MAREES TERRESTRES

BULLETIN D'INFORMATIONS

INTERNATIONAL CENTER FOR EARTH TIDES
CENTRE INTERNATIONAL DES MAREES TERRESTRES

Federation of Astronomical and Geophysical Data Analysis Services
(FAGS)

International Association of Geodesy - International Gravity Field Service
(IAG – IGFS)

Publié avec le soutien de l'Observatoire Royal de Belgique

BIM
1 4 2

15 SEPTEMBRE 2006

Editeur: Dr. Bernard DUCARME
Observatoire Royal de Belgique
Avenue Circulaire 3
B-1180 Bruxelles

BIM 142

15 septembre 2006

ABD EL-GELIL M., PAGIATAKIS S.,EL-RABBANY A.....
Pressure admittance function from least squares product spectrum of surface gravity and pressure 11305

NEUMEYER J., STÖBER C.....
Aspects of 3D air pressure reduction on gravity data (*abstract*) 11315

SIMON D.....
Gravimetric effects induced by vertical air mass shifts at Medicina (1998-2005), Wettzell, Bad Homburg , Moxa, Pecny and Wien (1998-2004)..... 11317

SIMON D.,KLÜGEL T., KRONER C.....
Comparison of variations of air mass attraction derived from radiosonde data and a meteorological forecast model 11323

HARNISCH G., HARNISCH M., FALK R.....
Hydrological influences on the gravity variations recorded at Bad Homburg 11331

MEURERS B.....
Long and short term hydrological effects on gravity in Vienna 11343

KRONER C.....
Hydrological signals in SG records at Moxa - a follow up 11353

NAUJOKS M., KRONER C., JAHR T., WEISE A.....
From a disturbing influence to a desired signal: Hydrological effects in gravity observations (*abstract*) 11359

VIRTANEN H., TERVO M., BILKER-KOIVULA M.....
Comparison of superconducting gravimeter observations with hydrological models of various spatial extents 11361

KLÜGEL TH., HARNISCH G., HARNISCH M.....
Measuring integral soil mosture variations using a geoelectrical resistivity meter 11369

KRAUSE P., FINK M., KRONER C.....
Soil moisture measurements and their impact on gravimetric measurements 11377

LONGUEVERNE L., FLORSCH N., BOUFIN F., VINCENT T., KAMMENTHALER M.....
Inclinometry and Geodesy: an hydrological perspective 11387

STEFFEN H., KAUFMANN G.....
Influence of the Hohenwarte reservoir on tilt and strain observations at Moxa 11399

TERVO M., VIRTANEN H., BILKER-KOIVULA M.....
Environmental loading effects on GPS time series 11407

WZIONTEK H., FALK R., WILMES H., WOLF P.....
Rigorous combination of superconducting and absolute gravity measurements with respect to instrumental properties 11417

CROSSLEY D., HINDERER J., BOY J.-P., de LINAGE C.....
Status of the GGP satellite project 11423

HINDERER J., de LINAGE C., BOY J.-P.....
How to validate satellite-derived gravity observations wit gravimeters at the ground? 11433

Pressure Admittance Function from Least Squares Product Spectrum of Surface Gravity and Pressure

Mahmoud Abd El-Gelil[1], Spiros Pagiatakis[1], and Ahmed El-Rabbany[2]
[1]York University, Toronto, Canada, Department of Earth and Space Science and Engineering
[2]Ryerson University, Toronto, Canada, Department of Civil Engineering

Abstract: Atmospheric pressure is one of the most significant disturbing noises to surface gravity measurements. This effect is usually removed by two different methods that are based on the availability of pressure data and their distribution in both time and space. The first and most accurate method is the convolution of the global surface pressure field with an appropriate Green's function; its downside is that it requires short sampling intervals currently unavailable. The second method determines a transfer function between pressure and gravity known as barometric pressure admittance. In this paper, we adopt an alternative approach for the determination of the admittance that is based on the least-squares (LS) product spectrum of the atmosphere pressure and gravity time series. It represents a reasonable gravity response to air pressure fluctuations in specific frequency bands (frequency dependent admittance), that is derived from a five-year data set from the Canadian Superconducting Gravimeter Installation – CSGI (Cantley, Canada). The results show improvements in the gravity spectrum, particularly in the diurnal and semi-diurnal bands and in higher frequency bands.

1. Introduction

Recent rapid improvements in technology have created extremely precise and accurate measuring systems that are sensitive to minute physical phenomena that were once much too small to be detected. The superconducting gravimeter is no exception; it is sensitive to changes in gravity that reach the nanogal level (1nGal = 10^{-11} m/s^2). Gravity variations are caused by many physical phenomena e.g. lunar and solar tides, Earth's rotation changes, atmospheric and ocean loading, and others (Hinderer and Crossley, 2000; van Dam and Wahr, 1998). This amazing device, with its high sensitivity and stability covers a very wide spectrum with periods from seconds to years (Crossley and Xu, 1998). It is, with no doubt, a challenge to the geophysicists to identify and/or separate minute signal(s) of interest in a specific band of interest (Sun et al, 2002).

In the last three decades, geophysicists and other researchers have been searching for very weak signals in the superconducting gravimeter records e.g., core modes and the Slichter triplet (Hinderer and Crossley, 2004; Jensen et al, 1995; Smylie and Jiang, 1993). Unfortunately, however, these weak signals can not be detected before removing or modeling other disturbances which are considered as noise. Otherwise, misleading results or wrong interpretation may arise. The atmospheric pressure is one of the most significant environmental phenomena that affect the surface gravity records. The atmospheric pressure effect on gravity is about one order of magnitude smaller than the solid Earth tides. For certain stations, this effect reaches 30μgal (Virtanen, 2004). There are basically two approaches to estimate or model the atmospheric pressure effect on the gravity records. The first one is the physical model and the second an empirical or experimental one using an admittance (transfer) function. In the physical model, the atmospheric parameters (e.g. pressure, temperature, and other) are measured on the Earth surface or at different altitudes and with very good spatial distribution. A Green's function is then used to estimate the loading and attraction effect (Boy et al, 2001; Boy et al, 1998; Kroner and

Jentzsch, 1999; Merriam, 1992a; Mukai et al, 1995; Neumeyer et al, 2004; Sun et al, 1995). The admittance approach deals with local atmospheric pressure measurements obtained in parallel with the gravity data (same time and location).

In the admittance approach, the regression analysis is usually applied to estimate a very simple transfer function between gravity and pressure. However, it is believed that this single scalar function is not adequate to remove the pressure effect because it is local in character and usually frequency and season dependent. The frequency dependant admittance that was first introduced by Warburton and Goodkind (1977) and elaborated by Crossley et al., (1995) and Neumeyer (1995) showed that it increases smoothly and monotonically from 0.2 μgal/mbar at low frequencies to about 0.35 μgal/mbar at high frequencies. However, Sun et al., (2002) found that the frequency-dependent admittance is 0.378 μgal/mbar at low frequencies and reduces to 0.147 μgal/mbar at high frequencies. Hu et al., (2005) applied the wavelet analysis to decompose the gravity and pressure signals into 14 bands. Different admittances were estimated for all the specific bands using regression between the decomposed signals. However, it is expected that a highly accurate empirical model can remove about 90 percent of the total pressure effect (Mukai et al, 1995; Spratt, 1982).

In this paper, a different procedure is adopted to estimate the pressure admittance that is based on the product spectrum from the least squares spectrum analysis. The common peaks in both gravity and atmospheric pressure are used to define and estimate the admittance. The significance level of the peaks in the product spectrum is well defined based on the probability density function derived from the LS spectrum. The common spectral peaks in both gravity and pressure series are suppressed in monthly data segments to estimate their amplitudes and phases in the band 700-2h. Finally, the weighted LS regression is used to estimate a smooth admittance as a function of frequency. The new admittance is then used to correct the gravity series (residual series) in an attempt to improve the signal to noise ratio for the purpose of obtaining better estimates of other effects or searching for weak signals.

3. Least Squares Spectral Analysis

We use the Least Squares Spectral Analysis (LSSA) to estimate the spectra of the gravity and atmospheric pressure series and subsequently produce their product LS spectrum. The benefits of the LSSA vs. Fourier analysis have already been presented widely but most recently in Craymer, (1998), Pagiatakis, (1999), and Pagiatakis, (2000) and need not be repeated here. We only present the fundamental formulas and emphasize the statistical properties of the LS spectrum.

We consider a time series $f(t_i)$ observed at discrete times t_i, $i = 1, 2, \ldots n$, not necessarily evenly spaced, which is essentially equivalent to the presence of gaps. This time series has also a variance-covariance matrix C_f that describes the uncertainty of the observed values. The LSSA spectrum is described by the percentage variance $s(\omega_i)$ of the spectral content at a specific frequency ω_i:

$$s(\omega_i) = \frac{f^T C_f^{-1} \hat{p}(\omega_i)}{f^T C_f^{-1} f}, \tag{1}$$

where $\hat{p}(\omega_i)$ is the projection of $f(t)$ onto the model space spanned by different base functions that can render the series stationary while simultaneously producing the LS spectrum (trigonometric base functions). The range of $s(\omega_i)$ is from 0 to 1. Pagiatakis (1999) showed that the probability density function (*pdf*) of the LS spectrum $s(\omega_i)$ follows the *beta* distribution defined by two parameters α =1 and β = (*m*-*u*-2)/2 where *m* is the number of data points and *u* is the number of unknown parameters estimated by the LS procedure.

4. Least Squares Product Spectra and Response function

Common peaks or common features in both gravity and atmospheric pressure can easily be defined through their product spectrum. Knowing that each individual factor spectrum follows the beta distribution, we derive the probability distribution of the product spectrum using standard statistical approaches (e.g. Hogg and Craig, 2005). After some development, we obtain the *pdf* for the sum of the natural logarithm of two spectra {z =ln(s_1)+ln(s_2)}, given by:

$$f(z) = \int_z^0 \beta_1\beta_2 e^z \left(1-e^{z-s_2}\right)^{\beta_1-1}\left(1-e^{s_2}\right)^{\beta_2-1} ds_2 \qquad (2)$$

where $\beta_i = 0.5(m_i - u_i - 2)$, m_i and u_i were defined earlier. The above *pdf* that underlines the product LS spectrum can be used to identify the significance of the common peaks in both series by using their product spectrum. Figure 1 shows the *pdf* for β_1 =*8500 and* β_2 = 3200. The vertical line in Figure 1 (at -15.73) shows the 95% confidence level.

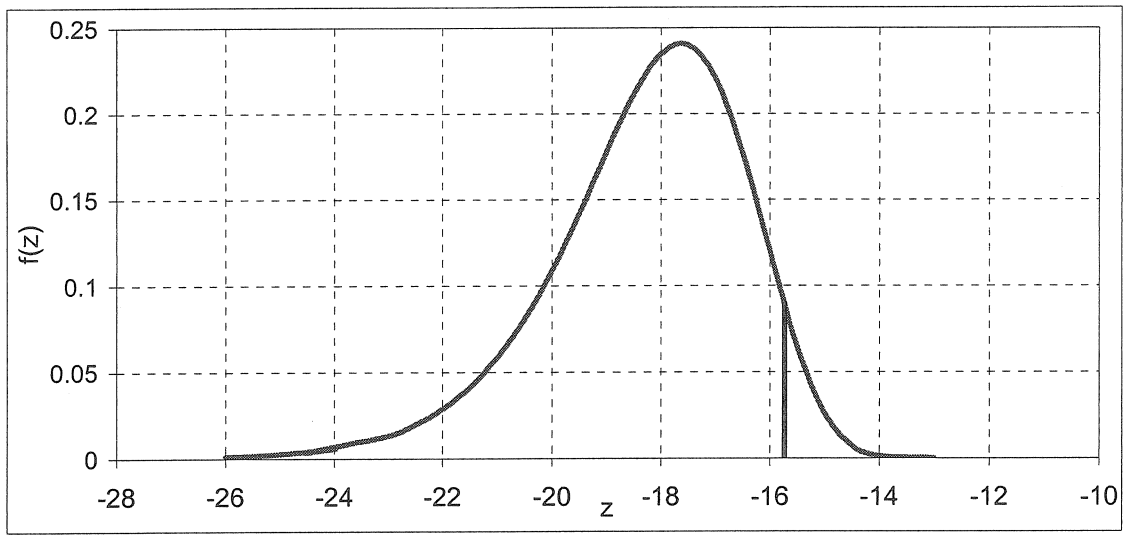

Fig. 1. The probability density function of the product spectrum

After producing the product spectrum between gravity and atmospheric pressure and using its *pdf* as a guide, we can identify statistically significant peaks above the 95% confidence level or higher. These peaks (actually their periods) are suppressed separately in the gravity and atmospheric pressure series to estimate their amplitude and phase:

$$g_i = a_{iG}\left(\cos\left[(\omega_i t) - \varphi_{iG}\right]\right), \tag{3}$$

$$p_i = a_{ip}\left(\cos\left[(\omega_i t) - \varphi_{ip}\right]\right), \tag{4}$$

where a_{iG}, a_{ip} are the amplitudes of gravity and atmosphere pressure constituents respectively, and φ_{iG}, φ_{ip} are their phases. All the above parameters have an associated covariance matrix estimated from the LS procedure. Only the statistically significant amplitudes and phases are used to estimate the pressure admittance. The magnitude and phase of the pressure admittance is then estimated from

$$\alpha(\omega_i) = \frac{a_{iG}}{a_{ip}}, \tag{5}$$

$$\Delta\varphi_i = \varphi_{iG} - \varphi_{ip}. \tag{6}$$

Applying the covariance law to Eq. (5) and (6) we calculate the standard deviation σ_α of admittance and σ_φ of its phase:

$$\sigma_\alpha = \left[\frac{1}{a_p^2}\left(\sigma_{a_G}^2 + \sigma_{a_p}^2\left(\frac{a_G^2}{a_p^2}\right)\right)\right]^{1/2} \tag{7}$$

$$\sigma_\varphi = \left[\sigma_{\varphi_G}^2 + \sigma_{\varphi_p}^2\right]^{1/2} \tag{8}$$

We note here that the admittance is calculated only at specific frequencies at which both gravity and atmospheric pressure data have significant amplitudes. We avoid the calculation of the admittance at frequencies where other phenomena may be present (i.e. in the semidiurnal or diurnal band) since they may contaminate it.

5. Data processing and Analysis

Two five-year-long time series of gravity and atmospheric pressure respectively starting 1st January 1998 are used to estimate the atmospheric pressure admittance from the Canadian Superconducting Gravimeter Installation – CSGI (Cantley, Canada). These five year records are segmented into monthly time series. First of all, the solid Earth tide effect is removed from the 1s gravity records using GWAVE (Merriam, 1992b). Secondly, the 1s gravity residual series (tide free) is then filtered using a Parzen weighting scheme that produces unequally spaced series along with their standard deviation at a sampling interval ranging from 2 to 5 minutes. The atmospheric pressure and its associated standard deviation are calculated by using the same scheme but at the sampling interval of 15 minutes. Thirdly, the ocean loading effect is also removed by least-squares fitting of eight most significant periods; this is done simultaneously with the estimation of the gravity spectrum using the LSSA software.

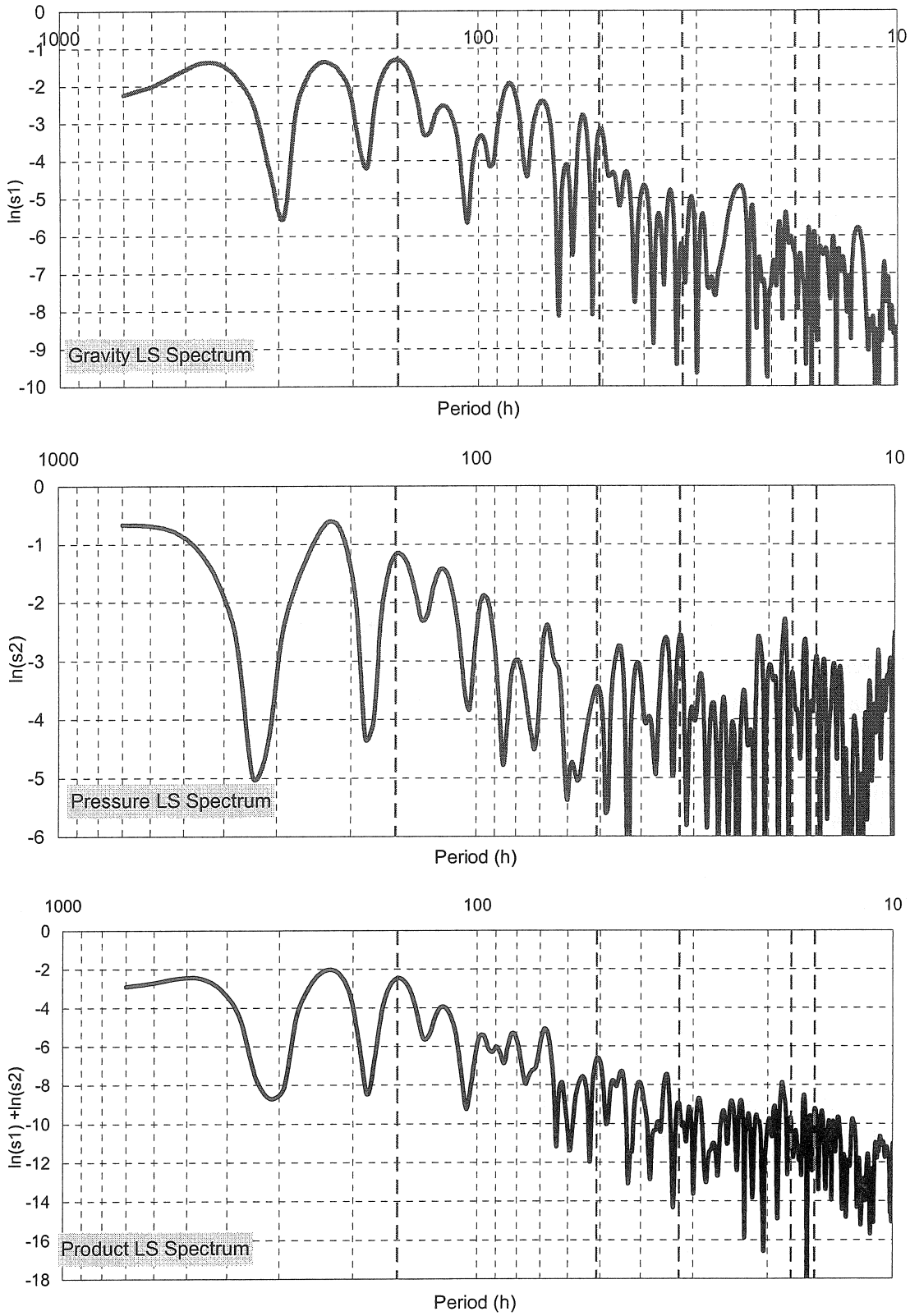

Fig. 2. LS spectra of gravity, pressure and of the product spectrum

The following steps are followed to estimate the admittance:

1. We produce monthly LS spectra for both gravity and pressure in the band 700-2h.
2. The natural logarithms of both spectra are taken and summed. The identification of the significant peaks in the product LS spectrum at 95% confidence levels is done rigorously using the probability density function of the product LS spectrum (Fig. 2).
3. The peaks in the product must be statistically significant at 95% confidence level in both gravity and pressure (Figure 2) to be considered in the next step.
4. We suppress these peaks in the monthly data to estimate their amplitudes and phases.
5. We use Eqs. (5)-(8) to estimate the admittance (amplitude and phase) along with their associated standard deviations.
6. The weighted LS regression is used to define the best fit to get a smoothed gravity response for pressure changes (Fig. 3)

$$\alpha(f) = 0.312501 - 0.291637e^{-\left(\frac{1}{32f}\right)}, \tag{9}$$

where f is the frequency cycle/hour (cph) and the phase difference $\Delta\varphi = 185.86 \pm 5.53$ degrees.

The results obtained from Eq. (9) are plotted in Fig. (3), which shows the admittance from 5-year data (monthly segments) with their error bars (1σ). Different fitting functions are tested (2^{nd}, 3^{rd} order polynomials and sine wave); however, Eq. (9) is the best fit with minimum quadratic norm. The red line shows a weighted LS regression that is expected to describe a smooth response over all frequencies without any resonance. The estimated frequency-dependent admittance tends to be constant for periods longer than about 100h and decreases exponentially in the band 100-3h. This means that the new admittance in the diurnal and semi-diurnal or higher frequency bands is smaller than the one estimated from previous studies (0.3μgal/mbar). The phase difference (phase response) is estimated from the weighted average.

Different tests are carried out to assess and validate this new admittance. LS gravity spectra of June, 1998 before and after the removal of the pressure effect using the constant (0.3 μGal/mbar) and the newly estimated frequency-dependent admittance are used in this comparison. Fig. 4 shows the spectrum in the band 100-10h, whereas Fig. 5 shows the 10-3h band. It is obvious that the frequency-dependent admittance improved the peaks but with more significant improvements in the 10-3h band. From Fig. 4, the gravity peak at period 56.689h, which is originally from the pressure (pressure spectrum not shown here) is reduced by 35% and 54% when applying the constant admittance and the new one, respectively. Craymer (1998) showed that the reduction of the LS spectrum peaks is equivalent to the inverse of the square of the signal-to-noise ratio (SNR). This means that the SNR is improved. Also, Fig. 4 shows the peak at 26.252h is improved when applying the new admittance (red color); however, this peak does not exist in the

pressure spectrum. Fig. 5 shows significant improvements in the peaks in that band (3-10h) when applying the new admittance compared with the constant one.

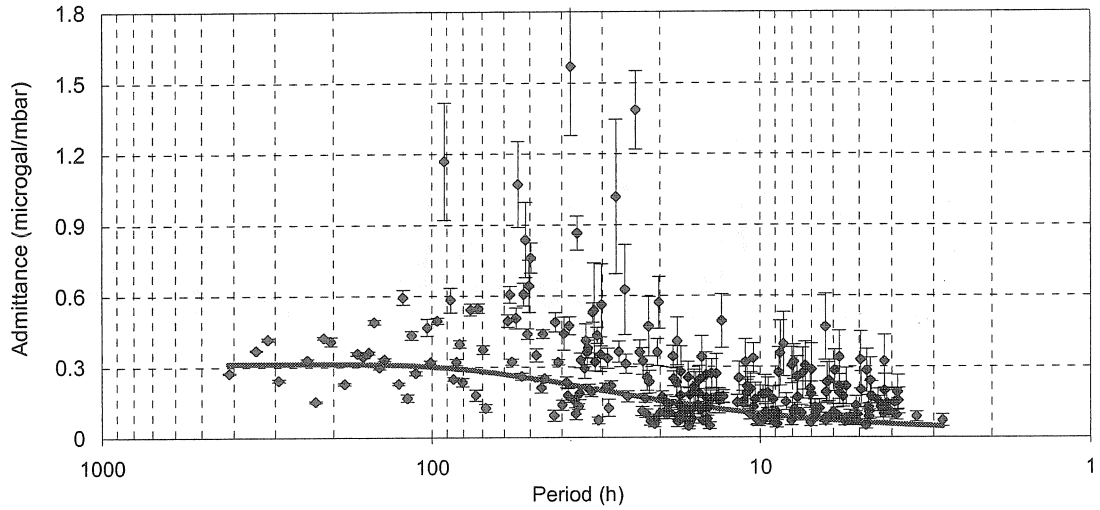

Fig. 3. Pressure admittance from the Least Squares Response Method

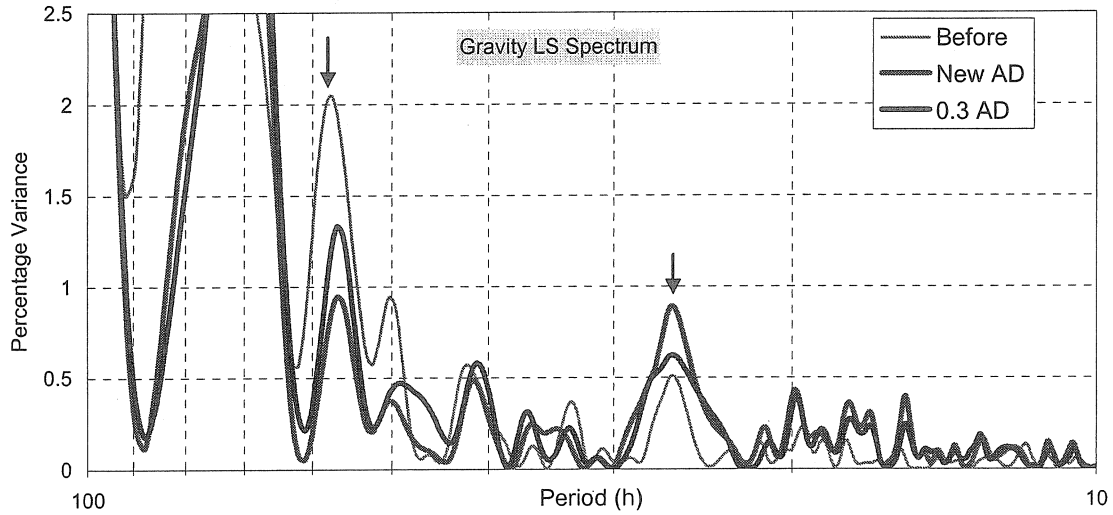

Fig. 4. LS spectrum before and after the application of the new admittance (10-100h)

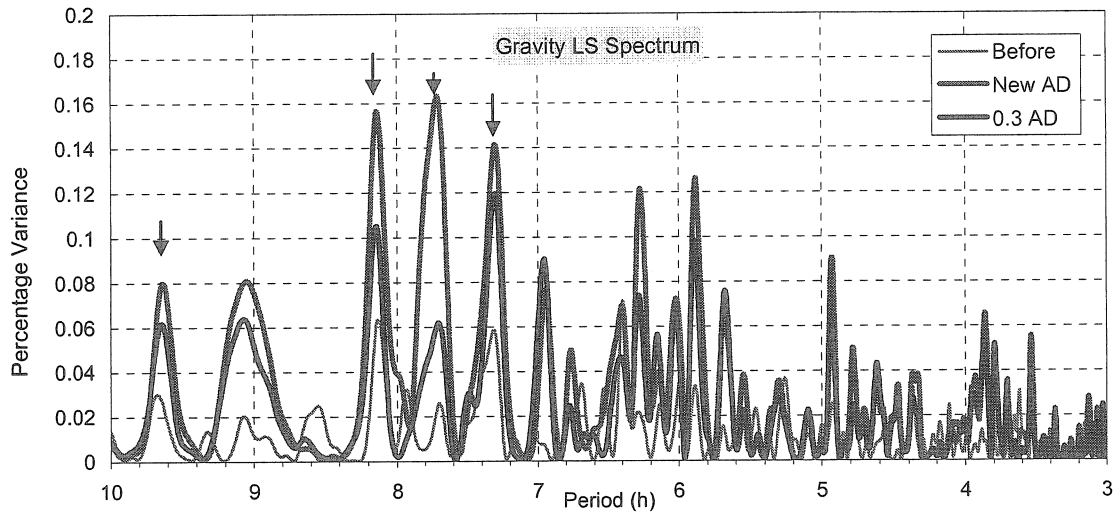

Fig. 5. LS spectrum before and after the application of the new admittance (3-10h)

6. Conclusion

The constant admittance is not adequate to correct the pressure effect. The new admittance is frequency dependent and it is relatively constant in the low frequency band (higher than few days), and it decreases exponentially starting from 100h. The spectrum in the high frequency band (10-3h) is improved significantly with peaks sharpened. Also, the signal-to-noise ratio of the gravity spectrum is improved with pressure peaks in the gravity either removed or reduced. Research is continuing to determine the seasonal variations of the pressure admittance.

References

Boy J.P., Gegout, P. and Hinderer Jacques, 2001. Gravity variations and global pressure loading, *Journal of the Geodetic Society of Japan,* 47, 267-272.

Boy, J.P., Hinderer, J. and Gegout, P., 1998. Global atmospheric loading and gravity, *Phys. Earth Planet. Inter.,* 109, 161-177.

Craymer, M.R., 1998. The least squares spectrum, its inverse transform and autocorrelation function: theory and some applications in geodesy, PhD thesis, University of Toronto, Canada.

Crossley, D., Jensen, O.G. and Hinderer, J., 1995. Effective Barometric Admittance and Gravity Residuals, *Phys. Earth Planet. Inter.,* 90, 221-241.

Crossley, D.J. and Xu, S., 1998. Analysis of superconducting gravimeter data from Table Mountain, Colorado, *G. J. International,* 135, 835-844.

Hinderer, J. and Crossley, D., 2004. Scientific achievements from the first phase (1997-2003) of the Global Geodynamics Project using a worldwide network of superconducting gravimeters, *Journal of Geodynamics,* 38, 237-262.

Hinderer, J. and Crossley, D., 2000. Time variations in gravity and inferences on the Earth's structure and dynamics, *Surv.Geophys.,* 21, 1-45.

Hogg, R.V. and Craig, A.T., 2005. *Introduction to mathematical statistics*. Prentice Hall New Jersey, (6th edition).

Hu, X.-G; Liu, L.-T; Hinderer, J.; Sun, H.P , 2005. Wavelet filter analysis of local atmospheric pressure effects on gravity variations. Journal of Geodesy, 79 (8): 447-459.

Jensen, O., Hinderer, J. and Crossley, D.J., 1995. Noise Limitations in the Core-Mode Band of Superconducting Gravimeter Data, *Phys. Earth Planet. Inter.*, 90, 169-181.

Kroner, C. and Jentzsch, G., 1999. Comparison of different barometric pressure reductions for gravity data and resulting consequences, *Phys.Earth Planet.Inter.*, 115, 205-218.

Merriam, J.B., 1992a. Atmospheric-Pressure and Gravity, *Geophysical Journal International,* 109, 488-500.

Merriam, J.B., 1992b. An ephemeris for gravity tide predictions at the nanogal level, *Geophysical Journal International,* 108, 415-422.

Mukai, A.; Higashi, T.; Takemoto, S.; Nakagawa, I.; Naito, I.., 1995. Accurate Estimation of Atmospheric Effects on Gravity Observations made with a Superconducting Gravity Meter at Kyoto, *Phys. Earth Planet. Inter.*, 91, 149-159.

Neumeyer, J., 1995. Frequency dependent atmospheric pressure correction on gravity variations by means of cross spectral analysis; Theoretical tidal model, calibration, and high precision tidal data processing [modified], *Marees Terrestres. Bulletin d'Informations,* 122, 9212-9220.

Neumeyer, J.; Hagedoorn, J.; Leitloff, J.; Schmidt, T., 2004 Gravity reduction with three-dimensional atmospheric pressure data for precise ground gravity measurements, *Journal of Geodynamics,* 38, 437-450.

Pagiatakis, S.D., 1999. Stochastic significance of peaks in the least-squares spectrum, *Journal of Geodesy,* 73, 67-78.

Pagiatakis, S.D., 2000. Application of the least-squares spectral analysis to superconducting gravimeter data treatment and analysis; Proceedings of the workshop on High precision gravity measurements with application to geodynamics and Second GGP workshop, *Cahiers Du Centre Europeen De Geodynamique et de Seismologie (ECGS),* 17, 103-113.

Smylie, D.E. and Jiang, X.H., 1993. Core Oscillations and their Detection in Superconducting Gravimeter Records, *Journal of Geomagnetism and Geoelectricity,* 45, 1347-1369.

Spratt, R.S., 1982. Modeling the Effect of Atmospheric-Pressure Variations on Gravity, *Geophysical Journal of the Royal Astronomical Society,* 71, 173-186.

Sun H-P, Ducarme, B. and Dehant V., 1995. Theoretical calculation of atmospheric gravity Green's functions, *Cahiers Du Centre Europeen De Geodynamique et de Seismologie (ECGS),* 11, 223-237.

Sun, H-P *et al.*, 2002. Tidal gravity observations obtained with a superconducting gravimeter at Wuhan/China and its application to geodynamics, *Journal of Geodynamics,* 33, 187-198.

van Dam T.M. and Wahr J., 1998. Modeling Environment Loading Effects: a Review, *Physics and Chemistry of the Earth,* 23, 1077-1087.

Virtanen, H., 2004. Loading effects in Metsahovi from the atmosphere and the Baltic Sea, *Journal of Geodynamics,* 38, 407-422.

Warburton, R.J. and Goodkind, J.M., 1977. Influence of Barometric-Pressure Variations on Gravity, *Geophysical Journal of the Royal Astronomical Society,* 48, 281-292.

Aspects of 3D air pressure reduction on gravity data

Juergen Neumeyer, Carsten Stöber

Ground gravity measurements based on a test mass (relative and absolute gravimeters) are influenced by mass redistribution within the atmosphere which induces gravity variations (air pressure effect) in μgal range (about 15 μgal for the Sutherland Superconducting Gravimeter (SG) station). These variations are disturbing signals in gravity data and they must be reduced very carefully for detecting weak gravity signals.

From European Centre for Middle Weather Forecasts (ECMWF) 3D air pressure data are available. These data are used for modelling of the Newtonian attraction term. The modelling shows a surface pressure independent part (SPI) of gravity variations induced by mass redistributions of the atmosphere in the μgal order.

For different SG sites and an Absolute Gravimeter location the 3D models have been applied and the SPI part was calculated. Its influence is shown on long periodic gravity variations, SG measured polar motion, comparison of SG with GRACE and hydrology model derived gravity variations. It will be shown how the application of the SPI part can increase the precision of the air pressure reduction on gravity data.

BIBLIOGRAPHY

1. Neumeyer J., Hagedorn J., Leitloff J., Schmidt T., 2004. Gravity reduction with three-dimensional atmospheric pressure data for precise ground gravity measurements. *Journal of Geodynamics*, 38, 437-450.

2. Neumeyer J., Schmidt T., Stoeber C., 2006. Improved determination of the atmospheric attraction with 3D air density data and its reduction on ground gravity measurements. *Symp. G3 on Earth Processes, Dynamic Planet 2005, Cairns, Australia, August 22-26 2005, Accepted for publication in Journal of Geodesy*

Gravimetric effects induced by vertical air mass shifts at Medicina (1998-2005), Wettzell, Bad Homburg, Moxa, Pecny and Wien (1998-2004)

by Dietrich Simon*
Frankensteinstr.4, D- 36469 Tiefenort, e-mail: reteid.simon@web.de

Abstract
The gravimetric effects of vertical air mass displacements were computed at the locations of six European stations, where superconducting gravimeters are recording. The modelling was made based on radiosonde data using the AMACON software of SIMON (2003). The length of the $g_c(t)$ model curves is 8 years (1998/01/01–2005/12/31) for Medicina station / Italy and 7 years (1998/01/01–2004/12/30), respectively, for the five other stations Bad Homburg/Germany, Wettzell/Germany, Moxa/Germany, Pecny/Czech Republic and at Vienna/Austria. As before the modelling was made with a general sampling rate of 24 hours (12 h of any day). Some examples of $g_c(t)$ model curves are given where the sampling rates are shorter.

1. Background of the modelling

Four years ago the existence of a gravimetrical component $g_c(t)$ induced by vertical air mass shifts in the case of a constant ground air pressure was firstly shown by SIMON (2002). The effect is caused by an unaccelerated rising of warmed (lighter) and the sinking of colder (heavier) air particles, respectively. The air mass attraction varies due to these vertical air mass shifts according to

$$A_c(t) = A(t) - A_p(t) = A(t) - r_{AP} * P(t) \qquad (1)$$

A(t): air mass attraction at the measuring point G,
P(t): surface pressure at the measuring point G
$A_p(t)$, $A_c(t)$: surface pressure-dependent and independent component of A(t)
r_{AP} = 0.40 μGal/hPa: regression coefficient (SIMON, 2003).

The corresponding component $g_c(t)$ of the gravity variation has the opposite sign. It is obtained from

$$g_c(t) = - A_c(t) + C, \qquad C = \text{constant} \qquad (2)$$

The seasonal warming /cooling of air masses is an effect of low regional variability. As a consequence the data of a network of eight radiosonde stations located in Germany, Austria, Poland and Italy were enough for the calculation of the $g_c(t)$ – variations at the mentioned six European gravimeter stations. The radiosonde stations were seldom situated in the direct vicinity of a gravimeter location, as for instance at Medicina and Vienna. Therefore the $g_c(t)$ modelling was made in most cases according the so-called 3 stations method (SIMON, 2003).

---

* Dietrich Simon, formerly BKG Frankfurt , Richard- Strauss- Allee 11, 60598 Frankfurt am Main

2. Results

The results of the computations are shown in the following figures:

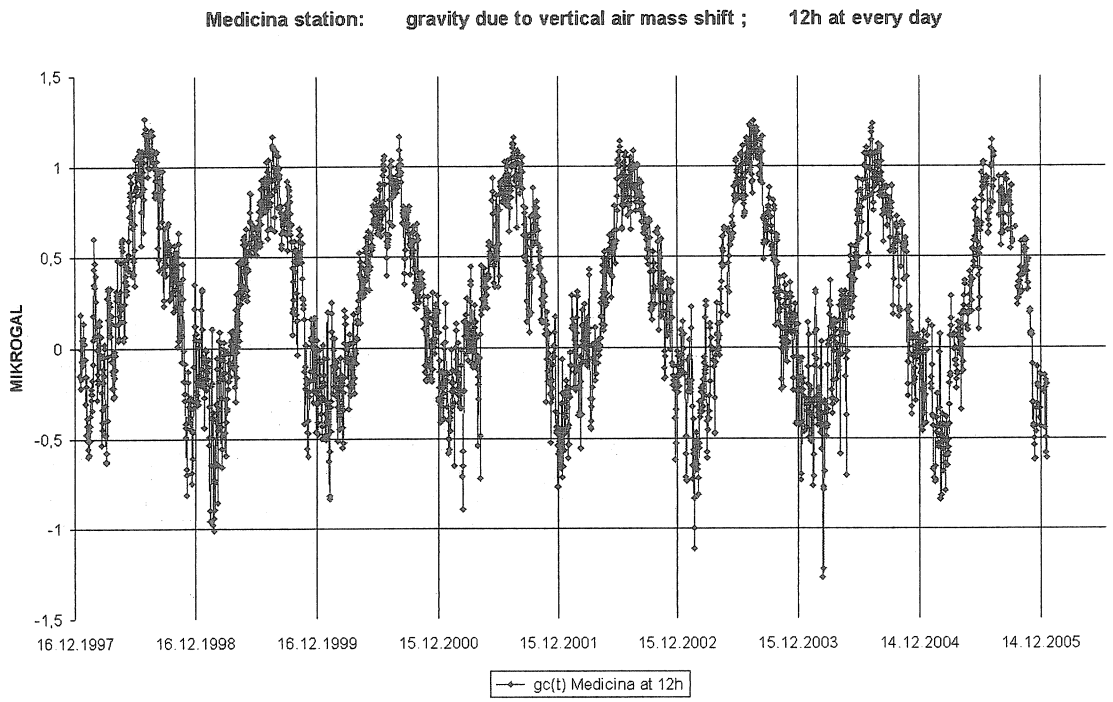

Fig.1: Medicina station 1998-2005: The $g_c(t)$ model curve , calculated from data of the neighbouring radiosonde station (distance: about 2 km).

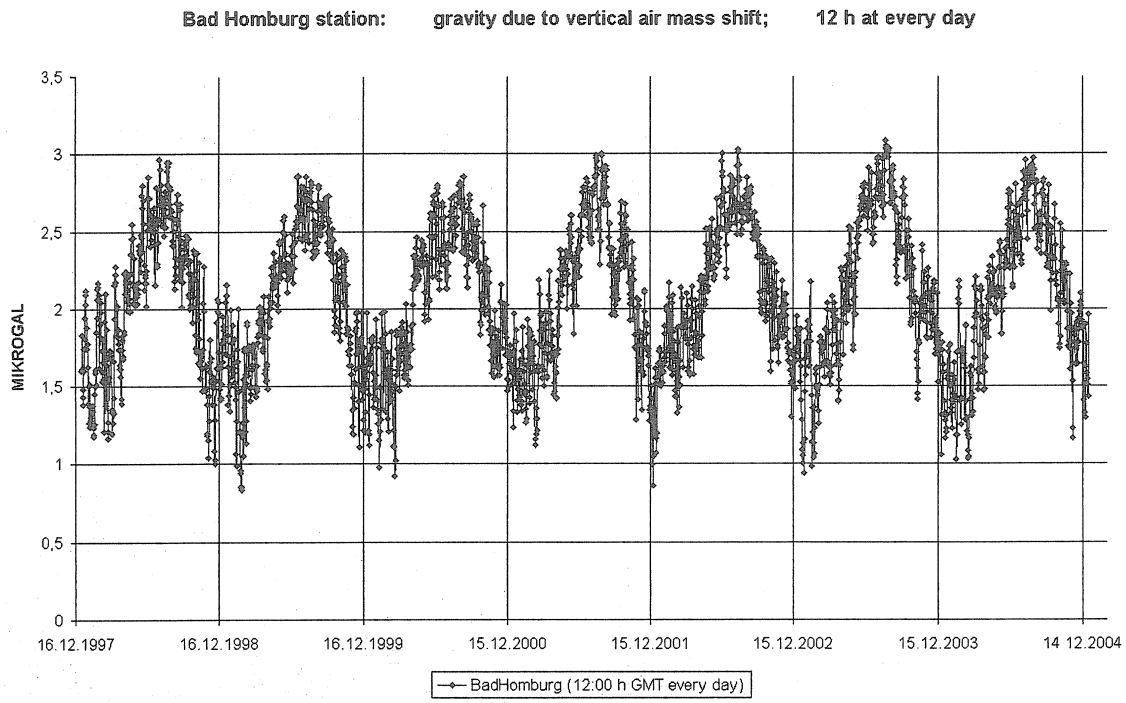

Fig.2: Bad Homburg station 1998-2004: The $g_c(t)$ model curve , calculated from data of the radiosonde stations at Stuttgart, Essen, and Meiningen, respectively.

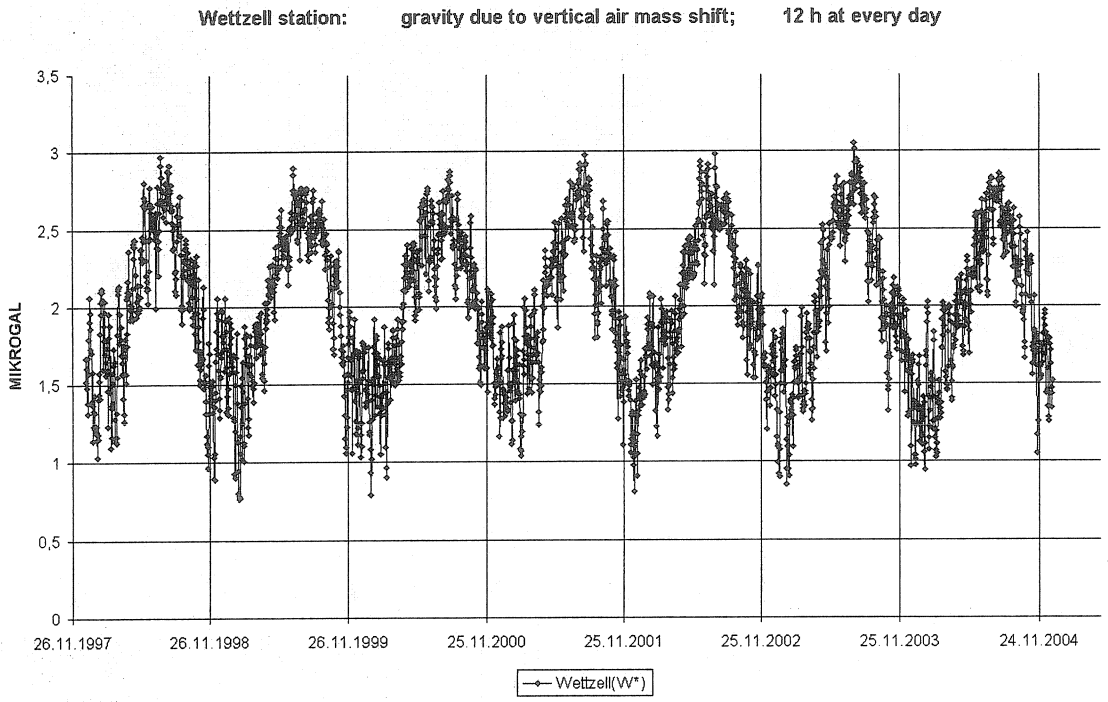

Fig.3: Wettzell station 1998-2004: The $g_c(t)$ model curve, calculated from data of the radiosonde stations at Munic, Lindenberg, and Meiningen, respectively.

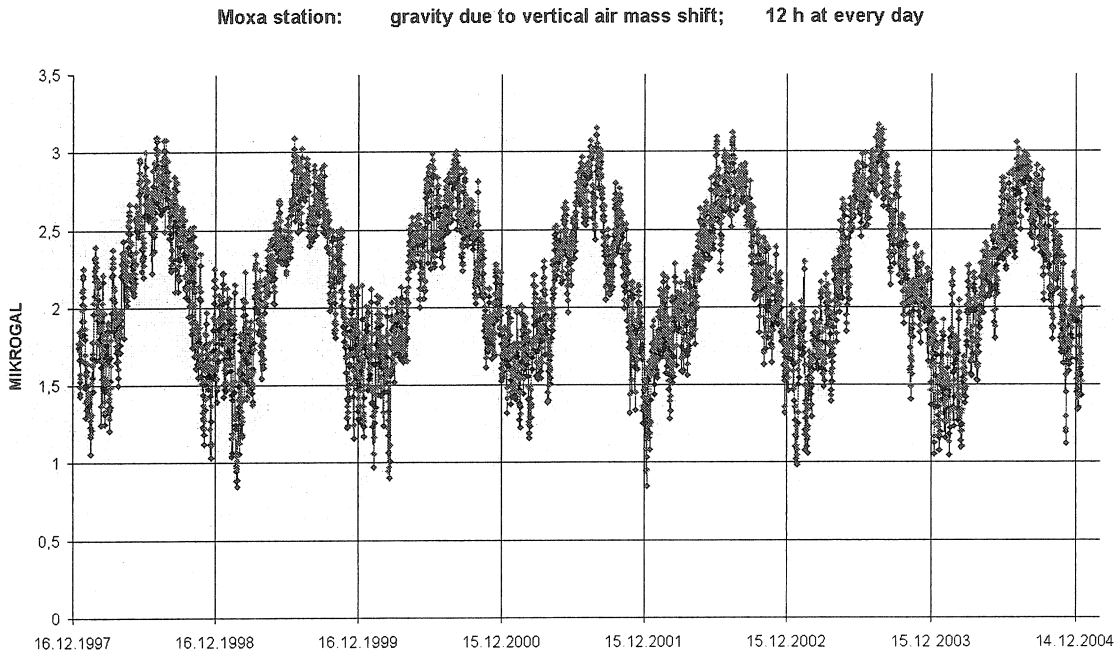

Fig.4: Moxa station 1998-2004: Two variants of $g_c(t)$ model curve, calculated firstly from radiosonde data of Munic, Lindenberg, and Meiningen, respectively, and secondly from radiosonde data of Munic, Wroclaw, and Meiningen.

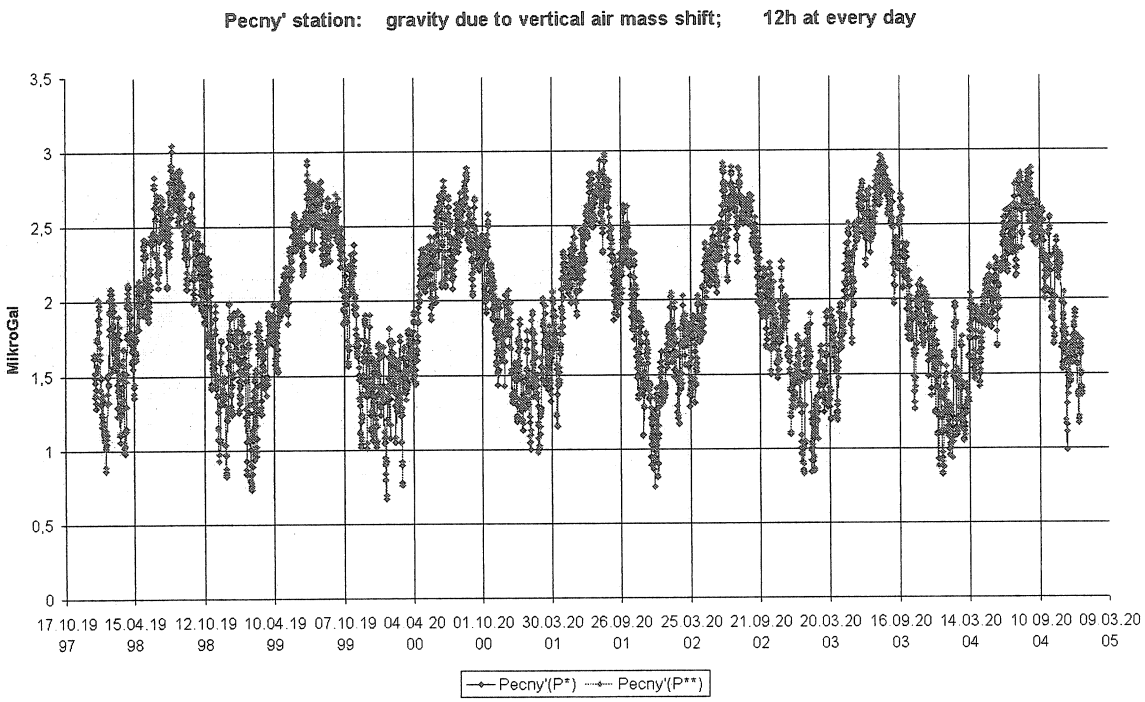

Fig.5: Pecny station 1998-2004: Two variants of $g_c(t)$ model curve, calculated firstly from the radiosonde data of Munic, Lindenberg, Vienna, and Wroclaw, respectively, and secondly by the radiosonde data of Munic, and Wroclaw, respectively.

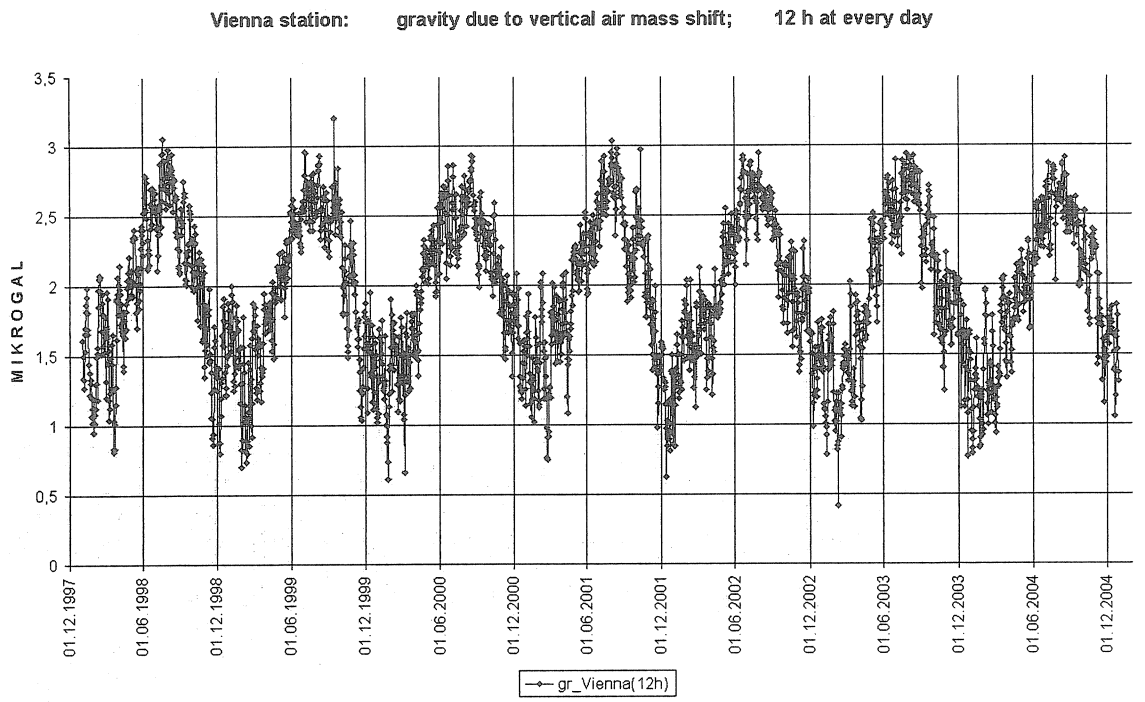

Fig.6: Vienna station 1998-2004: The $g_c(t)$ model curve , calculated from the data of the neighbouring radiosonde station (distance: < 0.2 km).

2. Comparison with the results of other modeling

KLUEGEL (2005) calculated the $g_c(t)$ curves of three of the before mentioned gravimeter stations Bad Homburg, Wettzell and Moxa, too. As 2 years ago (KLUEGEL, 2003) he used for this purpose instead of radiosonde data the data of the weather model LM of the German Weather Service (DWD), Offenbach. The modelling has been done for a longer time interval, covering one year (2003) now.

A first comparison of both types of the $g_c(t)$ curves was made in 2006, February. We found smaller double amplitudes of KLUEGEL's $g_c(t)$ variations at all the three stations. The empirically determined air pressure coefficients for the modelling of the $A_p(t)$-component were smaller, too: 0.35 μGal/hPa instead of 0.40 μgal/hPa. The discrepancy between the corresponding $g_c(t)$ variations practically disappeared after a multiplication of KLUEGEL's $g_c(t)$ model curves by a factor of 2.2.

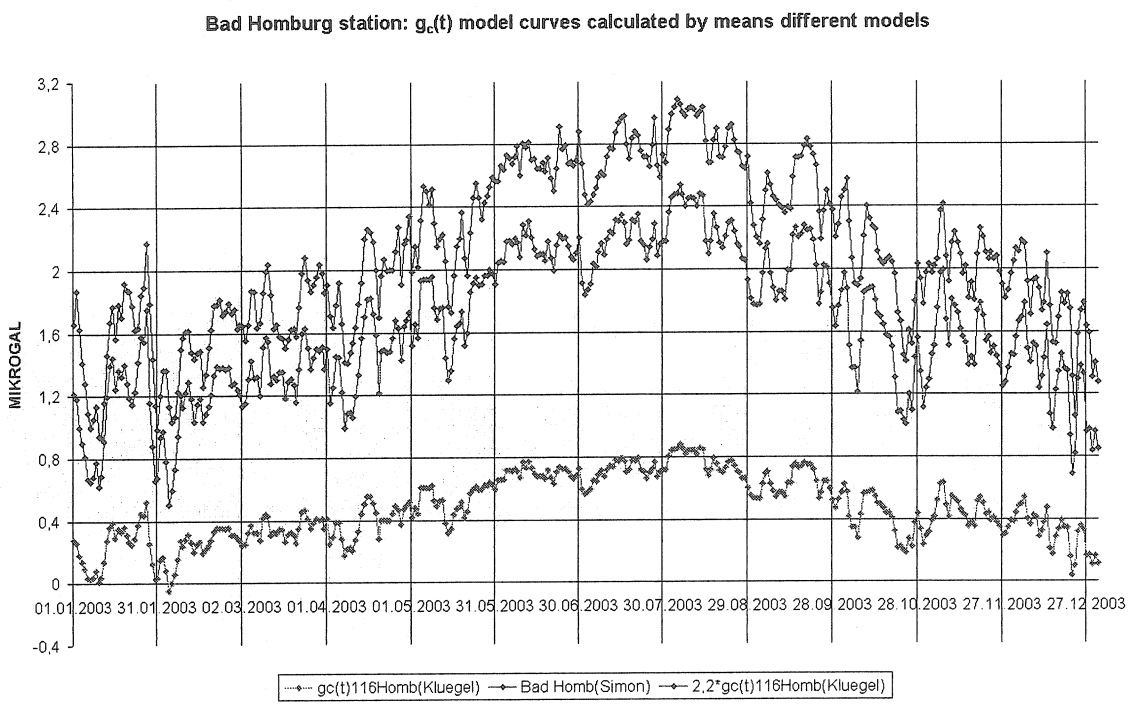

Fig.7: Gravimetric effects of vertical air mass shifts calculated either by means of radiosonde data and by weather model data (LM data) using different models.

The $g_c(t)$-curves of the Bad Homburg station for 2003 calculated by different models and data are compared in Fig.7. The upper curve was calculated by means of the model by SIMON (2003) and is based on radiosonde data. The middle $g_c(t)$-model curve is equal to the lowest one multiplied by the factor 2.2. The lowest curve was calculated by means of the model by KLUEGEL (2003) and is based on data of the local weather model data LM.

The reasons of the discrepancy between the $g_c(t)$-model curves are not completely known until now. The first results of a comparison of the calculations carried out in the last month for this purpose are shown in the paper of SIMON et al. (2006).

3. Conclusions

The figures of the $g_c(t)$-variations at the six European gravimeter stations in Fig.1–6 show that the amplitudes of the seasonal waves are relatively constant. Differences are mainly induced by variations of the regional climate from one year to the next one. Other effects such as e.g. the so-called "Sudden warming" or "Berlin phenomenon" (SCHERHAG, 1952) cause only short–time deviations from this normal behaviour.

Furthermore the regional variability of the $g_c(t)$-component is low (SIMON, 2003): The seasonal warming / cooling of the atmospheric air masses which produces the effect has practically the same qualities. As a consequence it seems to make sense to calculate this simple constructed $g_c(t)$ component separately and to subtract it from the total effect of air mass shift. The residuum thus obtained is not anymore a mixture of two effects with different origins. After the $g_c(t)$ elimination it is easier to find out the qualities of the remaining component which is primarily induced by horizontal air mass shifts.

References

KLUEGEL, TH., 2003. Bestimmung lokaler Einflüsse in den Zeitreihen inertialer Rotationssensoren. Schlussbericht z. DFG-Forschungsprojekt LOK-ROT, BKG Frankfurt a.M., Fundamentalstation Wettzell, March 2003

KLUEGEL, TH., 2005. Ergebnisse von Modellrechnungen zur Bestimmung der gravimetrischen Wirkungen von Luftmassenverlagerungen unter Verwendung von Daten des lokalen Wettermodells LM des Deutschen Wetterdienstes DWD ,Offenbach, pers. comm.

SCHERHAG, R., 1952. Die explosionsartigen Stratosphärenerwärmungen des Spätwinters 1951/52. Deutscher Wetterdienst US-Zone, Nr. 38

SIMON, D., 2002. Modelling of the field of gravity variations induced by the seasonal air mass warming during 1998-2000. Bull. d'Inf. Marées Ter., 136, 10821-10836.

SIMON, D., 2003. Modelling of the gravimetric effects induced by vertical air shifts. Mitt. BKG, Frankfurt a. M., vol. 21.

SIMON, D., KLUEGEL, TH., KRONER, C., 2006. Comparison of variations in air mass attraction derived from radiosonde data and a meteorological forecast model. Bull. d'Inf. Marées Terr., this issue.

Comparison of variations in air mass attraction derived from radiosonde data and a meteorological weather model

D. Simon[1], Th. Klügel[2], and C. Kroner[3]

[1] Frankensteinstr.4, D-36469 Tiefenort, Germany, formerly: Federal Agency for Cartography and Geodesy, Frankfurt a.M.

[2] Federal Agency for Cartography and Geodesy, Fundamental Station Wettzell, Sackenrieder Str. 25, D-93444 Bad Kötzting, Germany

[3] Institute of Geosciences, Burgweg 11, 07749 Jena, Germany

Abstract

For several years now endeavours are undertaken to improve the reduction of barometric pressure effects in continuous gravity observations. It is expected that a further improvement can be achieved by a more sophisticated consideration of the attraction effect of air mass fluctuations in a local to regional area around a gravimeter site. Two different approaches are compared for a number of stations: the computation of the attraction effect from radiosonde data and from a local high-resolution meteorological weather model. Differences in the two modelling approaches are discussed. First tentative explanations for deviations in the resulting attraction effects are given.

1. Objectives of the model comparison

For the computation of the gravimetric effect of air mass shifts often data of global meteorological models have been used besides classical regression reductions (e.g. MERRIAM, 1992; SUN, 1995; SUN ET AL., 1995; KRONER & JENTZSCH, 1999; NEUMEYER ET AL., 2004; BOY ET AL., 2002). A disadvantage of these model data is their small spatial resolution. Typically the grid distance is 0.5° which esp. affects the accuracy of the computed attraction component $A_p(t)$. $A_p(t)$ denotes the surface pressure dependent component of the total attraction effect A(t) and is given as $A_p(t)=A(t)-A_c(t)$ (Simon, 2002, 2003). It is caused by horizontal air mass movements, which cover a broad spatial and temporal spectral range. $A_c(t)$ denotes the component being independent of surface pressure.

According to KRONER (1997) it might be necessary to install several air pressure and temperature sensors in a local zone of about 50 km radius around a gravimeter site in order to determine the component $A_p(t)$ with an improved accuracy. An alternative was suggested in SIMON (2003) in order to improve the horizontal resolution: to use the local model LM of the German Meteorological Service (DWD) for the computation of the attraction component. The horizontal resolution of the model is about 14 km. 35 vertical layers with 36 layer boundaries are considered. The time resolution is 4 values per day. Using LM data KLÜGEL (2003) had already calculated the attraction effect for the gravimeter station Wettzell for a period of 16 days. With the support of the Federal Agency for Cartography and Geodesy (BKG) and in the frame of a joint project these computations were extended by KLÜGEL for the complete year 2003. The contributions A(t), $A_p(t)$, and $A_c(t)$ were computed for three locations of superconducting gravimeters (Wettzell, Bad Homburg, and Moxa) and two radiosonde stations (Meiningen and Munich).

In the next step the obtained model curves of air mass attraction should be compared with model curves derived from global meteorological models, radiosonde data, and the additional deployment of data from a local pressure network. On the basis of such a comparison a better estimate of the uncertainties in the modelling and an improved modelling should be achievable.

From a first comparison emerged that for all five stations for which a reduction based on radiosonde data was calculated the amplitudes of the $A_c(t)$-curve were 2.2 times larger than the amplitudes obtained using LM data. In the computations using radiosonde data a cylin-

drical air column with a radius of 113 km and a height of 31 km was considered. The model area for the LM data covered the same area, but the height of the air column was 23.6 km. For the elimination of the surface pressure proportional component $A_p(t)$ in the total attraction effect A(t) an air pressure coefficient of 0.35 µGal/hPa had to be usedinstead of 0.4 µGal/hPa for the radiosonde data. Multiplying the $A_c(t)$-curve derived from LM data by a factor of 2.2 yielded a good correspondence to the curves obtained with radiosonde data. The good agreement is found for both, annual variations and shorter-periodic contributions (SIMON, 2006).

2. Model differences as the origin of the factor 2.2

The systematic difference of the factor 2.2 between the model curves could be caused by different approaches or assumptions in the modelling. The main difference between the two model approaches is the following:

In the case of the model based on radiosonde data (SIMON, 2003) the variation of the air mass attraction due to warming / cooling of the air masses is computed for a circular-cylindrical air mass body with the vertical axis running through the location of the radiosonde station. The air pressure changes only vertically as observed with the radiosonde, and not laterally. This assumption only marginally changes the effect of the seasonal warming / cooling of the air layers on the computed attraction curves $A_c(t)$ of the air cylinder. The seasonal warming / cooling occurs in a very similar way for locations with a maximum distance of 226 km. The changes in the model cylinder will not differ much from those in the real air volume above the radiosonde station. The same assumption reduces the influence of horizontal air mass shifts on the total result.

The component $A_p(t)$ can even be totally eliminated in A(t) because of the lateral constance of air pressure in the model cylinder. For separation of the component $A_p(t)$ the surface pressure curve is simply multiplied by an empirically determined air pressure coefficient r (here 0.4 µGal/hPa) and subtracted from A(t). For the attraction component $A_c(t)_{radiosonde}$ follows:

$$A_c(t)_{radiosonde} = A(t)_{radiosonde} - r * p(t)) \quad (1)$$

$A_c(t)_{radiosonde}$: surface pressure independent component of A(t) in µGal
p(t) : surface pressure in hPa
$A(t)_{radiosonde}$: total attraction effec in µGal
r: regression coefficient in µGal/hPa.

In the model used by KLÜGEL (2003) the total volume around the considered station is divided into 225 rectangular piles each having a base of 14 * 14 km^2, thus covering the same area than the radiosonde model. Each pile consists of 35 layers reaching a total height of 23.6 km. The surface pressure is different at each grid point . The differences become larger with increasing distance.

The total attraction A(t) at the observation point (radiosonde station) is computed in this model by summing up all n contributions $A_n(t)$

$$A(t)_{LM} = \Sigma_n A_n(t). \quad (2)$$

The contributions $A_n(t)$ of the 225 piles to the total effect have similar $A_{cn}(t)$-components, but their $A_{pn}(t)$-contributions differ due to to the lateral variations of the surface pressure. Thus a difference emerges between the curve $A(t)_{LM}$ computed according to (2) and $A(t)_{radiosonde}$

$$A(t)_{LM} <> A(t)_{radiosonde}. \quad (3)$$

In order to determine the total attraction effect A(t) from $A_c(t)_{LM}$, which could better be compared to $Ac(t)_{radiosonde}$, it would have been necessary to compute the $A_{cn}(t)$ of the seasonal warming / cooling of the air masses from the partial attractions $A_n(t)$ and pressure functions $p_n(t)$ at each of the 225 grid locations

$$A_{cn}(t) = A_n(t) - A_{pn}(t) = A_n(t) - r_n * p_n(t). \quad (4)$$

From the sum of the attraction components

$$A_c(t)_{LM} = \Sigma_n A_{nc}(t) \quad (5)$$

the required attraction component $A_c(t)$ would follow. The attraction component $A_c(t)_{LM}$ is actually determined from the total attraction $A(t)_{LM}$ using the pressure curve p(t) from the observation point (radiosonde station)

$$A_c(t)_{LM} = A(t)_{LM} - r * p(t). \quad (6)$$

The annual wave thus obtained is too small. The quantitative consequences of the model difference on the attraction component $A_c(t)$ cannot be estimated yet. For verification extensive software modifications are necessary which are not realised up to now. The effects of other model differences on the computed air mass attraction could already be quantified. They partly explain the observed discrepancy between the two model approaches. The results of these studies are summarized in the following. The influence of the area extension and the neglection of the curvature of the earth in the model by Simon are not discussed here. A comprehensive discussion is given in the publications by SUN (1995) and SIMON (2003).

3. Additional sources for deviations

One additional verification is to check whether the same mean density values for the 35 air layers can be obtained using the same mean virtual temperatures from the meteorological model LM. The second question is whether these density values together with the model by Simon would yield different $A(t)_{LM}$ curves which are closer to the curves derived from radiosonde data.

3.1. Comparison of air density and latitude-dependent variation of earth acceleration

These test computations were carried out using LM data from one radiosonde station (Meiningen), for which already the air mass attraction A(t) and its components $A_c(t)$ and $A_p(t)$ had been calculated. At these stations also observed surface pressure data are available for comparison.

From the meteorological model the time series (6 h sampling rate) for the mean virtual temperature within all 35 air layers, the height of the layer boundaries and the pressure at the model surface can be obtained. The height of this surface typically deviates from the real earth's surface by some meters . At first the surface pressure curve for the real station height and the pressure variations for the 35 air layers were computed. In a second step the air density variations were calculated from these data using virtual temperatures.

For the computation of the air pressure at the boundary layers the actual gravity acceleration is required, which is a function of latitude and height. In the LM data based model the latitude-dependence of g was neglected and a constant average value for g has been used.

The consideration of this dependence of g leads to an increase in the peak-to-peak amplitude of the attraction effect A(t) and its two components $A_p(t)$ and $A_c(t)$ by 1-2% at maximum.

This increase results from air density differences of up to 11 g/m³, which esp. occur in layers with heights between 4000 and 10000 m. They correlate with mean reductions in the pressure magnitde at the upper and lower boundary of the layer. The mean air pressure e.g. diminishes by about 7 hPa in 5000-10000 m (Fig. 1).

Subtraction of the attraction component $A_p(t)=0.38$ [µGal/hPa]*p(t) [hPa] from the improved total attraction curve A(t) leads to the attraction component $A_c(t)$ caused by the seasonal warming / cooling of the air masses

$$A_c(t) = A(t) - A_p(t) = A(t) - r^*p(t). \quad (7)$$

The resulting $A_c(t)$-curve contains an annual wave with a peak-to-peak amplitude of about 2.4 µGal (Fig. 2). It is thus by a small amount larger than the one obtained from radiosonde data (1.8 µGal).

3.2. Effect of seasonal mass shifts in different heights

The LM and radiosonde data sets can be used to show how seasonal air density variations in certain heights contribute to the total effect. To investigate this an air mass package in a height of 23.6 km was divided into three parts. Each of these three volumes contributes about 1/3 to the total attraction effect A(t). The thicknesses of the volumes are 2997, 4867, and 15274 m. The corresponding air pressure coefficients are 0.18 µGal/hPa, 0.12 µGal/hPa, and 0.08 µGal/hPa. Thus it is ascertained to retrieve the coefficient of 0.38 µGal/hPa obtained for A(t)

$$A_c(t) = A(t) - 0.38^*p(t) = (A_l(t)+A_m(t)+A_u(t)) - (0.18+0.12+0.08) * p(t) \quad (8)$$

$A_l(t)$, $A_m(t)$, $A_u(t)$: contribution of the three layer packages to the total attraction effect

From Fig. 3 it becomes clear that during the summer months the air mass attraction increases in the 15 km thick upper layer. This increase compensates only partly the associated decrease

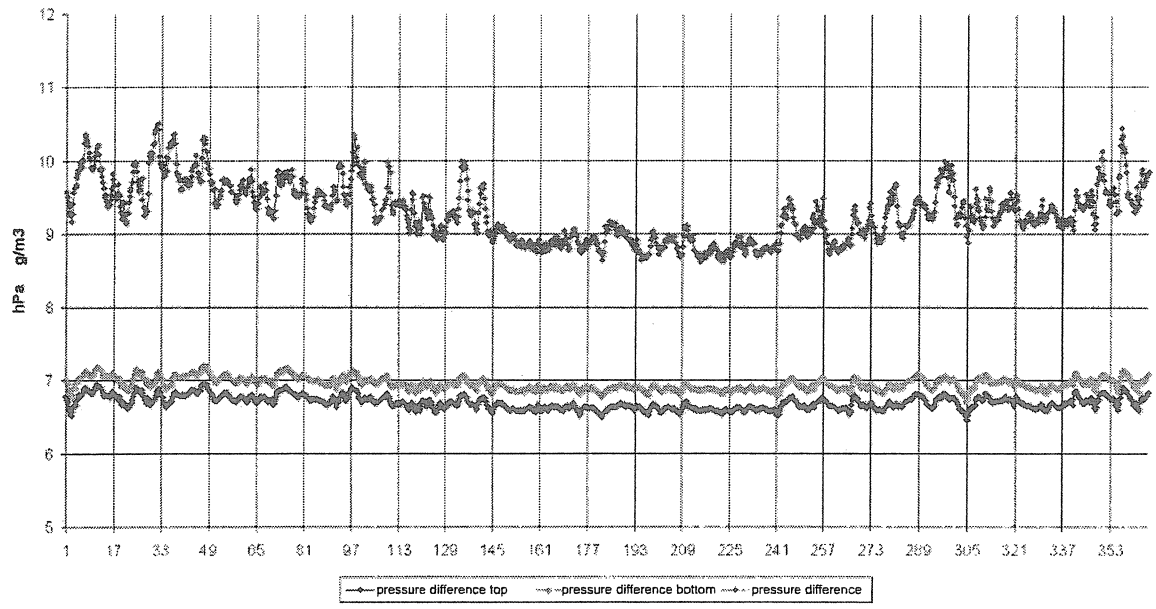

Fig. 1. Taking into account the latitude-dependence of g the mean air pressure reduces by 7 hPa and the mean air density by 13.8% in the layer 20 (5289 m- 5817 m), station Meiningen, year 2003.

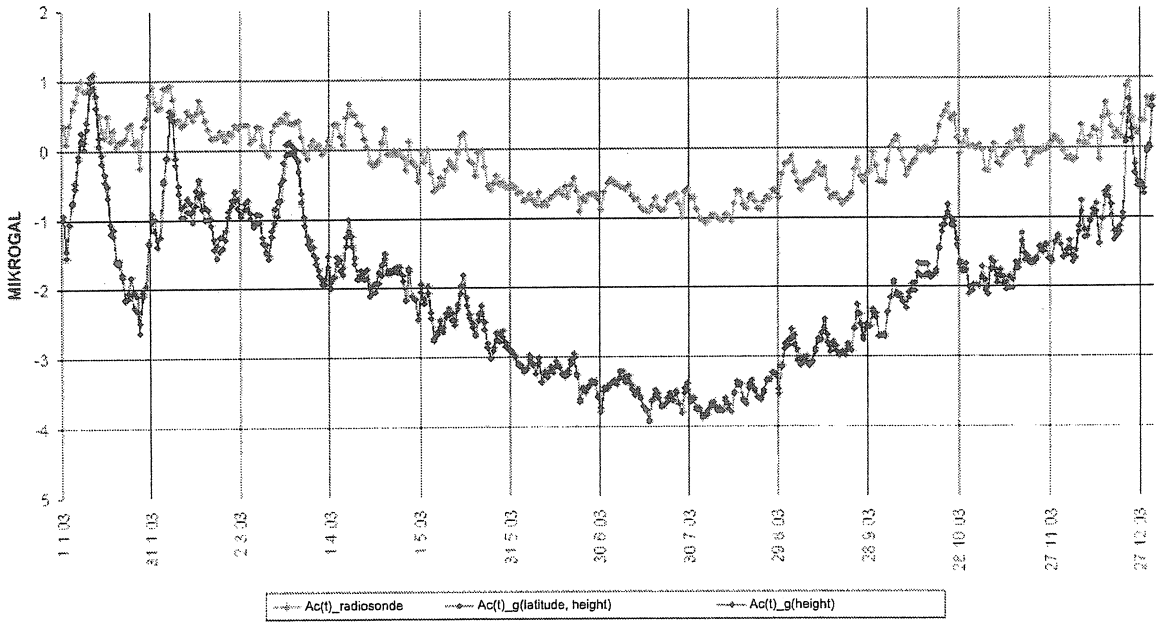

Fig. 2. Comparison of attraction component $A_c(t)$ derived from radiosonde and LM data, station Meiningen, year 2003.

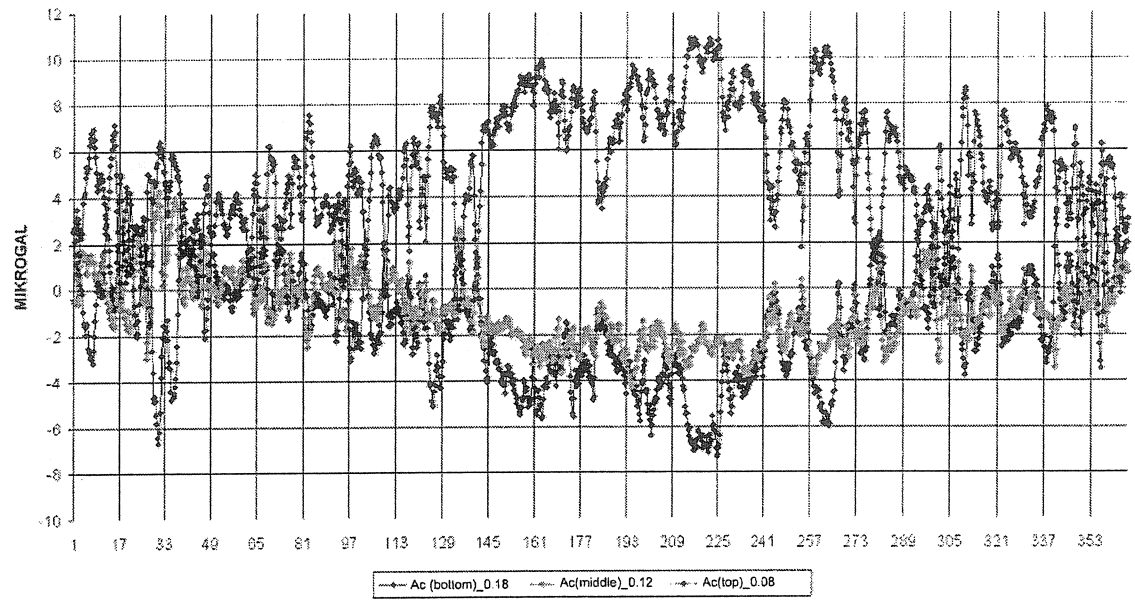

Fig. 3. Contribution of lower, middle, and upper air layer packages to the attraction component $A_c(t)$. The sum is given in Fig. 2 (lower curve); station Meiningen, year 2003.

in the lower and middle layers. This season-related decrease of the total attraction effect might be further reduced when considering an additional air mass package above 23.6 km in the modelling. In the radiosonde model the air mass cylinder is 7.4 km higher. NEUMEYER ET AL. (2004) even use data covering 50 air layers and reaching a height of 60 km.

3.3. Comparison with measured surface pressure

For a comparison of surface pressure variations computed from LM data for the true station height with observed surface pressure it should be considered that the computed curves might contain modelling errors.

In Fig. 4 the difference between modeled and observed surface pressure is shown for the radiosonde stations Meiningen and Munich. More or less regular deviations are visible. On the average the deviations are in the range of ±1 hPa. Larger differences in the order of 2-4 hPa and continuing over several time steps occur from time to time, but never at the same time at both stations.

3.4. Estimate of observation errors using modeled surface pressure curves

Differences between modeled and observed surface pressure curves could originate from modeling errors (see above), but can also be used to identify errors, drifts or additional influences in the barometer record. The pressure recordings at the gravimeter station Medicina are verified using data from the meteorological service which operates a meteorological station at the nearby radiosonde station. This way linear drifts of the pressure sensors at the gravimeter site could be determined (WOLF, pers. comm., 2003).

In Fig. 5 the differences between modelled and observed surface pressure variations are shown for the gravimeter stations Wettzell and Moxa. A deviation between observed and modelled values is clearly visible for Moxa observatory for one of the pressure records. The

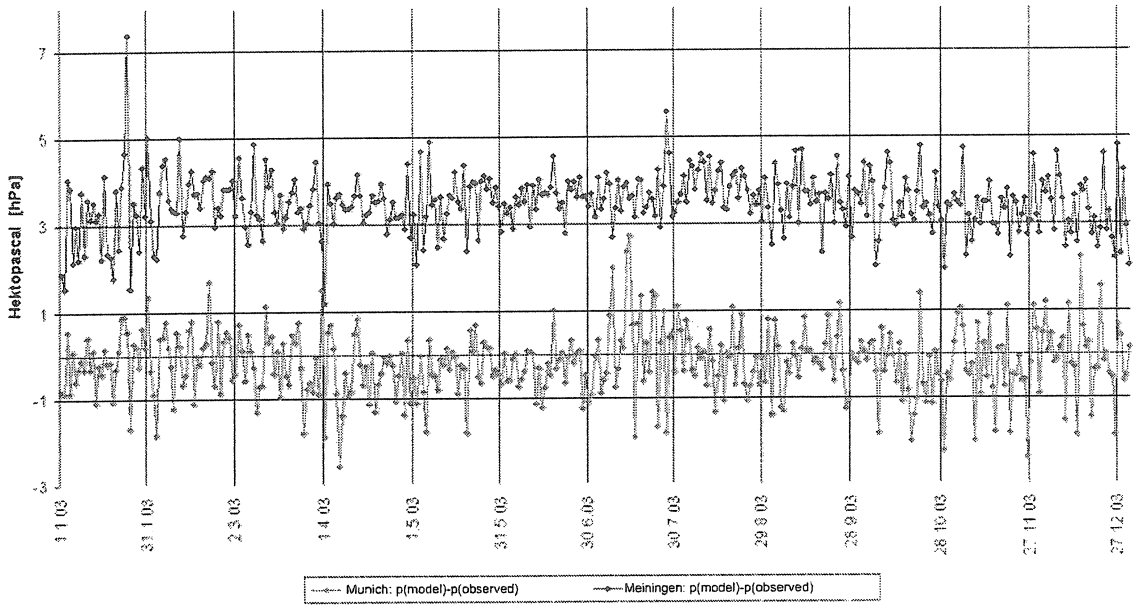

Fig. 4. Modelling errors of LM data-derived surface pressure variations, station Munich and Meiningen, year 2003. Deviations of more than 1 hPa do not occur at the same time at the two stations.

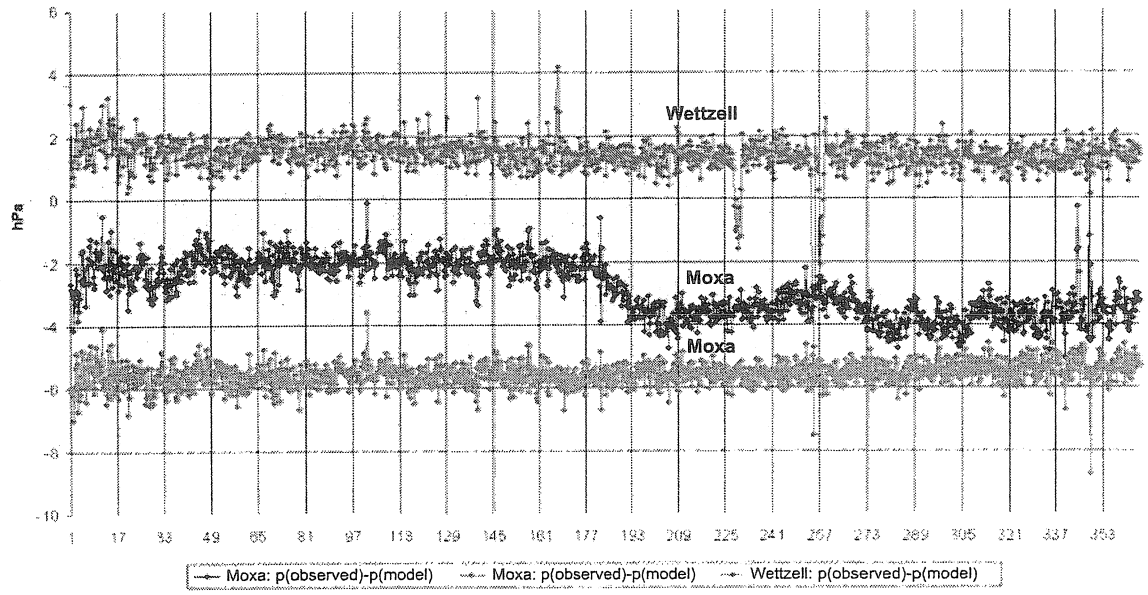

Fig. 5. Difference between modeled and observed surface pressure variations for stations Wettzell and Moxa, year 2003. For one of the records of Moxa observatory a clear deviation of the observed pressure changes from modelled ones can be seen.

second record shows no such discrepancy. On the other hand modelling errors can introduce artificial noise in the gravity residuals when using model data for air mass correction. When the $A_c(t)$-component is computed from (observed) radiosonde data, the resulting curves are smoother.

3.5. Modelling errors due to generalized topography

Another source for deviations between curves derived from LM and radiosonde data might be the generalized topography of the LM due to the model discretization. In present computations the lower boundary of the lowest air layer was on the average 12 m below true station height. This results in an additional air layer in the immediate vicinity of the gravimeter which is not present in reality. In the modelling with radiosonde data not only observed data enter, but the true station height is used.

4. Further factors of influence and consequences

Influence of the area size: As MERRIAM (1992) has pointed out firstly, about 90% of the total air pressure effect in gravity are due to pressure changes in a local zone with a radius of 0.5°. In the model computations discussed here a larger area is taken into account. The radius of 113 km used in this work corresponds to a cap with an angle of 1°.

Influence of earth's curvature: The air mass attraction was computed by SIMON (2003) for a ring model taking into account the curvature of the earth's surface. The differences between the attraction effect derived from the ring and the cylindrical model were neglegible.

Influence of the number of air layers used in the model and height of model cylinder: It is probably a reliable conjecture that the increase in the peak-to-peak amplitude of the annual wave from 1.8 µGal to 2.4 µGal is caused by a more appropriate capture of vertical mass shifts in the 35-layer model. In the computation based on the radiosonde data only 16 air layers enter. Apart from this the smaller height of the meteorological model could also be

a reason for the obtained discrepancies. Therefore comparative computations with global meteorological data as deployed by NEUMEYER ET AL. (2004) would be helpful. Here a maximum model height of 60 km with a larger number of air layers would be possible. Another possibility might be that the maximum height of 31 km in the computation with the radiosonde data is not sufficient for an appropriate precise computation of the $A_c(t)$-component.

Influence of the latitude-dependence of g and separation of $A_c(t)$-component: The influence of the latitude-dependence of g on A(t) and its components has been quantified. This dependence will be taken into account in future computations. The computation of $A_c(t)$ according to (4) and (5) needs still to be done. This requires some more extensive programming.

Assessment of the model comparisons: The authors think that the present model comparisons are necessary and have already yielded valuable information. The research is esp. important as long-term gravity changes become more and more of interest and smaller and smaller gravity signals are chased. The studies need to be continued and should include the model computations by Neumeyer and be done in close cooperation with him.

References

BOY, J.P, GEGOUT, P., AND HINDERER, J., 2002. Reduction of surace gravity from global atmospheric pressure loading. Geophys. J. Int., 149, 534-545.

KLÜGEL, Th., 2003. Bestimmung lokaler Einflüsse in den Zeitreihen inertialer Rotatiossensoren. Final report DFG-Forschungsprojekt LOK-ROT, BKG Frankfurt a.M., Fundamentalstation Wettzell, March 2003.

KRONER C., 1997. Reduktion von Luftdruckeffekten in zeitabhängigen Schwerebeobachtungen. Phd thesis, Institute of Geophysics, TU Clausthal.

KRONER, C. & JENTZSCH, G., 1999. Comparison of different barometric pressure reductions for gravity data and resulting consequences. Phys. Earth Planet. Int., 115, 205-218.

MERRIAM, J., 1992. Atmospheric pressure and gravity. Geophys. J. Int., 109, 488-500.

NEUMEYER J., HAGEDOORN J., LEITLOFF J., AND SCHMIDT T., 2004. Gravity reduction with three-dimensional atmospheric pressure data for precise ground gravity measurements. J. Geodynamics. 38, 437-450.

SIMON, D., 2002. Modelling of the field of gravity variations induced by the seasonal air mass warming during 1998- 2000. Bull. d'Inf. Marées Terr., 136, 10821-10836.

SIMON, D., 2003. Modelling of the gravimetric effects induced by vertical air shifts. Mitt. des BKG Frankfurt a. M., vol. 21.

SIMON, D., 2006. Gravimetric effects induced by vertical air mass shifts at Medicina (1998-2005), Wettzell, Bad Homburg, Moxa, Pecny and Wien (1998-2004), Bull. d'Inf. Marées Terr., this issue.

SMITHONIAN METEOROLOGICAL TABLES, 1951. 6 th Revised Edition. Published by the Smithonian Institution, Washington.

SUN, H.-P., 1995. Static deformation and gravity changes at the earth's surface due to atmospheric pressure. Phd thesis Cath. Uni. Louvain, Belgium.

SUN, H.-P., DUCARME, B., AND DEHANT, V., 1995: Correction of the atmospheric pressure on gravity measurements recorded by a superconducting gravimeter at Brussels. Proc. 12th Int. Symp. Earth Tides, Beijing, August 1993, Science Press, Beijing, 317-330

Hydrological Influences on the Gravity Variations Recorded at Bad Homburg

Günter Harnisch *, Martina Harnisch *, Reinhard Falk **
* formerly Bundesamt für Kartographie und Geodäsie (BKG)
** Bundesamt für Kartographie und Geodäsie (BKG)
Richard-Strauss-Allee 11, D-60598 Frankfurt am Main

Summary

The gravimetric observatory in the cellar of the Bad Homburg castle was established more than 25 years ago. In 1999 the double-sphere superconducting gravimeter GWR CD030 was installed and has been recording up to the present. Three ground water gauges at distances of between 200 m and 3.5 km show a clear correlation between the variations in the ground water level and the recorded gravity data in the long-term (annual) range. The comparison with the observed gravity variations was based on the "corrected minute data" (repair code 02), stored in the GGP data-bank. A regression coefficient of about 50 nm s^{-2}/m results from the amplitudes of the annual wave in the residual gravity (about 19 nm s^{-2}) and that of the ground water variations at the Meiereiberg gauge (about 37 cm). - In the daily and weekly range the correlation is less clear. It seems that during late winter and spring strong precipitation events are clearly reflected in the ground water level while in autumn no precipitational influences are to be recognized.

1. Introduction

With increasing accuracy of the gravimetric measuring techniques the correct consideration of hydrological influences has become increasingly important. At first the gravity effect of the varying soil moisture was assumed to be a limiting threshold of the accuracy achievable in gravimetric measurements (Bonatz, 1967). Later in special studies aimed at the detection of the small gravity variations resulting from weak tectonic processes the attempt was made to consider the disturbing hydrological influences by corrections derived directly from the measured soil moisture and the ground water level in the neighborhood of the measuring site (e.g. Elstner, 1987; Elstner et al., 1993). The interest in the consideration of hydrological influences again increased when the first superconducting gravimeters came into practical use (e.g. Peter et al., 1995; Harnisch and Harnisch, 1995). Meantime the estimation of corrections for the influence of precipitation and ground water variations is an essential part of detailed studies of different gravity effects, especially. in the long-term range (e.g. Lambert and Beaumont, 1977; Harnisch and Harnisch, 2002; Harnisch and Harnisch, 2006; Kroner, 2002; Llubes et al., 2004).

In contrast to the consideration of the local air pressure variations no standard procedure is available for the correction of the different hydrological influences. The reason is that generally the hydrologic conditions are very complicated and differ from site to site. To model the particular situation in detail and to estimate the varying density distribution beneath the surface a multitude of parameters and continuously measured data series would be needed (precipitation, topography of the ground water level and its variation with time, soil moisture, temperature, evolution of the plant cover, topography of the different soil layers, density and porosity within the layers, position of faults and clefts in the bedrock, etc.), which in practice cannot be provided completely and in time. Therefore statistical regression techniques are preferred, which relate the gravity effect to be eliminated with hydrological data (precipitation, ground water level, soil moisture) measured near the site of the gravity observations.

At Bad Homburg ground water data became available in the beginning of 2004. The surprisingly strong variations of the ground water level near the gravimetric laboratory (Schlosskirche gauge) and their correlation with the recorded gravity variations showed that in future, even at this very stable station hydrological influences on the gravity measurements have to be taken into account.

2. The gravimetric laboratory in the Bad Homburg castle

Bad Homburg is a town on the south eastern slope of the Taunus Mountains in the vicinity of Frankfurt a.M. The official addendum "v.d.Höhe" (= "before the heights") hints at the near Taunus Mountains. In the centre of the town on a local elevation is the castle with the White Tower, the oldest part of the castle from the 14th century. The other parts of the castle date from the 17th century, among them the Archive Wing (1679 – 1686), the southwestern part of the castle buildings.

The gravimetric laboratory in the basement of the Bad Homburg castle was built in 1978 in an old apple cellar in the Archive Wing. It was developed as a testing site for the BKG (formerly Institute for Applied Geodesy, IfAG). Nowadays there are two isolated huts with pillars for absolute gravimeters and for permanently recording superconducting gravimeters. Beginning with the TT40, one of the first superconducting gravimeters in practical operation, several other superconducting gravimeters, manufactured by GWR Instruments, San Diego, USA, have been operated or have been tested before continuous operation elsewhere (TT60, SG103, RG038, CD030). Also many calibration experiments have been carried out in the Bad Homburg castle with the moving platform as well (Richter, B. et al., 1995) as with comparison of superconducting and absolute gravimeters (Harnisch, G. et al., 2002). This laboratory has been used for more than 15 years as a reference site for the absolute gravity measurements within Germany and Europe (Wilmes and Falk, 2006).

3. The Gravity Data

At the end of 1999, the dual sphere superconducting gravimeter GWR CD030 was installed in the gravimetric laboratory. During the first year of operation the data series is distorted by several calibration activities of various kinds. Since that time the gravimeter has produced reliable data available in the GGP-ISDC (minute data; corrected minute data, rep. code 02; corrected minute data, rep. code 22; station log file). All data series begin with the February 9, 2001. In the present study the residual gravity has been derived from the corrected minute data, repair code 02 (i.e. corrected by P. Wolf, BKG).

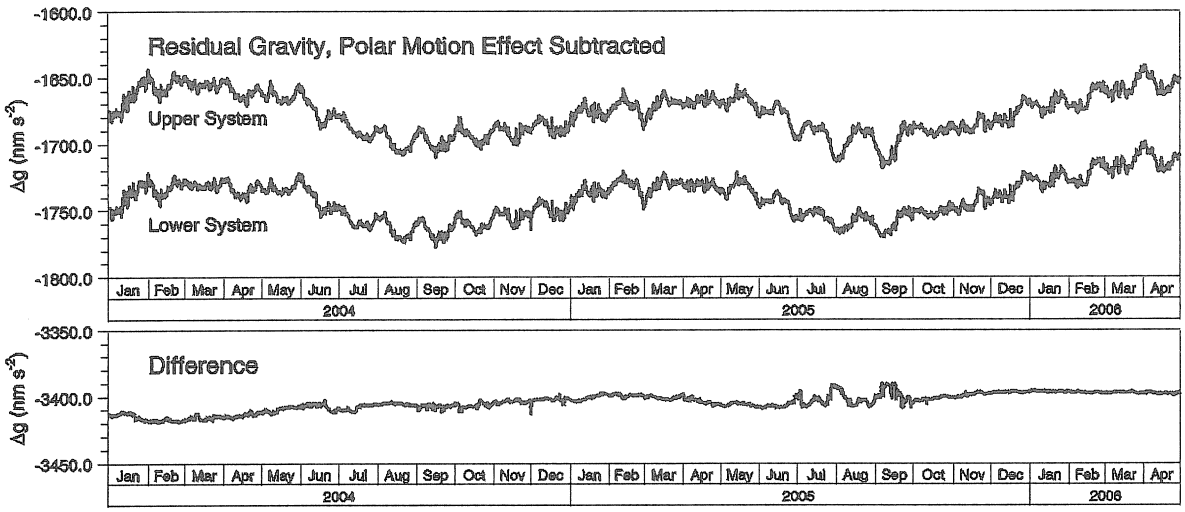

Fig. 1: GWR CD030, Bad Homburg, January 1, 2004 – April 30, 2006: **Upper frame:** Residual gravity of both systems of the gravimeter. Tidal model, gravity effect of the local air pressure and theoretical gravity effect of the polar motion subtracted. **Lower frame:** Difference of the residuals of both systems of the gravimeter.

The general problem of the use of gravity residuals is the preservation of the influences to be studied as completely as possible while all other known disturbing influences have to be eliminated. To this aim the tidal model was derived by a usual tidal analysis (ETERNA 3.30) including several long-term waves up to the annual wave Sa and the local air pressure. A second additional channel was used for the consideration of the theoretical gravity effect of the polar motion (IERS data, δ = 1.16). This way the parameters of the long-term tidal waves (e.g. Sa and Ssa) should be minimally influenced by the local air pressure and the polar motion. Nevertheless the parameters of Sa resulting from this tidal analysis are unrealistic. Obviously the annual tidal wave is affected by non-tidal influences with amplitudes und phases significantly different from those of Sa. Therefore the parameters of Sa are replaced by the "theoretical" values δ = 1.16 and the κ = 0.0. If this modified tidal model, the influence of the local air pressure (on the basis of the air pressure regression coefficient resulting from the actual tidal

analysis) and the theoretical gravity effect of the polar motion are subtracted from the observed gravity variations, an annual wave results with an amplitude of the order of 20 nm s^{-2} and with a maximum late in the winter. Generally this wave has to be interpreted as some non-tidal gravity effect in the annual range. In our special case it should be caused by the hydrological influences in question.

The data recorded by the two measuring systems of the double sphere gravimeter GWR CD030 are treated as the data of two independent gravimeters. In the upper frame, Fig. 1 shows the residual gravity of both systems of the gravimeter CD030, derived in the described way. The remaining gravity residuals look very similar in both systems. The instrumental drift is very small and therefore has not been eliminated. The difference between the residuals of both systems shows no systematic tendencies (Fig. 1, lower frame). Only noise and some disturbances due to icing problems in the year 2005 are visible.

4. Influence of the Castle Pond

The pond in the nearby landscape garden has a surface area of 11000 m^2 and a maximum depth of 1 m. The horizontal distance between the middle of the pond and the gravimetric laboratory is about 110 m. In the vertical direction the bottom of the pond is 15.3 m beneath the surface of the pillars in the gravimetric laboratory. Every two or three years the pond is emptied for repair or cleaning purposes. A rough estimation (approximation of the water volume in the pond by rectangular prisms) results in a maximum influence of about 8 nm s^{-2} if the pond has been totally emptied (Falk, 1995).

Concerning the absolute gravity measurements in the Bad Homburg castle the individual disturbing events resulting from the variations of the water level in the castle pond may be neglected. On the other hand gravity variations of the order of 8 nm s^{-2} should be detectable in the recordings of the superconducting gravimeter, at least from the theoretical point of view. However, in practice there is no chance because the weak "pond signal" changes very slowly. It extends over several months with a steep beginning (when the pond is emptied) and a moderate decrease (refilling of the pond). Moreover no exact notes are available which could enable a stacking of different events to separate them from the surrounding noise.

5. The hydrological situation around the Bad Homburg castle

The local hydrological influences are essentially determined by the grouping of the different buildings of the castle. Above the gravimetric laboratory there is the solidly built Archive Wing. Its large roof and the gutters let the precipitation immediately run off and this way the infiltration of water into the ground near the gravimeter is hindered. Similarly the strong sealing of the soil surface acts in the castle area. For all these reasons the precipitation near the gravimetric laboratory cannot contribute to the formation of ground water and therefore clear precipitation signals are to be expected neither in the ground water residuals nor in the gravity.

In order to understand the occurrence of ground water around Bad Homburg the catchment area has to be taken into account. In this context the hillside position of Bad Homburg also plays an important role. The ground water is formed in higher regions of the Taunus Mountains and flows down towards the plain of the Main River. On its way the water is dammed by the castle hill. There it can pass neither upward (due to impermeable layers above the aquifer) nor laterally; and therefore the pressure in the aquifer grows. This is the typical behavior of a confined aquifer. In consequence, at the Schlosskirche gauge (about 110 m northeast of the gravimetric laboratory) variations of the pressure in the borehole are to be observed which have no influence on the observed gravity variations. In this way the position of the mean ground-water level at the Schlosskirche gauge about 8 m above the level of the Meiereiberg gauge may also be explained. Heavy rainfall in the catchment area causes frequent and strong variations of the pressure in the Schlosskirche gauge. During the vegetation period evapotranspiration reduces the formation of ground water.

In the nearby valley of the Heuchelbach covering layers are nearly totally missing above the aquifer. Therefore the Meiereiberg gauge which was drilled there (about 200 m south of the gravimetric laboratory) should react to local precipitation more clearly than the Schlosskirche gauge. Nevertheless the local formation of ground water is minimal and therefore it causes only a moderate rise of the ground water level.

6. Influence of precipitation

Since 1998, daily weather data (precipitation, maximum and minimum temperature) have been noted in the castle gardener's house (distance to the gravimetric laboratory about 130 m). The precipitation is measured with a simple glass gauge, read every day in the early morning (about 6:30 a.m.).

A second measuring site at a distance of 1.35 km to the southwest of the gravimetric laboratory was installed by the municipality of Bad Homburg. It is equipped with an automatically recording precipitation gauge. The precipitation data recorded at the municipal station should be very reliable. Unfortunately the data series begins only on May 10, 2005.

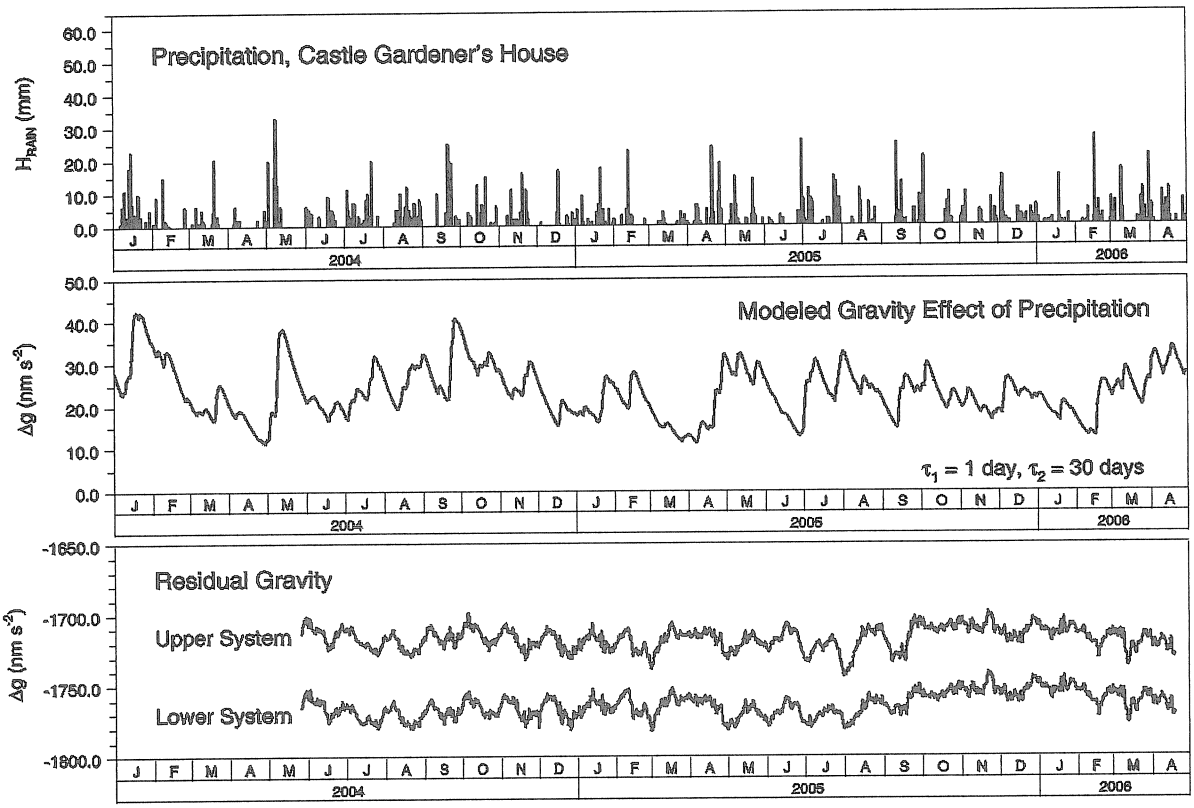

Fig. 2: Bad Homburg, precipitation at the castle gardener's house. **Upper frame:** Daily sums of precipitation. **Middle frame:** Modeled gravity effect, resulting from the exponential model (Crossley et al., 1998) with τ_1 = 1 day and τ_2 = 30 days. **Lower frame:** Residual gravity of both systems of the gravimeter GWR CD030, corrected for the influence of ground water (Meiereiberg gauge, conversion factors 51.7 nm s^{-2}/m and 49.8 nm s^{-2}/m for upper and lower system, respectively.).

In a first step the discrete rain volumes recorded by the rain gauges are transformed to a continuous data series. For this purpose the exponential model proposed by Crossley et al. (1998) was used. Two time constants describe the infiltration of water into the ground ("recharge time constant" τ_1) and the following gradual dry out ("discharge time constant" τ_2). In the present study of hydrological influences at Bad Homburg τ_1 = 1 day and τ_2 = 30 days were chosen, keeping in mind, that the basic assumptions for the exponential model are not fulfilled (homogeneous half-space, unsealed flat surface) and therefore the use of this model can be only a very formal step. However, the "modeled gravity effect of precipitation" has the great advantage that in computations it can be better handled than the discrete data coming directly from the rain gauges. If the precipitation (daily sums or modeled gravity effect) is compared with the recorded gravity variations no significant influence of the precipitation can be recognized (Fig. 2).

7. Ground water

Ground water data are available from the three gauges Schlosskirche, Meiereiberg and Seulberg. Some information on these gauges is summarized in Tab.1. The variation in the ground water level at these gauges is plotted in Fig. 3. The very similar behavior of the ground water variations at the three gauges is surprising. However, the amplitudes are different. The strongest variations occur at the Schlosskirche gauge. But these are first of all variations of the pressure in the confined aquifer as it has been discussed already in section 5.

From the Seulberg gauge (about 3.5 km northeast to the Bad Homburg castle) only weekly values are available. Nevertheless the general tendency in the ground water variations is very similar to that at the other two gauges. An advantage of the Seulberg gauge is the length of the data series, which goes back to 1951 and among other things it covers the TT40 data series recorded 1981 – 1984 at Bad Homburg.

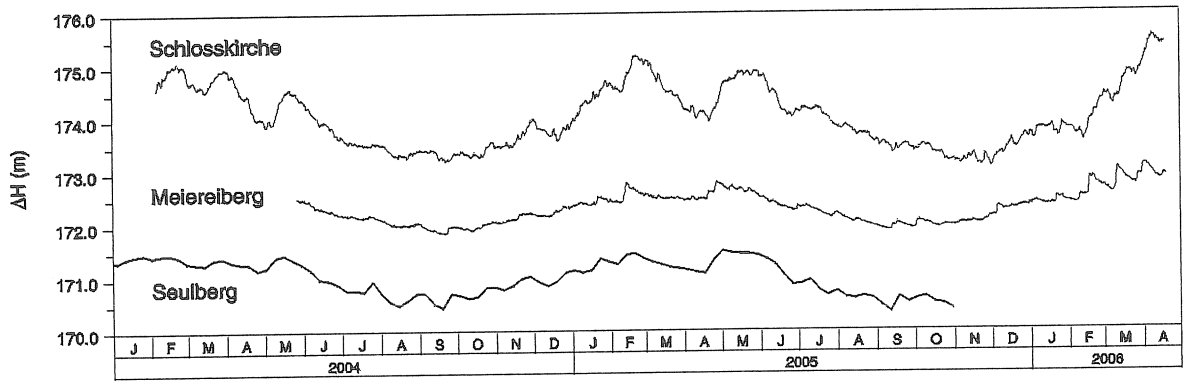

Fig. 3: Groundwater variations at the gauges Schlosskirche (Offset -5.5 m), Meiereiberg (Offset +0.7 m) and Seulberg (Offset -0.5 m)

Tab.1: The ground water gauges Schlosskirche, Meiereiberg, Seulberg

	Schlosskirche	Meiereiberg	Seulberg
Height of the terrain	191.94 m	174.1 m	174.31 m
Mean ground water level	179.49 m	171.57 m	171.80 m
Distance to the gravimetric laboratory	110 m	200 m	3.5 km
Range of the ground water variations (peak-to-peak amplitude of an annual wave)	(1.38 ± 0.64) m	(0.75 ± 0.21) m	(0.66 ± 0.41) m
Sensor	SEBA Dipper II	SEBA Dipper II	Manual sounding
Sampling rate	1 hour	1 hour	1 week
Begin of the dataset	February 5, 2004	May 26, 2004	April 9, 1951

At first glance the influence of precipitation on the ground water gauges Schlosskirche and Meiereiberg seems to be inconsistent (Fig. 4). Some significant anomalies in the ground water which obviously are caused by strong precipitation are marked by double arrows. All these events occur in the first half of the year. This may be explained by the growth of vegetation in summer and the early autumn. From section 5 we know that vegetation reduces the infiltration of precipitation into the ground. However, the two gauges have to be considered differently. While the anomalies at the Schlosskirche gauge are caused mainly by precipitation in the extended catchment area and increased by the pressure in the confined aquifer, the anomalies at the Meiereiberg gauge also include local influences.

The gravity residuals remaining after the tidal model, the influence of the local air pressure and the influence of the polar motion have been eliminated show long-term undulations like annual waves (Fig. 1, upper frame, Fig. 5, uppermost curves in both frames). The amplitudes are (19.33 ± 0.08) nm s^{-2} (upper system) and (18.59 ± 0.06) nm s^{-2} (lower system). A brief visual comparison with the similar behavior of the ground water makes it seem probable that the variations in the gravity residuals are caused by the influences of the ground water. The amplitudes of the annual wave in the ground water level are (0.69 ± 0.32) m (Schlosskirche gauge) and (0.37 ± 0.11) m (Meiereiberg gauge). If ratios of the correspondent amplitudes are formed, conversion factors ("regression coefficients") result of the order of 28 nm s^{-2}/m (Schlosskirche gauge) and 50 nm s^{-2}/m (Meiereiberg gauge). Detailed values are given in Tab. 2. Corrections based on these conversion factors clearly diminish the undulations in the gravity residuals (Fig. 5, middle and lower curves in both frames). Especially if the data of the Meiereiberg gauge are used, the influence of ground water variations seems to be totally eliminated.

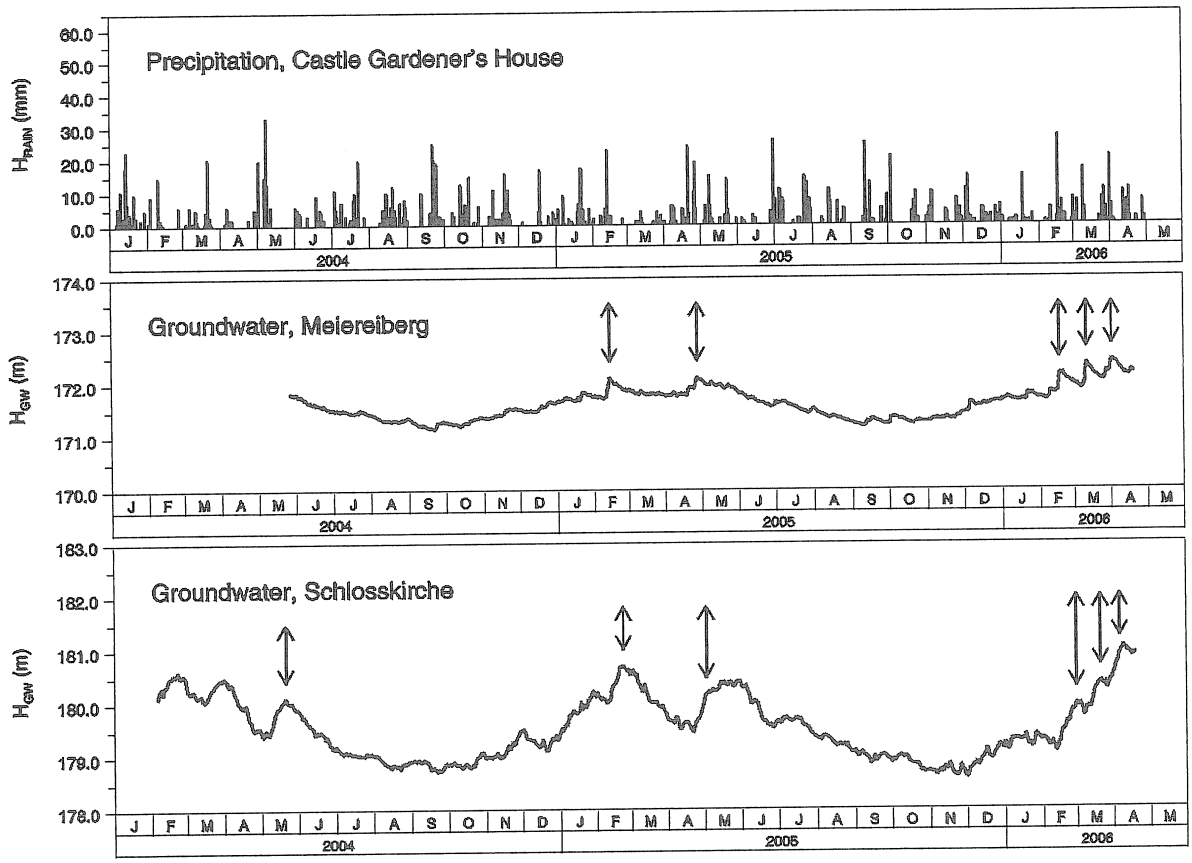

Fig. 4: Influence of precipitation on the ground water gauges Schlosskirche and Meiereiberg. **Upper frame:** Daily total precipitation. **Middle frame:** Ground water variations at the Meiereiberg gauge. **Lower frame:** Ground water variations at the Schlosskirche gauge. The double arrows mark times at which clear influences of precipitation on the ground water gauges may be recognized.

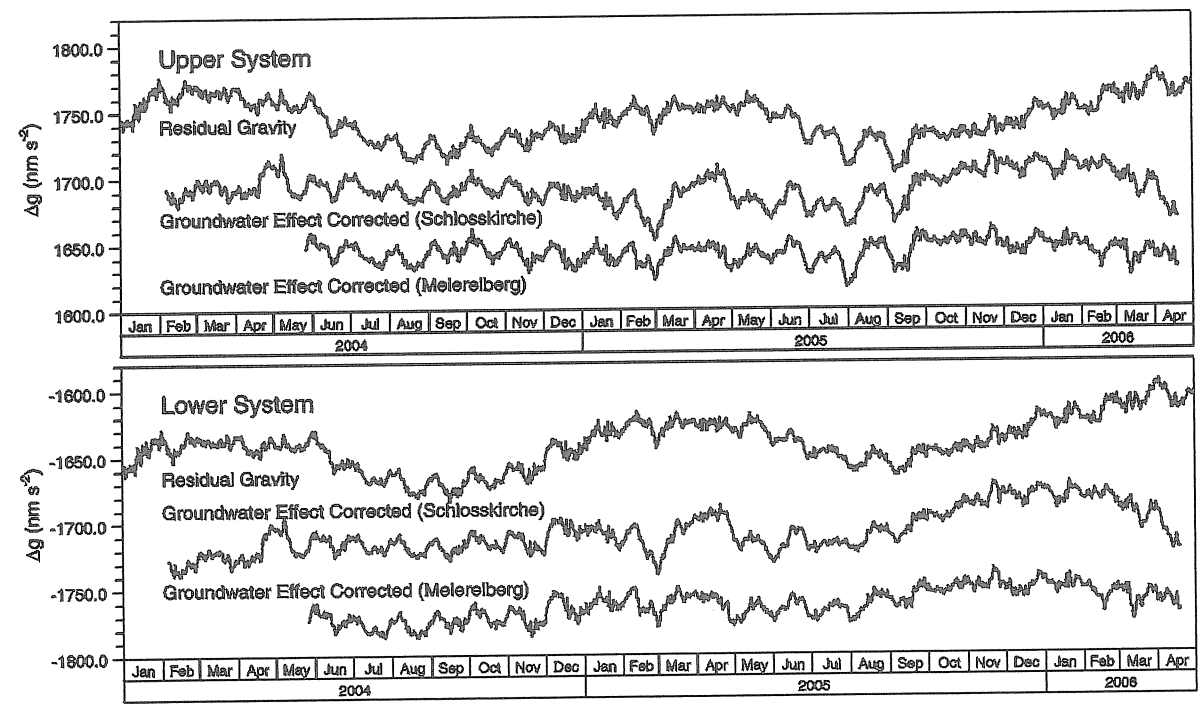

Fig. 5: GWR CD030, January 1, 2004 – April 30, 2006. Residual gravity. Air pressure influence and gravity effect of the polar motion subtracted. Ground water corrections based on the Schlosskirche gauge as well as the Meiereiberg gauge. **Upper frame:** Upper system. **Lower frame:** Lower system.

Tab. 2: Influence of ground water variations on gravity measurements at the Bad Homburg castle. Conversion factors ("Regression coefficients").

GWR CD030	Ground water gauges	
	Schlosskirche	Meiereiberg
Upper system	28.0 nm s^{-2}/m	51.7 nm s^{-2}/m
Lower system	26.9 nm s^{-2}/m	49.8 nm s^{-2}/m

8. Possible other explanations for the observed gravity variations

Generally the interpretation of gravity variations in the annual range is problematic. Many processes in nature recur at nearly annual periods but not necessarily with the same or a similar phase (e.g. variations of the temperature throughout the year, rainfall and snow, seasonal development of the plant cover, foliation and defoliation of the trees). In the rating of the tidal model resulting from the tidal analysis of the recorded gravity data the strongly deviating δ- and κ-values of the annual wave were rejected and replaced by the theoretical values $\delta = 1.16$ and $\kappa = 0$. Therefore it may be asked whether the annual wave in the gravity residuals is a real one and whether it is possible to explain this wave by hydrological influences. We consider two alternative explanations: Gravity variations induced by the three-dimensional redistribution of air masses and seasonal motions of the earth's surface, detected by GPS observations.

8.1. Three-dimensional anomalies of the air density

Usually the distribution of the air density in the atmosphere is assumed to be in agreement with the model of the standard atmosphere. On this basis the gravity variations caused by variations of the air density may be derived from the local air pressure alone. Simon (2003) studied the influence of discrepancies between the standard atmosphere and the real density distribution in the atmosphere derived from data of radiosondes. As a very important result he found out that after the air pressure corrections based on the local air pressure have been applied there remains a seasonal gravity variation with an amplitude (peak to peak) of the order of 10 nm s^{-2}, slightly different from station to station (about 6 nm s^{-2} at Miami and 16 nm s^{-2} at Ny Ålesund).

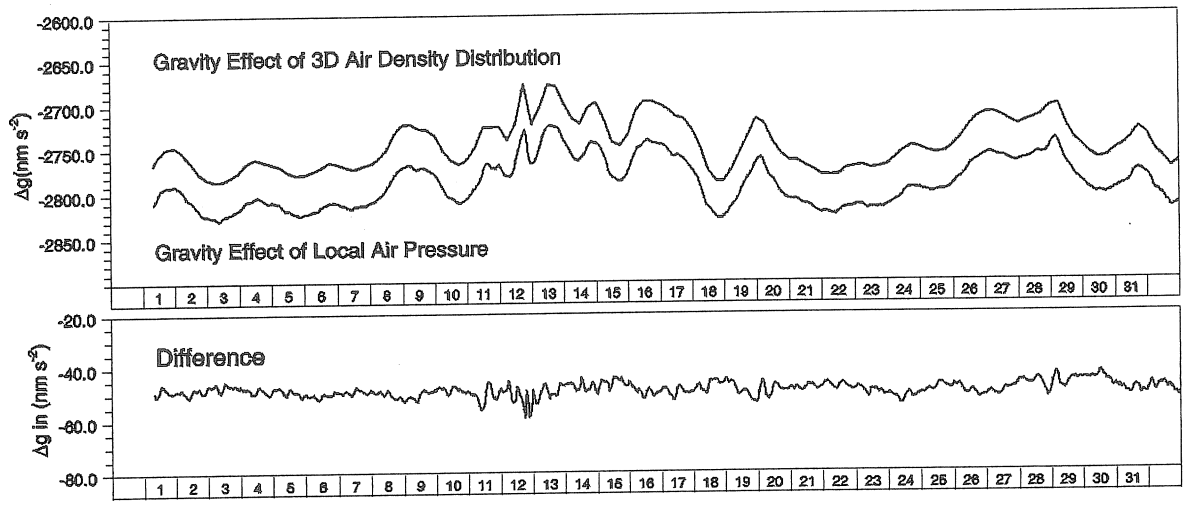

Fig. 6: Gravity effect of density anomalies in the atmosphere, January 1 – 31, 2005. **Upper frame:** Comparison of the estimates based on the local air pressure and on the 3D-model. **Lower frame:** Difference of the two models.

On the basis of three-dimensional air density data from the European Centre for Medium-Range Weather Forecasts (ECMWF) Neumeyer (2004) calculated the total gravity effect of the atmosphere (attraction term as well as elastic deformation of the earth's surface due to the atmospheric loading) at selected stations. The ECMWF data are referred on a grid with meshes of $\Delta\varphi$ and $\Delta\lambda = 0.5°$ and in vertical direction on 60 pressure levels up to a height of 60 km; the spacing in time is 6 hours. The 3D-model includes the model developed by Simon completely, based on vertical anomalies of the air density alone; the different origin of the air pressure data used by both the authors is unimportant.

The 3D-model also includes the gravity effect of the local air pressure. Therefore the correction of air density anomalies has to be based on the 3D-model alone. In practice that means that the 3D-model has to be subtracted from the measured gravity data before they are analyzed and no air pressure channel has to be introduced into the tidal analysis as it is done usually.

For a monthly period the estimates based on the local air pressure and the 3D-model are compared in Fig. 6. As may be seen from the lower frame the difference between both estimates varies more or less randomly and remains below about 10 nm s^{-2}.

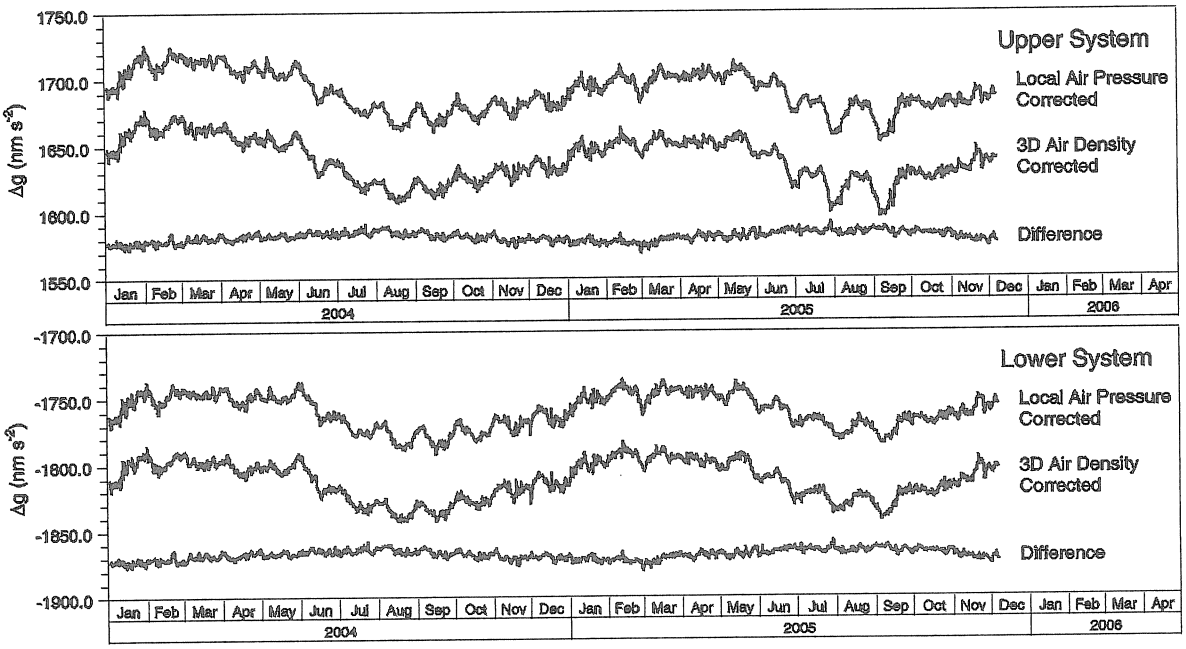

Fig. 7: GWR CD030, January 1, 2004 – December 7, 2005. Residual gravity. Air pressure influence and gravity effect of the polar motion subtracted. Consideration of air density variations based as well on the local air pressure (upper curve) as also the 3D-model (middle curve). Difference of he two estimates (lower curve). **Upper frame:** Upper system. **Lower frame:** Lower system.

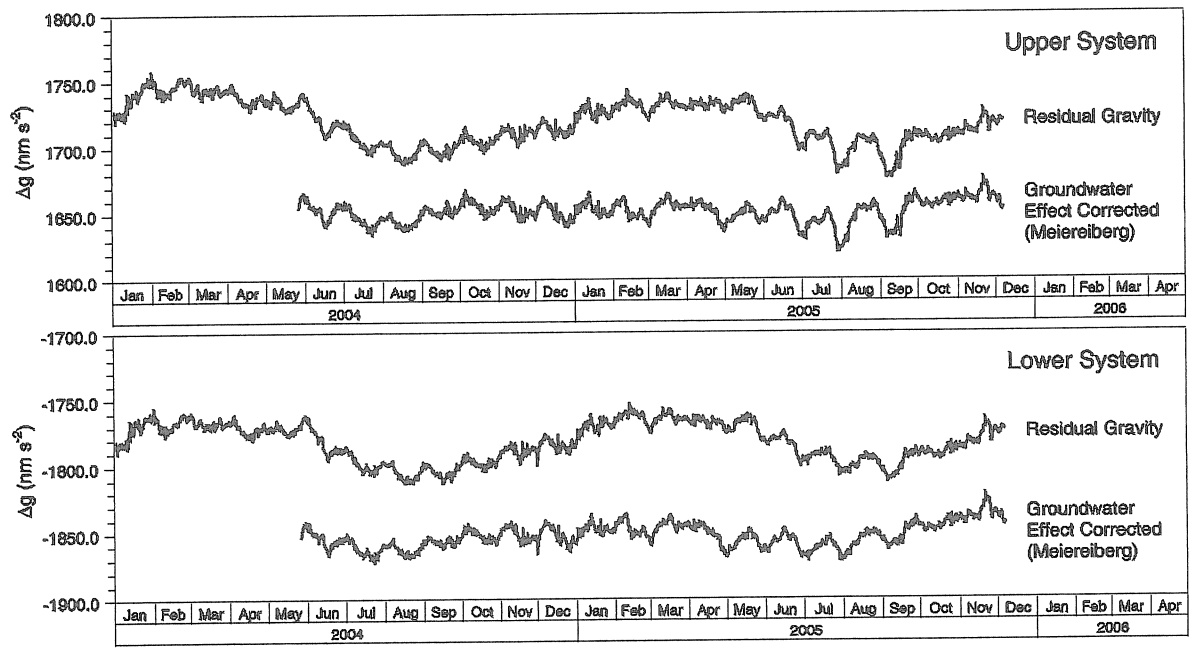

Fig. 8: GWR CD030, January 1, 2004 – December 7, 2005. Residual gravity. Air pressure influence and gravity effect of the polar motion subtracted. Air density correction based on the 3D-model. Ground water correction based on the Meiereiberg gauge. **Upper frame:** Upper system. **Lower frame:** Lower system.

If the gravity residuals are compared resulting from both estimates of the air pressure influence the slight seasonal variation of the order of 10 nm s^{-2} becomes visible (Fig. 7), also described by Simon (2003). Moreover it is very important that the plots of the gravity residuals (Fig. 8) are very similar to the correspondent plots based on the local air pressure correction (Fig. 5), i.e. also the consideration of the spatial distribution of the air density (3D-model), cannot explain the annual wave remaining after the polar motion influence has been subtracted from the standard residuals.

If the gravity residuals based on the 3D-model are compared with the variations of the ground water level in the Meiereiberg gauge regression coefficients of 44.6 nm s^{-2}/m (lower system) and 63.6 nm s^{-2}/m (upper system) result which are very similar to those derived in section 7 from the gravity residuals based on the local air pressure correction (49.8 nm s^{-2}/m respectively 52.9 nm s^{-2}/m).

8.2. GPS Observations at the Bad Homburg castle

At the beginning of 2005, a GPS antenna was installed on the Bad Homburg castle. It is mounted on a brick wall at a height of about 20 m. The distance to the gravimetric laboratory is about 70 m. The first year of observations shows a slight undulation in the daily values of the vertical component (Fig. 9, upper frame). For comparison, in the middle frame the daily means of the air temperature at the Frankfurt a.M. airport have been recorded and in the lower frame the gravity residuals of both systems of the gravimeter GWR CD030 are plotted. Obviously the motion of the earth's surface derived from the GPS data is in opposite phase to the variations of the gravity residuals of both systems of the gravimeter. This would mean that the gravity changes could be totally or partly explained by the local uplift and subsidence of the earth's surface.

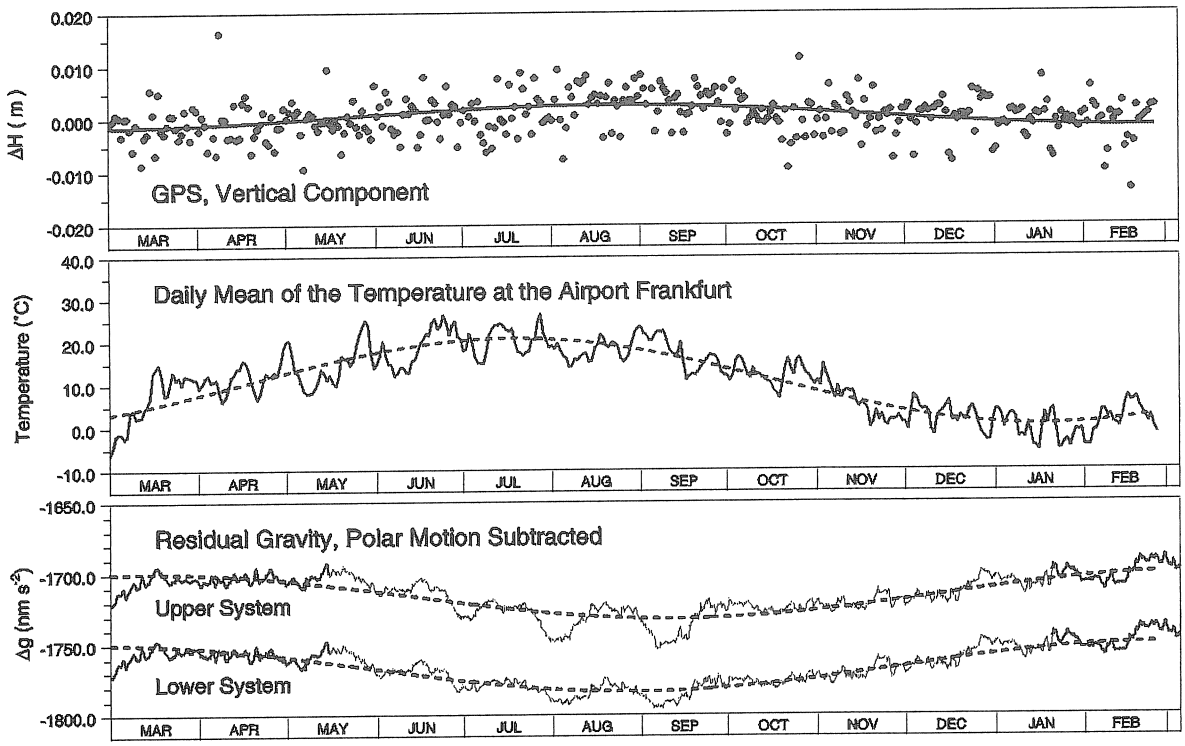

Fig. 9: GPS, Bad Homburg castle, March 1, 2005 – February 23, 2006. **Upper frame:** Vertical displacement of the GPS antenna. **Middle frame:** Daily mean temperature at the airport Frankfurt a.M. **Lower frame:** Gravity residuals of both systems of the gravimeter GWR CD030. Solid and dotted lines: annual waves with the amplitudes 2.1 mm (GPS, vertical component), 10.2 K (Mean daily temperature), 16.3 nm s^{-2} (Residual gravity, upper system) and 16.8 nm s^{-2} (Residual gravity, lower system).

For a more detailed examination of the mutual dependences, sinusoidal functions with annual period were fitted to the data series. The resulting amplitudes are (2.1 ± 0.4) mm for the vertical component of the GPS data and (16.8 ± 0.1) nm s^{-2} respectively and (16.3 ± 0.1) nm s^{-2} for the lower and the upper system of the gravimeter GWR CD030. If the free air gravity gradient of 3 nm s^{-2}/mm is used, the annual wave in the GPS data could explain annual gravity variations with amplitudes of 6.2 nm s^{-2}. That is only about 37 % of the observed annual variation of the gravity residuals. Due to a smaller vertical gradient the true effect of the vertical motions should be less than this value.

Up to now in the present discussion the GPS data have been assumed to describe real motions of the earth's surface around the GPS antenna. However, the variations can also be explained otherwise, e.g. by thermal expansion of the masonry. To this aim in the middle frame of Fig. 9 the mean daily temperatures at the airport Frankfurt a.M. (about 20 km to the south of Bad Homburg) are shown together with a sinusoidal function fitted to these data. The amplitude of this annual wave is (10.2 ± 0.3) K. If a coefficient of $5 \cdot 10^{-6}$/K is assumed, the thermal expansion of the masonry could explain annual variations of the GPS antenna with amplitudes of 1.0 mm, i.e. about 50 % of the observed motion. In view of the phase shift obviously existing between the temperature variations and the vertical motion of the GPS antenna (see Fig. 9) it is very questionable whether a significant influence of the temperature really exists.

In summary, it can be stated that the vertical motions detected by the GPS observations may influence the gravity measurement, but they cannot explain the main part of the annual wave in the gravity residuals.

9. The TT40-Series, recorded 1981 – 1984 at the Bad Homburg castle.

In the well known TT40-series recorded 1981 – 1984 at the Bad Homburg castle the gravity effect of the polar motion clearly could be detected (Richter, 1987). Now it is possible to correct retrospectively also this data series for hydrological influences. In the upper frame of Fig. 10 the variations in the ground water level at the Seulberg gauge are shown and in the lower frame from top to bottom the results of three main steps of the data processing:

- Gravity residuals, corrected for the instrumental drift (by subtraction of a polynomial of second degree)
- Polar motion influence eliminated (IERS data, $\delta = 1.16$)
- Ground water influence eliminated (regression coefficient 31.2 nm s^{-2}/m)

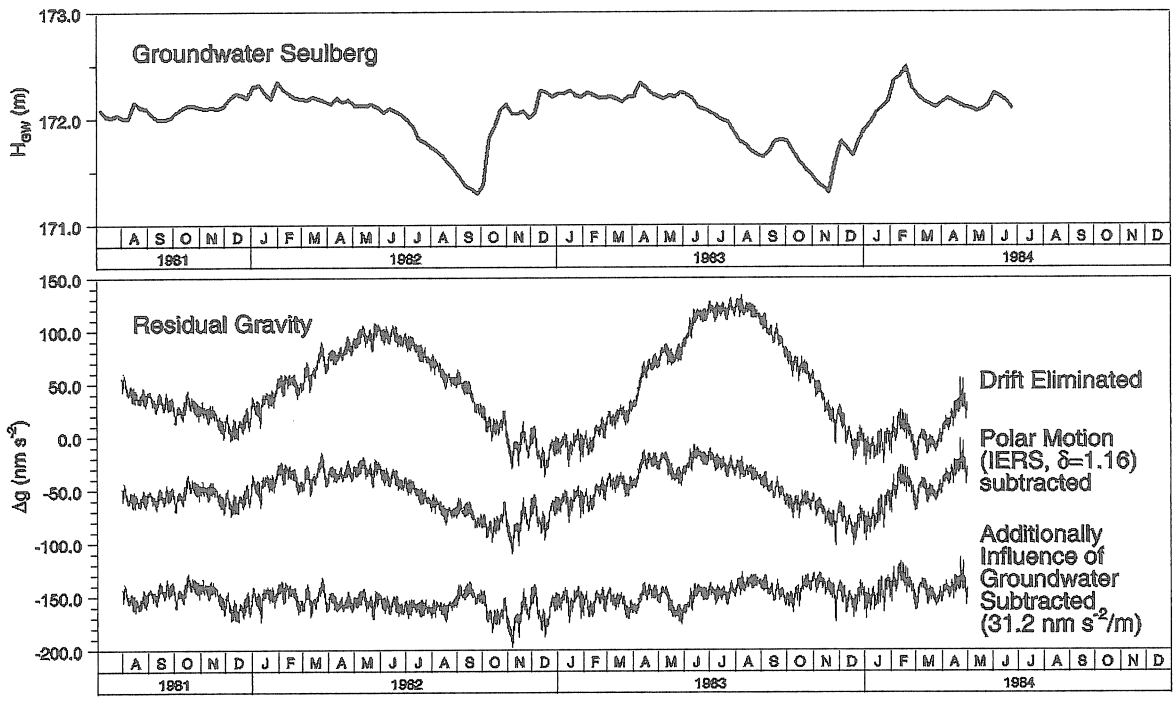

Fig. 10: Influence of ground water corrections on the TT40 data series, recorded 1981 – 1984 at the Bad Homburg castle. **Upper frame:** Ground water level at the Seulberg gauge. **Lower frame:** Effect of the ground water correction on the gravity residuals.

The ground water regression coefficient was derived from the comparison of the ground water variations in the Seulberg gauge with the gravity residuals of the TT40 during the period 1981 - 1984. The shape of the middle curve in the lower frame of Fig. 10 is caused mainly by the ground water influence. After this influence has also been eliminated the gravity residuals take the expected straightened shape (lower curve in the lower frame).

Results, Conclusions

- The study presented here is the first such attempt with the gravity data recorded by the gravimeter GWR CD030 at Bad Homburg.
- The recorded gravity data are significantly disturbed by hydrological influences.
- The gravity residuals remaining after the tidal model, the influence of the local air pressure and the gravity effect of the polar motion have been subtracted may be approximated by an annual wave with an amplitude of about 20 nm s^{-2}. Obviously this wave is caused by hydrological influences.
- From comparisons with the ground water gauges conversion factors ("regression coefficients") of the order of 50 nm s^{-2}/m (Meiereiberg gauge) and 28 nm s^{-2}/m (Schlosskirche gauge) result. Most effective are corrections derived from data of the Meiereiberg gauge.
- Other influences or effects (consideration of the 3D air density distribution; displacements of the earth's surface detected by GPS) cannot explain the annual wave in the gravity residuals alternatively, at least not completely.
- The studies concerned with hydrological influences on gravity measurements at Bad Homburg should be continued.

Acknowledgements

The authors thank

- **Peter Wolf** (BKG Frankfurt a.M.), who painstakingly provided maintenance to the gravimeter, preprocessed the data and stored them into the GGP-ISDC,
- **Dr. Walter Lenz** (Büro Hydrogeologie und Umwelt GmbH, Giessen), who provided valuable information on the hydrologic regime in the region of Bad Homburg,
- the **Hessisches Landesamt für Umwelt und Geologie**, Landesgrundwasserdienst, which made the 50 years of ground water data from the Seulberg gauge available,
- the castle gardener **Peter Vornholt**, who made available his notes on precipitation in the vicinity of the Bad Homburg castle,
- **Dr. Jürgen Neumeyer** (GFZ Potsdam), who calculated the 3D air density model for the station Bad Homburg and made it available for this study,
- **Peter Franke** (BKG Frankfurt a.M.), who processed and made the GPS-data from the station „Bad Homburg, Castle" available.

References

Bonatz, M., 1967. Der Gravitationseinfluss der Bodenfeuchte. ZfV 92, pp. 135-139.

Crossley, D. J., S. Xu , van Dam, T., 1998. Comprehensive Analysis of 2 years of SG Data from Table Mountain, Colorado. Proc. 13th Int. Symp. Earth Tides, Brussels, July 1997. Obs. Royal Belgique, Brussels, pp. 659 – 668.

Elstner, C., 1987. On common tendencies in repeated absolute and relative gravity measurements in the central part of the G.D.R. Gerlands Beitr. Geophysik, **96**, pp. 197-205.

Elstner, Cl., Falk, R. Harnisch, G., Becker, M., 1993. Results and Comparisons of repeated precise gravity measurements on the gravimetric West-East-line. Proc. 7th Intern. Symp. "Geodesy and Physics of the Earth", Potsdam, Oct. 5 - 10, 1992. IAG Symposia, Nr. 102, Springer-Verlag Berlin Heidelberg New York, pp. 176 – 180.

Falk, R., 1995. Abschätzung einer möglichen Beeinflussung des Schwerewertes des Absolutpunktes in Bad Homburg auf Grund von Wasserstandsschwankungen des Schloßteiches. [Potsdam], 10.5.1995, unpublished.

Harnisch, M., Harnisch, G., 1995. Processing of the data from two superconducting gravimeters, recorded in 1990 - 1991 at Richmond (Miami, Florida). Some problems and results. Marées Terrestres, Bull. Inf., Bruxelles **122**, pp. 9141 – 9147.

Harnisch, M., Harnisch, G., Falk, R., 2002. Improved Scale Factors of the BKG Superconducting Gravimeters, Derived from Comparisons with Absolute Gravity Measurements. Marées Terrestres, Bull. Inf., Bruxelles **135**, pp. 10627-10638

Harnisch, M., Harnisch, G., 2002. Seasonal Variations of Hydrological Influences on Gravity Measurements at Wettzell. Marées Terrestres, Bull. Inf., Bruxelles **137**, pp. 10849 – 10861.

Harnisch, G., Harnisch, M., 2006. Hydrological influences in long gravimetric data series. J. Geodynam., **41**, pp. 276 - 287.

Kroner, C., 2002. Zeitliche Variationen des Erdschwerefeldes und ihre Beobachtung mit einem supraleitenden Gravimeter im Geodynamischen Observatorium Moxa, Habilitationsschrift, Chemisch-Geowissenschaftliche Fakultät, FSU Jena, 149 p.

Lambert, A., Beaumont, C., 1977. Nano variations in gravity due to seasonal groundwater movements; implications for the gravitational detection of tectonic movements. J. Geophys. Res., **82**, pp. 297 – 305.

Llubes, M., Florsch, N., Hinderer, J., Longuevergne, L., Amalvict, M., 2004. Local hydrology, the Global Geodynamics Project and CHAMP/GRACE perspective: some case studies. J. Geodynam., **38**, no. 3-5, pp. 355 - 374.

Neumeyer, J., Hagedoorn, J., Leitloff, J., Schmidt, T., 2004. Gravity reduction with three-dimensional atmospheric pressure data for precise ground gravity measurements. J. Geodynamics, **38**, pp. 437 – 450.

Peter, G., Klopping, F., Berstis, K.A., 1995. Observing and modeling gravity changes caused by soil moisture and groundwater table variations with superconducting gravimeters in Richmond, Florida, U.S.A. Cahiers du Centre Européen de Géodynamique et de Séismologie, Luxembourg **11**, pp. 147 – 159.

Richter, B., 1987. Das Supraleitende Gravimeter. Anwendung, Eichung und Überlegungen zur Weiterentwicklung. Dt. Geodät. Kommiss., C 329, 126 p.

Richter, B., Wilmes, H., Nowak, I., 1995. The Frankfurt calibration system for relative gravimeters. Metrologia, **32**, pp. 217-223

Simon, D., 2003. Modelling of the gravimetric effects induced by vertical air mass shifts. Mitt. Bundesamt Kartogr. Geodäsie, 21, 100 + XXXII p.

Wilmes, H., Falk, R., 2006. Bad Homburg - a regional comparison site for absolute gravity meters. Cahiers du Centre Européen de Géodynamique et de Séismologie, Luxembourg, **26**, pp. 29 - 30.

Long and short term hydrological effects on gravity in Vienna

Bruno Meurers[1)]

[1)] Institute of Meteorology and Geophysics, University of Vienna, UZA II, Althanstrasse 14, A–1090 Wien, Austria. bruno.meurers@univie.ac.at

Abstract

Some typical hydrological effects (precipitation, groundwater) observed in the gravity time series of the superconducting gravimeter (SG) Vienna are analyzed in detail. The contribution focuses on short-term meteorological events (heavy rain) associated with rapid gravity drops and on long-term hydrological loading effects. In contrast to precipitation data in high temporal resolution, unfortunately no groundwater table and soil moisture observations are available at the station. Groundwater table variations observed at distant wells are anti-correlated to the long term (seasonal) gravity signal although the aquifer is below the SG sensor. Newtonian water loading effects of different origin like rain, groundwater table fluctuations or snow cover are estimated using high resolution terrain models. The area in very close vicinity of the station (<100 m) turns out to play the dominating role. The gravitational effect of water level variations of the nearby Danube River is estimated to be less than 3 nms^{-2}.

Introduction

Geodynamical gravity signals are affected by surface mass variations due to atmospheric processes and redistribution of the atmosphere's water content by precipitation, evapotranspiration and water flow. Surface mass changes and associated elastic loading cause long-term but also short-term (< 1 h) gravity signals of several 10 nms^{-2}. In order to separate geodynamical signals it is necessary to understand the effect of these environmental processes. Recent studies (e.g. Kroner 2001, Harnisch and Harnisch, 2002, Boy and Hinderer 2006, Kroner and Jahr 2006, Van Camp et al. 2006) underline the importance of acquiring and evaluating additional environmental parameters like soil moisture, precipitation, groundwater and continental water storage. A ten years' time series of high resolution gravity and air pressure data is available obtained by the superconducting gravimeter (SG) GWR C025 which has been operating since August 1995 in the seismic laboratory of the Central Institute of Meteorology and Geodynamics (ZAMG) in Vienna (Austria). Investigating long-term gravity effects is difficult at this station because of two reasons:

- High station noise hampers sufficiently accurate instrumental drift determination by absolute gravimeter observations.
- No groundwater table or soil moisture sensor is available in close vicinity of the SG.

This paper tries to clarify which environmental signals can be expected in Vienna and estimates the effects taking the topographic conditions into account. Previous investigations have clearly demonstrated that in case of rainfall the area in close vicinity of the station plays the dominating role (Meurers 2000, Meurers et al. 2006).

Hydrological and topographic situation

The SG in Vienna is installed in the base floor of a large building. The underground consists of late Tertiary Vienna basin sediments. The uppermost soil is characterized by interbedded strata of sand, silt and gravel. Several drillings within the building area detected a water-

bearing formation about 14 m below ground. A well exists close to the SG site for extracting industrial water. Its actual water table corresponds to the findings of the subsoil examination. The SG sensor is located about 8-9 m below ground i.e. rain and increasing soil moisture are expected to generate a gravity decrease while raising groundwater table should cause gravity increase. Water load modeling is very sensitive to the topography and to the local station geometry. It is important to consider impermeable areas like buildings or sealed surface from where water is drained immediately. Additionally, within the building area soil moisture does not contribute to gravity variations either (Fig. 1). The building is located on a gentle topography slope. The surface close to the station is well above the SG. However, this does not hold for the distant terrain. Therefore the gravity effect of mass distributed above and below the station partly compensates each other (Fig. 2).

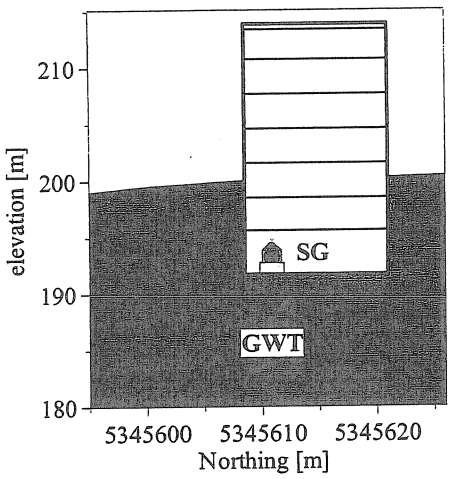

Fig. 1: Location of the SG sensor on the base floor of the ZAMG building, about 8 m below topography surface, GWT: Groundwater table.

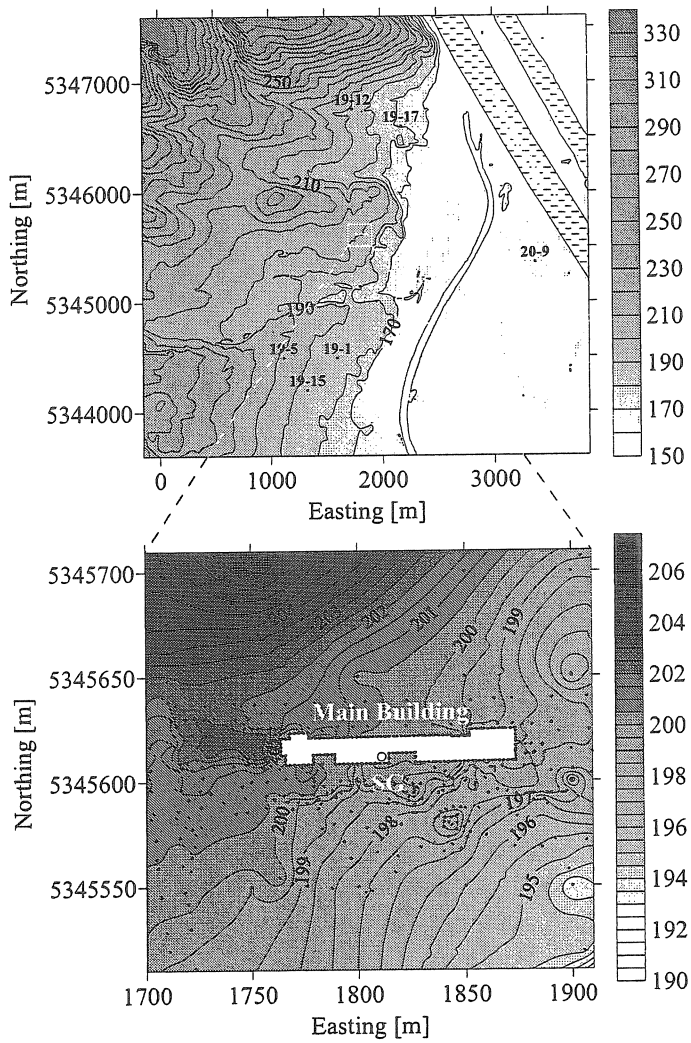

Fig. 2: Topography within the vicinity of the SG station. Black dots indicate the location of selected groundwater measuring points from where groundwater table data is available. Note the different contour interval [m] in the lower panel where black dots represent the DTM data. The blanked area represents the building where no water is stored in the soil. SG sensor elevation: 192 m.

Long- and short-term rain effects

Precipitation data in high temporal resolution show that even small rain events are immediately imaged by corresponding gravity signals. The dominance of the local contribution permits to apply simple rainfall admittance in order to correct for the rain effect routinely (Meurers et al. 2006). Fig. 3 demonstrates that only the close vicinity contributes to the gravity effect due to the specific topography. The gravity drop during rain events can often be explained by the water mass load, but in numerous cases the Newtonian effect of vertical air mass redistribution (vertical density variation without air pressure change) plays also an

essential role (Meurers 2000). Fig. 4 shows one typical example where the model reflects the cumulative rainfall effect correctly but indicates additional atmospheric effects at the beginning. In Vienna the model fits 50% of all rain events perfectly. However, even in most of the other cases the water load model is able to explain the dominating part of the residual drop especially when heavy rain fall is involved.

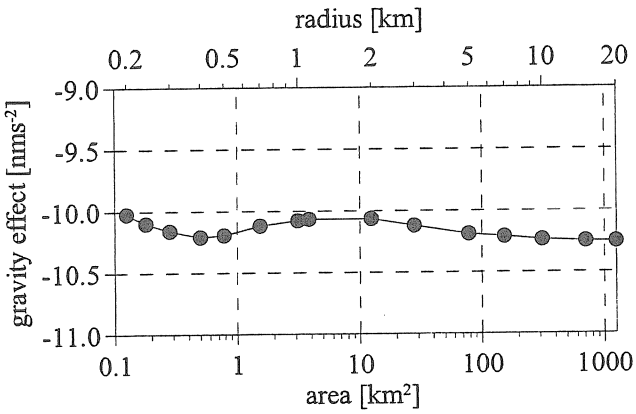

Fig. 3: Gravitational effect of a circular water layer (thickness 40 mm) spread on topography and centered at the SG sensor position for different radii. The gravity effect does not much vary with the extension of the contributing mass load due to compensation effects of distant layer parts.

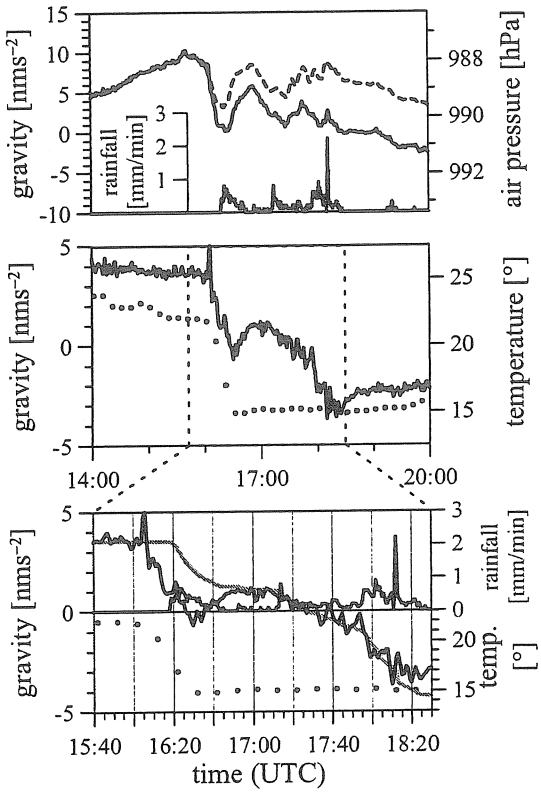

Fig. 4: Gravity variations caused by heavy rain and meteorological processes. Vienna, 2000 05 18.
Top: air pressure (dashed), tide free gravity measurements (black) and rainfall samples (black).
Middle: gravity (black) corrected for the air pressure effect [admittance factor: −3.53 nms^{-2}/hPa]. Air temperature (dots).
Bottom: exaggerated section of the middle panel, water load effect (grey), 1 min rainfall samples (black). The model reflects the cumulative rainfall effect correctly but indicates additional atmospheric effects at the beginning.

The rain admittance concept does not consider water flow due to run-off and evapotranspiration. Therefore rain water load *rwl* has been defined according to eq. (1) by considering a discharge process similar as proposed by Crossley et al. (1998):

$$(1)\quad rwl(t) = \sum_{j=-\infty}^{0} r(t + j\,\delta t)\frac{1}{2}\left(e^{j\,\delta t/\alpha} + e^{j\,\delta t/\beta}\right)$$

t is the time and δt = 1 min the sampling interval of the rainfall r. The discharge parameters α accounts for fast run-off after the rain fall event and β for much slower evapotranspiration.

They have to be tuned in such a way, that rain related gravity signals are minimized. Fig. 5 shows examples for three selected heavy rain events.

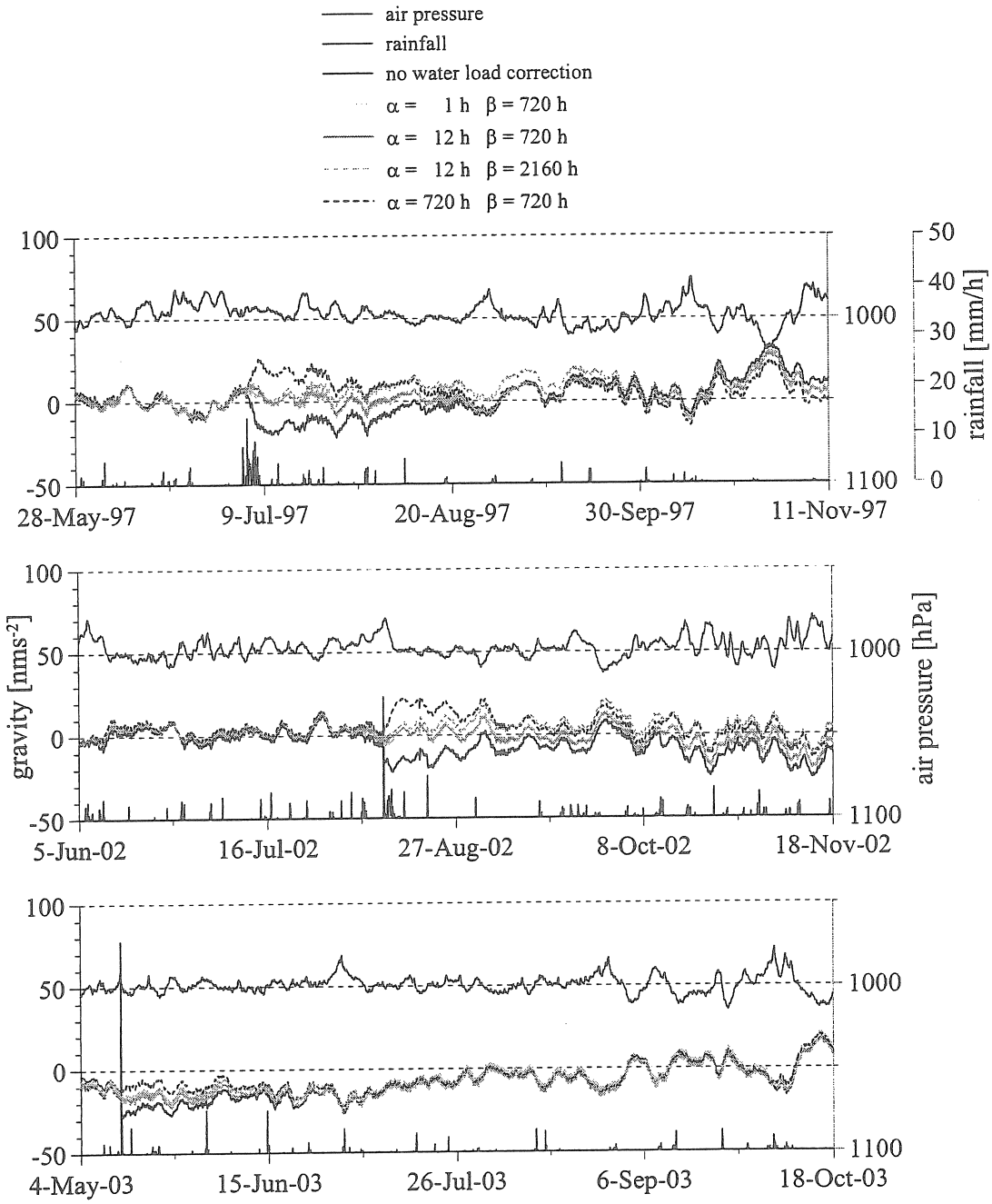

Fig. 5: Influence of the discharge parameters on gravity. Drift free gravity after subtracting the air pressure effect [admittance factor: -3.53 nms^{-2}/hPa] is displayed as dashed line (no water load correction) or different grey tones (water load correction assuming different discharge parameters). Air pressure and hourly rainfall are shown additionally. The best result is obtained for $\alpha = 12$ h and $\beta = 720$ h or even much slower discharge ($\beta = 2160$ h).

There is a link between soil moisture and the slow discharge process. Rain water is the most important supplier for soil moisture. That part of rain, which does not run off at the surface or evaporate immediately, invades the soil from where it is removed later by water flow and evapotranspiration.

Groundwater table variations

No groundwater information is available at the SG site. However, several measuring points of the municipal office of hydraulic engineering can be used to investigate trends and seasonal variations. Groundwater data is sampled there once a week in average. The wells utilized in this study are marked in Fig. 2 and Fig. 6. Because they are scattered over the entire area of Vienna they certainly do not represent a common aquifer. Besides, those stations located in the lowland near the Danube River (21-1, 22-212) are influenced by activities of the hydroelectric power plant South of Vienna. Others may be affected by industrial water extraction as well. Nevertheless, clear common seasonal features and trends are visible in the groundwater table data of all wells (Fig. 6).

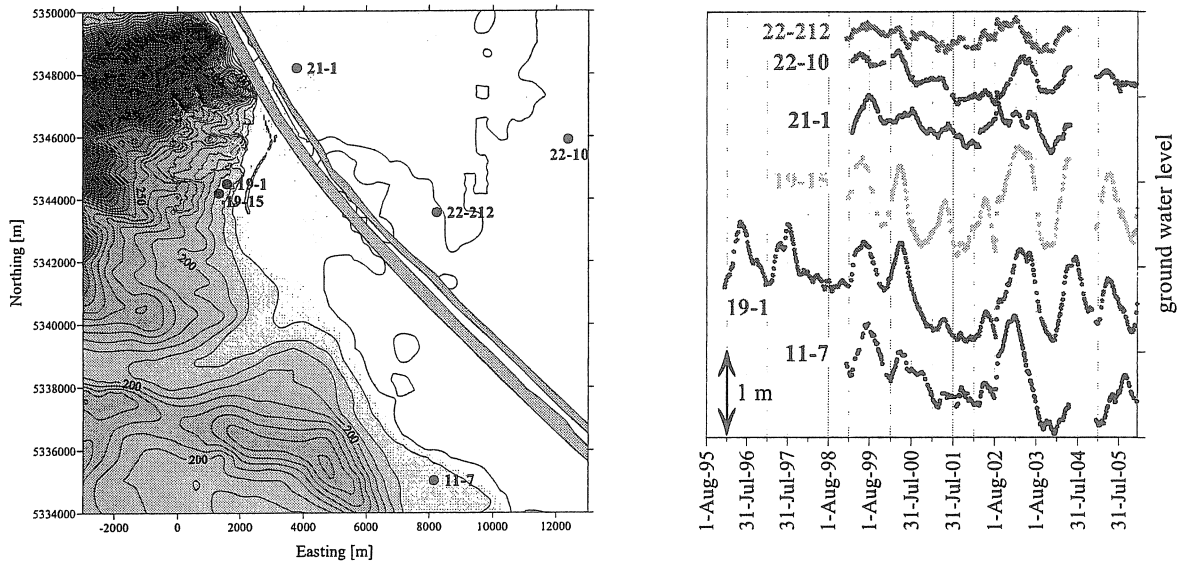

Fig. 6: Elevation map of Vienna (left) and groundwater table variations (right) observed at selected wells (marked as dots in the map).

Fig. 7 compares the drift-free gravity with the groundwater table data of well 19-1 that is located next to the SG (both smoothed by applying a running mean procedure).

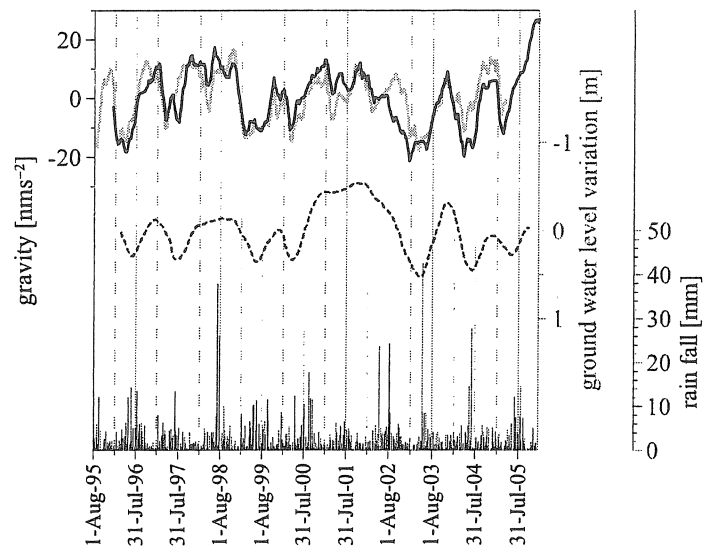

Fig. 7: Smoothed gravity (black) and groundwater table variations (dashed) at well 19-1. Rainfall is displayed too. The grey line indicates gravity after rain water load correction by applying the rain admittance and discharge model (α = 12 h, β = 2160 h)

Surprisingly gravity and groundwater table are anti-correlated although the SG sensor is located above the aquifer. There are different explanations:

- Either there is no groundwater table variation at the SG site or the effect is overcompensated by soil moisture or other sources. However, applying the discharge model and different discharge parameters does not essentially change the seasonal gravity fluctuations. Contrarily, this correction seems to enhance the pattern of low gravity in late winter and high gravity in late summer or autumn (Fig. 7, grey line). This favors an alternate interpretation, that
- gravity reflects long-term effects caused by continental water storage (e.g. elastic deformation) that correlate with local groundwater table variations. Of course, this has still to be verified by calculating the load contributions.

In order to check the pure Newtonian effect of water load 3D modeling has been performed assuming the aquifer being located below and alternatively above the SG sensor in spite of the fact that the latter contradicts what we presently know about the groundwater table at the SG site.

A water layer of constant thickness (1 m, porosity of 10%) and at constant depth below the ground represents the aquifer. As in case of rain effect calculations, a polyhedral surface defined by Delaunay triangulation (e.g. Renka 1996) of the irregularly scattered terrain model data approximates the upper and lower layer boundary. The digital terrain model (DTM) consists of different data sets with distance dependent resolution. The average point interval varies from 10 m next to the SG to 20 km in far distant zones. By applying the method of Götze and Lahmeyer (1988) the corresponding gravity effect can be calculated precisely.

Fig. 8 shows again that the area more than a few 100 m apart from the sensor does not contribute significantly to the gravity effect in Vienna. If the aquifer is assumed to be located above the SG sensor the result depends strongly on the layer depth due to the missing contribution from inside the building. The extremum estimate is obtained when the depth to the aquifer vanishes (Fig. 8, open triangles). Even in this unrealistic case a much larger fluctuation than observed would be required to explain the seasonal gravity effect by groundwater table variation.

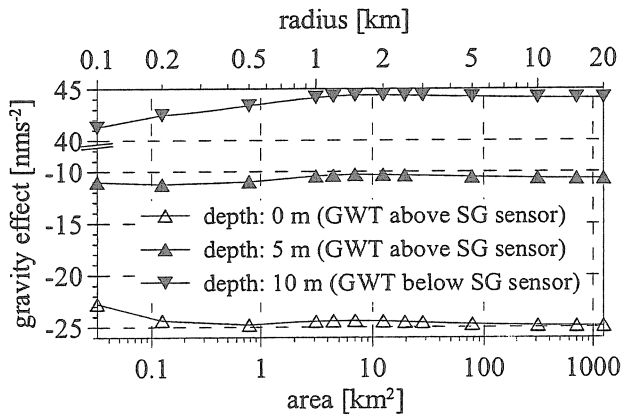

Fig. 8: Newtonian effect of a circular water layer (thickness 1 m, parallel to topography) representing the aquifer in a depth of 0 m, 5 m (aquifer above the SG sensor) and 10 m respectively (aquifer below the SG sensor) for different radii.

Groundwater table variations within the Vienna basin, the elevation of which is less than that of the SG sensor everywhere, have also been estimated. Assuming a porosity of 10% the gravity increases just by less than 2 nms^{-2} per groundwater table increase of 1 m. This is far below the amplitude of observed seasonal gravity fluctuations.

Newtonian gravity effect of snow cover

Snow generates gravity signals, which differ from those of rain, because

- snow does not invade the soil, and
- no run-off occurs at the surface

unless snowmelt starts. Possible seasonal effects have been estimated based on climatological findings (Fig. 9). At the same time this study also estimates the gravity effect of far distant (> 20 km) load of different origin. Between 100 m – 100 km remote from the station the Newtonian effect of surface water or snow is partly compensated (Fig. 10). Due to earth curvature this does no longer hold for distant areas where load always increases the observed gravity.

Fig. 9 demonstrates that far distant zones do not contribute significantly to gravity even in case of snow accumulation. Again, solely the very close vicinity is critical. Extending the snow cover area beyond a circle of about 100 m radius changes the gravity effect by less than 1-2 nms^{-2}.

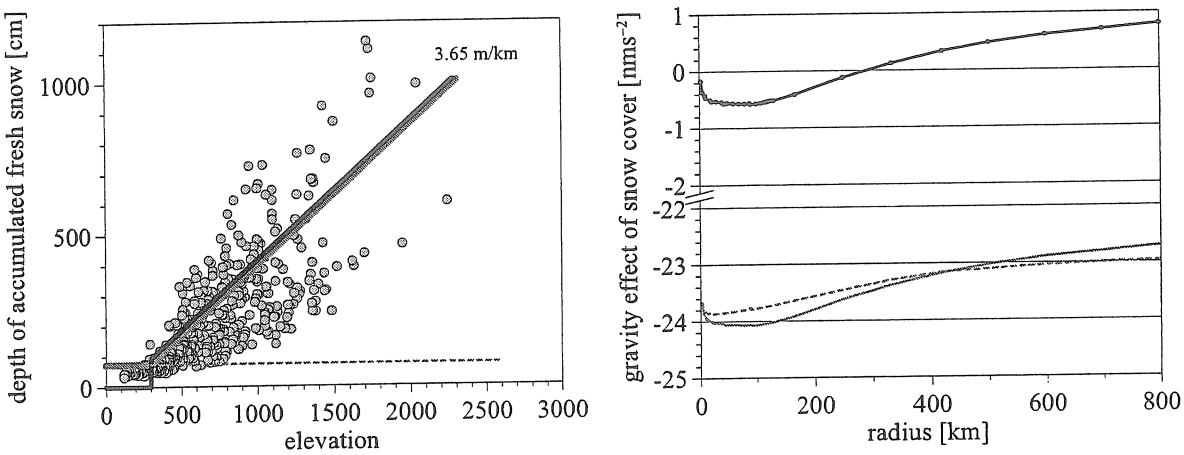

Fig. 9: Mean depth of accumulated fresh snow per year at climatological stations in Austria (dots) and snow cover models (left); modeled gravity effect at the SG site in Vienna (right): height dependent snow depth (grey, solid line), height dependant snow depth but no snow cover below 300 m (black), constant snow depth of 0.745 m (grey, dashed line).

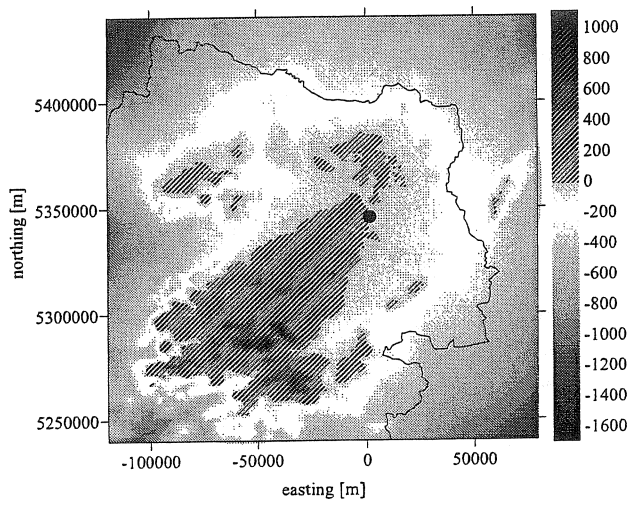

Fig. 10: Relative topography referred to the SG sensor in Vienna (dot). Due to earth curvature the Newtonian effect of water load increases gravity at the SG site except of the close vicinity and those parts located in SW and S mainly.

Newtonian gravity effect of Danube River high water

The Danube River is located below the SG sensor. Water level actually varies by up to 5 m in case of high water (e.g. August 2002, Fig. 11). Within the Vienna area an artificial flood discharge streamlet has been constructed parallel to the river for flood regulation, which is opened occasionally. This reduces the water level increase of the main river to 2 m approximately while the water level of the channel varies between 5 m at the beginning and 2 m at the end. The corresponding gravity effect has been estimated as 0.65 nms^{-2}/m. Because high water is developing over a couple of days these small signals can not be separated.

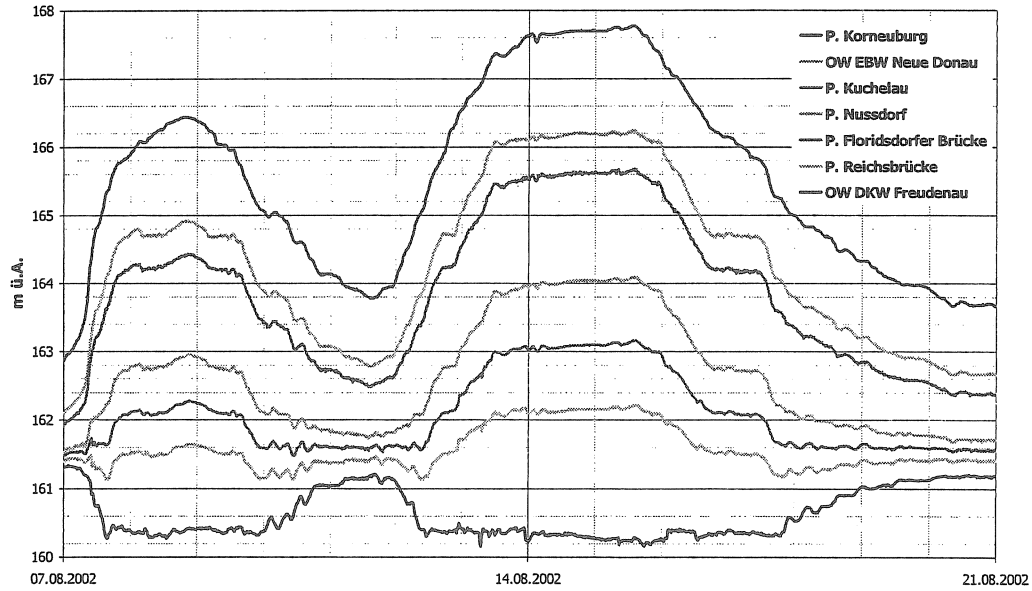

Fig. 11: Water level variations [m] of Danube River in the Vienna region for the flooding event of August 2002 (Gutknecht, 2004). The upper 3 lines represent the situation before flood regulation gets effective contrary to the lower 4 lines.

Conclusions

No groundwater data is available at the station itself, but it is known from drillings that the first water bearing stratum is located below the SG. Gravity and groundwater table variations as observed in wells about 1 km apart are anti-correlated. This indicates that the gravity effect of groundwater table variations either is small at the SG site or overcompensated by much stronger signals caused by soil moisture and/or other sources. Applying different discharge models does not essentially influence the long-term gravity fluctuations but enhances the typical pattern of low gravity in late winter and high gravity in autumn. It has still to be verified by analyzing large-scale load contributions if continental water storage signals (e.g. elastic deformation) causes the long-term gravity variations.

3D modeling of large-scale (ground-) water or snow load shows that the area in very close vicinity of the station (<100 m) turns out to play the most dominating role as long as the Newtonian effect is considered. Extending the load area beyond a circle of about 100 m radius up to a distance of 1000 km generates an additional gravity increase as small as 1-2 nms^{-2}. Water level variations of the nearby Danube River cause very low amplitude signals of less than 3 nms^{-2}.

References

Boy, J.P. and Hinderer, J. (2006): Study of the seasonal gravity signal in superconducting gravimeter data, J. Geodyn. 41, 227-233.

Crossley, D.J., Xu, S. and van Dam, T. (1998): Comprehensive analysis of 2 years of SG data from Table Mountain, Colorado. In: Proceedings of the 13th International Symposium on Earth Tides, Brussels, July 1997. Obs. Royal Belgique, Brussels, 659–668.

Götze, H.J. and Lahmeyer, B. (1988): Application of three dimensional interactive modeling in gravity and magnetics, Geophysics, 53, 1096-1108.

Gutknecht, D. (2004): Abflussbildung bei Hochwasser. Symposium FLOOD RISK Analysis of the Floods of August 2002, 24./25. November 2004, Vienna.

Harnisch, M., Harnisch, G. (2002): Seasonal variations of hydrological influences on gravity measurements at Wettzell. B. Inf. Marées Terr. 137, 10849-10861.

Kroner, C. (2001): Hydrological effects on gravity data of the geodynamic observatory Moxa, J. Geod. Soc. Japan 47(1), 353-358.

Kroner, C. and Jahr, Th. (2006): Hydrological experiments at Moxa observatory, J. Geodyn. 41(1-3), 268-275.

Meurers, B. (2000): Gravitational effects of atmospheric processes in SG gravity data, In: Ducarme, B. and Barthélemy, J. (eds.), 2000: Proc. Workshop: „High Precision Gravity Measurements with Application to Geodynamics and Second GGP Workshop", Luxembourg, 1999, Conseil de L'Europe, Cahiers du Centre Européen de Géodynamique et de Séismologie, 17, 57-65.

Meurers, B., Van Camp, M. and Petermans, T. (2006): Correcting gravity time series using rain fall modeling at the Vienna and Membach stations and application to Earth tide analysis, J. Geod. (submitted).

Renka, R. J. (1996): "ALGORITHM 751. TRIPACK: Constrained two-dimensional Delaunay Triangulation Package", ACM Trans. Math. Software, 22, 1, 1-8.

Van Camp, M., Vanclooster, M., Crommen, O., Petermans, T., Verbeeck, K., Meurers, B., van Dam, T., and Dassargues, A. (2006): Hydrogeological investigations at the Membach station, Belgium and application to correct long periodic gravity variations, J. Geoph. Res., in print.

Acknowledgement

Cooperation with Geophysical and Climatological Divisions of the Central Institute for Meteorology and Geodynamics, Vienna, is gratefully acknowledged as well as financial support by Austrian Science Foundation, project P16480-GEO. Thanks to Peter Janac (Vienna City Administration, Municipal Department 45 - Water Engineering) for providing groundwater data.

Hydrological signals in the SG records at Moxa – a follow-up

Corinna Kroner

Institute of Geosciences, Friedrich-Schiller-University Jena, Burgweg 11, D-07749 Jena, Germany

Abstract.

The existence of hydrological signals with their various sources in the records of the superconducting gravimeter (SG) at Moxa observatory is well known for several years. A part of this influence is directly related to rainfall affecting gravity from the short-periodic tides up to some weeks. The immediate (roof) area above the gravimeter which is thought to be a major source for this hydrological effect was covered with plastic foil in order to reduce effects. The results of this effort are presented.

1. Introduction

Hydrological signals in the records of the dual sensor superconducting gravimeter (SG) CD034 which operates at the Geodynamic Observatory Moxa, are known for a couple of years (e.g. Kroner, 2001). One characteristic of the hydrological influence is the occurrence of an immediate gravity decrease of several nm/s² associated with rainfall events (Fig. 1). A systematic change in gravity related to precipitation has not been found yet. Effects can widely vary even within one season: 14 mm of rainfall e.g. might produce a gravity effect of 7 nm/s², while 3 mm precipitation can result in a gravity decrease of 6 nm/s². The amplitude spectrum of the accumulated rain (Fig. 2) shows in which spectral bands a significant effect is to be expected in gravity. As can been seen from Fig. 2 the short-periodic tides (diurnal and higher periods) will clearly be affected by rain, but also strong effects should occur around 4, 10, 20, and between 30 and 40 days which will increase the noise in the gravity records and diminish the signal-to-noise ratio. Therefore, it is highly desirable to reduce this influence by any means. A fairly simple method for a reduction is to compute a regression coefficient between water level data of a 50 m deep borehole in front of the observatory and the gravity residuals. This procedure removes at least part of the hydrological effect (Kroner, 2001).

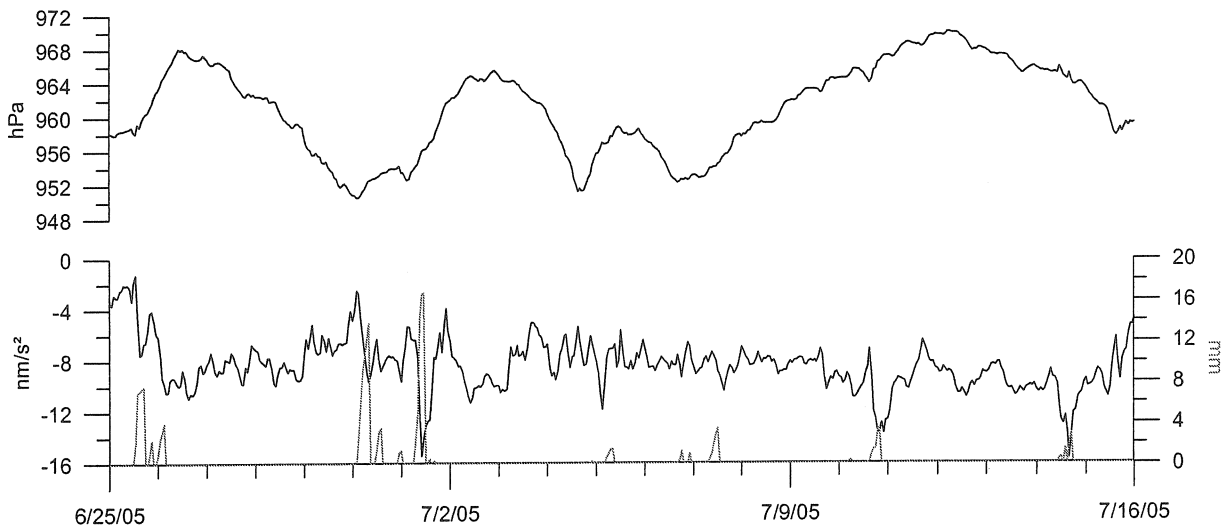

Fig. 1. Example of rainfall induced signals in gravity residuals. The gravity data were reduced with regard to earth tides, drift, polar motion and barometric pressure effects (3d-reduction+local regression coefficient). The precipitation given in grey corresponds to accumulated rain per event. The upper panel shows the local barometric pressure variation for comparison.

During the last years a number of experiments have been carried out to enhance the understanding of the hydrological effects from different contributing areas in the near vicinity of the SG and to develop reduction algorithms (Kroner, 2001; Kroner & Jahr, 2006). Apart from this, additional hydrological sensors for continuous soil moisture and water level monitoring were installed in the gravimeter vicinity. From one experiment in which the roof area above the gravimeter was irrigated it could be demonstrated that a non-negligible effect comes from changes in the water mass in this volume which consists of soil and gravel. To get an estimate of the effect due to rainfall events from this area it was assumed that one third of the total amount of precipitation runs off, one third evaporates and one third percolates. By applying this simple rule of thumb gravity variations of some nm/s² originate solely from this area (Fig. 3). From this follows, if it were possible to avoid or reduce changes in the amount of water stored in the roof area, the total of the hydrologicallyinduced effects in gravity could be reduced and the signal-to-noise ratio in the gravity data improved.

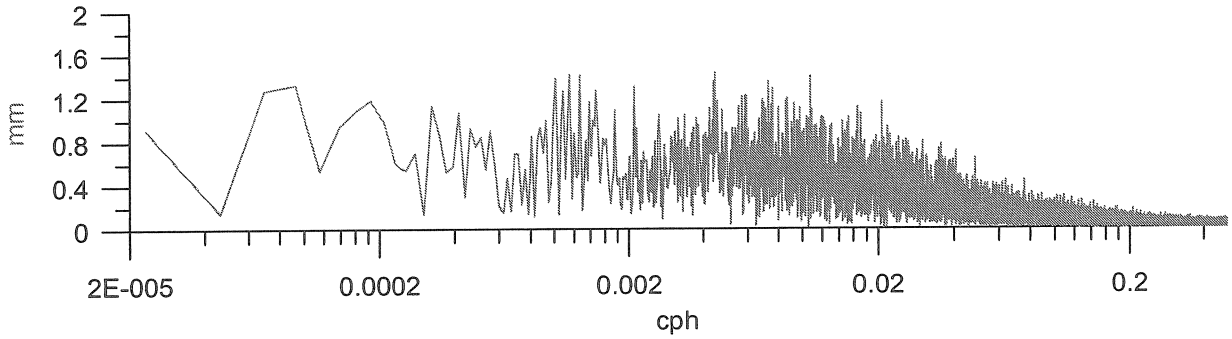

Fig. 2. Amplitude spectrum of the accumulated precipitation per event, 01/01/2001-12/07/2005.

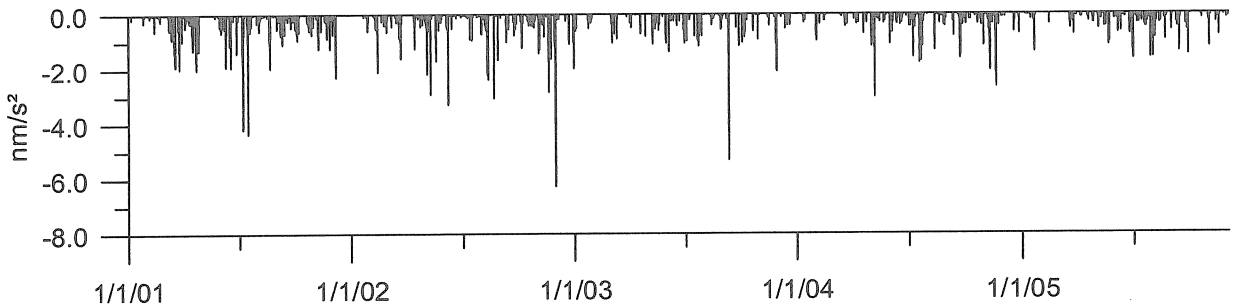

Fig. 3. Estimate of gravity effect caused by rainfall on roof area, 01/01/2001-12/07/2005. Periods with snow are excluded.

2. Coverage of roof surface

Bsed on the result of the irrigation experiment and the estimate of the hydrological effect originating from the roof area, in summer 2004 a project was started to cover the roof area. The first step was to remove all the vegetation from weeds up to small trees. After this the area had to be provided with a slope and the surface had to be levelled off with an excavator, among other things getting rid of a 0.5 to 1 m high hump in the middle of the roof. At the same time bigger roots and larger rocks were removed. Due to bad weather and a slippery surface work had to stop in September and could only be continued in summer 2005. Due to the long break the roof once more was covered with vegetation which thus had to be removed for cond time. After the preparation of the surface was finished a 4 cm thick layer of gravel (density: 1660 kg/m³) was put onto the roof which should help to avoid damage of the plastic foil by remaining small rocks. The major part of the roof then was covered with plastic foil of 1 mm thickness. Only a small part in the back which directly borders to the rock, in which the observatory is built, was left uncovered due to the rocky and unequal surface. Fig.

4 gives an impression of the roof area before work was begun and afterwards. The total area which is covered by foil since September, 7th 2005 amounts to 311 m². At the location of the SG the surface is 6 m above the instrument, at its lowest point, 13 m to the west the surface has a height of 3.6 m above the gravimeter.

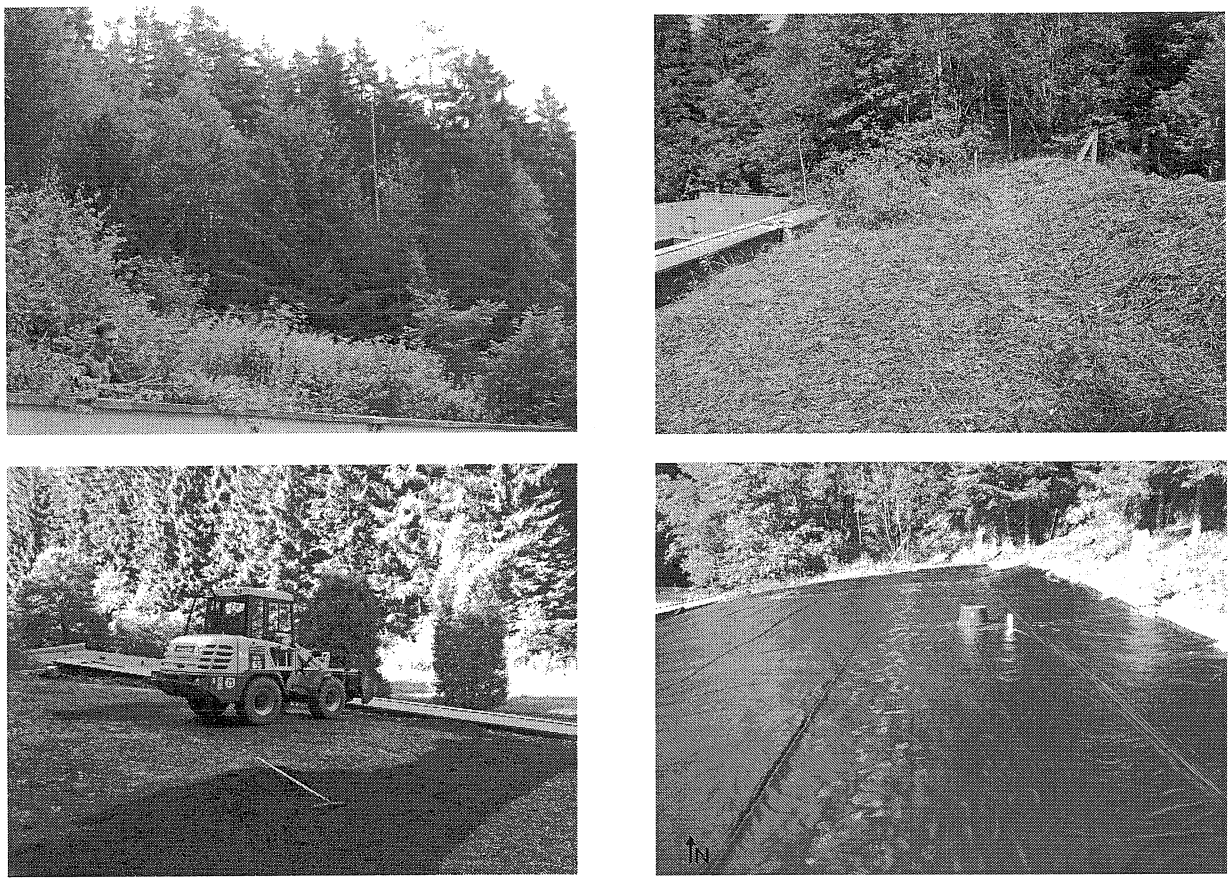

Fig. 4. Upper panel: Impressions of the roof area before work was started and after removal of vegetation; bottom panel: Putting gravel on the flattened suface and final condition of surface.

The additional mass of about 40 t on the roof produced a gravity decrease of 19 nm/s² in the record of the lower sensor of the SG and of 19.7 nm/s² in the data of the upper sensor (Fig. 5). The order of magnitude of the effect could be recovered in an estimate considering the dimensions and the geometry of the area with respect to the SG and assuming a gravel layer of homogeneous thickness.

Fig. 6 shows the gravity residuals before and after the roof was covered. For comparison the accumulated precipitation per rain event and the soil moisture changes on the roof directly above the SG in a depth of 0.3 m and 1.0 m are given. The soil moisture variations are monitored with TDR probes (TRIME-EZ). The sampling rate is 15 min. From the change in the soil moisture signatures it becomes clear that the foil screens the roof surface against short-term hydrological variations as intended, hopefully also against part of the long-term variations. Before the coverage most rain events produced clear soil moisture variations mostly in the data of the upper probe. At the same time also effects in the gravity residuals can be found. After the roof coverage practically no fluctuations exist in the soil moisture data which can be related to rain. The results are not so unambiguous with regard to gravity. We still have a gravity decrease related to rain events as expected because most of the area from which precipitation induced effects originate is still the same. The question is whether the size of the gravity decrease is now noticeably reduced or not. In the short period of data that is available after the roof coverage, we have e.g. rain events of 12 and 15 mm which produce a decrease in gravity of 5 nm/s² and rain events of 4.5 mm which result in a gravity change of

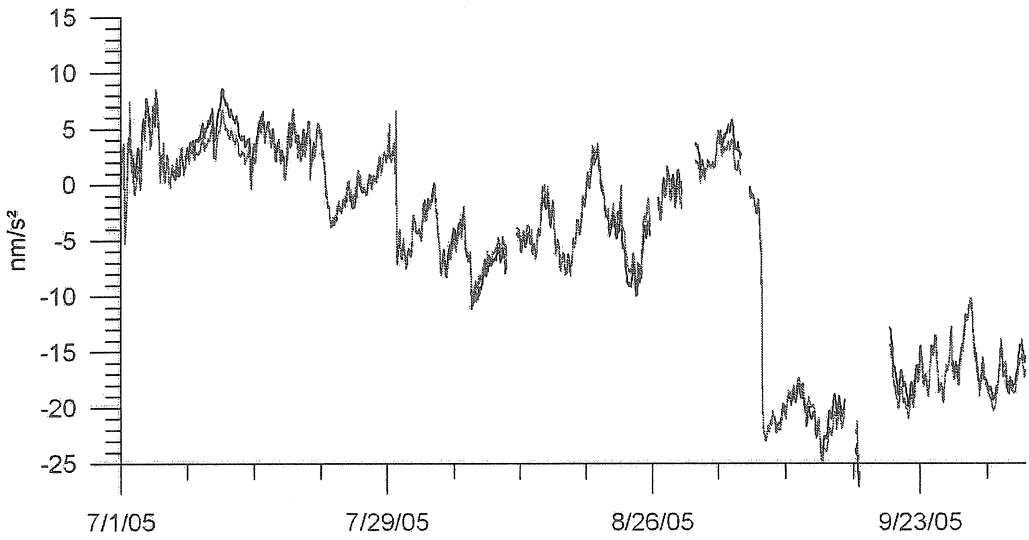

Fig. 5. Decrease in gravity residuals due to additional mass on roof; — lower sensor, — upper sensor.

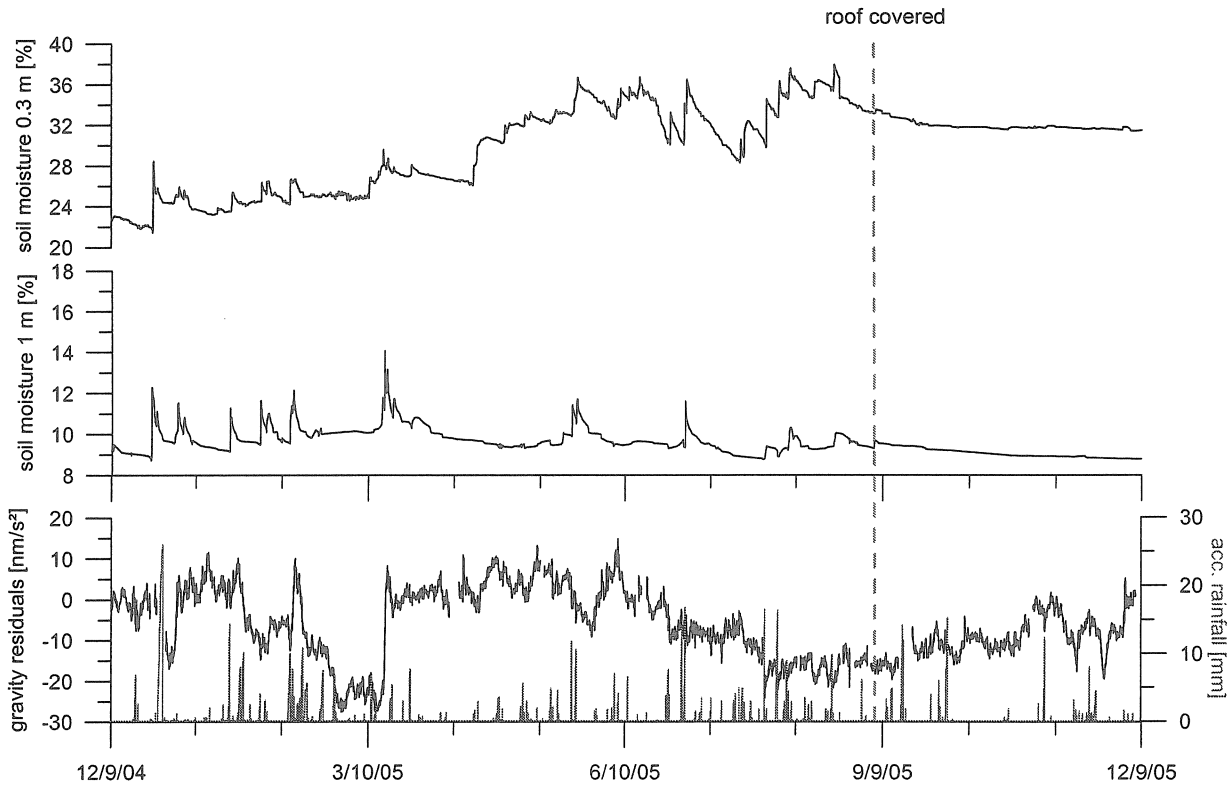

Fig. 6: Comparison of gravity residuals before and after the roof was covered with foil and accumulated precipitation per rainfall; the upper two curves show soil moisture changes in a depth of 0.3 and 1.0 m on the roof directly above the location of the SG. The decrease in gravity in the second half of December 2004 and between mid-February and mid-March is caused by snow.

2.5 nm/s². The general impression is that of a slight reduction of the gravity effects, but truth to tell the time span is still much too short for a meaningful assessment. The winter period (December 2005 until end of March 2006) can not be taken into account since the snow load remains the same independent of the roof coverage.

3. Conclusions

With the coverage of the roof surface at Moxa observatory it is intended to prevent esp. short-term hydrological fluctuations which affect the observations with the superconducting gravimeter situated directly below. This should lead to an improved signal-to-noise ratio. The clear diminishing of the soil moisture fluctuations to practically no variation shows the effectiveness of the coverage which results in an almost constant amount of water stored in the gravel and soil volume on the roof when periods of a few hours up to some weeks are considered. Whether the roof coverage is as effective as expected with regard to gravity is not clear yet since the period of observation after the covering took place is still too short.

Acknowledgements

The covering of the roof surface required a lot of hard work. Without the willing, tireless hands of colleagues and students this project could not have been realized. Many thanks to Raphael Dlugosch, Holger Hartmann, Thomas Jahr, Sonja Kuhlmann, Wernfrid Kühnel, Matthias Meininger, Britta Merten, and Marco Naujoks.

References

Kroner, C., 2001. Hydrological effects on gravity data of the Geodynamic Observatory Moxa. J. Geod. Soc. Japan, vol. 47, no. 1, 353-358.

Kroner, C. & Jahr, Th., 2006. Hydrological experiments around the superconducting gravimeter at Moxa Observatory. J. Geodyn., vol. 41, 1-3, 242-252, doi:10.1016/j.jog.2005.08.011

From a disturbing influence to a desired signal: Hydrological effects in gravity observations

M. Naujoks, C. Kroner, T. Jahr, and A. Weise
Institute of Geosciences, FSU Jena

Hydrological effects in an order of magnitude of up to several μGal are observed worldwide in gravity data, particularly in the high resolution recordings of superconducting gravimeters. Because they superpose other geodynamic signals, their reduction is necessary. For the development of a reduction model the understanding of the underlying hydrological processes is of central importance. Especially in areas with strong topography and/or inhomogeneous subsoil a simple reduction model based on hydrological measurements at the observatory is not sufficient. If the gravity variations in the observatory surrounding caused by hydrological variations and the hydrological parameters are observed two-dimensional it should be possible to model the influence of hydrological variations on the gravity recordings at the observatory and develop a reduction model. Because generally there is no superconducting gravimeter available for two-dimensional gravity measurements, the question raises whether by repeated gravity measurements with field gravimeters hydrological variations can be detected significantly in the μGal range. On the other hand the hydrological effects observed in the gravity data are of interest to hydrologists and hydrogeologists because they contain information about mass distributions and their changes in the subsoil, e.g. groundwater movement. Gravity measurements, in particular two-dimensional gravity measurements, detect hydrological variations integral - in contrast to the hydrological measurements which contain only information about the point of the measurement. Thus, information is also won about areas, in which hydrological measurements are not or hardly possible. That way gravity measurements can help to understand hydrological processes better. They also can be a boundary condition for hydrological modelling.

At the Geodynamic Observatory Moxa in Germany a local gravity network was established. Using excellent LCR field gravimeters the gravity differences between these observation points were measured in nine campaigns so far. The hydrological variations observed by the superconducting gravimeter as well as by water level, soil moisture and run off measurements are significantly provable as gravity changes in the range of some μGal between different observation points of the network by repeated gravity measurements using field gravimeter. In particular differences in gravity differences are observed between observation points in the valley and at the steep slope to the east of the observatory. They are bigger during dry weather and smaller during wet weather conditions. This indicates significant hydrological variations in the slope. For a better understanding of the hydrologically caused gravity changes as well as for the evaluation of hydrological models existing for the observatory surrounding 3D gravity modelling is carried out. Based on the free air anomaly a 3D gravity model of the observatory surrounding is developed. In the model the measured hydrological variations are converted to density changes of the subsoil. It is analysed in which areas and in which range hydrological variations appear, which are significant for the gravity observation points. First results indicate a good agreement in the range of the measured and modelled gravity changes.

Comparison of superconducting gravimeter observations with hydrological models of various spatial extents

H. Virtanen, M. Tervo, M. Bilker-Koivula,
Finnish Geodetic Institute
P.O.Box 15, FIN-02431 Masala, Finland
heikki.virtanen@fgi.fi

We have compared temporal gravity variations of the superconducting gravimeter T020 with various water storage models and observations at Metsähovi, Finland. We have used local data, regional and global hydrological models. The regional model is a highly accurate model for Finland, called the Watershed Simulation and Forecasting System (WSFS). The global model is the Climate Prediction Center global soil moisture data set (CPC), which correlates well with WSFS. We have exploited both regression methods and loading calculations using Green's function formalism to calculate gravity effects of these sources.
Gravity residuals are strongly correlated with local groundwater level, which clearly seems to correlate with the regional water storage. The important question is how to separate the effect of the near-field water storage from the loading effect of the regional or of the global water storage. Using regression methods exclusively, it is not possible to separate the various factors. Though, the local hydrological conditions have slowly altered and it offers a possibility to separate these phenomena.

Introduction

The superconducting gravimeter GWR T020 has been recording in Metsähovi almost continuously since August 1994. The gravity data correlates well with the local groundwater level (Fig. 1). In the gravity studies local hydrology has been conventionally corrected with regression on water level, observed by nearby borehole (Virtanen, 2000; 2001; 2006). Regression coefficients vary from 25 to 28 $nms^{-2}m^{-1}$. In addition, we have corrected the effect of the Baltic Sea loading (Virtanen, 2004).
We have treated only the local hydrology and the Newtonian attraction due to it. We have recently extended these studies to include regional and global water storage and its loading effect i.e. both the vertical deformation and the Newtonian attraction. We can crudely divide hydrological effect on gravity into three parts, depending on a distance. First is the local scale up to few kilometers, next, the regional scale up to several 100 km and then the continental or global scale. Theoretical studies show, that we are capable to detect gravity effect of local and global scale with superconducting gravimeter. However, the regional scale should be practically below the observational limit (Llubes et al., 2004).
We used two hydrological models: The Climate Prediction Center global soil moisture data set (Fan and Van den Dool, 2004) and the Watershed Simulation and Forecasting System (WSFS) of the Finnish Environment Institute (Vehviläinen and Huttunen, 2002). We have compared (Virtanen et al. 2005a; 2005b) the time series of T020 with both models, using regression methods and loading calculations. A key question is the separation of the attraction of near-field water storage from the loading effect of the regional water storage, as these two are strongly correlated. It seems, that using only regression methods it is not possible to separate the various factors and we will need stepwise modeling methods.
Hydrological phenomena appear to be a main cause for the regional gravity variation detected by

the gravity satellites CHAMP and GRACE. In several studies (Crossley and Hinderer, 2002; Crossley et al., 2004; 2005; Neumeyer et al. 2004; 2006; Virtanen et al. 2005a; 2005b) a correlation between regional gravity variation detected by the satellites and point gravity variation detected by the SGs has been pointed out. The question is again, which part of the SG response is driven by the regional hydrological loading and which part by the local hydrological attraction.

Data and processing

We have used hourly gravity hourly data of superconducting gravimeter T020 at Metsähovi. The data set starts on December 1994 and ends on December 2005, being over 11 years. The data is almost continuous, except the one longer data gap (4 four months in 2003) due to failure of the data acquisition system (DAS). We have removed from refined and drift corrected gravity data tides, pole tide and effect of air pressure. The procedures of data processing are described in detail by Virtanen (2004; 2006). The gravity residuals are shown top in Fig. 5, including all hydrological effects and non-tidal loading of the Baltic Sea. All data used in the calculations were sampled to hourly values regardless of original sampling rate. Hourly values are interpolated from monthly values using near rigid splines. The grid loading calculations were done using a slightly modified programme NLOADF (Agnew, 1997). In other calculations we have applied the program TSOFT (Van Camp and Vauterin, 2005)

At a distance of 3 m from the T020 there is a 33 m deep borehole in the bedrock, with a diameter of 11 cm, for monitoring the groundwater (GW). The level has been measured manually since November 1994. In March 1998 a pressure sensor for the level measurements was installed in the borehole and connected to the DAS. The range of GW is 2.6 m (-4.5 m – 7.1m below surface). The low pass filtering (0.25 d) was applied on the data (Fig. 5 [B]).

We have used a very-high class regional hydrological model for Finland, Watershed and Forecasting System (WSFS) shown in Fig. 3 (Vehviläinen and Huttunen, 2002). Original data is in 1×1 km grids and includes all components of hydrological cycle. The data in this study is as daily average values (mm) of total Finnish water storage. We have water storage in mm for whole span of the analysis. The range is 250 mm. We have original grid data from June 2003 to December 2005, totally 31 months. We have averaged daily grids (664 km×1214 km) to monthly values of 0.5°×0.5° grid to calculate actual loading effect to gravity using Green's functions formalism (Tervo et al., 2006). Daily values in gravity unit (nms^{-2}) are regressed on the total water in units of mm. The results are shown in Fig. 4. The correlation is very good and we get coefficient: 0.058 $nms^{-2}mm^{-1}$. Thus, the regional water storage should give about 15 nms^{-2} effect on gravity.

There are several global hydrological models available. In this study we have used Climate Prediction Center global soil moisture data (Fan and Van den Dool, 2004). This data set (CPC) are given in monthly 0.5°×0.5° grid of water in mm. This model was selected because it gives rather good data of snow (Dirmeyer et al., 2004). We have modified this global grid to preserve mass balance (MB). The model gives soil moisture in land areas only. We have smoothed increasing/decreasing water to even layer on oceans. Global yearly rainfall is about 35 mm.

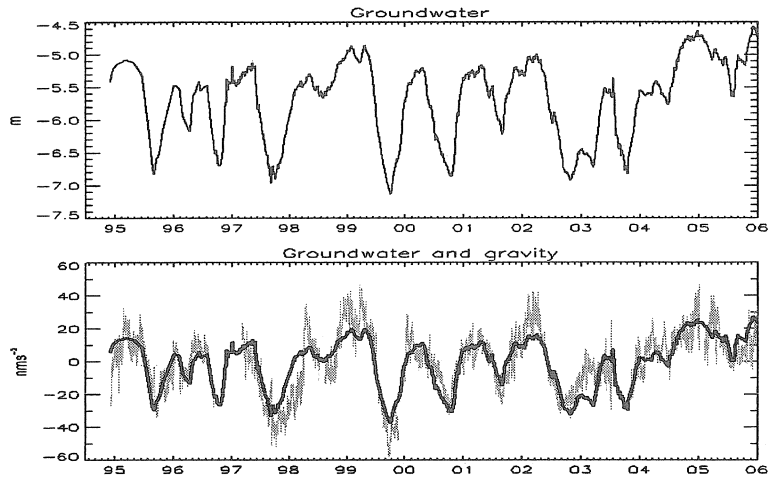

Fig. 1. The classical treatment of gravity data. Top: groundwater level at Metsähovi from 1 December 1994 to 31 Decemb 2005. Bottom: Gravity residuals with fitted groundwater level. The regression coefficient varies from 25 to 28 nms^{-2} depending on the correction of the Baltic Sea. Correlation coefficient is 0.83.

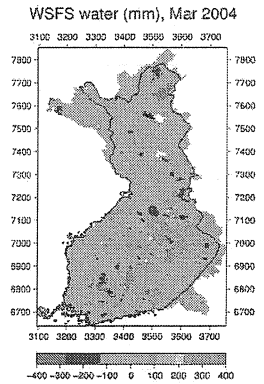

Fig. 2. The region of WSFS consist of Finland and connected watersheds

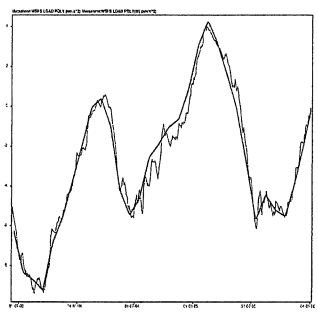

Fig. 3.The regression of loading gravity to mean value of total water storage in Finland (0.058 nms^{-2}mm^{-1}) 15.6.2003 – 15.12.2005.

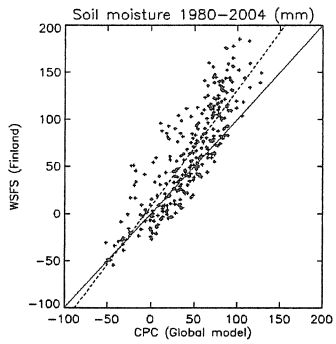

Fig. 4. WSFS vs. global model CPS, which is masked to the same area as WSFS

Next, we have calculated loading gravity effect using Green's function formalism. Monthly global gravity loading was then interpolated to hourly values (Fig. 5 [D]). The range of gravity variations is 30 nms^{-2}. For comparison we calculated the gravity load from CPC grid for the same area as WSFS and we found the maximum gravity effect of 5 nms^{-2} (Fig. 5 [E]). As additional data set we have data from snow water equivalence (Fig. 5 [F]) from station in distance about 40 km (MHR, 1994). We have used precipitation data (Fig. 5 [G]), too. The data is from Helsinki-Vantaa airport, at distance of 30 km (Meteorological Yearbook of Finland, 1994-; Ilmastokatsaus, 1999-). The data correlates well with local measurements, which do not work in winter.

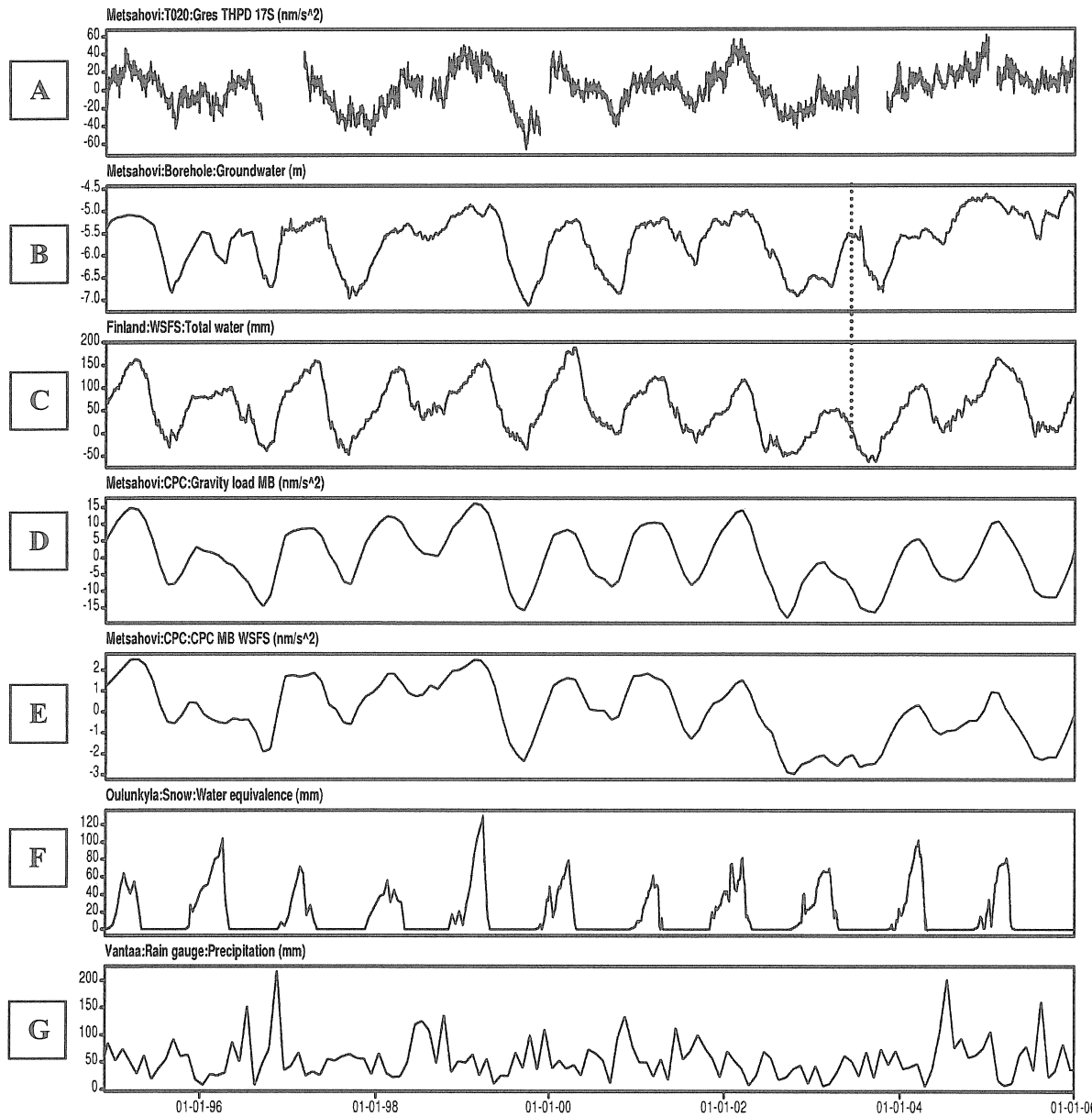

Fig. 5. From top to bottom: [A] Gravity residuals, [B] groundwater level at Metsähovi, [C] WSFS model for Finland, [D] CPC gravity load, [E] CPC gravity load for the region of WSFS, [F] Water equivalence of snow, [G] Precipitation at Helsinki-Vantaa airport. The dotted line in panels [B] and [C] shows approximately the time of change of local hydrological conditions.

Table 1
Results of gravity data of SG T020 vs. different hydrological models.

Treatment	Classical	Coeff.	Unit	Corr.	RMS	- %
1	GTPHD		nms^{-2}		20.07	0
2	GTPHD/GW	27.72	$nms^{-2}m^{-1}$	0.824	11.23	44
3	[2]/HSL	21.42	$nms^{-2}m^{-1}$	0.436	10.24	49
	New					
4	GTPHD-CPCMB		nms^{-2}		16.73	17
5	[4]/GW	19.49	$nms^{-2}m^{-1}$	0.695	12.03	40
6	[5]/HSL	19.24	$nms^{-2}m^{-1}$	0.371	11.17	45
7	[1]-[5]*GW-[6]*HSL		nms^{-2}		10.88	46
8	[7]/WSFS	0.070	nms^{-2}/mm	0.355	10.17	49
9	[7]/SNOW	0.127	nms^{-2}/mm	0.303	10.37	48
10	[7]/PREC	-0.006	nms^{-2}/mm	0.015	10.88	46
11	[7]/CPC(WSFS)	1.691	nms^{-2}/nms^{-2}	0.216	10.62	47
12	[8]/SNOW	0.045	nms^{-2}/mm	0.114	10.10	50
13	[8]/PREC	0.024	nms^{-2}/mm	0.069	10.15	49
14	[7]/WSFS/SNOW	0.053	nms^{-2}/nms^{-2}			
		0.064	nms^{-2}/mm	0.377	10.07	50

GTPHD: Edited gravity residuals, where effects of tide, pole tide, air pressure and drift were removed, GW: local groundwater, HSL: Baltic Sea level in Helsinki, CPCMB: Modified CPC model, WSFS: Total water storage for Finland, CPC(WSFS): Global model masked for WSFS area, SNOW: Water equivalence of snow, PREC: Precipitation.

Results and comparisons

We can see directly that hydrological data are strongly correlated (Fig, 5. [B-E] and Fig. 4.) In addition, water equivalence of snow correlates with WSFS. Using only regression methods it is not possible to separate the various factors and we need stepwise modelling. Results are given in the table 1. In classical treatments (hereafter TR) we have not used regional or global hydrological data. We compare results of all calculations to TR 1 (-%), where no reduction has been done. First we have calculated regression with local groundwater (TR2) and further with the Baltic Sea level. In the new treatment (TR4 - TR15) we have taken into account regional and global hydrology. First, we have deducted from gravity data the global effect (TR4) and then we have repeated TR2 and TR3. We have used coefficient from TR5 and TR6 and subtracted GW and HLS effect from gravity data (TR7). Next, we have calculated regressions on regional data of WSFS (TR8), snow (TR9), precipitation (TR10) and CPC model masked for WSFS area (TR11). With residuals of TR8 we have done regressions on snow (TR12) and precipitation (TR13). Finally, we have used data of TR7 and a simultaneous regression on snow/precipitation (TR14) have been done.

Summary and conclusions

The classical treatments show that both local groundwater and the Baltic Sea level are important in the data processing. After removing the global hydrological effect the regression coefficient of GW diminished about 30% and change of coefficient for sea level is small (TR2,3,5 and 6). Therefore, we get an important result: 2/3 of hydrological effects are due to local factors. Another interest result is: The effect of Finnish water storage (WSFS) is observable (TR8). The regression gives 0.070 nms^{-2}/mm, which is comparable to the result shown in Fig. 3. The correlation coefficient of snow is lower, which is understandable due to lack of data in summer. Regression on precipitation seems to be insignificant (TR10). Results using global model CPC(WSFS) show (TR11) that WSFS gives better results as expected. The best result is achieved using gravity data, which is corrected for local factors and simultaneous regression on WSFS and snow.
As conclusion we can say that separation between local and regional hydrology factors seems to be possible, which is remarkably due to high accurate watershed model WSFS. The SG T020 at Metsähovi is capable to monitor regional water storage. Global contribution must be taken into account in the data processing. We have used in this study only one global monthly hydrological model. In future, we continue studies with other global models, which are preferably given more frequently (e.g. Rodell et al., 2004).
However, the most effective hydrological effects are local. The level of local groundwater has been a conventional tool to correct this effect (Virtanen, 2001). Hydrological conditions have slowly changed at Metsähovi since 2003 (Fig. 5 [B,C]). Storms have destroyed the forest around gravity laboratory and a nearby swamp has been dried up. The change of level of groundwater is smaller than before. However, it correlates well with WSFS and with gravity still. In the future, the SG might observe changes in regional water storage more sensitively. The accurate modelling of local hydrology will play an important role in studies of hydrological effects on gravity. Modelling includes soil moisture measurements in wider area, observing weather parameters and detailed studies of structure of bedrock near SG. It means developing complete 3-D hydrogeological-meteorological model for a local hydrological cycle.
We can use gravity methods to improve hydrological models of different spatial extensions, local, regional and global, nationally and internationally.

Acknowledgements

The Finnish Institute of Marine Research has kindly made tide gauge data in Helsinki available to us. The HIRLAM data for air pressure correction is due to Finnish Meteorological Institute. The Finnish Environment Institute has provided the data of Watershed Simulation and Forecasting System (WSFS).

References

Agnew, D. C., 1997. NLOADF: a program for computing ocean tide loading. J. Geophys.Res. 102 (B3), 50109-51110.

Crossley, D., and Hinderer, J., 2002. GGP Ground Truth for Satellite Gravity Missions. Bull. d'Inf. Marées Terr. 136, 10735-10742.

Crossley, D., Hinderer, J., Boy, J-P., 2004. Regional gravity variations in Europe from superconducting gravimeters. J. Geodyn. 38 (3-5), 325-342.

Crossley, D., Hinderer, J., Boy, J-P., 2005. Time variations of the European gravity field from superconducting gravimeter. Geophys. J. Int., 161, 257-264.

Dirmeyer, P. A., Z. Guo, and X. Gao, 2004. Validation and forecast applicability of multi-year global soil wetness products. Journal of Hydrometeorology, 5., 1011-1033.

Fan, Y., Van den Dool, H. (2004). The CPC global monthly soil moisture data set at 1/2 degree resolution for 1948-present. J. Geophys. Res. 109, D10102, doi:1029/2003JD004345.

Ilmastokatsaus, 1999-2005. Finnish Meteorological Institute, (Monthly survey in Finnish).

Llubes, M., Florsch, N., Hinderer, J., Longuevergne, L., Amalvict, M., 2004. Local hydrology, the Global Geodynamics Project and CHAMP/GRACE perspective: some case studies. J. Geodynamics 38, 355-374.

Meteorological yearbook, 1994-1998. Finnish Meteorological Institute, SVT, Official Statistics of Finland

MHR, 1994-2005. Monthly Hydrological Report, Finnish Environment Institute, Hydrology and Water Management Division, 1994 – 2005, Helsinki.

Neumeyer, J., Schwintzer, P., Barthelmes, F., Dierks,O., Imanishi, Y., Kroner, C., Meurers, B., Sun, H.-P., Virtanen, H., 2004. Comparison of Superconducting Gravimeter and CHAMP Satellite Derived Temporal Gravity Variations. Ed. C. Reigber et. Al. Earth Observations with Champ, Results from Three Years in Orbit. Springer, 31-36.

Neumeyer, J., Barthelmes, F., Dierks, O., Flechtner, F., Harnisch, M., Harnisch, G., Hinderer, J., Imanishi, Y., Kroner, C., Meurers, B., Petrovic, S., Reigber, Ch., Schmidt, R., Schwintzer, P., Sun,H.-P., Virtanen, H., 2006. Combination of temporal gravity variations resulting from Superconducting Gravimeter recordings, GRACE satellite observations and global hydrology models. J. Geodesy, doi: 10.1007/S00190-005-0014-8.

Rodell, M., P. R. Houser, U. Jambor, J. Gottschalck, K. Mitchell, C.-J. Meng, K. Arsenault, B. Cosgrove, J. Radakovich, M. Bosilovich, J. K. Entin, J. P. Walker, D. Lohmann, and D. Toll, 2004. The Global Land Data Assimilation System. Bull. Amer. Meteor. Soc. 85, 381–394.

Tervo, M., Virtanen, H., Bilker-Koivula, M., 2006, Environmental loading effects on GPS time series, Bull. d'Inf. Marées Terr. (ibid).

Van Camp, M., and Vauterin, P., 2005. Tsoft: graphical and interactive software for the analysis of time series and Earth tides, Computers & Geosciences 31 (5), 631-640.

Vehviläinen, B. and Huttunen, M., 2002. The Finnish watershed simulation and forecasting system (WSFS). XXI Conference of the Danubian countries on the hydrological forecasting and hydrological bases of water management. Bucharest, Romania. 2-6 September 2002.

Virtanen H., 2000. On the observed hydrological environmental effects on gravity at the Metsähovi station, Finland. In B. Ducarme and J. Barthélemy (eds): Proceedings of the Workshop: High Precision Gravity Measurements with Application to Geodynamics, and Second GGP Workshop. Munsbach Castle (Grand Duchy of Luxembourg), March 24th to 26th. Cahiers du Centre Européen de Géodynamique et de Séismologie, Vol. 17, 169–175.

Virtanen, H., 2001. Hydrological studies at the gravity station Metsähovi in Finland. J. Geod. Soc. Japan 47 (1), 328–333.
Virtanen, H., 2004. Loading effects in Metsähovi from the atmosphere and the Baltic Sea. J. Geodynamics 38, 407–422.
Virtanen, H., 2006. Studies of Earth Dynamics with the Superconducting Gravimeter, Academic Dissertation in Geophysics, University of Helsinki, http://ethesis.helsinki.fi/.
Virtanen, H., Bilker, M., Mäkinen, J., Poutanen, M, Tervo, M., Vehviläinen, B., Huttunen, M., Mäkinen, R., 2005a. Comparison of modeled variation in water storage in Finland with GRACE and superconducting gravimeter observations. Geophysical Research Abstracts 7, 06248, 2005.
Virtanen, H., Bilker, M., Mäkinen, J., Tervo, M., Vehviläinen, B., Huttunen, M, Mäkinen, R., Peltoniemi, M., Hokkanen, T., Pirttivaara, M., 2005b. Comparison of modelled variation in water storage in Finland with superconducting gravimeter observations and with GRACE. Abstract in Dynamic Planet, Cairns, Australia, 22-26 August 2005.

Measuring integral soil moisture variations using a geoelectrical resistivity meter

Thomas Klügel [1], Günter Harnisch [2] & Martina Harnisch [2]
[1] Bundesamt für Kartographie und Geodäsie, Fundamentalstation Wettzell, thomas.kluegel@bkg.bund.de
[2] formerly: Bundesamt für Kartographie und Geodäsie

1 Introduction

The attractional effect of time-varying mass distributions of environmental origin is a limiting factor in high resolution terrestrial gravimetry. Beside atmospheric air mass fluctuations, which is the largest environmental signal, mass fluctuations of water in the underground play an important role (e.g. Harnisch & Harnisch 2005, and references cited herein). After removing the Earth tides, the pole tide, and air pressure effects, the residual time series of superconducting gravimeters often show signals showing some correlation with hydrological data. One example from the Wettzell gravimeter shows a clear improvement of the residual gravity when groundwater corrections are applied (figure 1). At other stations a groundwater correction doesn't work well or groundwater data are not available. In some cases the modeled gravity effect of precipitation using the charge/discharge model of Crossley et al. (1998) helps reducing the hydrological signal. But both sensors do not contain the whole information how much water is stored in the underground.

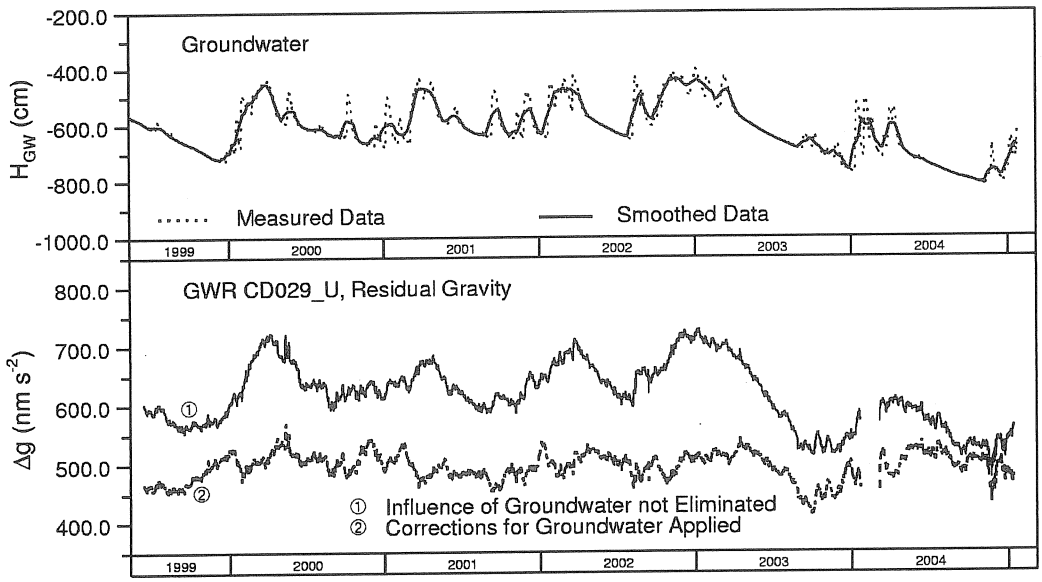

Figure 1: Hydrological correction of residual gravity at Wettzell using groundwater data

Regarding the basic equation of the hydrological cycle (figure 2)

Precipitation = Evapotranspiration + Surface Runoff + Subsurface Runoff

it is very difficult to determine the present distribution of water in the different subsystems, because many parameters controlling the water flow are time dependent. The amount of water going back to the atmosphere by evapotranspiration is strongly affected by temperature, wind and vegetation cover. The surface runoff depends on the slope, soil type, rain intensity, vegetation and soil moisture, whereas the latter three are also functions of time. Subsurface runoff is extremely difficult to estimate.

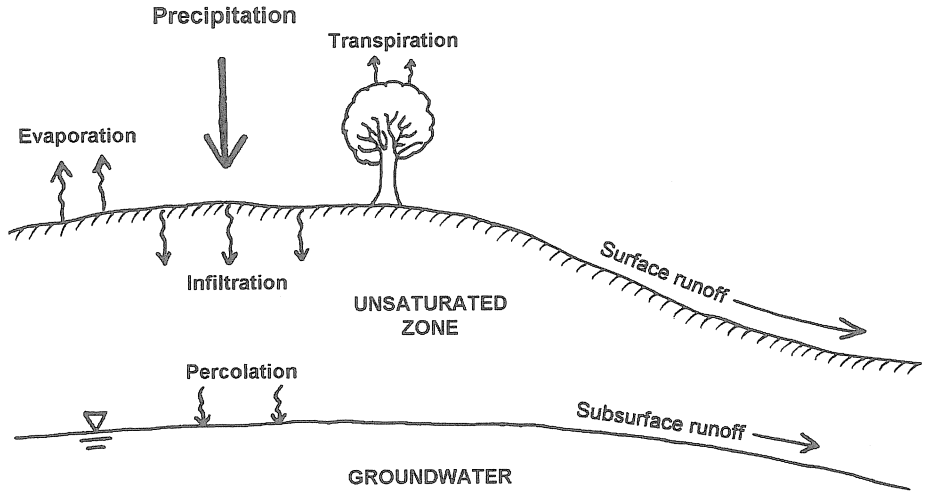

Figure 2: Sketch illustrating the hydrological cycle

In terms of measurements, there is easy access to precipitation and groundwater level. But how much water is stored in the unsaturated zone? One appoach to solve this is the use of hydrological models, where the unknown quantities in the hydrological cycle are estimated on the base of meteorological, geographical and geological data (e.g. J2000 hydrological model, Krause et al. 2006). The other approach is to measure soil moisture.

2 Measuring soil moisture

There are many soil moisture sensors commercially available working in different ways and measuring different quantities. An overview of different sensor types is given in table 1. However, all sensors measure a physical property in the immediate vicinity of the sensor, generally probing less than 1 liter. How representative are these data for the whole matter affecting the gravimeter, and can the data extrapolated vertically or laterally? One could tackle this problem by an 3-D array of soil moisture sensors, but besides the costs, the installation is time-consuming and not practicable at depths greater than 2-3 m. As an alternative, electrical resistivity survey techniques acting at the surface and penetrating the underground yield an integral information of the electrical conductivity and easily reaches depths of several meters without digging or drilling.

Table 1: Sensor types for measuring soil moisture

Sensor type	Measured quantity
Gypsum block	Electrical conductivity
Tensiometer	Water tension
Time domain reflectometry (TDR)	Propagation delay of electromagnetic pulses (ε)
Frequency domain reflectometry (FDR)	Frequency shift of electromagnetic waves (ε)
Heat dissipation sensor	Thermal conductivity
Neutron probe	Energy loss of neutrons (H-atoms)

3 *Electrical resistivity survey*

The basic principle of electrical resitivity survey is sketched in figure 3. Two current electrodes C1 and C2 are supplied with a constant electrical current of DC or AC type. The potential drop between the two electrodes P1 and P2 being located in a defined distance between (or even outside) the current electrodes is a function of the resistivity of the soil. There is a sensitivity maximum at a certain depth, depending on the electrode configuration. The bigger the spacing of the electrodes is, the deeper is the sensitivity maximum. In this way information of different depth in gained. A 2-D or even 3-D mapping of the specific resistivity of the underground can be done by varying systematically the spacing and the location of the electrodes. The unit is [Ωm], which is the 1-D specific resistivity [Ω/m] times the cross sectional area of the probed body [m^2].

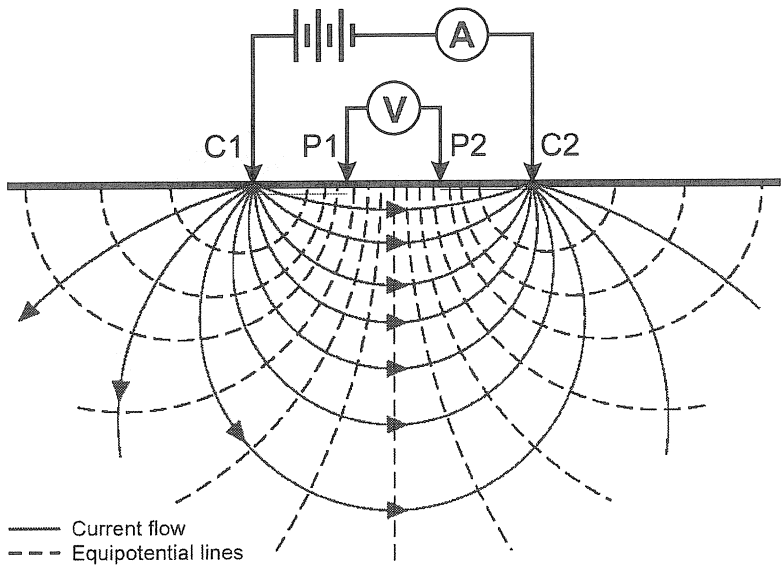

Figure 3: Basic principle of electric resistivity survey

The electrical resistivity is mainly controlled by the material. Some rough values are 1-30 Ωm for clay, 10-50 Ωm for silt, 50-2000 Ωm for Sand and 10^3-10^6 Ωm for crystalline rocks. The material is taken as constant in time. Time-variable parameters affecting the electrical resistivity of the soil are water content and temperature. Variations of the salinity also affect the resistivity, should however play a minor role in silicate rocks.

Standard electrical resistivity meters have two current and two potential electrodes. Using this configuration, information at 1 location and 1 depth is obtained. In order to get spatial information, re-location of the electrodes is required. This procedure is not practicable for countinuous monitoring.

Since several years multielectrode devices are available, where a big number of electrodes are permanently installed. The configuration can be set up software-controlled that each electrode can operate as current or potential electrode. More than 100 electrodes can be operated simultaneously. All possible configurations are scanned automatically yielding data for different locations and depths. The obtained data set has to be inverted to get the true spatial information of the specific resistivity. An example of a section inversion using the RES2DINV software is given in figure 4. The measurement has been performed at the Fundamental Station Wettzell using 50 electrodes with 1 m spacing (figure 5).

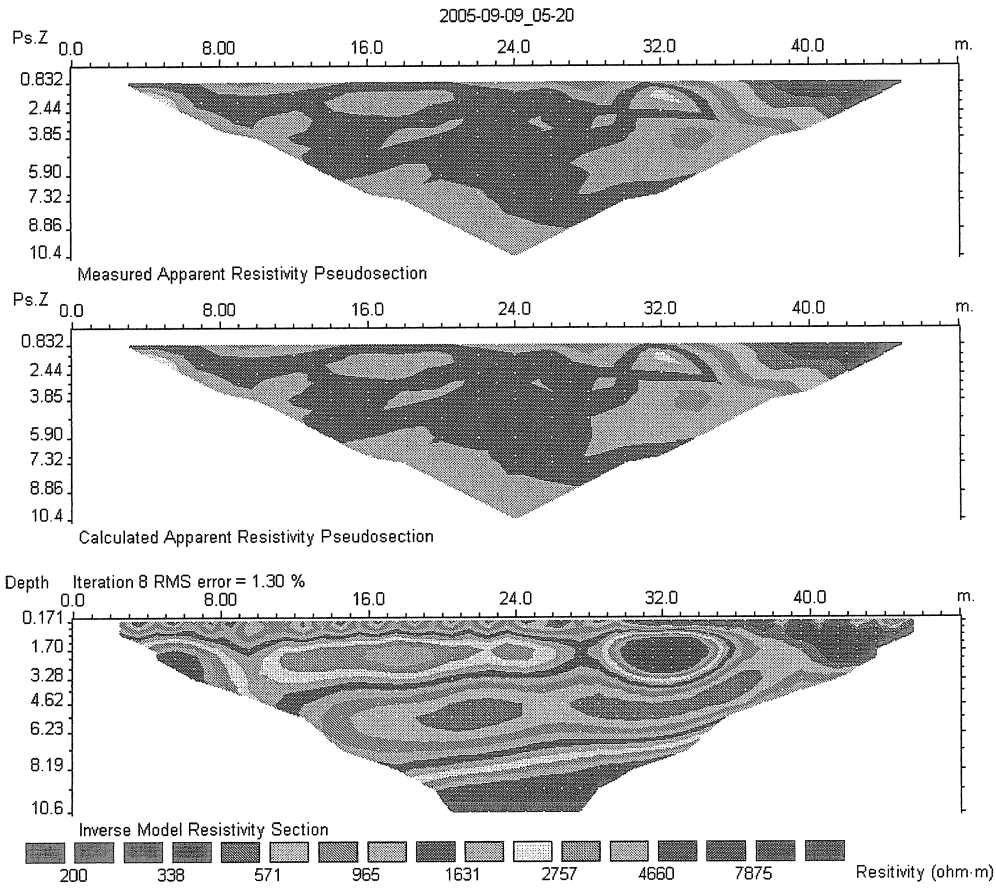

Figure 4: Inverted section of geoelectric test line Wettzell; location given in figure 5

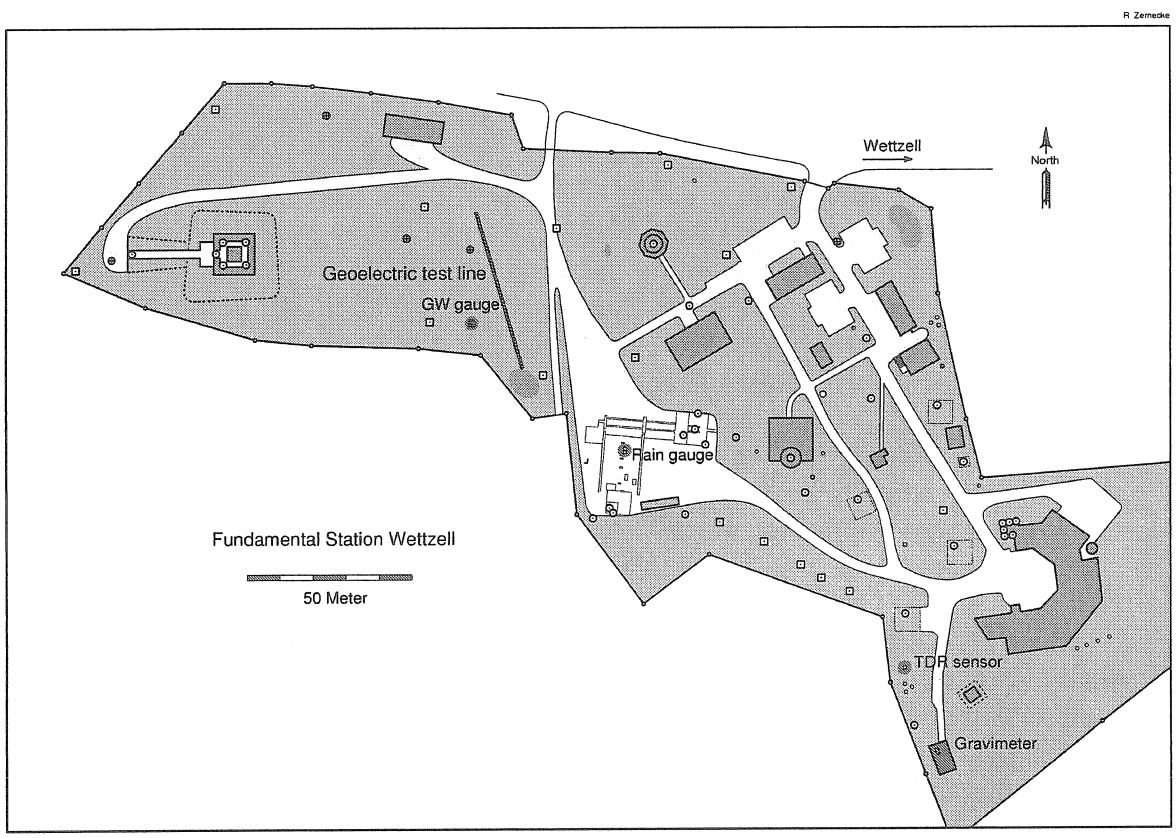

Figure 5: Map of the Fundamental Station Wettzell showing the locations of the geoelectrical test line, the groundwater and rain gauge, the soil moisture sensor and the gravimeter site.

4 *Continuous monitoring*

Electrical resistivity survey is normally used to map the kind and distribution of the underground material. The software controlling the scanning process is interactive and stops after a full cycle is complete. In order to create time series, the software has been modified in a way that a new cycle starts automatically after a given time interval. Each cycle creates one data file. Time series has been generated by extracting data points for a common location and apparent depth from each file. The result is shown in figure 6 for one selected depth, indicating lateral variations of the resistivity by one order of magnitude due to different materials (compare with figure 4). In a second step all data points representing one depth but different locations has been averaged and normalized with respect to the first data point. The resulting time series (figure 7) show no longer variations due to lateral inhomogeneities, but a systematic variation of the time series with depth.

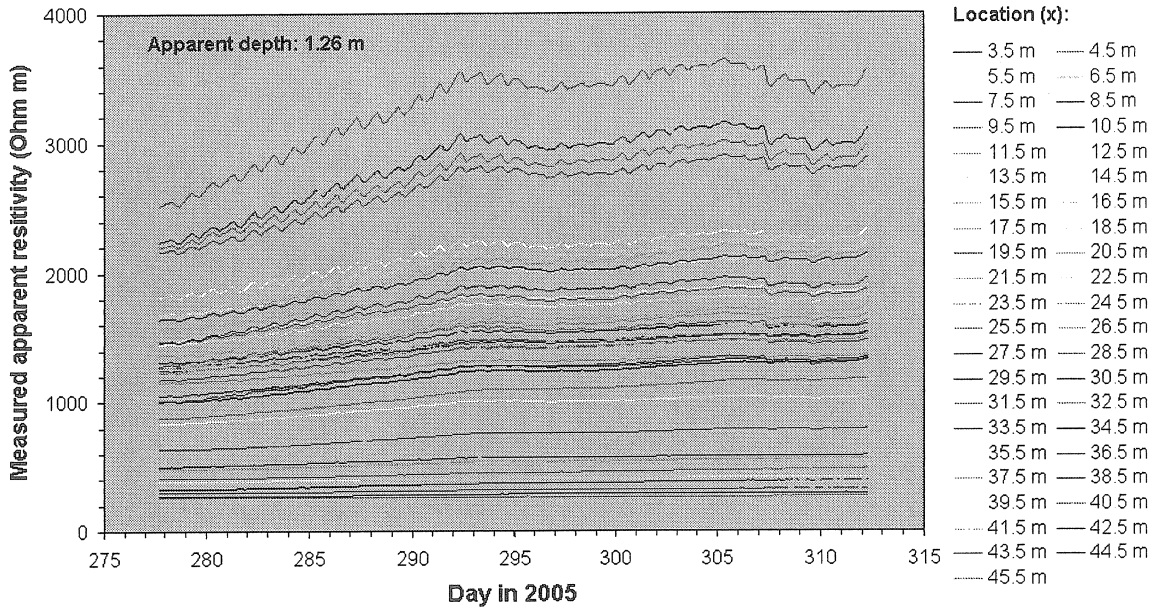

Figure 6: Time series over 35 days with constant spacing (depth) and varying location

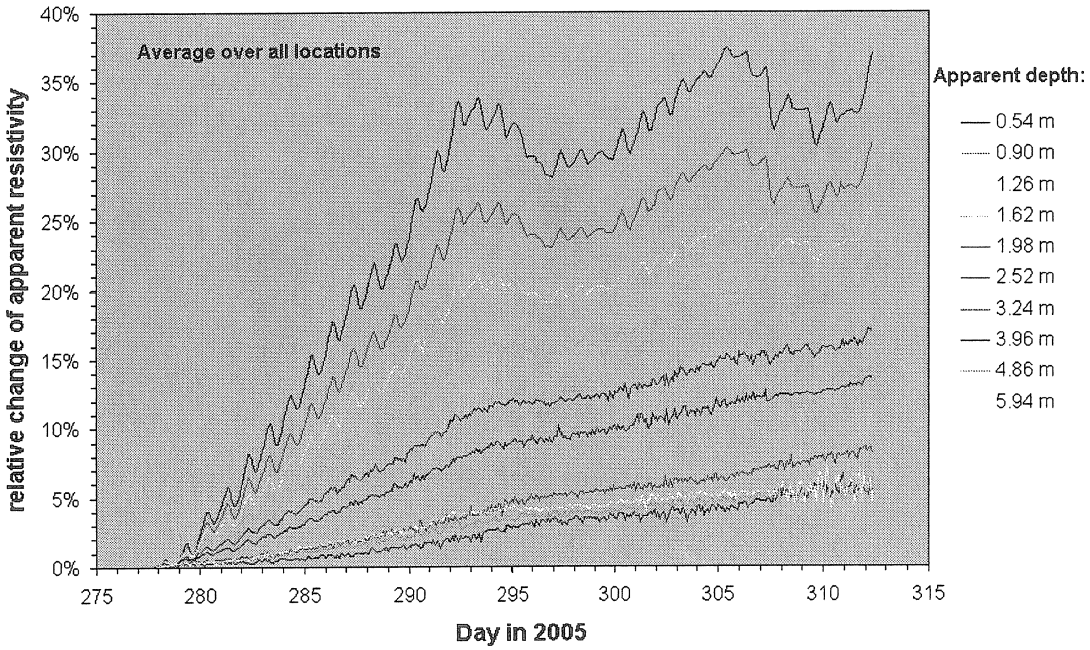

Figure 7: Time series normalized and averaged over all locations, constant spacing (depth)

5 Results

The obtained time series over 35 days show a general increase of the apparent resistivity with some long period variations, and clear daily cycles. Both signals become weaker with depth. In terms of soil moisture, the increase of resistivity could be interpreted as a drying of the soil during these sunny autumn days. The daily cycles however are not likely to be a soil moisture effect. The minimum occurs in the evening hours, which should be the maximum in the case of soil moisture. This is obviously a temperature effect causing a higher ion mobility in the uppermost soil layer during the warm evening hours. There is no phase shift with increasing depth, indicating that also measurements with big spacing are influenced by surface effects.

As no soil temperature data were available to verify the temperature hypothesis, a synthetic temperature curve has been generated using a simple one-dimensional heat flow model and air temperature data as boundary condition. The comparison of the model temperature in 0.3 m depth with the resistivity in 0.5 m depth (figure 8) shows a clear anticorrelation of both curves, indicating that the temperature has a major impact on the measured resistivity. A rough estimate is 2% resistivity change per degree temperature change.

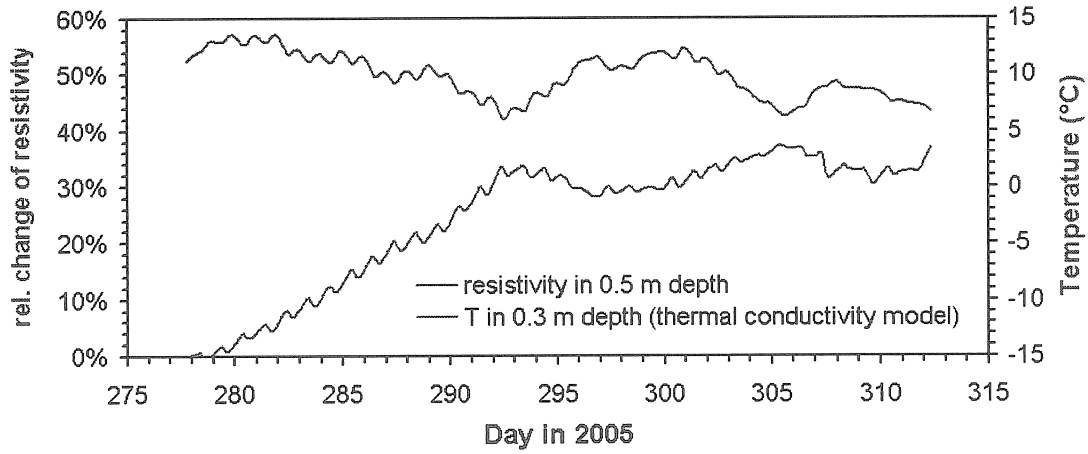

Figure 8: Comparison with 1-dimensional thermal conductivity model, basing on air temperature data

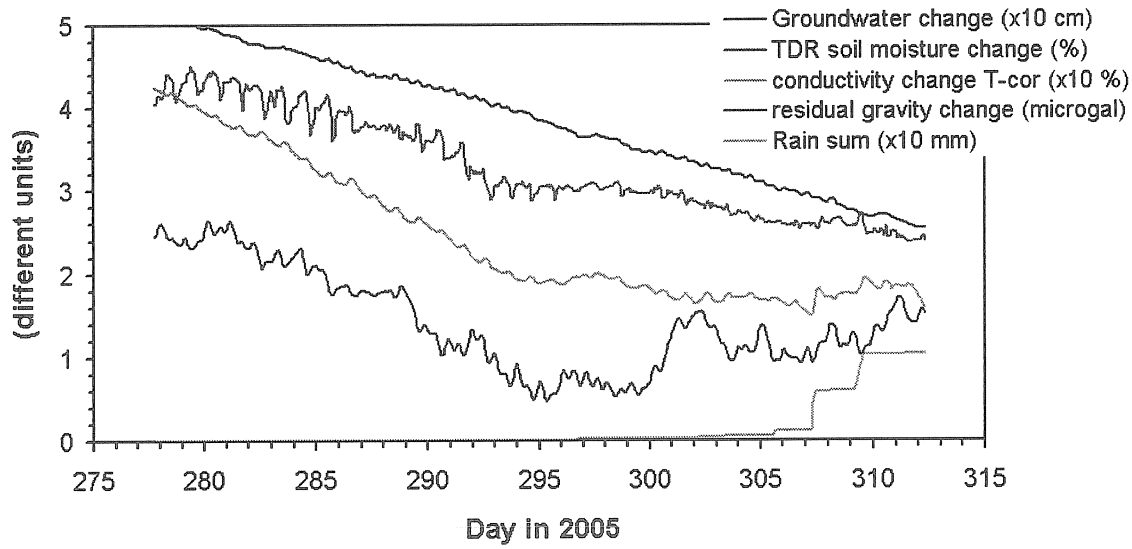

Figure 9: Comparison with other hydrological data and residual gravity time series

When taking the temperature corrected conductivity (inverted resistivity) as a reading of soil moisture and comparing it with other hydrological data, there is a partial correlation

observable (figure 9). The general trend is present in all data sets, whereas some signatures are visible in the conductivity data only. The residual gravity time series however shows only a weak correlation with the conductivity data. This might have different reasons,

- the location is not representative,
- the residual gravity still contains other signals (atmosphere),
- the contribution of soil moisture to gravity is weak,
- the presented method is inadequate.

From these first results it cannot be stated if this method is adequate to obtain an integral information of the soil moisture, but they encourage to further investigations. This includes relocation of the test site closer to the gravimeter, monitoring of the soil temperature, and creation of longer time series.

6 References

Crossley, D.J., Xu, S. & van Dam, T., 1998: Comprehensive analysis of 2 years of SG data from Table Mountain, Colorado. Proc. 13th Int. Symp. Earth Tides, Brussels 1997: 659-668.

Harnisch, G. & Harnisch, M., 2006: Hydrological influences in long gravimetric data series. J. Geodyn. 41: 276-287.

Krause, P., Fink, M., Kroner, C., Sauter, M. & Scholten, T., 2006: Hydrological processes in a small headwater catchment and their impact on gravimetric measurement. Workshop on Analysis of Data from Superconducting Gravimeters and Deformation Observations regarding Geodynamic Signals and Environmental Influences, Jena, March 27 - 31, 2006.

Soil moisture measurement and simulation and their impact on gravimetric measurements

P. Krause (1), M. Fink (1), C. Kroner (2)
(1) Department of Geoinformatics - FSU Jena, Germany
(2) Department of Applied Geophysics - FSU Jena, Germany

1. Abstract

An interdisciplinary research project which comprises scientists from hydrology, hydrogeology, geophysics and soil sciences has been launched in the neighbourhood of the Geodynamical Observatory Moxa in Germany. For this project the small (Ac 2 km²) catchment which surrounds the observatory has been instrumented with soil moisture and groundwater probes at various locations as well as additional precipitation gauges and a climate measurement station for monitoring of climatological and hydrological parameters in high spatial and temporal resolution. Secondly, a fully distributed and spatially high resolved hydrological model, based on the modelling system J2000, has been set up for continuous simulation of the hydrological processes in the catchment in daily and hourly time steps.

The main purpose of the project was to explore the hydrological influence on the gravity change monitored by a high sensitive superconducting gravimeter, which is part of a world wide network of similar instruments. The gravimeter readings show significant influence of groundwater, soil water contents and snow coverage on the measurements. Those influences interfere with geodynamic signals which are of geophysical interest. However the recorded responses carry interesting information from a hydrological point of view, because a method for direct, integrative and non-invasive measurement of soil water contents and groundwater variations would be available, if the hydrological influence on the response of the gravimeter records could be extracted.

This paper provides an overview of the test site and its geophysical, hydrogeological and hydrological measurement network set up for the project. In particular, the response of the superconducting gravimeter on hydrological variations is shown. Results of the relationship between the gravimetric data, measured hydrological parameters and the modelled hydrological dynamics are also demonstrated.

2. Introduction

A superconducting gravimeter (SG) is an important part of the equipment at the Geodynamical Observatory Moxa in Germany. It is a well known fact that gravimeter data is affected by various environmental influences like barometric pressure, tides, polar motion which can be corrected by regression models. The influence of hydrological variations in the surrounding catchment are, however, is not as well understood. The influence of changing groundwater tables has been discussed by many authors (e.g. Lambert and Beaumont 1977, Kroner 2001, Harnisch and Harnisch 2002). Beside groundwater, there are other sources of influence like soil moisture, snow, interception and sap flow which have not been considered in all details in previous work. The magnitude of the hydrological influences depends on the location of the water mass in relation to the gravimeter, which is somehow problematic in Moxa, because the gravimeter is placed in a building at the end of a steep and more than 40 m high slope on the valley floor of a small catchment. As a result, most of the terrain surface north, west and east of the observatory is higher than the gravimeter's location.

Because the gravity data contain integrated information of hydrological mass shifts (Kroner and Jahr, 2005), the signal can be a valuable source for hydrologists for model assessment and validation. Some preliminary assessments and experiments from scientists from Jena, Göttingen, and Wageningen (NL) have show that the gravimeter signal can be used for hydrological model validation and process studies.

To obtain more information about the soil moisture variations and their influences on the gravimeter data, the catchment was equipped with five FDR probes which record soil moisture variations in different depths on different locations. Additionally a soil mapping campaign was carried out to provide better soil information as a baseline for hydrological modelling.

In addition to these measurements, the hydrological model J2000 (Krause 2002) was parameterised and applied in an hourly mode in the period from the 19th of February to the 4th of October 2004. The period was selected because complete time series were available. Due to the short length of the time period, no model calibration was performed; moreover, the parameters obtained in daily mode in a

catchment nearby were transferred. As a result, the model produces a poor fit of the basin's runoff (Figure 1) with a significant overestimation of the high flood peak and the following periods. The basic idea was not to set up a perfect model for the catchment to reproduce the runoff at the outlet but to obtain spatially distributed values of the models state variables. In particular, spatially distributed values of soil water content for the entire catchment were estimated for comparison with measured values to determine if the soil moisture dynamics are reproduced more or less correctly. Additionally, the modelling approach was intended to serve as a baseline to investigate and identify specific model components that need to be modified to be suitable for the small and dynamic catchment of the Silberleite.

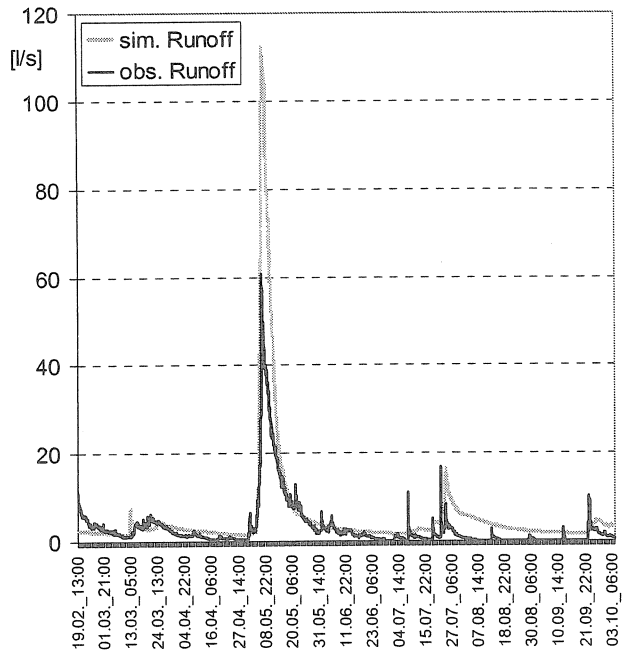

Figure 1: Observed and simulated runoff

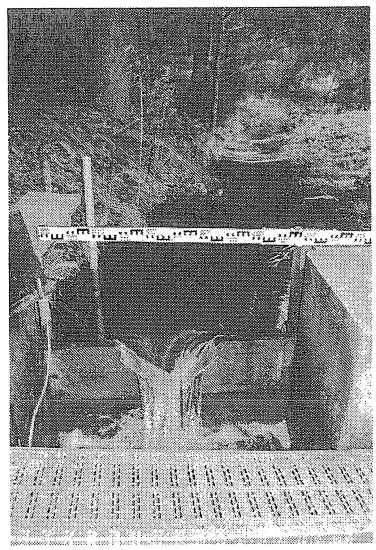

Figure 2: V-notch Silberleite

3. The Moxa test site

The Moxa test site is located in Thuringia, Germany 30 km south of Jena. In the 1960s, a seismological observatory was established at the Moxa site near the outlet of a small catchment drained by a small creek, the Silberleite. In 1999, the observatory was equipped with a superconducting gravimeter for geophysical monitoring of the earth's temporal gravity field variations. Because such an instrument is affected by climatological influences (e.g. temperature, air pressure, humidity), a climate station was installed on the roof of the building to monitor rainfall, air pressure, temperature, relative humidity, wind speed and wind direction. The water level of the Silberleite is recorded with a diver beside a V-notch near the observatory (Figure 2) and the runoff volume is measured once per day manually.

The catchment of the Silberleite has an area of 1.9 km² and is shown in Figure 3. It has elevations range between 540 m to 450 m at the outlet. As shown in the map, nearly the whole catchment is covered by coniferous forest and only two small parts are used as agricultural areas (west and east).

The geological underground consists of crystalline schist (Lower Carboniferous) and is strongly fractured in the top layer. Because of tectonic reasons, the fractures are mostly oriented vertically resulting in preferential flow paths for fast infiltration of subsurface water. It has to be noted that the valley floor between the observatory and the Silberleite has been filled up with debris resulting from the construction of the observatory and a tunnel for geophysical measurements. This debris can be considered an ideal and very permeable groundwater aquifer which drains water from/to the stream bed.

The soil types have been mapped recently to produce a high resolved soil map (Scholten et al. 2004) which is based on more than 30 soil profiles. The soils are mostly silty to loamy with partly significant clay fractions and a considerable rock fraction. At the valley floors, groundwater influenced soils can be found. For the entire area, 15 different soil types have been distinguished and parameterised during the mapping campaign.

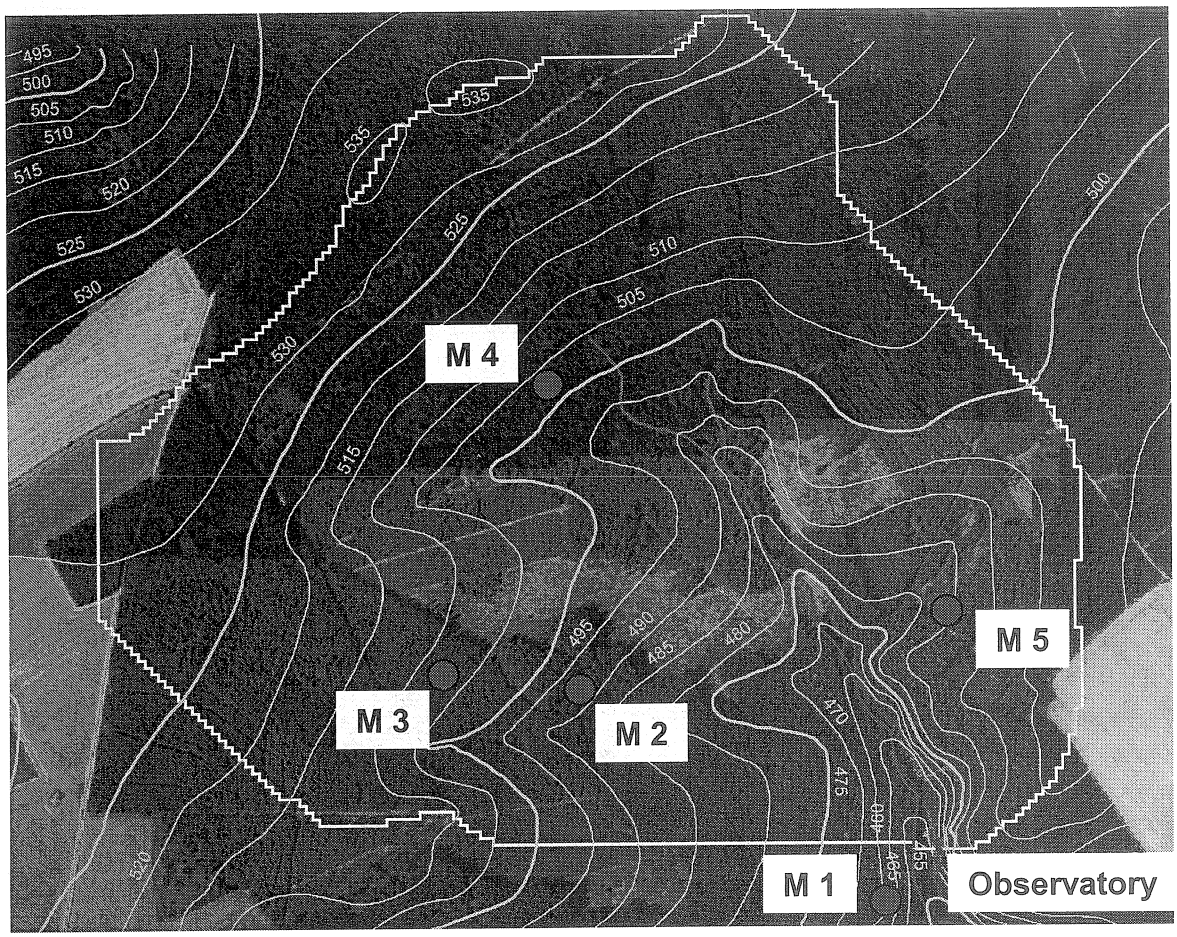

Figure 3: The catchment of the Silberleite, the soil moisture measurement sites and the observatory.

4. The superconducting gravimeter

The superconducting gravimeter (SG), installed in 1999 in Moxa, belongs to a world-wide network of 21 instruments (Crossley et al., 1999) which monitor variations of the earth's gravity field. The principle layout of the SG consists of a Niob sphere which levitates in a defined null position in a magnetic field generated by superconducting coils. Whenever a mass change above or below the gravimeter occurs, the sphere tends to move in direction of the mass increase. The voltage which is needed to keep it at the null position is recorded as relative gravity change. Because of the sensitivity of the instrument, it is affected by various influences such as barometric pressure, earth tides, polar motion, instrumental drift and hydrological influences. For all influences beside hydrology, models exist by which the gravity readings can be reduced resulting in the residual gravity which is referred to in this paper. Because of the complexity and variability of the hydrological processes, it is difficult to apply simple correction terms to remove the hydrologic influences. Some approaches for stochastic correction can be found in Kroner (2001) and Kroner and Jahr (2005). A more promising way would be the use of a hydrological model combined with in situ measurements to simulate all relevant hydrological processes distributed with a certain degree of precision. The development and application of such a model is the main objective of the current project carried out by the authors of this paper.

5. Soil moisture measurements

To provide a base for the assessment of the influence of soil moisture on the gravimeter signal, five Frequence Domain Reflectrometry (FDR) C-Probes have been installed in the catchment. The locations were selected in such a way that an understanding of the distribution of the soil moisture variations could be obtained by the measurements. Therefore, locally distributed sites with different soil types were selected for instrumentation. Unfortunately, the slope east of the observatory, which has the major influence on the gravimeter signal, was not permeable enough for an installation. The FDR installations are marked as red dots in Figure 3.

The FDR-Method is based on the measurement of the dielectrical capacity of the surrounding medium. Soil moisture measurement relies on the fact that the dielectrical constant of the mineral soil (3-5) is significantly different than that of water (~78). The installed probes create an electrical signal with a frequency that depends on the dielectrical constant of the surrounding and can be directly related to soil moisture.

The C-probes (Figure 4, ADCON) allow the installation of up to six single sensors each at different depths. Each probe is installed in the soil in a plastic tube and integrates a radius of 10 cm which is equivalent to a soil volume of 1.9 l. Because the signal strength is decreasing with distance, it can be assumed that 95% of the signal stems from the surrounding 5 cm. During the installation of the probes, great care must be taken to ensure that the soil material is disturbed as little as possible. The uncertainty of such sensors is reported to be less than 5% if they are properly calibrated.

Additionally, each C-probe was equipped with a precipitation gauge with an accuracy of 0.2 mm. The temporal interval of the soil moisture and precipitation recording was set to 15 minutes and the recordings are transferred via telemetry network directly to the observatory from which are can be acquired via a modem. The installation was established in June 2004 and has worked nearly without failures since then.

Figure 4: C-Probe used for soil moisture measurement.

5.1 Soil moisture readings and simulation

In the following paragraphs, the soil moisture readings from the 25th of June to the 4th of October 2004 will be presented and discussed. Additionally, the conceptual model J2000 (Krause, 2002) was parameterised and applied in hourly time steps for the period of the 19th of February to the 4th of October 2004. Due to the short time period, the model was not calibrated very well which is obvious from the comparison of simulated and observed runoff (Figure 1).

The soil module of J2000 simulates the soil water balance integrated over the entire soil profile of each spatial unit with two storage units defined by the different pore volumes: A middle pore storage (MPS) is defined by the useable field capacity and a large pore storage (LPS) is defined by the air capacity of the soil. The water from infiltration is distributed between the storage units based on the saturation of the MPS. As a result, the amount of infiltration to the MPS is higher when there is less water stored in MPS and vice versa. MPS can only be depleted by evapotranspiration, whereas LPS is the source for percolation and interflow. In the following sections, the relative saturation of MPS and LPS together are compared to measured soil moisture time series.

Location M1 is situated in the South-East just beyond the catchment border. The location is approximately 50 m away from the Silberleite, but some 7 to 10 m above the creek itself. The soil was mapped as cambisol with a loamy silt texture with reasonable loess contingents. It has an average depth of 60 to 70 cm. The topsoil has a depth of 4-5 cm, followed by a 45 cm B-horizon, followed by a 5 cm thick C-horizon. The A and B horizons consist of silt with large clay contents, whereas the C-horizon consists of loamy to sandy silt. The rock fraction is 30% in the B and 75% in the C-horizon.

Location M1 was equipped with a C-probe with four sensors in 10, 30, 50 and 70 cm. The recorded volumetric water contents [in %], the precipitation and the simulated volumetric soil water content at the location are shown in Figure 5. From the figure the rising water content with increasing depth can be seen as well as the decreasing dynamics.

The deepest sensor shows a strong reaction at single precipitation events in August and September which it did not show at the beginning in June and July where more precipitation was recorded. The same behaviour can be observed for the sensor in 50 cm in July. This can be interpreted as fast preferential flow through the soil profile through macro pores or by lateral inflow of interflow or a combination of both processes. The modelled soil moisture, which is an integrated value of the whole soil profile, was in the range of the measurements, but shows a damped dynamic. The peaks during the pre-

cipitation events are simulated but not reproduced very well. This may be due to the model conceptualisation, which does not consider preferential flow in macro pores.

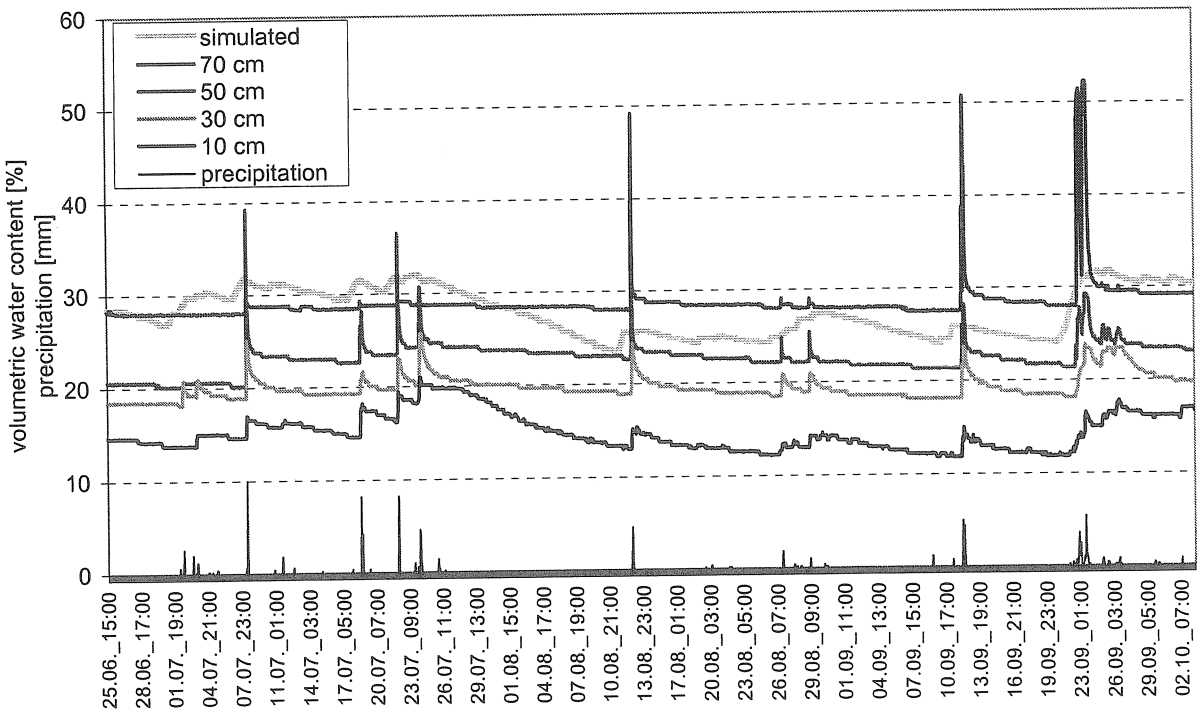

Figure 5: Observed volumetric soil water content in different depths, precipitation and simulated soil water content at location M1.

Location M2 is situated North-West of M1 and about 40 m higher on the slope. The soil was mapped as cambisol with clayey silt texture in the upper horizons and sandy to loamy silt in the C-horizon. It has an average depth of ~ 60 cm. The topsoil has a depth of 7 cm, followed by a 35 cm B-horizon a 15 cm C-horizon. The rock fraction is 15% in A, 22% in B and 30% in the C-horizon. The location was equipped with a C-probe with five sensors covering a depth from 10 down to 60 cm. The observed and simulated volumetric soil water content is shown in Figure 6.

In comparison to M1 this location shows a more dynamic behaviour of the soil moisture, in particular at the upper sensors. This could partly be explained by the higher precipitation rates resulting from a less dense tree cover at this location. A second explanation can be seen in the location up hill, which results in less lateral inflow. Similar to M1, M2 shows a fast reaction of the lower sensors on precipitation. The simulated soil water content at this location shows, again, a damped dynamic and a slight overestimation at the beginning of the period. In the middle, the volumes match with the recordings despite the ridge at the end of August and beginning of September which was only a small peak in the recording. The reason for the ridge in the modelled soil water may be related to the missing macro pore consideration in the model and possible underestimation of interception.

Location M3 is located about 50 m upslope from M2. It is a very flat site at which nearly no lateral inflow is thought to occur. The soil was mapped as cambisol with clayey silt texture in all horizons. It has an average depth of ~ 60 cm, with a topsoil of 6 cm, followed by a 54 cm B-horizon. A C-horizon was not mapped. The rock fraction is 30% in the B-horizon. The observed and simulated volumetric soil water content is shown in Figure 7.

The recordings at M3 exhibit a behaviour which is surprisingly non-dynamic. All sensors show very low fluctuations throughout the entire period. The modelled soil water content is much more dynamic than the readings but is more or less in the same range. A further investigation of the measurement equipment may be needed for this location.

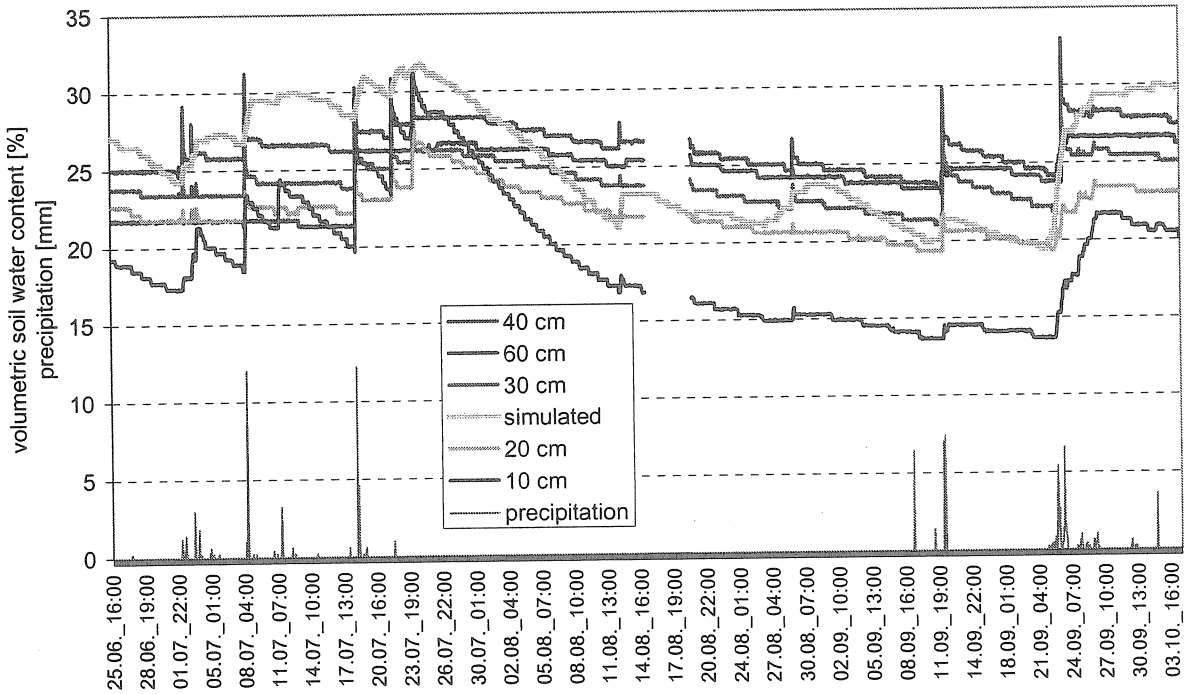

Figure 6: Observed volumetric soil water content in different depths, precipitation and simulated soil water content at location M2.

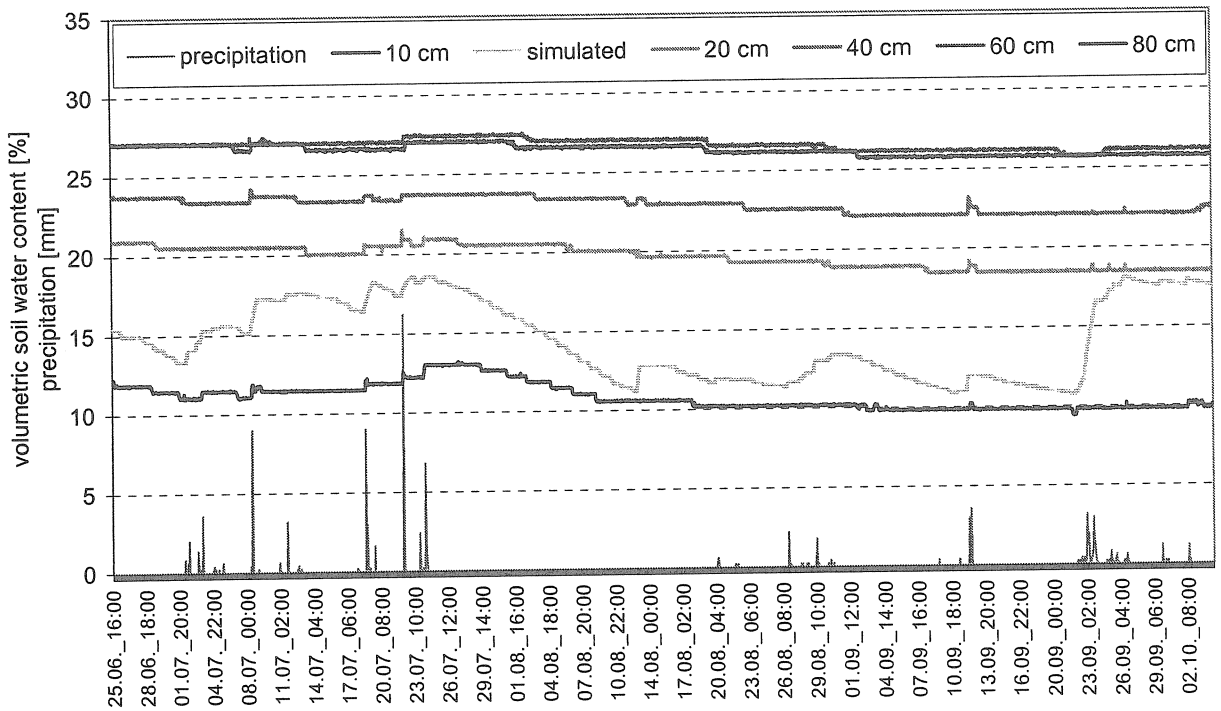

Figure 7: Observed volumetric soil water content in different depths, precipitation and simulated soil water content at location M3.

Location M4 is situated east of the spring area of the Silberleite in the northern part of the catchment about 10-15 m above the creek. The soil was mapped as a stagnic gleysol made of clayey silt in the upper horizons and clay in the lowest one. It has an average depth of 40 to 50 cm, with a topsoil of 5 cm, followed by a 30 cm Bg1-horizon and a 6 to 10 cm Bg2-horizon. A C-horizon was not mapped.

The rock fraction is low with ~10% in the Bg1-horizon. The observed and simulated volumetric soil water content is shown in Figure 8.

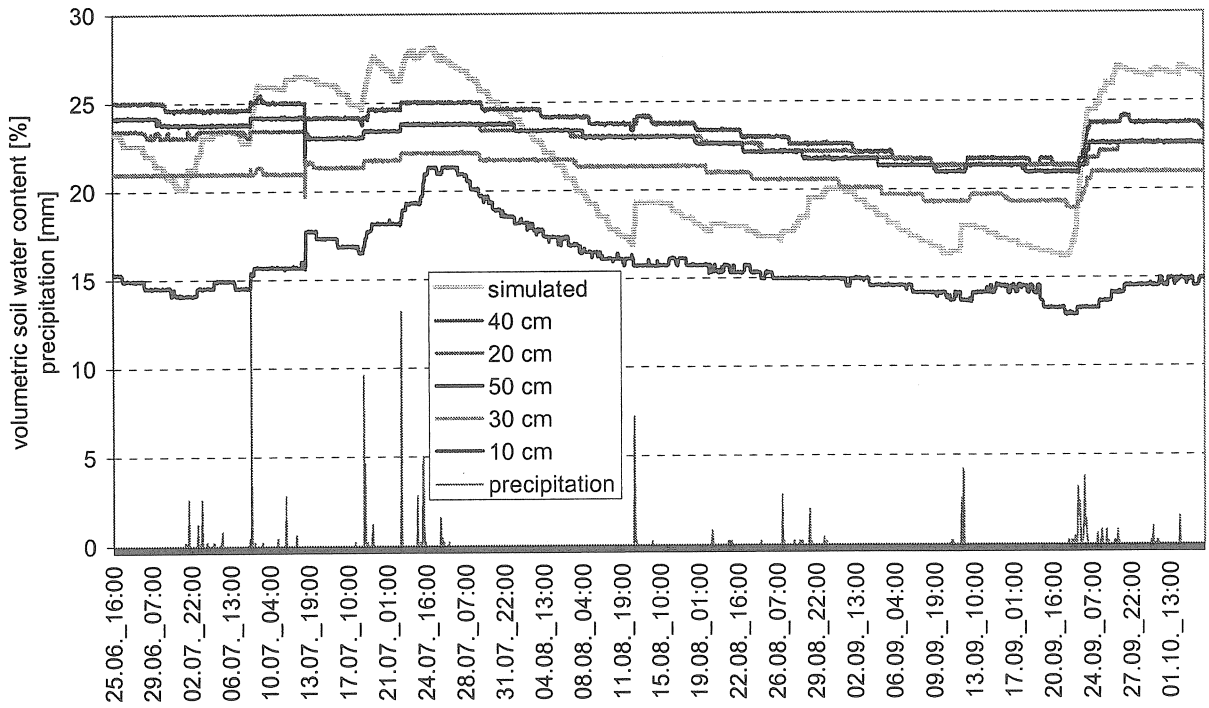

Figure 8: Observed volumetric soil water content in different depths, precipitation and simulated soil water content at location M4.

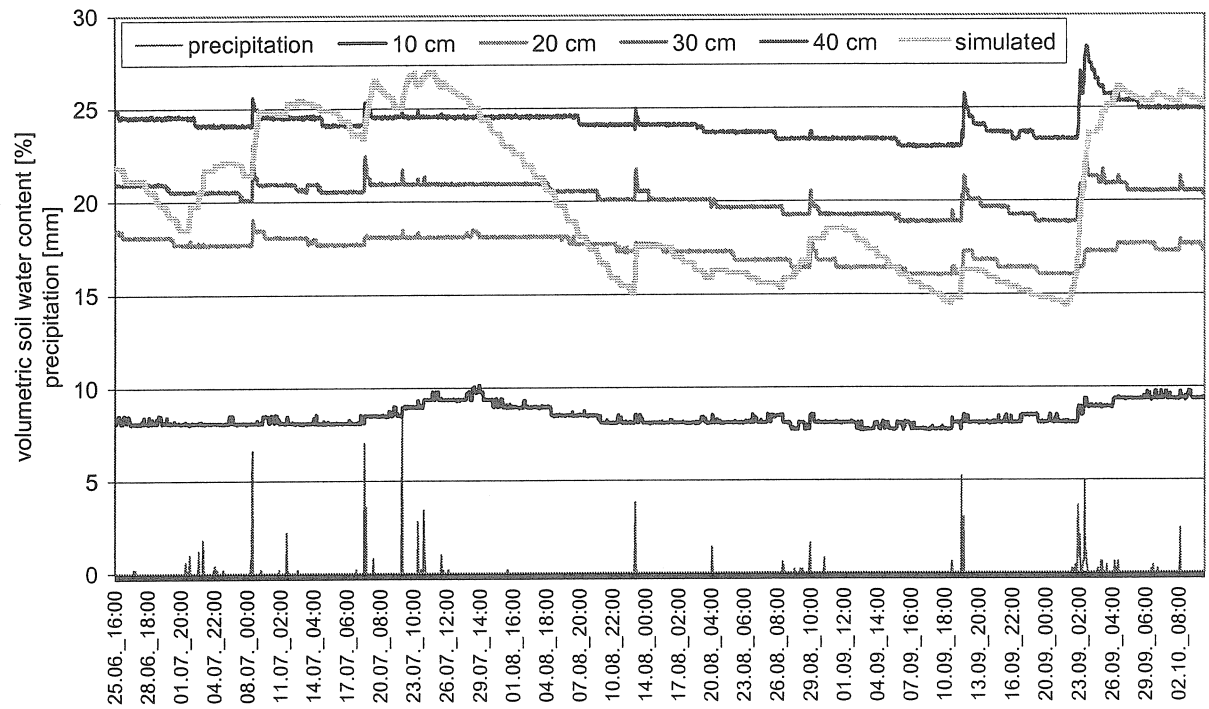

Figure 9: Observed volumetric soil water content in different depths, precipitation and simulated soil water content at location M5.

The recordings at M4 show a dynamic behaviour in the upper 10 cm which is more and more damped with increasing depth. The dynamic reaction of the lower sensors during precipitation events seen at the M1 and M2 sites was not found at this site. This may be due to the stronger saturation throughout the entire period preventing fast preferential flow through the soil. The modelled soil water content is,

again, much more dynamic but more or less in the correct range. In particular, the drying trend in the modelled simulation during August and September can only be seen as a slight trend in the recordings. The wetting conditions simulated with the model due to the precipitation at the 23 of September can be observed in the recordings of the lower sensor but with dampened amplitude.

Location M5 is situated in the eastern part of the catchment north and above the observatory. The soil was mapped as a cambisol with silty loam texture in all horizons. The soil has an average depth of 50 to 60 cm, with a topsoil of 22 cm, followed by a 20 cm B-horizon and a 9 to 10 cm C-horizon. The rock fraction is higher than in the other profiles with ~50% in the B-horizon and ~70% in the C-horizon. The observed and simulated volumetric soil water content is shown in Figure 9.

The recordings at M5 show a very steady behaviour in all depths. In the middle and at the end of the period, quick reactions of the lower three sensors on single precipitation events can be observed. The drying up after an event is much slower than it was in M1 and M2. The topsoil of the profile is very dry throughout the entire period and reacts only very slightly on precipitation events. The simulated soil water content at M5 shows a strong drying of the soil profile during July and September resulting in a dynamic behaviour which can not be seen in the sensor readings. For the most part, the modelled soil water content is in the range of the measurements and single events are simulated, but most of the time the amplitude is too large.

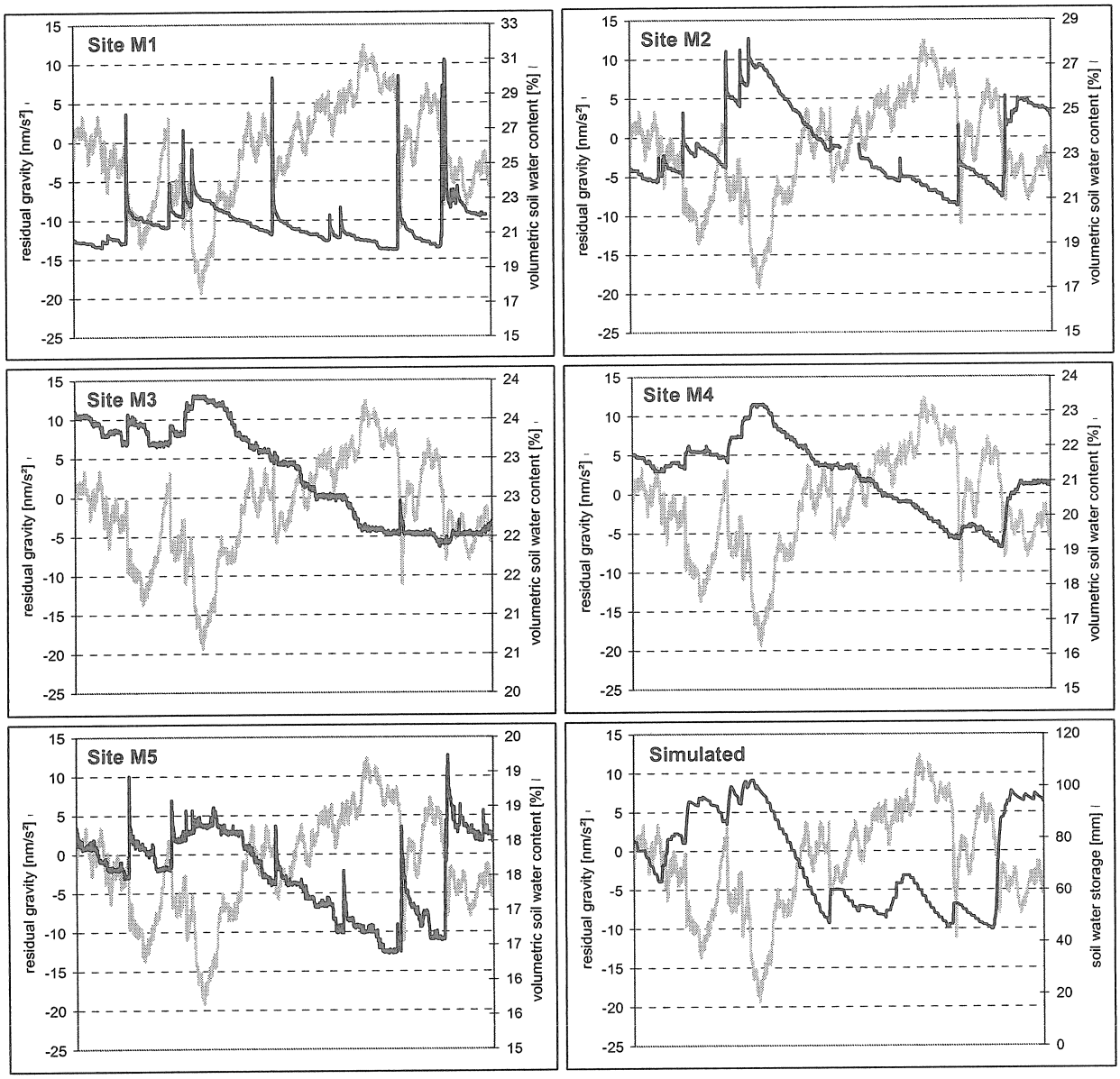

Figure 10: Comparison between residual gravity (grey), measured soil water content (black) at site M1 to M5 and simulated soil water storage as catchment mean for the period between 25.06.04 and 2.10.04.

6. Gravimeter readings and hydrological processes

The next step was the comparison between the residual gravity and the measured and simulated soil water contents. The results of the comparisons are shown in Figure 10. For each plot, a depth weighted mean time series for each site was calculated from the readings of the single sensors and plotted against gravity. It has to be noted that for the second y-axis, different resolutions were set to produce a better view of the dynamics. Additionally, the modelled soil moisture content as a catchment average was used for the comparison. Because M1 and M2 are the closest sites to the observatory, they are of higher interest than M3 and M4 which are further away. Site M5 is also of major importance because it is the only site which lies on the same side of the Silberleite and it has the same soil type as the slope above the observatory.

The inverse behaviour of the gravity reading compared to soil moisture can be clearly seen in the figure. This is most obvious during the continuous decrease of soil moisture of the fairly dry period in the middle of the time series which results in a continuous increase in the gravity data. The heavier rainfalls at the end of the period are replenishing the soil moisture storages leading to a decreasing gravity. This can be seen at the plots of site M2, M4, M5 but also in the simulated soil moisture. From the figure, the immediate reaction of the gravity readings on soil moisture changes can also be seen. This is most obvious at the two low gravity recordings in the first third of the time series. Here, single precipitation events are producing a direct reaction of the gravimeter signal in form of a sharp decrease in the reading that flattens a little bit after several hours.

7. Discussion

A more detailed view of the processes is provided in Figure 11 for twelve days at the beginning of the period. The measured precipitation at the observatory is plotted against the residual gravity and the measured soil water content at site M2.

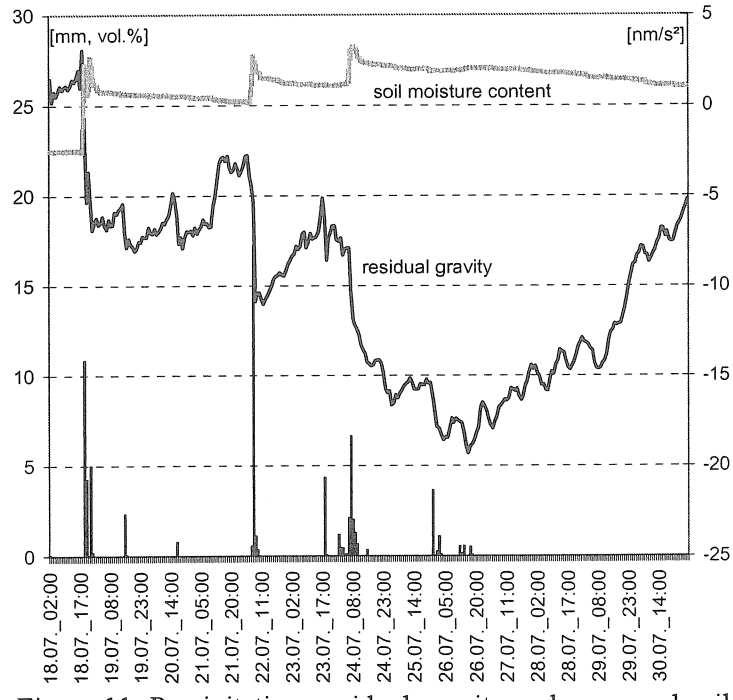

Figure 11: Precipitation, residual gravity and measured soil water content at site M2

This can be interpreted as mass movement from above the gravimeter as a combination of hydrological processes: (1) When precipitation occurs it is stored as interception or on top or inside the topsoil. The mass of the water leads to a sudden decline of the gravity reading. During the rain event nearly no evapotranspiration from this water occurs, but some of the water infiltrates into the soil profile. (2) When precipitation stops the intercepted water is continuously evaporated from the plant surface and the topsoil which leads to an increase in the gravimeter readings because of the mass reduction a top of it. (3) Water which has infiltrated into the soil profile is partly taken out by plant transpiration and partly percolating into the withering zone of the underlying bedrock. As shown at site M1 the process of fast percolation due to preferential flow paths is important in the catchment. Transpiration and percolation leads again to an increase of the gravity reading because of reduced mass. (4) Water in the withering zone percolates partly into the bedrock in fissures and fractures and is partly moving down-slope as interflow, which again leads to an increase of the gravity reading. (5) Once the water has reached a level below the gravimeter level gravity increases due to the additional mass below the instrument. The described behaviour is reproduced during the events at site M1, M2 and M5 and can also be reproduced with the simulated soil water storage. Kroner and Jahr (2005) described an irrigation experiment coupled with measurements in the vicinity of the gravimeter which is further evidence that the assumptions are correct.

Beside soil moisture, other hydrological processes e.g. snow accumulation, interception and groundwater can have significant influence on the gravimeter reading, which are not addressed in this paper but are currently being investigated at the Moxa site by the authors of this paper.

8. Conclusion

In this paper, the influence of soil moisture on the residual gravity monitored by a superconducting gravimeter (SG) in Moxa, Germany was shown. Measured soil moisture readings from five sites have been compared with the residual gravity of the SG. In addition, the distributed hydrological model J2000 was applied in the catchment to (1) provide a comparison between measured and simulated soil moisture values and (2) to provide distributed model results for the entire catchment. The modelling results showed that the J2000 was able to reproduce the range and trend of the soil moisture variations at the five sites. The comparisons of the observations of soil moisture with the J2000 estimates indicate that the model estimates are generally in the same range of the observations but contain a dynamic variability that is generally not observed in the data. Further analysis of the gravimeter signals and the in situ measurements should provide a means for further improvement of the model simulation capabilities in future work.

The findings of the study underpin the importance of soil moisture variations for the explanation of the hydrological influences on the gravimeter signal. A clear reaction of the residual gravity due to soil moisture variations was detected. This was most evident during single precipitation events where an increase of soil moisture could be observed which could be correlated to a sharp drop of gravity at the SG. During longer dry periods when the soil moisture decreases slowly, a slow recover of the gravity signal could be observed.

Acknowledgement: Thanks to Douglas Boyle (DRI, Reno, Nevada) for many advices and proof reading of this paper.

9. References

Crossley, D., J. Hinderer, G. Casula, O. Francis, H.-T. Hsu, Y. Imanishi, G. Jentzsch, J. Kääriäinen, J. Merriam, B. Meurers, B. Richter, K. Shibuya, T. Sato and T. van Dam, 1999: Network of superconducting gravimters benefits a number of disciplines, EOS Trans. Am. Geophys. Union 80 (11)

Harnisch, M. and G. Harnisch, 2002: Seasonal variations of hydrological influences on gravity measurements at Wettzell, Bull. d'Inf. Marées Terr. 137, 10849–10861.

Krause, P., 2002: Quantifying the impact of land use changes on the water balance of large catchments using the J2000 model, Physics and Chemistry of the Earth 27 (2002), 663-673

Kroner, C., 2001: Hydrological effects on gravity data of the Geodynamic Observatory Moxa, J. Geod. Soc. Japan vol. 47 no. 1, 353–358.

Kroner, C. and T. Jahr, 2005: Hydrological Experiments around the superconducting gravimeter at Moxa Observatory, Journal of Geodynamics (accepted)

Lambert, A. and C. Beaumont, 1977: Nano Variations in Gravity due to Seasonal Groundwater Movements; Implications for the Gravitational Detection of Tectonic Movements, J. Geophys. Res. 82, 297-305

Scholten, T., T. Behrens, H. Dahlke, H. Förster, K. Gülland, H. Kika, J. Lippelt, U. Poppe & K. Schmidt (2004): Bodenkundliche Karte 1:10.000 für das Einzugsgebiet der Silberleite am Geodynamischen Observatorium Moxa. Friedrich-Schiller-Universität Jena.

Inclinometry and geodesy: an hydrological perspective

Proceedings of GGP Workshop, Jena, March 27-31 2006

Laurent Longuevergne [1 2] , Nicolas Florsch [2] , Frédéric Boudin [3] , Thierry Vincent [4] , Michel Kammenthaler [4]

Abstract

Two orthogonal, precise and low drift tiltmeters have been installed in the Vosges mountains in order to study environmental surface loading. The first results show the great sensitivity (10^{-10} radians), stability (negligible drift) of the instrument, and its ability to be used as a tool to study hydrological loading. This work focuses on local and regional hydrological physical modelling, with a stepwise refinement of mass balance calculations on a geodetic purpose. We show that meteorological forcing mainly drives stock variations inside a hydrological unit, it is therefore necessary to take great care of precipitation and evapotranspiration. Uncertainty assessment on stock variations is also raised, and shows that hydrological models bring good estimation of short term water stock variations, but that long term geodetic variations provide complementary information for stored water modelling.

Keywords : tiltmeter, catchment, hydrological modeling, precipitations, evapotranspiration, uncertainty assessment.

[1]Corresponding author, E-mail: laurent.longuevergne@ccr.jussieu.fr
[2]UMR Sisyphe, Université Pierre et Marie Curie, Paris, France
[3]Institut de Physique du Globe, Paris, France
[4]Volunteer

1 Introduction

TheGGP Workshop on analysis of geodetic data geodynamic signals and environmental influences, which took place in Jena in March 2006 showed the growing interest of the geodetic community to understand hydrological contribution on geodetic signals. Several different approaches to the problem have been presented, depending on the goal of the study:

A geodetical approach:

- remove hydrological noise from time series in order to search out external and internal dynamical phenomenon (Kroner et al., this issue),
- validate satellite-derived gravity observations with ground observations, in this case, only local contribution has to be removed (Hinderer et al., this issue).

A hydrological approach:

- Provide a complementary tool to study local and regional hydrology, indeed geodesy is a "direct" measurement of total mass variation of water (Naujoks et al., this issue),
- validate global hydrological models in the case of GRACE measurements (Neumeyer et al., this issue).

If points of view are various, we are confronted to the same difficulties. First, the question of spatial scales to be taken into account is inseparable of environmental signals (Llubes et al., 2004) since meteorological forcings are distributed on the earth surface. Another difficulty, for local scale in particular, is the way of describing the complex nature of stored water variations with sufficient precision and only a few measurements. Several lines of research have been explored:

- Study correlations between environmental observations and calibration on geodetic data. The problem is that correlation does not give a satisfactory systematic description of hydrological contributions, since it depends on the phenomena that are integrated in the study (Tervo et al., this issue). Generally, environmental signals are mixed and correlated - in particular annual signals.
- Extract global signal thanks to data processing, using a set of observations at different locations (Crossley et al., this issue).
- Isolate hydrological processes and understand water flow, by implementing full scale tests (Kroner et al., 2004) or by measuring stored water with an independent method (Kügel et al., this issue).
- using hydrological models (Krause et al., this issue), for each spatial scale. This is the most difficult solution, but allows to answer to a lot of questions (for example, separation of spatial scales (Virtanen et al., this issue), etc)

This work opts for physical modelling and is illustrated by tilt data collected by a new instrument installed in the Vosges Mountains. A stepwise refinement of water mass balance calculations is applied on regional stored water variations, and could be extended to local modelling. Physical processes are first described - in particular hydrometeorological forcings that drive mass balance equation. Then conceptual hydrological models are introduced in order to describe more accurately mass variations. Finally, uncertainty assessment on stock variations is raised.

Table 1: Order of magnitude of the regional hydrological contribution in Sainte-Croix-aux-Mines

Phenomenon	Time span	Equivalent water height [mm]	Amplitude [nrad]
Storm	1 hour	20	20
Winter rainfall	1 day	20	20
Beautiful days	1 week	-20	-5
Catchment stocking-destocking	1 year	200	50
Instrument resolution	1 measure	0.1	0.1

2 Tiltmeter: a privileged instrument for surface loading studies

2.1 Scale invariance of tilt deformation field

Tiltmeters are a privileged geodetic instruments for studying surface loading since they are sensitive to all local, regional and global scales (Rerolles et al., 2006). In this sense they are a little different from gravimeters that are only sensitive to global and local scales (Llubes et al., 2004).

For instance, an analytical solution of tilt loading T can be calculated from green tilt functions (Pagiatakis, 1990), for local and regional scales (see figure 1) when dealing with a full layer water Δh loading uniformly a ribbon which width is b at a distance r of the instrument $||T|| = 2.k(0).\Delta h.ln(1 + b/r)$. The tilt effect can be written as a separated function of the mechanical behavior of the crust $k(0)$, the geometry of the ribbon and the equivalent height of a full water layer. The scale invariance is illustrated by this example since the deformation is linked to the ratio between the surface and the distance of the loading mass.

In table 1 we can see that hydrology induces geodetic signals at all time scales. Moreover, 1 mm rainfall is equivalent to a 1 nrad tilt deformation because precipitation are concentrated in the bed of the valley. For longer term variations, the whole valley should be taken into account. Notice that the $10^{-10} nrad$ resolution of the tiltmeter that has been installed is at least 1 order of magnitude better than awaited deformations due to hydrology.

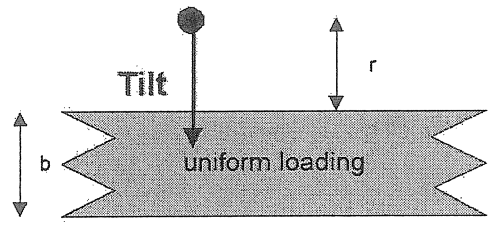

Figure 1: Top view of surface loading on a valley.

2.2 New tiltmeters installed for this study

Two orthogonal hydrostatic long base tiltmeters designed by Frederic Boudin from IPGP have been installed in an old mine in the Vosges Mountains, right in front of BFO observatory. Figure 2 shows the hourly and daily raw data of the tiltmeter. No drift can be extracted from this data for the moment, and this is due to the perfect coupling that has been achieved between rock and instrument.

Observed monthly rainfall and water flow of a nearby river are also presented. We can see poor correlation between observed tilt signal and rainfall. On the contrary, tilt is really close to the water flow of the nearby river since water flow is an integrative measurement of the amount of water in a system - what geodesy sees too. During last winter, there was a really poor precipitation rate. Precipitation only occured in March, that's why tilt - and water flow - signals did not get higher before the beginning of March.

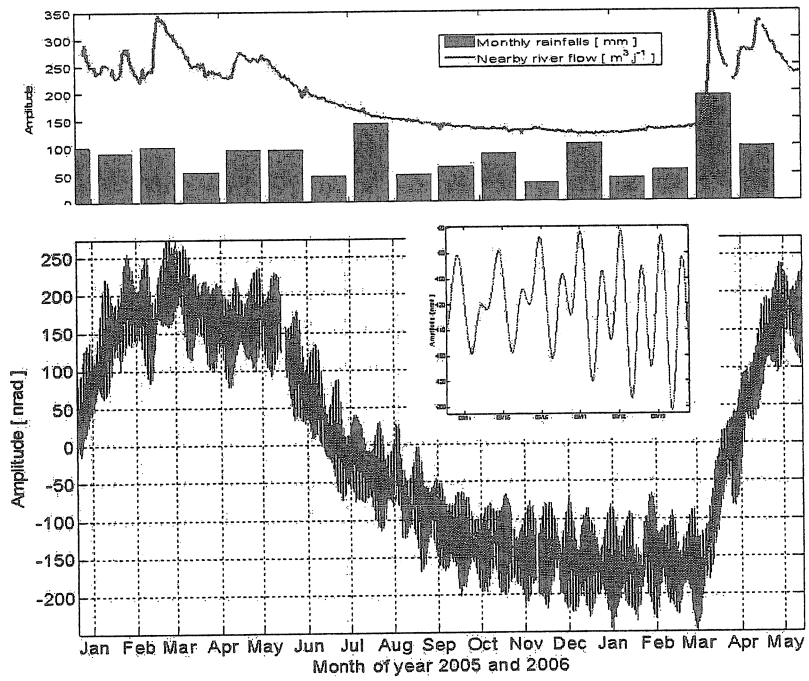

Figure 2: Above: Monthly rainfall and water flow of a nearby river. Underneath: First-year measurements (decimated hourly and daily data from 30sec data).

3 Modelling hydrology on geodetic purpose

3.1 Mass balance

3.1.1 Definition of an hydrological unit

Before mass balance equation is used, an hydrological unit should be defined: the catchment, which is first designed as a topographic catchment (see figure 3). As a consequence, we are almost sure that each water drop falling within the catchment frontier goes out at the single outlet i.e. the gauging station. Mass balance ΔW can be written as $\Delta W = P - ETR - Qs - Qg$, where P is precipitation, ETR is real evapotranspiration, Qs and Qg are respectively surface flow and groundwater flow out of the hydrological unit. On the one hand, rainfall and surface flow can be measured, real evapotranspiration can be evaluated; on the other hand, groundwater flow is difficult to measure or evaluate, but represents around 2 to 10% of surface flow, so for the moment, it can be neglected. Hydrologists are used to distribute this stock ΔW on the catchment area $S_{catchement}$, so stock is expressed as an equivalent full water layer Δh in millimeters, or, it is the same, in kilograms per square meter. Next subsections present major difficulties in calculating mass balance in a catchment.

The Liepvrette catchment (see figure 3) is 100 km^2. The presence of snow caps should be noted and need a special modelling tool in order to take into account this mass of water that does not

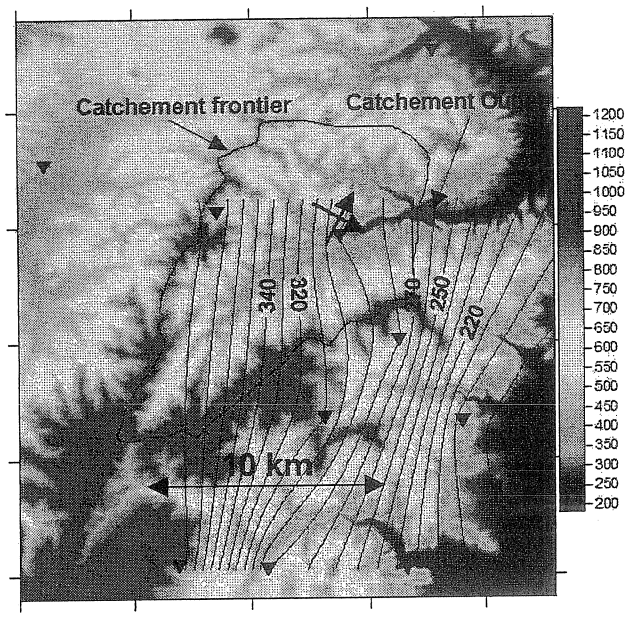

Figure 3: Topography of the Liepvrette valley. Both arrows show the directions of the 2 tiltmeters. The Black line rounding the summits is called the topographic catchment, its single outlet (red triangle) is equipped with the gauging station. Superposed isolines 100 days cumulative rainfall in mm, used rain gauges seen as blue triangles.

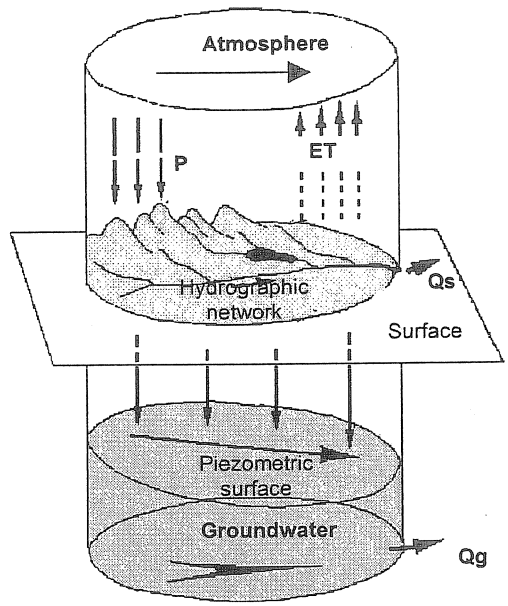

$$\Delta W = P - ET - Qs - Qg$$

$$\Delta W = \Delta h . S_{catchement}$$

Figure 4: sketch showing water circulation at catchment scale and associated mass balance equation.

stream immediately (Degree day, HBV tool, etc). One other important property is the 1 day concentration time, i.e. the mean time, fallen precipitation take to escape from the catchment. This time limit separates transient and quasi-static behavior of the hydrologic system.

3.1.2 Precipitation variability

One major uncertainty in catchment hydrology is the variability of precipitation field, which is significant in mountainous areas. Figure 3 shows 100 day total precipitations and its variability over the catchment. In this case, a single measure near the instrument underestimates the precipitation near the crest of 40%, and so induces a 20% mass loss in the balance.

3.1.3 Evapotranspiration

Another difficulty is dealing with evapotranspiration. From observed meteorological forcing (temperature, wind speed, insolation) potential evapotranspiration (PET) can be estimated using different approaches: temperature methods (e.g. Thornthwaite formula), radiation methods (e.g. Turc's approach) and combination methods (e.g. Penman - Monteith). It is called potential because this calculation represents the evaporing power of atmosphere. Evaluating real evapotranspiration (RET) is then a bit more difficult since it depends on the water available in the soil for the vegetation.

Turc's law was developed in Western Europe for regions where relative humidity is greater than 50%. This law only need information on temperature and duration of insolation. Daily potential evapotranspiration in $mm.day^{-1}$ can be written as $ETP = 0.013\frac{Tm}{Tm+15}.(Rg + 50)$ where Tm is the mean daily temperature, Rg is the daily global solar radiation in $kJ.m^{-2}.day^{-1}$ dependent on the duration of insolation and the astronomical solar insolation which can be found in tables. For 45 degrees

Table 2: Order of magnitude of potential evapotranspiration in millimeters calculated by Turc's law and translated for tiltmeters

	Summer	Winter
Potential evapotranspiration	$3-4\ mm.day^{-1}$	$0-1\ mm.day^{-1}$
	$1\ nrad.day^{-1}$	$0\ nrad.day^{-1}$

Table 3: Annual variation of stored water in millimeters for different evapotranspiration calculations and translated for tiltmeters. RET is estimated using GR4J rainfall-runoff model (see next chapter)

	2002 – 2003	5-year mean
ET = RET	290 mm	190mm
	70 $nrad$	45 $nrad$
ET = PET	420 mm	230 mm
	100 $nrad$	55 $nrad$
ET = 0	250 mm	80 mm
	65 $nrad$	20 $nrad$

latitude situations, potential evapotranspiration is 0 to 1 mm a day in winter and 3 to 4 mm a day in summer (see table 2).

This is an important issue because it does change the annual amplitude in stocked water. When calculating mass balance with observed rainfall and water flow, for different evapotranspiration cases (see table 3), great differences are found. For the Liepvrette catchment, a 5-year mean shows that the annual term of water balance is 20 % smaller when using real evapotranspiration than potential evapotranspiration, but twice as important as ignoring evapotranspiration. When dealing with exceptionally dry years, real annual term is 30 % smaller when using real evapotranspiration than potential evapotranspiration, but only 20 % greater than without evapotranspiration. Indeed, in summer 2003 no water was available for vegetation to make it evaporate.

3.1.4 Temporal contribution and Water budget

Figure 5 shows the temporal cumulative contribution of each meteorological forcing on water balance. Evapotranspiration is a very annual term, water flow is also annual in opposite phase, but also contains short term variations. The water balance can then be calculated by subtracting the sum of these two last terms and cumulative precipitation. Rainfall brings major part of short term contribution, then, for longer term contribution, evapotranspiration and water flow should be considered. Annual amplitude contributions is presented in table 4.

3.1.5 Stock estimation on geodetical purpose

On a temporal point of view, water balance variations are driven by meteorological forcing. So, it is important to correctly appreciate precipitations and evapotranspiration before starting hydrological modelling. Then, water flow outside the hydrological unit is important because it contains short term as well as long term contribution.

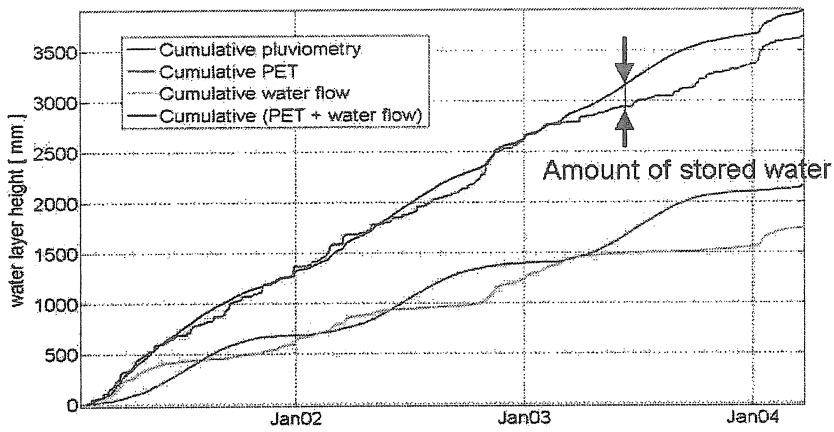

Figure 5: Cumulative temporal contribution of precipitations, evapotranspiration and runoff.

Table 4: Mean annual water budget for Liepvrette catchment.

Mean annual rainfall	$1100mm$
Mean annual PET	$700mm$
Mean annual runoff	$500mm$
Mean annual budget	$-100mm$?

We will show (see figure 8) that a simple calculation of mass balance using sound precipitation and evapotranspiration gives a good first order evaluation of local or regional water stock variation in a single hydrological unit.

Finally, a geometrical model is necessary to distribute the calculated full layer water height on the hydrological unit. Figure 6 is obtained under the assumption that mass variations are concentrated in the bed of the valley. The discrepancies between the model and observations are certainly due to the fact that internal processes (inside the hydrological unit) of water redistribution are not taken into account.

3.2 Hydrological models

In order to calculate more precisely longer period contribution, real evapotranspiration and groundwater flow should be evaluated, so it is necessary to use hydrological models. This section focuses on catchment modelling. For land surface schemes and soil modelling, please refer to GSWP project http://www.iges.org/gswp/ .

3.2.1 Overview of hydrological models

As far as catchment hydrology is concerned, two kinds of hydrological models can be chosen.

On the one hand, conceptual models describe the global behavior of a catchment using simplification of physical processes. Its major advantage is that they contain a few parameters, so they are very robust. Unfortunately it is difficult to extract internal processes because of the poor physical meaning of the model. Some models can be cited, depending on the major processes that should be taken into account: GR4J (Perrin et al., 2003), Topmodel (Beven et al., 1979), Sacramento (Burnash et al., 1973),

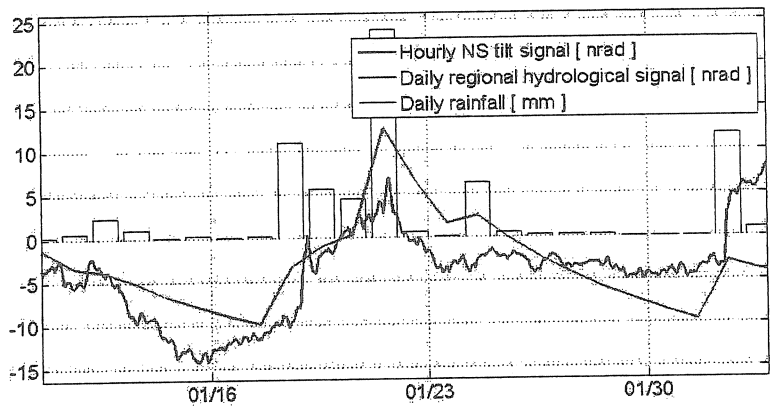

Figure 6: Controntation between observed tilt signal and modelled tilt signal. Note that time sampling is not identical.

HBV (Bergstrm et al., 1973), IHACRES (Jakeman et al. , 1990). A geodetic application was attempted by (Yamauchi, 1987).

On the other hand, physical models can be used. They have a theorical advantage, but contain too many parameters and are not very robust. One other advantage is that these models describe water circulation processes, so the position of the water masses are known. For example SHE (Abbott et al., 1986), SWATCH (Morel-Seytoux et al., 1989). The semi-distributed hydrological model presented by (Krause et al., this issue) is intermediary.

3.2.2 Calibration

Hydrological models are designed to represent catchment behavior at basin outlet, so they are calibrated on stream flow data, and hydrologists traditionally use the nash criteria F which is a quadratic index (Nash et al., 1970):

$$F = 1 - \frac{\Sigma(Q_{observed} - Q_{simulated})^2}{\Sigma(Q_{observed} - E(Q_{observed}))^2}$$

A perfect model is marked 1, a good model is greater than 0.6 and F is negative for bad models. A long time serie is often needed, because most information are contained in extreme situations (shallow water, high water, quick streaming, etc)

Hydrologists often adopt a parsimonious behavior towards hydrological modelling because a 3 or 4-parameter model is sufficient to correctly describe stream flow at basin outlet (Beven, 1989, Sorooshian, 1991). Indeed, flow data does not contain all information about internal processes of the catchment (Ambroise, 1991, Grayson et al., 1982).

3.2.3 Application of GR4J rainfall-runoff model

A first experimentation is to apply a conceptual model. For example, GR4J (Perrin et al. 2003) is a 4-parameter model describing flows within a catchment with 2 buckets (so called "soil" bucket or production store, and "groundwater" bucket or routing store), discharge laws and delay laws (see figure 7).

Precipitation is first intercepted (evapotranspiration is subtracted). The soil bucket is then used to calculate real evapotranspiration as a function of the level of the production store. Discharge and / or excess of precipitation is divided into two flow components according to a fixed split: 90% is routed by a unit hydrograph UH1 (delay law) and then a non linear routing store (interpreted as groundwater

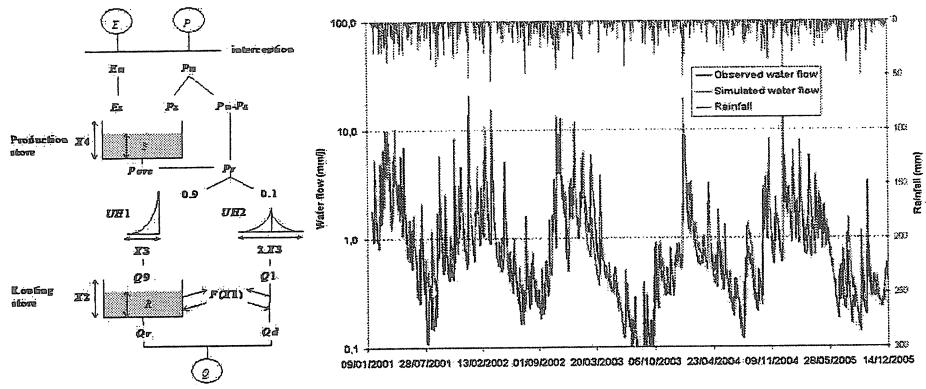

Figure 7: Left: Description of internal processes of GR4J. Right: Observed and simulated water flow using GR4J

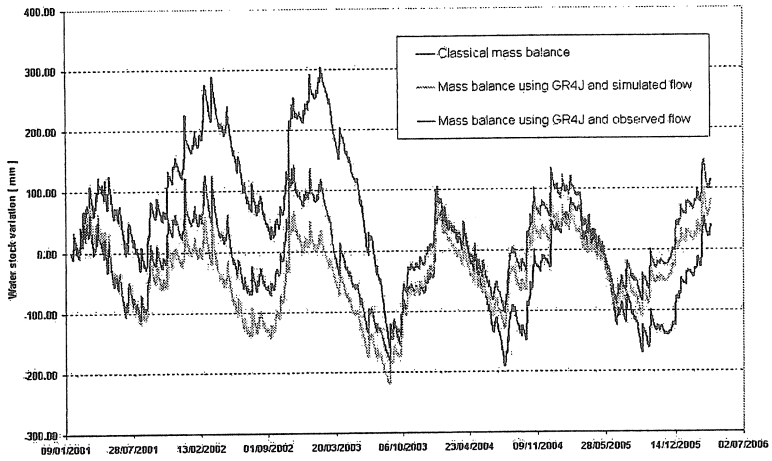

Figure 8: Variation of stored water calculated using 3 differents methods. A linear trend has been removed

store), the remaining 10% is routed by a single unit hydrograph UH2 direct to basin outlet. A groundwater exchange term (that can be interpreted as groundwater flow out of the hydrological unit) is also calculated.

The model has been calibrated on the logarithm of the water flow (see figure 7) in order to describe the annual variations as correctly as possible. Nash criteria is 0.8 which is very good.

3.3 Stored water variations

Stored water within the catchment for 3 cases is shown in figure 8. The blue one is classical mass balance, where processes are respected, but amplitudes are overestimated. The green and red curves are calculated using GR4J rainfall runoff model, either using modelled water flow or observed water flow. We can see the differences, and next question is: Can we evaluate uncertainty on stored water variations?

4 Assessing uncertainties in for stored water variations

This question of uncertainty assessment in hydrological modelling is now a central theme for hydrologists. It is a necessity for two reasons: In terms of likelihood, multimode in model parameter distribution is often observed, and equifinality is often obtained between models when dealing with stream flow data.

A few statistical methods exist, for example First-order approximations near global optimum (Kuczera et al.), Generalized Likelihood Uncertainty Estimation (GLUE) method (Beven et al.), Markov Chain Monte Carlo (MCMC) methods (Vrugt et al.), Pareto Optimization Methods (Hoshin et al.). In this work the application of the SCEM-UA algorithm is presented. This is a Bayesian inversion algorithm designed to infer the traditional best parameter set and its underlying posterior distribution by launching parallel Markov chains.

Figure 9 shows the most likely model and the uncertainty according to a 95 % parameter confidence interval. Stream flow is correctly described by the model. One problem is that the observation are seldom inside the uncertainty interval. Two reasons are to be put in an obvious: the fact that uncertainties on observations have not been taken into account, and that a 4-parameter model is unable to provide more information than given in this case.

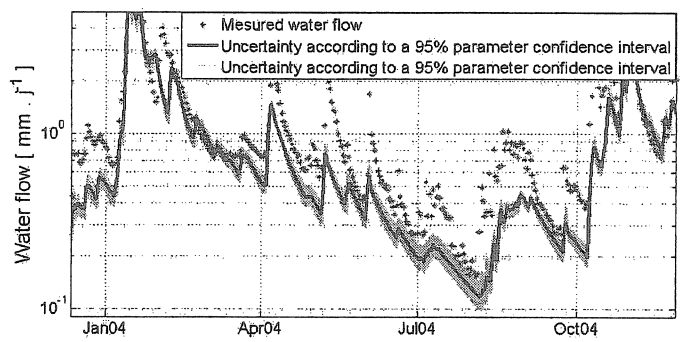

Figure 9: Most likely model (in blue) and uncertainty associated to water flow modelling (green) according to a 95 % parameter confidence interval. Red dots are water flow measurements.

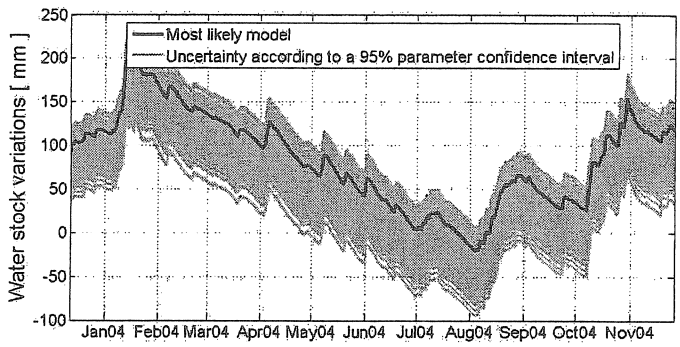

Figure 10: Most likely model (in blue) and uncertainty associated to modelled stored water variations (green) according to a 95 % parameter confidence interval.

When looking to stored water variations (see figure 10), it is interesting to note that short term is correctly described but cumulative errors appear when dealing with stored water variations, particularly in summer if low water stream is not correctly described. In this case geodesy could bring information to longer period variations, for the annual water budget in particular.

5 CONCLUSION

This work focuses on regional (and local) hydrological physical modelling, with a stepwise refinement of mass balance calculations. Water balance variations are driven by meteorological forcings; hence it is important to correctly evaluate precipitation and evapotranspiration. For short term stored water variations (1-2 days), precipitation is a major contributor, for longer term variations, evapotranspiration and water flow outside the hydrological unit must be taken into account. Simple conceptual hydrological models, calibrated on water flow measurements, allow a more accurate description of nonlinear processes, i.e. real evapotranspiration and groundwater flow out of the catchment. Uncertainty assessment on stock variations is also raised. It shows that hydrological models bring good estimation of short term water stock variations, and that long term geodetic variations could provide complementary information for stored water modelling.

Acknowledgments:

The authors want to thank Corinna Kroner and the organization staff in Jena for this GGP Workshop. This study, has been carried out within the framework of the ECCO-PNRH program "Hydrology and Geodesy".

References

[1] *Abott, M.B., Bathurst, J.C., Cunge, J.A., O'Connel, P.E. et Rasmussen, J. (1986). An introduction to the European Hydrological System - système hydrologique européen, SHE, 1. History and philosophy of a physically-based, distributed modelling system, J. Hydrol., 87, 45-59.*

[2] *Ambroise, B. (1991). Hydrologie des petits bassins versants ruraux en milieu tempéré - processus et modèles. Séminaire du Conseil scientifique du Département Science du Sol de l'INRA Dijon, 26-27 mars 1991.*

[3] *Bergström, S. et Forsman, A. (1973). Development of a conceptual deterministic rainfall-runoff model. Nordic Hydrology, 4, 147-170.*

[4] *Beven, K.J. et Kirkby, M.J. (1979). A physically based, variable contributing area model of basin hydrology. Hydrological Sciences Bulletin, 24(1), 43-69.*

[5] *Beven, K. (1989). Changing ideas in hydrology - The case of physically-based models, J. Hydrol., 105, 157-172.*

[6] *Beven, K. (1993). Prophecy, reality and uncertainty in distributed hydrological modelling, Adv. in Water Resources, 16, 41-51.*

[7] *D.S. Bowles et P.E. O'Conel (eds.), NATO ASI Series C, vol. 345, 443-467, Kluwer Academic Publ.*

[8] *Burnash, R.J.C., Ferral, R.L. et McGuire, R.A. (1973). A generalized stream flow simulation system - Conceptual modelling for digital computers, U.S. Department of Commerce, National Weather Service and State of California, Department of Water Resources.*

[9] *Crossley, D., Hinderer, J., Boy, J.P., De Linage, C. (2006): Status of the GGP satellite project, thi issue.*

[10] *Jakeman, A.J., Littlewood, I.G. et Whitehead, P.G. (1990). Computation of the instantaneous unit hydrograph and identifiable component flows with application to two small upland catchments. Journal of Hydrology, 117, 275-300.*

[11] Grayson, R.B., Moore, I.D. et McMahon, T.A. (1992). Physically Based Hydrologic modelling, 1. A terrain-based model for investigative purposes, Water Resour. Res., 28(10), 2639-2658.

[12] Hinderer, J., De Linage, C., Boy, J.P.(2006): How to validate satellite-derived gravity observations with gravimeters at the ground?, this issue

[13] Krause, P., Fink, M., Kroner, C., Sauter, M., Scholten, T. (2006): Hydrological processes in a small headwater catchment and their impact on gravimetric measurement, this issue.

[14] Kroner, C., (2006): Hydrological effects in the SD record at MOXA - a follow up, this issue.

[15] Kügel, T., Harnisch, G., Harnisch, M., (2006): Measuring integral soil moisture variations using a geoelectrical resistimeter, this issue.

[16] Llubes, M., Florsch, N., Hinderer, J., Longuevergne L., Amalvict, M. (2004): Local hydrology, the Global Geodynamics Project and CHAMP/GRACE perspective: some case studies, Journal of Geodynamics 38, 355374.

[17] Morel-Seytoux H, Alhassoun S. (1987). SWATCH. Swiss watershed model for simulation of surface and subsurface flows in stream-aquifer system. Department of Civil Engineering, Colorado State University, 297 p.

[18] Naujoks, M., Kroner, C., Jahr, T., Weise, A.(2006): From a disturbing influence to a desired signal: Hydrological effects in gravity observations, this issue.

[19] Nash, J.E. et Sutcliffe, J.V. (1970). River flow forecasting through conceptual models, 1, A discussion of principles, J. Hydrol., 10, 282-290.

[20] Neumeyer, J., Barthelmes, F., Petrovic, S.(2006): Preparation of gravity variations derived form Superconducting Gravimeter recordings, GRACE and hydrological models for comparison, this issue

[21] Pagiatakis, S. D. (1990). The response of a realistic earth to ocean tide loading. Geophys. J. Int. 103: 541-560.

[22] Perrin, C., Michel, C., Andrassian, V. (2003). Improvement of a parsimonious model for stream flow simulation, Journal of Hydrology 279(1-4), 275-289.

[23] Rerolle, T., Florsch, N., Llubes, M., Boudin, F., Longuevergne, L. (2006): Inclinometry, a new tool for the monitoring of aquifers?, Comptes-Rendus de l'acadmie des sciences, accepted.

[24] Rodell, M., P. R. Houser, U. Jambor, J. Gottschalck, K. Mitchell, C.-J. Meng, K. Arsenault, B. Cosgrove, J. Radakovich, M. Bosilovich, J. K. Entin, J. P. Walker, D. Lohmann, and D. Toll (2004), The Global Land Data Assimilation System, Bull. Amer. Meteor. Soc., 85 (3), 381-394, 2004.

[25] Sorooshian, S. (1991). Parameter estimation, model identification and model validation: conceptual-type models. In Recent advances in the modelling of Hydrologic systems,

[26] Tervo, M., Virtanen, H., Bilker-Koivula, M.(2006): Environmental loading effects on GPS time series, this issue.

[27] Virtanen, H., Tervo M., Bilker-Koivula, M.(2006): Comparison of superconducting gravimeter observations with hydrological models of various spatial extents, this issue

[28] Vrugt J.A., H.V. Gupta, W. Bouten, and S. Sorooshian (2003). A Shuffled Complex Evolution Metropolis algorithm for optimization and uncertainty assessment of hydrological model parameters, Water Resources Research, 2003

[29] Yamauchi, T., (1987) Anomalous strain response to rainfall in relation to earthquake occurrence in the Tokai area, Japan. Journal of Physics of the Earth, 35: 19-36.

Influence of the Hohenwarte reservoir on tilt and strain observations at Moxa

Holger Steffen* and Georg Kaufmann
Institute of Geological Sciences, FU Berlin
Malteserstr. 74-100
D-12249 Berlin / Germany

Abstract

The Geodynamic Observatory Moxa is located around 4 km to the north of the Hohenwarte reservoir, a medium-sized artificial reservoir, holding on average 182 Mill. m^3 of water. The data of the installed seismometers and strainmeters at Moxa are successfully used for studies of the Earth's interior structure and properties. It is possible to observe tilt changes in the range of 10^{-9} rad and displacement changes of 10^{-9} strain.

We explore the possibility that registrations of the seismometers and strainmeters are influenced by deformation changes induced by lake-level fluctuations of the Hohenwarte reservoir, both on a short-term seasonal time scale and a long-term decadal time scale. We use the Finite Element method to calculate deformations in vicinity of the Hohenwarte reservoir. We show that the influence of lake-level fluctuations of up to 30% to tilt and strain registrations at the observatory is larger than the resolution of the instruments, with differences of at most 48 nrad for the tilt and 6 nstrain for the strain. Thus, at the location of Moxa, the influence of lake-level changes on the registrations is significant.

1 Introduction

Artificial reservoirs are important for flood protection, for providing drinking water and for the generation of electricity. Besides that, the filling of reservoirs with water induces a load on the Earth's surface, deforming the crust and mantle and producing tilt and strain deformations. These deformations have been studied extensively in the literature (see Steffen & Kaufmann, 2006, for a review).

The Hohenwarte reservoir in the southeast of Thuringia is the 3rd largest reservoir in Germany with a volume of 182 Mill. m^3, covering an area of 7.3 km^2. The

*E-Mail: hsteffen@zedat.fu-berlin.de

dam was built between 1936 and 1943, and put into operation in 1941. The balance reservoir is the Eichicht reservoir in the west with a volume of 5.21 Mill. m^3 and an area of 0.71 km^2 (Fig. 1). In 4 km distance to the reservoir, the Geodynamic Observatory Moxa is situated, equipped with sensitive seismometers and strainmeters. With these instruments it is possible to observe tilt changes in the range of 10^{-9} rad and displacement changes of 10^{-9} strain. We explore the possibility that registrations of the seismometers and strainmeters are influenced by deformation changes induced by lake-level fluctuations of the Hohenwarte reservoir. We therefore use the Finite Element (FE) method to calculate the deformations in vicinity of the Hohenwarte reservoir.

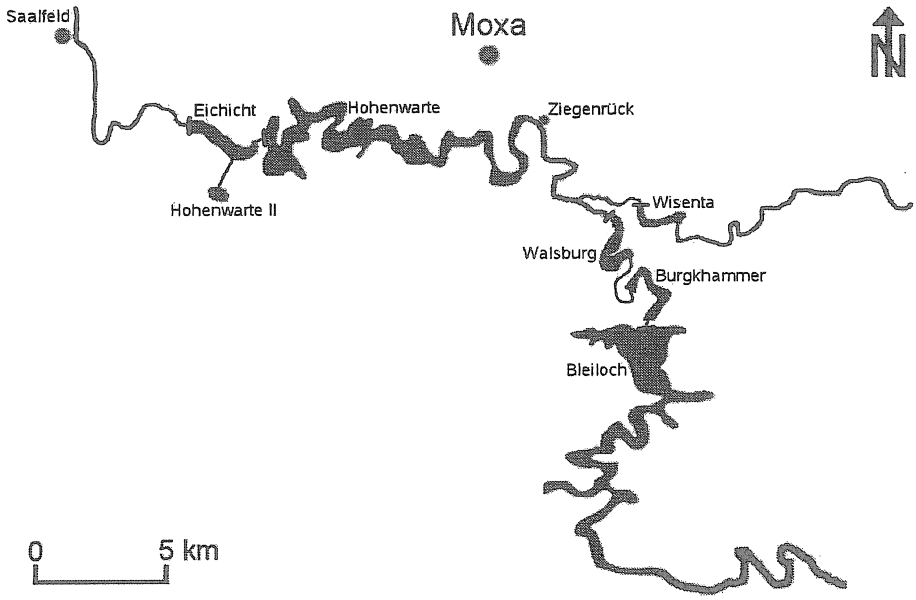

Figure 1: Overview of the reservoirs along the river Saale in the southeast of Thuringia, Germany, and the location of the Geodynamic Observatory Moxa.

2 Model description

We model the water impounded in the Hohenwarte reservoir as surface load on a flat, viscoelastic earth by means of the FE method. The Earth model is a cube with 100 km side length, consisting of a 25 km thick crust and the 75 km thick upper mantle. For the crust a linear, elastic rheology and for the upper mantle a viscoelastic rheology is used. The viscosity for the upper mantle is set to 5 x 10^{20} Pa s, taken as an average of upper-mantle viscosities beneath Europe (Steffen & Kaufmann, 2005). Thus, this model allows the relaxation of stress in the upper mantle. The material parameters and

the dimensions for the element layers are summarised in Steffen & Kaufmann (2006). The model is meshed with 130000 hexahedra elements. The central area, between 40 and 60 km in each horizontal direction, is meshed using elements with a horizontal side length of 250 m. The remaining 10 element rows of the 40 km wide peripheral frame have a variable side length from short side lengths near the center to long side lengths for the outer elements.

The full water load of 182 Mill. m^3 for Hohenwarte and of 5.21 Mill. m^3 for Eichicht is applied uniformly over the shape of each reservoir (Fig. 2), which is approximated by 135 (Hohenwarte) and 14 (Eichicht) element surfaces of the central area. Thus, the reservoir areas correspond to 8.44 km^2 and 0.88 km^2, respectively. The load is generated by dividing the water volume of each reservoir by the modelled area, multiplied with water density (1000 kg/m^3) and gravity (9.81 m/s^2). The full load of the Hohenwarte and the Eichicht reservoir corresponds to constant water columns of 22 m and 6 m, respectively.

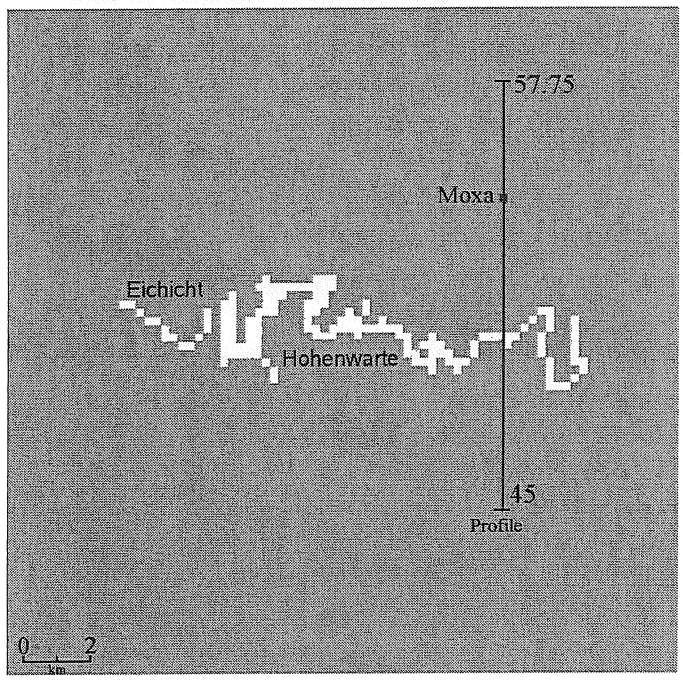

Figure 2: Top view of the model center (20 km x 20 km) with the shape of the reservoirs (white) and the profile for the deformations. The location of the observatory is marked. Numbers indicate locations in km relative to the entire grid of 100×100 km used.

The load initially increases linearly over 2 years, after the dam was closed in 1941. This simulates the filling of the reservoir starting at 0% of water volume and ending after 2 years with a maximum water volume of 100%. Then, two cycles of lake-level changes simulating the annual hydrological cycle follow (Fig. 3). Within 6 months, the

reservoir volume is reduced to 70% (summer) and after another 6 months increased again to 100% (winter). After the two cycles the load is kept constant at 100% till the year 2011. With this approximation, it is possible to both study seasonal changes and to save computations time for the long-term evolution until the present.

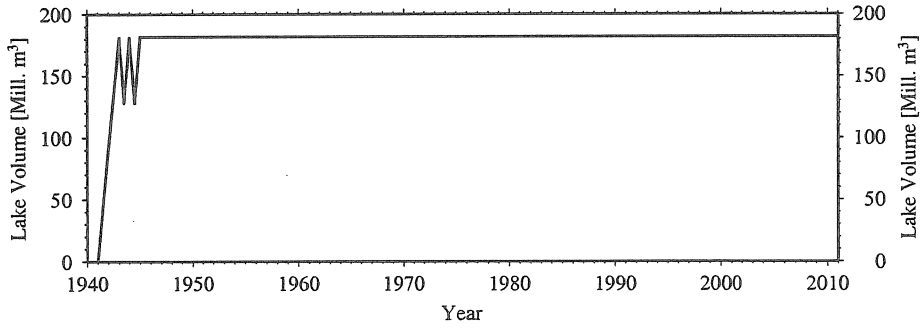

Figure 3: Lake volume as function of time.

3 Results

An extensive study of the deformations in vicinity of the Hohenwarte reservoir can be found in Steffen & Kaufmann (2006). In this study, we focus on the results for Moxa observatory.

The deformation of the model by the time-dependent water load is calculated, and strains and tilts are shown along the profile of Fig. 2. The profile starts south of the reservoir and runs in NS–direction. The location of Moxa observatory is at 54.25 km on the profile.

3.1 Short-term seasonal variations

Tilt: Fig. 4 shows on top the tilt in the NS– and EW–component at different load times. To compare the results, the tilts at different times of an annual cycle are taken when the reservoir is filled-up (winter, solid) and 70%-filled (summer, dotted). The tilt changes on the profile reflect the location of the reservoir and which reservoir border is tangent to the profile. The tilt only shows eye-catching changes when the reservoir is crossed at 50 km. The amplitude is affected by the load sum in the vicinity of each point and is in winter at most 3 μrad northward in the NS–component. Between winter and summer significant differences in the amplitude of the tilts are found. The tilt difference between winter and summer is at most 30% of the full load in winter and therefore a result of the elastic behaviour. Changes in the direction of the tilt are not observed.

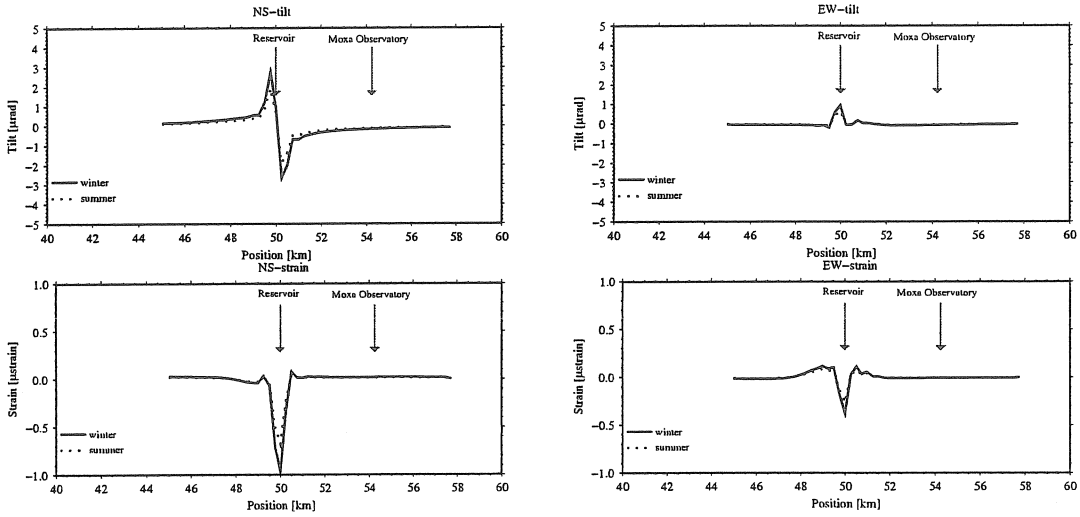

Figure 4: Top: Tilt in the NS– component (left) and EW–component (right) obtained at different load times. Tilt northward and eastward positive. Bottom: Strain in the NS–component (left) and the EW–component (right) obtained at different load times. Extension positive.

Strain: Fig. 4 shows at the bottom the strain in the NS– and EW–component at the two different load times winter (solid) and summer (dotted). The maximum amplitude is found in winter with around 1 μstrain compression. The strain changes reflect the location of the reservoir in compression. The profile demonstrates this behaviour clearly when the reservoir is crossed around 50 km. As for the tilts, between winter and summer significant differences in the amplitude of the strains are found. At the location of the reservoir, the difference between winter and summer is at most 30% of the full load in winter and again a result of the elastic behaviour. No changes in the direction of the strain are detected.

Tilt and strain at Moxa: Tab. 1 summarises for the location of the Moxa observatory the differences in tilt and strain for both components between winter (100%–filled) and summer (70%–filled). The difference in the EW–component is around 22 nrad and in the NS–component around 48 nrad. The strain differences results for the EW–component in only around 2.5 nstrain and for the NS–component in around 6 nstrain. These differences between winter and summer should be observable with the sensitive instruments at Moxa (see Kroner et al., 2005, for a description), if lake-level variations are in the order of 30%.

3.2 Long-term variations

Fig. 5 shows the vertical deformation on the surface at Moxa for the load cycle (Fig. 3). The deformation at Moxa for a full reservoir in winter is about 0.85 mm, and 0.60 mm in summer, when the lake-level is 30% lower. There is clearly no big influence of

Table 1: Difference in tilts and strains in both components between winter and summer at the location of Moxa observatory.

	NS	EW
tilt [nrad]	48	22
strain [nstrain]	6	2.5

the viscoelastic mantle on the vertical deformation due to the loading period of the Hohenwarte reservoir. After 70 years, the viscoelastic part is only about 0.22 μm of vertical deformation. The differences in the vertical deformation induced by short-term load changes are caused by the elastic crust. There is no influence of the viscoelastic mantle on tilt and strain in this case.

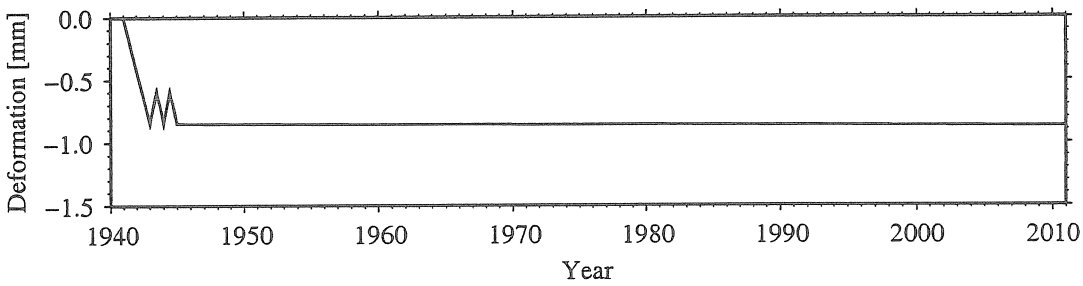

Figure 5: Vertical deformation over 70 years obtained at Moxa.

4 Conclusions

Artificial reservoirs such as the Hohenwarte reservoir in Germany induce additional loads on the Earth's surface. The resulting effects in tilt and strain deformations can be observed with sensitive instruments in the Geodynamic Observatory Moxa, which is located in a distance of 4 km to the reservoir. The influence of lake-level changes on the registrations is significant. For lake-level fluctuations up to 30% tilt and strain differences at the observatory are larger than the resolution of the instruments. Differences of at most 48 nrad for the tilts and 6 nstrain for the strains are established and should be observable. The vertical deformation is more affected by load changes with a difference of around 0.25 mm between winter and summer. The influence of the viscoelastic mantle after a long time-period is negligible.

Acknowledgements

We employ the modelling software ABAQUS. This research was funded by the DFG (research grant KA1723-1).

References

Kroner, C., Jahr, T., Kuhlmann, S. and Fischer, K. D. 2005. Pressure-induced noise on horizontal seismometer and strainmeter records evaluated by finite element modeling. *Geophys. J. Int.* **161**, pp. 167 - 179, doi:10.1111/j.1365-246X.2005.02576.x

Steffen, H. and Kaufmann, G. 2005. Glacial isostatic adjustment of Scandinavia and northwestern Europe and the radial viscosity structure of the Earth's mantle. *Geophys. J. Int.*, **163/2**, pp. 801-812, doi:10.1111/j.1365-246X.2005.02740.x.

Steffen, H. and Kaufmann, G. 2006. Numerical modelling of deformation changes induced by lake-level fluctuations of the Hohenwarte reservoir, Thuringia, Germany. *J. Geodyn.*, 41(4), pp. 411-421, doi:10.1016/j.jog.2005.08.004.

Environmental loading effects on GPS time series

Maaria Tervo, Heikki Virtanen, Mirjam Bilker-Koivula
Finnish Geodetic Institute
P.O. Box 15, 02431 Masala, Finland
maaria.tervo@fgi.fi

Metsähovi is a permanent GPS-station in Finland. It is situated on the south coast, with the distance to the Baltic Sea being only 15 km. The effect of tidal loading is small since its distance to the ocean is 800-1000 km, therefore the other loading effects can be seen more clearly. We have studied the effects of non-tidal loading of the Baltic Sea and loading caused by atmospheric pressure and water storages on solid Earth in the height time series of GPS. When all known factors are taken into account, the variance in the GPS height time series diminishes up to 31%. Regression coefficients for the different factors were found to be –0.2 mm/hPa for the local air pressure, -9 mm/m for the nearby tide gauge recording and -0.05 mm/mm for the total water storage of Finland. The effect of local aquifers and global soil moisture need to be studied more carefully, because all the water storages correlate and give therefore similar results.

1 Introduction

The geographic distribution of atmospheric, hydrologic and oceanic masses varies in time and this in turn loads and deforms the surface of the Earth. The interactions between the solid Earth and the changing masses can be seen in gravity but also in vertical motion observed by GPS. There are several studies on the topic in both gravity and vertical motions. Combination of different loading factors has been studied (Van Dam and Wahr, 1998, Dong et al., 1996), as well as loading by single factors, such as continental water (van Dam et al., 2001, Llubes et al., 2004) or atmospheric loading (Boy et al., 1998, Van Dam et al. 1994). There is also a recent study in non-tidal loading by storm surges (Fratepietro et al., 2006). The loading phenomenon especially in gravity at Metsähovi has been studied before by Virtanen and Mäkinen (2003), Virtanen (2004) and Virtanen (2006). Studies of watersheds with gravity can be found in Virtanen et al. (2006).

We have studied the three best known and most significant loading factors in Finland, namely loading caused by air pressure, by non-tidal sea level changes and by changes in the watersheds. These loading factors are compared and correlated with the vertical motion observed by GPS for a time period of 8 years.

2 Methods

To see different factors and their effects on the vertical movements we have used two approaches. The first one is simple regression, which was used for the loading factor time series with the GPS time series. The second approach was to use Green's function formalism and coefficients to calculate and model the loading and create loading time series. After that the loading was reduced from the vertical movements. The flow chart for the data processing can be seen in figure 1.

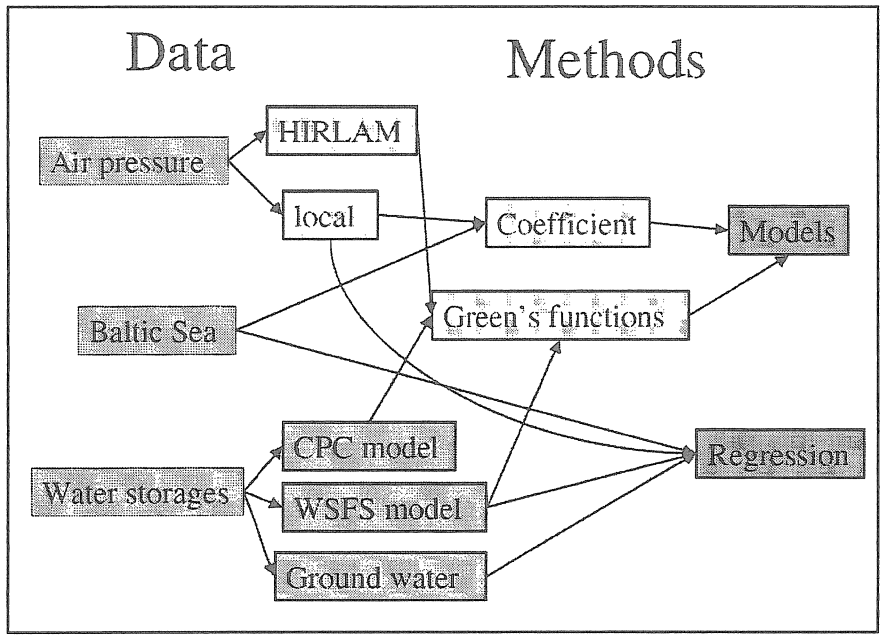

Figure 1. The flow chart for the data processing, on left the different datasets and on right the processing methods used for them. Data will be explained more thoroughly in chapter 3.

3 Data

The GPS time series has been calculated by the IGS process center at Jet Propulsion Laboratory (JPL) (available at http://sideshow.jpl.nasa.gov/mbh/series.html). It is shown in figure 2. The time series has been calculated using the GIPSY software and precise point positioning strategy. We used the radial component from here on referred to as height or vertical motion. The only correction to the data was the removal of the trend mainly caused by post-glacial rebound.

There are two sources of air pressure data. The local air pressure (fig. 3) was measured in Metsähovi next to GPS antenna. The numerical weather model data (High Resolution Limited Area Model, HIRLAM) were provided by the Finnish Meteorological Institute. The HIRLAM model has 6-hourly values and for this study we have used a subgrid that covers about 10° around Metsähovi. The grid size is 44 km × 44 km.

The Baltic Sea level time series is the hourly sea level at the Helsinki tide gauge (fig. 3), measured by Finnish Institute of Marine Research. The tide gauge is about 30 km from Metsähovi, but open sea is only 15 km from the station.

For the water storages there were three different datasets. The local aquifer was observed in a groundwater well at Metsähovi, some tens of meters from the GPS antenna. The regional watershed time series and grids (Watershed Simulation and Forecasting System, WSFS, Vehviläinen and Huttunen, 2002) were provided by the Finnish Environmental Institute, the time series can be seen in figure 3. The WSFS grids were originally daily 1 km × 1 km datasets and they were smoothed to 0.5° × 0.5° grids in this study. The global grid data were taken from the Climate Prediction Center (CPC, Fan and van den Dool, 2004). It is a monthly soil moisture data set with 0.5° resolution. CPC model was chosen because, despite its simplicity, it simulates the interannual variability of soil moisture reasonably well (Dirmeyer et al., 2004)

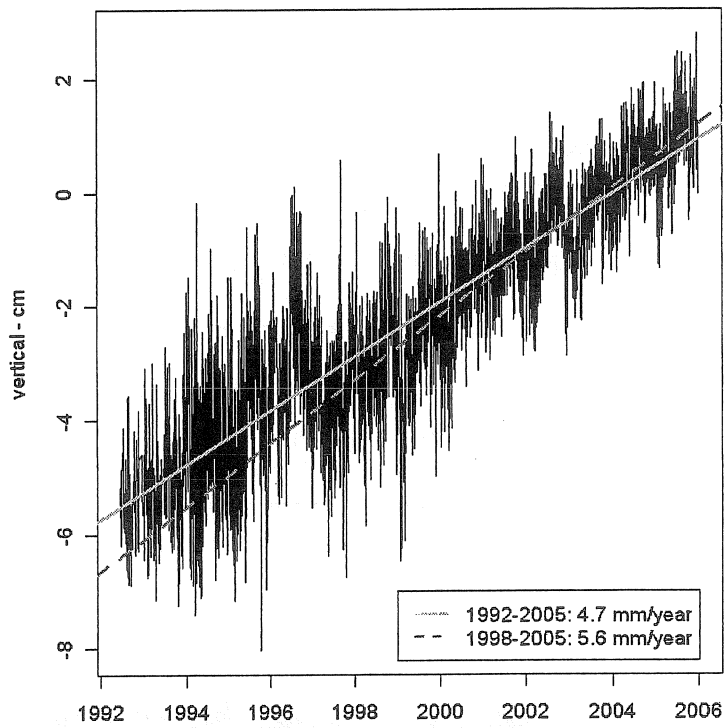

Figure 2. The radial component of Metsähovi IGS time series 04/1994 – 12/2005, computed by JPL.

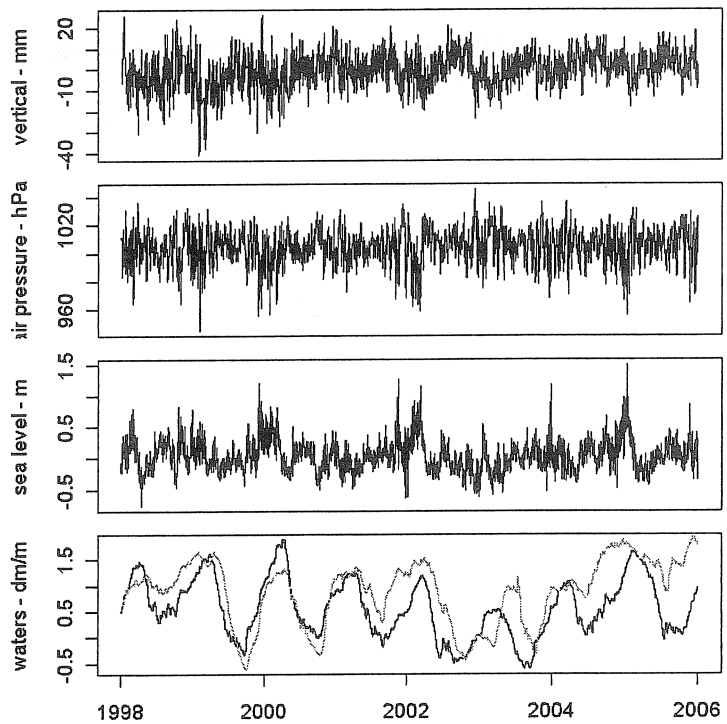

Figure 3. The time series data 01/1998 – 12/2005. On top the GPS height (standard deviation 7.4 mm) of Metsähovi corrected for land uplift, second from top is the local atmospheric pressure, second from bottom the sea level time series of Helsinki tide gauge and at the bottom the total water storage of Finland (black, in dm) and local groundwater in Metsähovi (grey, in m).

4 Loadings

The air pressure and watershed grids were processed to loading time series using Green's function formalism. The watershed calculations were done with the program NLOADF (Agnew, 1997) using the Gutenberg-Bullen Earth model. The CPC grid was used for the whole time span and a mixed model of CPC and WSFS was used when it was available, starting from June 2003. The sea level time series was transformed to loading by using a simple coefficient (-9 mm/m). For reference, a simple coefficient was also used for the air pressure (-0.23 mm/hPa). The coefficients were taken from previous study with superconducting gravimeter (Virtanen, 2004). To correct the apparent annual variation in the GPS time series a fitted sine function has been used at the institute. We have used it as a reference and to be able to compare our results with previous ones. The maximum of the sine is in September and the amplitude is 3.7 mm. Amplitude of the height change due to CPC loading is 3.8 mm and maximum is also in September, meaning that watersheds (and loading caused by them) are at minimum in the autumn. The calculated loadings for the whole time series can be seen in figure 4 and in figure 5 for the year 2004.

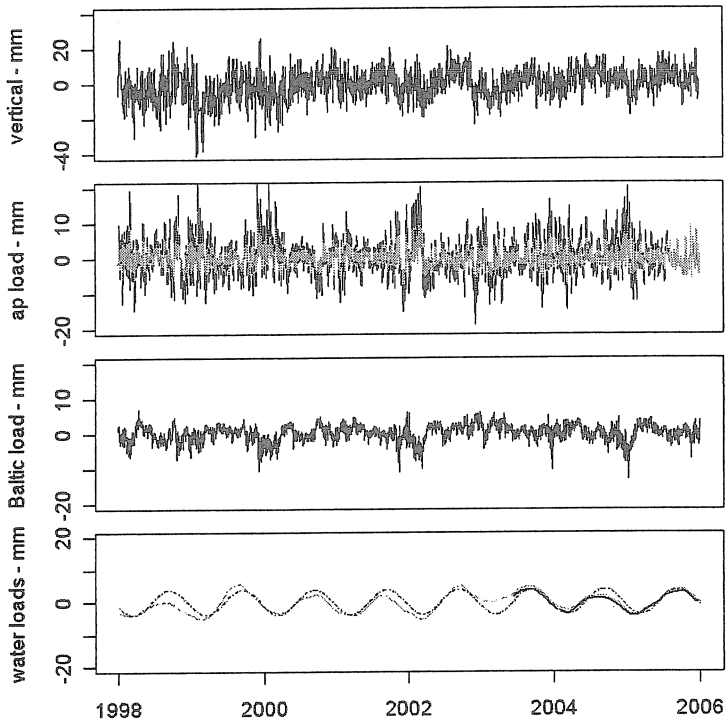

Figure 4. The calculated loadings for the different factor 1998 – 2005. On top the GPS time series, second from top the atmospheric pressure loads from HIRLAM (black) and using coefficient (grey), second from bottom the load caused by Baltic Sea and on bottom the calculated watershed loads (CPC model on grey, mixed model on black, starting 06/2003) and a sine function (grey, dashed line). All the loading factors have the same scale (40 mm).

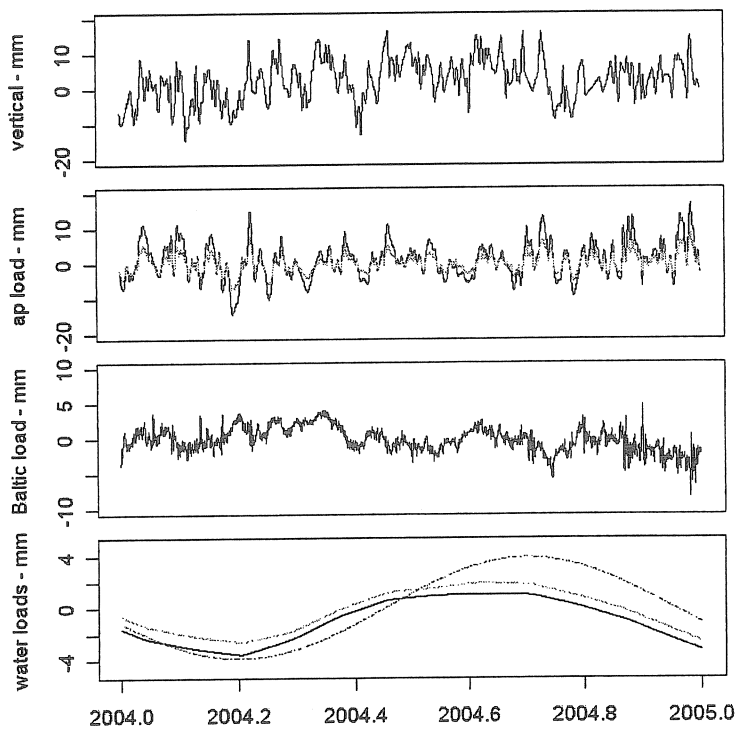

Figure 5. The same as fig. 4, but for a shorter stretch of time, only year 2004. Note that the scales vary.

5 Results

Results of the calculations can be seen in table 1. In table 2 the same results are shown for time period of one year. First, the regression was calculated (referred to as "Regression" in tables 1 and 2), starting with the air pressure alone, then with air pressure and sea level and so forth using the time series of figure 3. Second, the time series from the loading calculations (fig. 4) were reduced from the GPS time series (referred to as "Models" in tables 1 and 2). The best result (reduction in variance 31%) is achieved using a simple regression for GPS time series together with air pressure, sea level height and total water storage of Finland.

Table 1. Results for 1998-2005. The "Regression" –part shows the results of the regression analysis, the different constants, correlation coefficients, standard deviations and reduction in the standard deviation respect to the original time series. The "Models" –part shows the standard deviations when the different loading models were reduced. Abbreviations are explained below the tables.

1998 - 2005 REGRESSION	ap mm/hPa	sea mm/m	gw mm/m	tw mm/mm	corr	std mm	%
vertical						7,3540	
ap	-0,2132				0,3352	6,9284	5,8
ap+sea	-0,2767	-6,8576			0,3854	6,7857	7,7
ap+sea+tw	-0,2933	-5,2908		-0,047	0,5243	6,2620	14,8
ap+sea+gw	-0,2763	-6,028	-1,3285		0,4003	6,7392	8,4
vertical - cpc						6,8523	6,8
ap	-0,2283				0,3853	6,3232	14,0
ap+sea	-0,3028	-8,0512			0,4538	6,1061	17,0
MODELS							
ap	-0,23					6,9311	5,8
ap+sea	-0,23	-9				6,8431	6,9
ap+sea+cpc	-0,23	-9				6,4157	12,8
ap+sea+sinus	-0,23	-9				6,1817	15,9
ap+sea+tw	-0,23	-9		-0,05		6,4162	12,8
hrl+sea+cpc	HRL	-9				6,4605	12,1

Table 2. Same as table 1, but for year 2004.

2004 REGRESSION	ap mm/hPa	sea mm/m	gw mm/m	tw mm/mm	corr	std mm	%
vertical						5,6048	
ap	-0,2773				0,5325	4,7438	15,4
ap+sea	-0,3261	-7,2132			0,5848	4,5463	18,9
ap+sea+tw	-0,3244	-6,5816		-0,051	0,6496	4,2610	24,0
ap+sea+gw	-0,3292	-8,9954	2,072		0,5977	4,4935	19,8
MODELS							
ap	-0,23					4,7548	15,2
ap+sea	-0,23	-9				4,7098	16,0
ap+sea+cpc	-0,23	-9				4,3442	22,5
ap+sea+wsfs	-0,23	-9				4,2950	23,4
ap+sea+sinus	-0,23	-9				4,4177	21,2
ap+sea+tw	-0,23	-9		-0,05		4,6982	16,2
hrl+sea+cpc	HRL	-9				4,3144	23,0
hrl+sea+wsfs	HRL	-9				4,4757	20,1

vertical	gps radial	*ap*	air pressure	*tw*	total water of Finland
corr	correlation	*hrl*	HIRLAM load	*gw*	ground water
std	standard deviation	*sea*	Baltic Sea	*cpc*	CPC model load
%	reduction of std in %	*sinus*	sine function	*wsfs*	WSFS model load

6 Discussion

The results show that environmental factors can be seen in the GPS vertical time series. The different watershed time series and grids correlate, so the different models give

quite similar results. When using loading results for the period of eight years, the fitted sine function gives the best result. For a period of one year, the sine is not the best. We assume that for longer periods the sine is a mean for the process and therefore fits better, averaging out the small variation. For shorter time periods the averaging does not work and therefore the more realistic CPC or WSFS model give the best results.

Van Dam and Wahr (1998) have calculated coefficients for different loading effects in their review paper. They find a difference in loading of coastal and non-coastal sites. For Metsähovi the admittance of air pressure was found to be –0.129 mm/hPa and for Onsala in Sweden –0.122 mm/hPa. We found –0.21 mm/hPa for Metsähovi, this could be due to more detailed and local data. The amplitude of annual sine amplitude due to hydrologic variability was 2.1414 mm for Onsala in Van Dam and Wahr. The hydrologic effect has been calculated using sparser grid and a shorter period of time than we have used and that probably explains the over 1.5 mm difference.

The GPS time series we have used is coarse, we do not have much information about the processing. We assume it is quite standard processing, no corrections for snow on the radome or any other typical northern problems. There may also be a problem with aliased tidal signals due to 24-hour solutions (Penna and Stewart, 2003). Despite all this, the environmental factors diminish the variation.

Atmospheric pressure calculations give interesting results: the simple coefficient calculations gives better results than the complicated HIRLAM-calculation as can be seen in tables 1 and 2. For the longer time series the difference is small, only 0.05 mm in the standard deviation but for the one-year period the difference is 0.18 mm. This could be explained by the fact, that GPS does not see the mass movements in the atmosphere and therefore the local pressure gives adequate results. This has to be studied in more detail with more stations.

Local aquifer behaviour has changed in the past years. A swamp near Metsähovi has been dried and the variation in the groundwater well has diminished remarkably. We expect that in the future we can distinguish between the regional and local watersheds because of this changed situation using both GPS and superconducting gravimeter located nearby. The results of the vertical motion show so far only a weak signal of the difference.

In this study data from only one tide gauge was used to represent the level of the Baltic Sea. In the future, we hope to improve our calculations by using a grid model for the Baltic Sea level height. We presume it will give better results than the time series of one point alone. We are also planning to calculate PPP time series for all the Finnish permanent GPS stations to get more accurate knowledge of the loading processes in Finland.

7 Conclusions

Environmental loading effects can be found in GPS time series. Different factors need to be observed. For example, the loading caused by nearby sea cannot be corrected properly without knowledge of air pressure. The periodic fluctuation found in the time series can be traced back to the fluctuations in the water storages, but it is not fully explained by it. In some cases, e.g. Metsähovi, groundwater correlates well with total

water storage and therefore can be used for the water storage correction if no other information is available. The reduction of all the known factors diminishes the variance in the GPS height up to 31 %. With shorter time spans the reduction is even greater.

Acknowledgements. We would like to thank the Finnish Meteorological Institute, the Finnish Institute for Marine Research and the Finnish Environmental Institute for providing the datasets. This study was partially supported by the Finnish Funding Agency for Technology and Innovation TEKES (decision number 40414/04).

References

Agnew, DC, 1997, NLOADF: A program for computing ocean-tide loading, *Journal of Geophysical Research,* **102**, 5109-5110

Boy, J.P., J. Hinderer. and P. Gegout, 1998. Global atmospheric loading and gravity, *Physics of the Earth and Planetary Interiors,* **109**, 161-177

Dirmeyer, P. A., Z. Guo, and X. Gao, 2004, Validation and forecast applicability of multi-year global soil wetness products. *Journal of Hydrometeorology,* **5**, 1011-1033

Dong, D., R. S. Gross, and J. O. Dickey, 1996, Seasonal variations of the Earth's gravitational field: an analysis of atmospheric and ocean tidal excitation, *Geophysical Research Letters,* **23**, 725-728.

Fan, Y., and H. van den Dool, 2004, Climate Prediction Center global monthly soil moisture data set at 0.5° resolution for 1948 to present, *Journal of Geophysical Research*, **109**, D10102, doi:10.1029/2003JD004345

Fratepietro, F., T. F. Baker, S. D. P. Williams, and M. Van Camp, 2006, Ocean loading deformations caused by storm surges on the northwest European shelf, *Geophysical Research Letters*, **33**, L06317, doi:10.1029/2005GL025475.

Llubes M., N. Florsch, J. Hinderer, L. Longuevergne and M. Amalvict, 2004, Local hydrology, the Global Geodynamics Project and CHAMP/GRACE perspective: some case studies, *Journal of Geodynamics,* **38**, 3-5, 355-374

Penna N.T. and M.P. Stewart, 2003, Aliased tidal signatures in continuous GPS height time series, *Geophysical Research Letters,* **30(23)**, doi:10.1029/ 2003GL018828

van Dam, T., G. Blewitt, and M.B. Heflin, 1994, Atmospheric pressure loading effects on GPS coordinate determinations, *Journal of Geophysical Research,* **99**, 23939-23950

van Dam, T., J. Wahr, P.C.D. Milly, A.B. Shmakin, G. Blewitt, D. Lavallee, and K.M. Larson, 2001, Crustal displacements due to continental water loading, *Geophysical Research Letters*, **28**, 651-654

van Dam, T. M., and J. M. Wahr, 1998, Modeling environmental loading effects: a Review, *Physics and Chemistry of the Earth,* **23**, 1077-1086

Vehviläinen, B. and M. Huttunen, 2002, The Finnish watershed simulation and forecasting system (WSFS). XXIst Conference of the Danubian countries On the hydrological forecasting and hydrological bases of water management. Bucharest-Romania. 2-6 September 2002

Virtanen, H., Mäkinen, J., 2002, The effect of the Baltic Sea level on gravity at the Metsähovi station, *Journal of Geodynamics,* **35/45**, 553565.

Virtanen, H. 2004, Loading effects in Metsähovi from the atmosphere and the Baltic Sea, *Journal of Geodynamics,* **38/35**, 407422.

Virtanen, H., 2006, Studies of Earth Dynamics with the Superconducting Gravimeter, Academic Dissertation at the University of Helsinki (http://ethesis.helsinki.fi/)

Virtanen, H., M. Tervo and M. Bilker-Koivula, 2006, Comparison of superconducting gravimeter observations with hydrological models of various spatial extents, BIM (ibid.)

Rigorous Combination of Superconducting and Absolute Gravity Measurements with Respect to Instrumental Properties

H. Wziontek, R. Falk, H. Wilmes, P. Wolf

Bundesamt für Kartographie und Geodäsie (BKG), Germany

Abstract

Precise monitoring and a conclusive interpretation of temporal gravity variations at a given station is based upon accurate knowledge about the properties of the used instruments. The combination of concurrent sets of superconducting and absolute gravity measurements allow both. Whereas the absolute gravimeters provide the scale and reference level, the superconducting gravimeters enable to investigate gravity variations and to exploit the sources of the changes. The method proposed here permits to derive the scale function and zero drift of the superconducting gravimeter as well as a reliable survey of the instrumental stability of different absolute meters with high precision without the need of gravity reductions.

keywords: absolute gravity, calibration, superconducting gravimeter, site of regional comparison.

Motivation

For a conclusive interpretation of temporal variations in gravity obtained from superconducting gravimeters as well as to establish the gravity standard with absolute gravimeters, the instrumental properties of both meter types are of fundamental importance. While the sensor of the superconducting gravimeters (SG) shows a low but very stable drift rate, which must be precisely estimated to expose long-term and secular changes in gravity, absolute gravimeters (AG) are based on direct realization of physical standards. Thus drift can be excluded and calibration is not needed, but regular supervision of the instruments is necessary and – especially after maintenance – checks for possible offsets are essential. In contrast, the continuous time series of highest precision obtained from the SG has due to the relative nature of the measuring principle no absolute scale. This makes calibration of the sensor unavoidable.

Taking advantage of the different characters of both gravimeter types, a combination of their measurements should allow to resolve their instrumental properties and, in a later step, the determination of long-term gravity changes. The large amount of parallel gravity observations with different absolute gravimeters at SG stations available at BKG permits such an investigation. While a comparison at relatively short periods with the only objective to derive a constant scale factor for the SG is a common approach, see e.g. [Hinderer et al., 1991, Francis et al., 1998, Falk et al., 2001, Amalvict et al., 2002, Harnisch et al., 2002, Imanishi et al., 2002], a more complex combination of the data of several epochs can be carried out, in order to simultaneously estimate drift, check for offsets and determine the scale function for the SG as well.

Such an approach should be suitable to overcome the problem of different, possibly inconsistent reductions for the time varying gravity field. Instead of calculating a reduced mean from all drop values of an epoch of absolute gravity measurements, it should be alternatively possible to proceed with every single drop instead and average their values implicitly. To verify such a basic approach, first attempts based on synthetic data as well as data from the Station Bad Homburg were carried out.

Functional relationships

The instrumental properties of the SG under consideration are functions of scale[1] and drift[2]. The relation between the voltage equivalent to the current through the feedback, U_{SG} and gravity g_{SG} can be written in the general form

$$g_{SG} = g_0 + f_E(t)\left[f_D(t) + U_{SG} + \sum \Delta U\right], \tag{1}$$

where f_E and f_D are arbitrary functions of time for scale and drift. The steps ΔU occurring after disturbances must be determined separately during preprocessing and are not subject of this study. To leave open the possibility to extent the approach, simple polynomial representations were chosen for scale and drift:

$$f_E(t) = \sum_0^{n_E} e_i t^i, \quad f_D(t) = \sum_0^{n_D} d_i t^i.$$

[1] mostly considered constant and called calibration factor

[2] change of the systems zero point with time

Most likely, the scale can be assumed to be a constant function ($n_E = 0$) and the drift should be linear[3] ($n_D = 1$). This results in a linear relationship between gravity and observations. If the observations can not be fitted adequately, a time dependence of higher order should be introduced.
For AG, the observations are the direct measurements of time t and distance s from which the gravity values $\bar{g}_{AG}$ are derived by a procedure described in [Niebauer et al., 1995]. Each single drop experiment results in a gravity value which is used further instead of the original observations. Outliers in the drop-data are assumed to be detected by suitable criteria and removed during preprocessing. Despite their absolute characteristics, offsets between different instruments are possible and stronger changes caused by maintenance of equipment, mechanical wear or misalignment may result in an offset with respect to previous observations or other instruments. The observation equations can be written as

$$g_{AG} = \bar{g}_{AG}(s,t) + O_j, \tag{2}$$

with possible instrumental offsets

$$O_j = \begin{cases} c_j & \bigvee \quad t \in [t_j, t_{j+1}] \\ 0 \end{cases},$$

which are expected to be constant during predefined intervals $[t_j, t_{j+1}]$ (e.g. maintenance-intervals).
One important problem of the combination of AG and SG measurements are non-uniform gravity reductions used in practice to remove the time dependent parts of the gravity signal. Besides different reduction models and parameters for Earth tides, atmospheric effects, loading effects etc., even different software and processing schemes may lead to different residual gravity values. Especially with respect to the determination of drift and offset parameters with highest precision, primary observations instead of incomparable residuals will be used. This is possible because both sensors are collocated and are sensitive to the same (time dependent) gravity signal. The resulting gravity value of each single drop experiment from the AG is associated with a value from SG registration by means of a simple linear interpolation[4]. This results in a huge amount of observations with a large scatter, but as it will be shown, scale and drift as well as offset parameters are separable.
The observation equations for the combination are achieved by treating only the absolute gravity values as the measured quantity, whereas the SG data are considered as error-free parameters. This can be motivated by the distinct precision levels: A single drop has a standard deviation of about $100nms^{-2}$, while the SG measurements have a sensitivity of $0.01nms^{-2}$. From equations (1) and (2) follows

$$g_{AG} + v = g_0 + \sum_0^{n_E} e_i t^i \left[\sum_0^{n_D} d_i t^i + \tilde{U}_{SG} \right] + O_j, \tag{3}$$

where $\tilde{U}_{SG}$ are the step-free SG data. Based on this functional model, a least squares adjustment ($\sum v^2 \rightarrow Min$) of the parameters d_i, e_i and O_j can be carried out. Because the AG measurements do not have a uniform accuracy level, a suitable weighting scheme depending on standard deviation and scatter between drops respectively groups of drops (so called sets) should be used to attenuate less reliable observations.
The vast number of observations should not suggest a highly over-determined equation system. On the contrary, the resolution of drift and offset parameters does not depend on the quantity of single drops but on the number of independent measurement epochs. While one AG measurement epoch is typically consistent of 10 to 25 sets with 150 drops, only the scale function is retrievable from these several hundred observations[5]. For each drift parameter d_i and instrumental offset O_j one additional AG measurement epoch is necessary. Therefore, the minimum number of independent epochs is $n = 3$.

Tests with synthetic data

Because of the large scatter of the AG drop-data, the question arises, whether all unknown instrumental parameters are resolvable within a least squares procedure. To check this, synthetic data on the basis of predicted tidal signals for four distinct epochs (2001-2005), each lasting about 48h hours with a sampling-rate of $60\,s$, were generated.
The simulated observations were obtained by adding Gaussian noise with an amplitude of $2nms^{-2}$ for SG and $100nms^{-2}$ for AG observations. The input data are shown in figure 1 and the chosen parameters with their corresponding adjustment results are documented in table 1. It is to be seen, that within the limits of the single standard deviation, all parameters can be retrieved. An exact reproduction of the initial values cannot

[3] initial nonlinear run-in effects are not considered here
[4] interpolation is only necessary because of different sampling rates and/or a time shift between sampling instances
[5] furthermore dependent on tidal amplitude and temporal extent of the AG measurement

Table 1: Chosen parameters and the corresponding adjustment results for synthetic data

	predefined	resultant
constant scale $e_0[nms^{-2}V^{-1}]$	750.00	750.55 ± 1.31
linear drift $d_1[nms^{-2}a^{-1}]$	50.00	50.37 ± 1.05
offset $O_1[nms^{-2}]$	-20.00	-22.70 ± 4.76

be expected since every time limited random sequence has a systematic component, which effects a change in the originally chosen parameters. Thus it is demonstrated, that the algorithm should be capable to determine the instrumental parameters from the scattered AG observations.

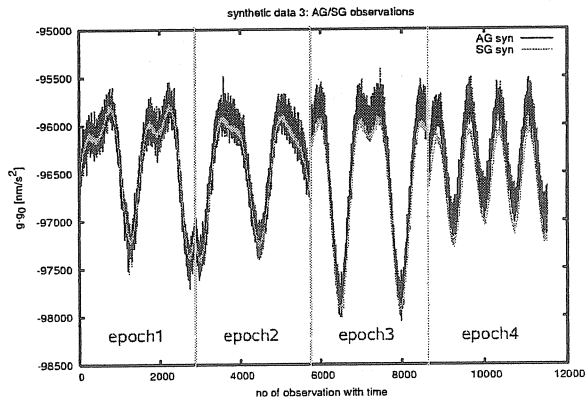

Figure 1: Synthetic data derived from tidal prediction over 4 epochs, each lasting 48 hours.

Preliminary results with observed data at Station Bad Homburg in 2005

The station Bad Homburg (BH) was developed during the last years to a station of regional comparison [Wilmes and Falk, 2006]. Beside the continuous gravity time series obtained from the dual sphere superconducting gravimeter SG30, regular absolute gravity measurements with various meters and high repetition rates were carried out. The objective is to ensure the gravity standard, monitor long-term gravity changes and to supervise diverse AG. With 18 measurement epochs during the year 2005 performed with five different instruments partially operating side by side, this station seemed ideally suited for the described comparison.

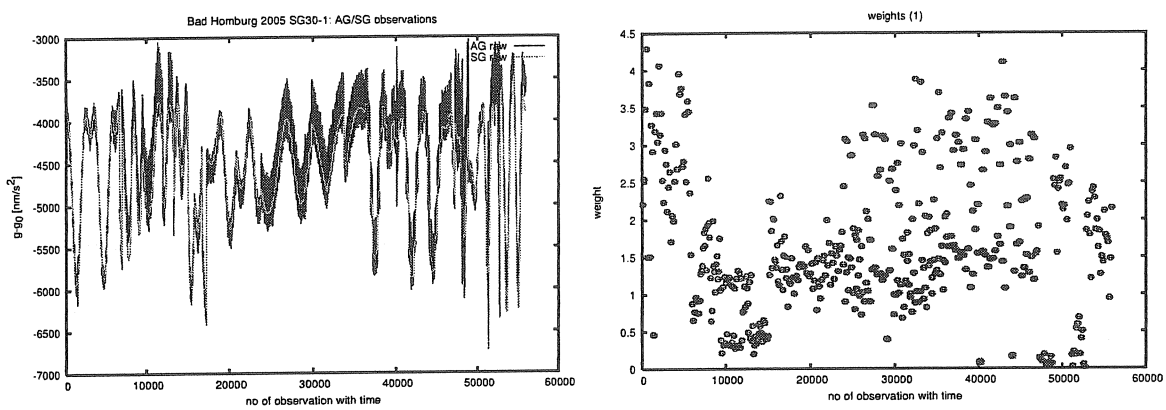

Figure 2: a) Dedicated AG and SG observations for station BH. b) weights for AG observations derived from drop scatter.

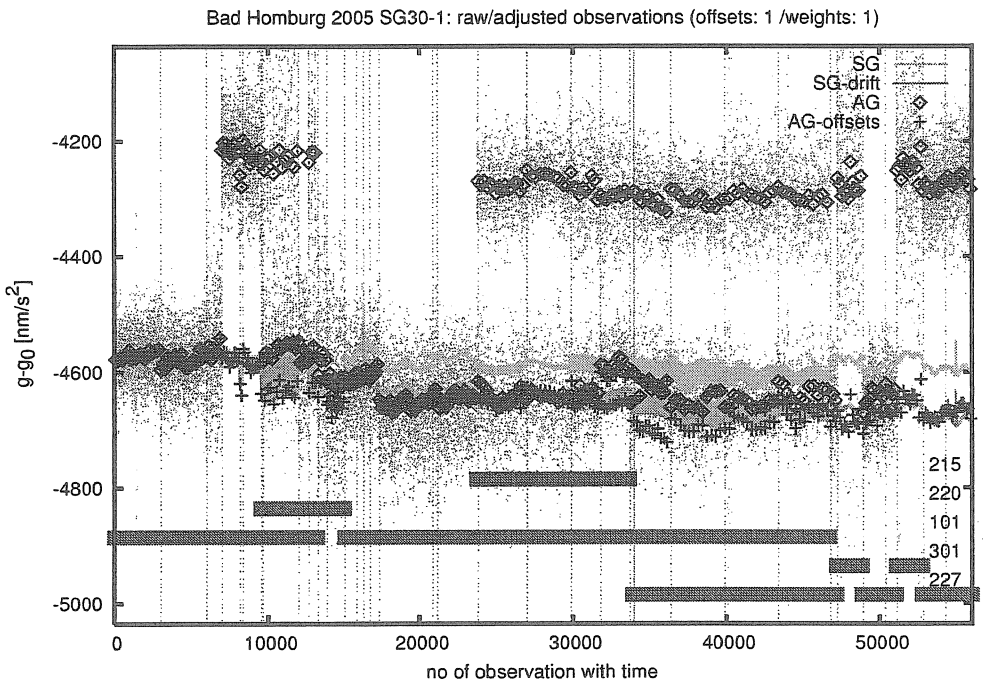

Figure 3: Observations before and after adjustment: SG: orange (grey) resp. green (light grey); AG: blue (dark grey) diamonds resp. red (grey) pluses. Single AG observations are denoted with gray dots, while markers indicate mean values of a set. During parallel operation of AG, different monuments had to be used, resulting in a constant offset in gravity. Dashed vertical lines indicate the beginning of a measurement epoch. The (pink) bars at the lower part of the plot symbolize the presence of different FG5 gravimeters annotated on the right. Values at the abscissa are the observation numbers, ordered with increasing time, not the time itself.

Preprocessing of SG data was done with the help of the well-known remove-restore approach. Tidal and atmospheric constituents are removed from the signal only for the purpose of data correction (spikes, gaps, disturbances) which were performed with the program TSOFT[Van Camp and Vauterin, 2005] and restored afterwards. The manual identification and removal of steps is probably the most important part of the preprocessing since the SG values are treated error free and unrecognized steps influence drift as well as AG offsets. Because of the different accuracy levels of AG and SG measurements, step amounts can not be obtained from the combined approach. However, a raw identification of overlooked steps is still possible.
AG data from four different FG5 instruments (FG5-101, FG5-227, FG5-301 from BKG, FG5-215 from Geodetic Observatory Pecny, Czech Republic and FG5-220 from University Hannover, Germany) were reprocessed with same reductions, preferences and software versions to ensure homogeneous datasets and consistent outlier-criteria. The elimination of outliers was done on the basis of the $3-\sigma$ criterion with respect to the mean over a set[6]. Beside statistical also different deterministic outlier criteria based on instrumental properties were investigated. The dedicated observations and the weights derived from drop scatter are shown in figure 2.
In case of parallel operation of AG, different monuments had to be used, causing a constant offset in gravity. In this case, the functional model from equation (3) has to be extended by an additional offset parameter M_k, describing the gravity difference between distinct points k.

Table 2: *Preliminary* instrumental parameters for double sphere gravimeter SG30 from combination with different AG for year 2005.

	SG30-1 (lower sphere)	SG30-2 (upper sphere)
constant Scale $e_0[nms^{-2}V^{-1}]$	-741.23 ± 0.31	-682.06 ± 0.29
linear drift $d_1[nms^{-2}a^{-1}]$	-92.33 ± 1.25	-83.05 ± 1.27

The advantage of the dual sphere system SG30 lies in the possibility to check the results independently. The preprocessing of the time series of both sensors (including determination of steps) is autonomous and will affect

[6] as a rule: 1 set = 150 drops

the adjustment results in a different manner. Further, the instrumental properties of both sensors are different, but the resulting offsets for the AG should be the same.
Although procedure and data are still under investigation, preliminary even though promising results can be given here (see figure 3). The adjustment of more than 55000 drops leads to (constant) values for the SG scale very near to those actually used. However, both values are slightly larger about 1.7 resp. 2.8 $nms^{-2}V^{-1}$. The SG drift rates for both sensors look widely similar and reasonable, the values are shown in table 2.
The residuals after adjustment show no significant deviations from a normal distribution. Merely some measurements have a distinctly larger scatter, but are symmetric as can be verified by the histogram presented in figure 4. Hence it can be infered, that no significant systematic errors nor model deficits distort the parameter estimation.

Table 3: *Preliminary* results for AG offsets from combination with SG30 for year 2005. Instrument FG5-101 held fixed.

j	serial	SG30-1		SG30-2	
		O_j $[nms^{-2}]$	rms $[nms^{-2}]$	O_j $[nms^{-2}]$	rms $[nms^{-2}]$
1	FG5-101	0.00	–	0.00	–
2	FG5-227	36.31	0.81	36.36	0.82
3	FG5-301	42.15	3.18	43.40	3.19
4	FG5-220	37.62	2.21	34.20	2.22
5	FG5-215	14.46	0.90	22.41	0.90

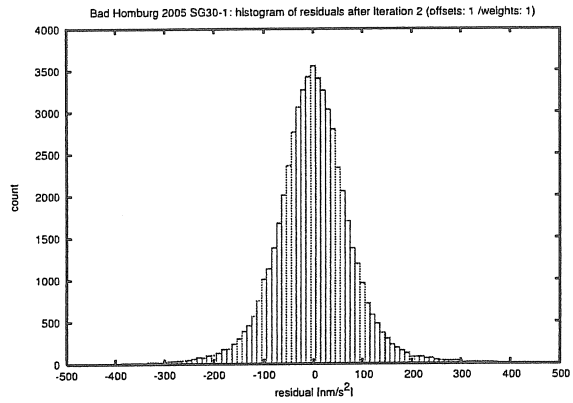

Figure 4: Histogram of the residuals after adjustment for SG30-1.

Further, the estimated gravity difference $361 \pm 1[nm/s^2]$ between the monuments AA and BA matches very well the value $356 \pm 15[nm/s^2]$ obtained from relative measurements with spring gravimeters. Therefore it can be assumed, that the obtained offsets for the AG (table 3) are expedient as well. The instrument with the longest tradition, FG5-101 held fixed[7]. All offsets are significant with respect to their standard deviations and they agree between both calculations within their bounds of error, except for instrument FG5-215, for which the difference seems to be significant with respect to the (too optimistic) error estimation. The results will soon be examined and validated with an extended dataset, since some instruments are included only with a small number of independent measurement epochs.

Conclusions

The proposed method of a strict combination based on most primary observations without any gravity reduction applied, works successfully. The simultaneous estimation gives reasonable results. For SG, a constant scale and a linear drift can be resolved well, while for AG, plausible offsets for fixed periods are obtained. Additionally, gravity differences between different points could be reliably specified. It can be concluded, that this method is an eligible basis for the analysis of temporal gravity variations and the supervision of AG.
In future investigations, correlation between drift and offsets should be examined more in detail and the combination should be extended to common subsets of AG at different SG locations. For the SG, different periods of constant parameters should be defined in order to take into account changes in the instrumental properties.

[7]this choice is arbitrary

Acknowledgment

The authors thank V. Palinkas and J. Kostelecky, Research Institute of Geodesy, Topography and Cartography, Geodetic Observatory Pecny, Czech Republic, and L. Timmen, Institut für Erdmessung, University of Hannover, Germany for providing the raw data of measurements with FG5-215 and FG5-220.

References

M. Amalvict, J. Hinderer, P. Gegout, S. Rosat, and D. Crossley. On the use of AG data to calibrate SG instruments in the GGP network. *Bulletin d'Information des Marées terrestres*, 135:10621–10626, 2002. URL `http://www.astro.oma.be/ICET/bim/text/amalvict.pdf`.

R. Falk, M. Harnisch, G. Harnisch, I. Nowak, B. Richter, and P. Wolf. Calibration of the Superconducting Gravimeters SG103, C023, CD029 and CD030. *Journal of the Geodetic Society of Japan*, 47(1):22–27, 2001.

O. Francis, T. Niebauer, G. Sasagawa, F. Klopping, and J. Gschwind. Calibration of a superconducting gavimeter by comparison with an absolute gravimeter FG5 in Boulder. *Geophysical Research Letters*, 25(7):1075–1078, 1998.

M. Harnisch, G. Harnisch, and R. Falk. Improved Scale Factors of the BKG Superconducting Gravimeters, derived from Comparisons with Absolute Gravity Measurements. *Bulletin d'Information des Marées terrestres*, 135:10627–10638, 2002. URL `http://www.astro.oma.be/ICET/bim/text/harnisch.htm`.

J. Hinderer, N. Florsch, J. Makinen, H. Legros, and J. Faller. On the calibration of a superconducting gravimeter using absolute gravity measurements. *Geophysical Journal International*, 106:491–7, Aug. 1991.

Y. Imanishi, T. Higashi, and Y. Fukuda. Calibration of the superconducting gravimeter T011 by parallel observation with the absolute gravimterer FG5 #210 - a Bayesian approach. *Geophysical Journal International*, 151:867–878, 2002. URL `http://www.blackwell-synergy.com/doi/abs/10.1046/j.1365-246X.2002.01806.x`.

T. Niebauer, G. Sasagawa, J. Faller, R. Hilt, and F. Klopping. A new generation of absolute gravimeters. *Metrologia*, 32:159–180, 1995.

M. Van Camp and P. Vauterin. Tsoft: graphical and interactive software for the analysis of time series and Earth tides. *Computers & Geosciences*, 31:631–640, 2005.

H. Wilmes and R. Falk. Bad Homburg - a regional comparison site for absolute gravity meters. In O. Francis and T. van Dam, editors, *International Comparison of Absolute Gravimeters in Walferdange (Luxembourg) of November 2003*, volume 26 of *Cahiers du Centre Européen de Géodynamique et de Seismologie (EGCS)*, pages 29–30, Luxembourg, 2006.

Status of the GGP Satellite Project

David Crossley[(1)], Jacques Hinderer[(2)], Jean-Paul Boy[(2)], and Caroline de Linnage[(2)]

[(1)] Department of Earth and Atmospheric Sciences, St. Louis University, 3507 Laclede Ave., St. Louis, MO, USA 63103 (crossley@eas.slu.edu),
[(2)]Ecole et Observatoire des Sciences de la Terre / IPG Strasbourg, 5 Rue Descartes, Strasbourg 67084 Cedex, France (Jacques.Hinderer@eost.u-strasbg.fr).

Abstract
As has been recognized for several years, attempts to validate GRACE satellite data using any kind of ground data immediately runs into the problem of horizontal scale lengths. Over Europe we have only 7 GGP stations operating since GRACE observations began and these are insufficient to give more than a simple averaging of local hydrology variations. Yet the approach from averaging ground stations is conceptually correct and would be effective if we had numerous stations all situated at the ground / atmosphere interface. Here we review how a combination of surface and underground stations (i.e. those measuring gravity below a local soil moisture horizon) can be used to validate satellite data. We show results from several GRACE models with the European GGP data since 2002.

Keywords: Superconducting gravimeter, GRACE, hydrology, GGP, GLDAS

Introduction
This study is a continuation of previous results from the comparison of ground and satellite gravity data over Europe that we began in 1989 (e.g. Crossley et al., 2003, 2004; Hinderer et al. 2006) and have subsequently called the GGP satellite project. The purpose of the early papers was to find a suitable method of averaging the ground gravity stations so they could be compared to the time-varying gravity fields produced monthly from the GRACE data (e.g. Wahr et al., 1998, 2004). In recent work we have also become aware of the need to modify our comparison with hydrology models (e.g. the GLDAS model of Rodell et al. 2004) according to whether the station lies above or below the local soil moisture horizon.

The question of averaging is characterized in Figure 1, which shows gravity stations located at the surface of the Earth. In the traditional view, used for example in atmospheric pressure modeling (e.g. Merriam 1992), gravity variations are divided into 3 zones of influence depending on distance from the station, Fig. 1(a). If this view is applied to the problem of hydrology variations, it suggests that to obtain a regional gravity field one should correct gravity stations for local hydrology. This is very difficult to do in practice because of the generally unknown nature of the subsurface porosity and permeability, as well as the profound effects of topography on the drainage and runoff from rainfall. In addition the storage of groundwater is a complex problem except in areas where the subsurface is geologically simple (e.g. perhaps sedimentary basins).

Fig. 1(b) is intended to suggest that a satellite averages all hydrology to arrive at a regional estimate. There is no distinction between L, R, and G, except in the averaging function implied in the sampling at an altitude of about 450 km (GRACE) and in the subsequent field reconstruction process for spherical harmonic coefficients or Gaussian averaging functions. Thus it has been our philosophy that a suitable average of ground-based stations should approximate a valid regional gravity field, without the necessity of making difficult decisions about how to subtract 'local' hydrology from ground-based, i.e. superconducting gravimeter (SG) measurements.

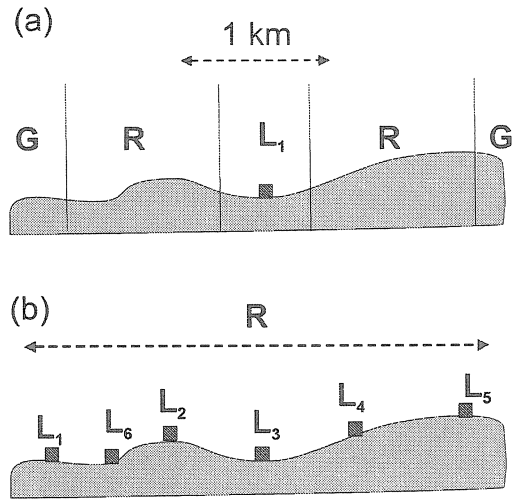

Figure 1. (a) The traditional division of a region around a gravity station into Local Regional, and Global sectors, compared to (b) the satellite averaging a sum of local gravity variations.

GGP Data

The data we use is similar to that described in previous publications (listed above). We have the 7 SG stations located within a region of approximately 1000 km in central Europe. Of these only Medicina (MC) is south of the Alps (Fig. 2). The difference is that now we are using data up to the end of October 2005, both from GGP and from GRACE. The GGP data has been stored at the ICET / GFZ database in Brussels and is freely available. It is 1 minute uncorrected data (i.e. just decimated from the original sampling). There are several approaches to processing the data for the current type of study, but the overriding factor is to correctly remove disturbances and offsets and this must be done with manual intervention, even when using a software package such as TSOFT.

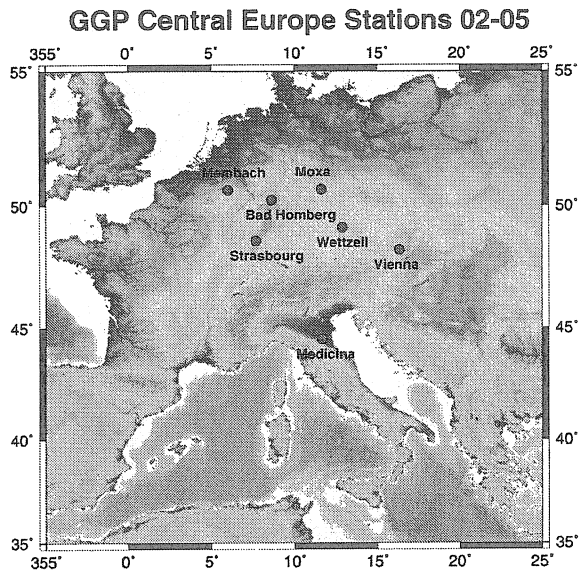

Figure 2. SG stations included in this study. Most have been in operation since 1997, and all since the beginning of GRACE (May 2002).

Here we use a traditional series of sequential processing steps: (a) fix all the problems in the local pressure data from the station, (b) construct and remove a synthetic tide based on local gravimetric factors (δ,κ) together with a nominal local pressure effect using a barometric admittance of -0.3 μGal hPa^{-1}, (c) replace obvious spikes, gaps and disturbances with a liner interpolation, decimate to 1 hr, (d) remove IERS polar motion, and (e) identify and remove offsets together with an overall linear drift function for each

data set, and (f) decimate to 1 day and 1 month data sets.

Of the various processing steps, the most critical is the removal of offsets that if left uncorrected would render the time series unusable for this application. We carefully removed between 2 and 20 offsets per station (often verified with the station operators) and at the same time subtracted a linear drift between -4.1 and +3.2 μGal / year. This linear drift is mostly of instrumental origin but it does include any real tectonic gravity drift in the array. Only after the offsets and drift are corrected can we combine the data series from each of the sensors from the dual sphere instruments (BH, MO, and WE).

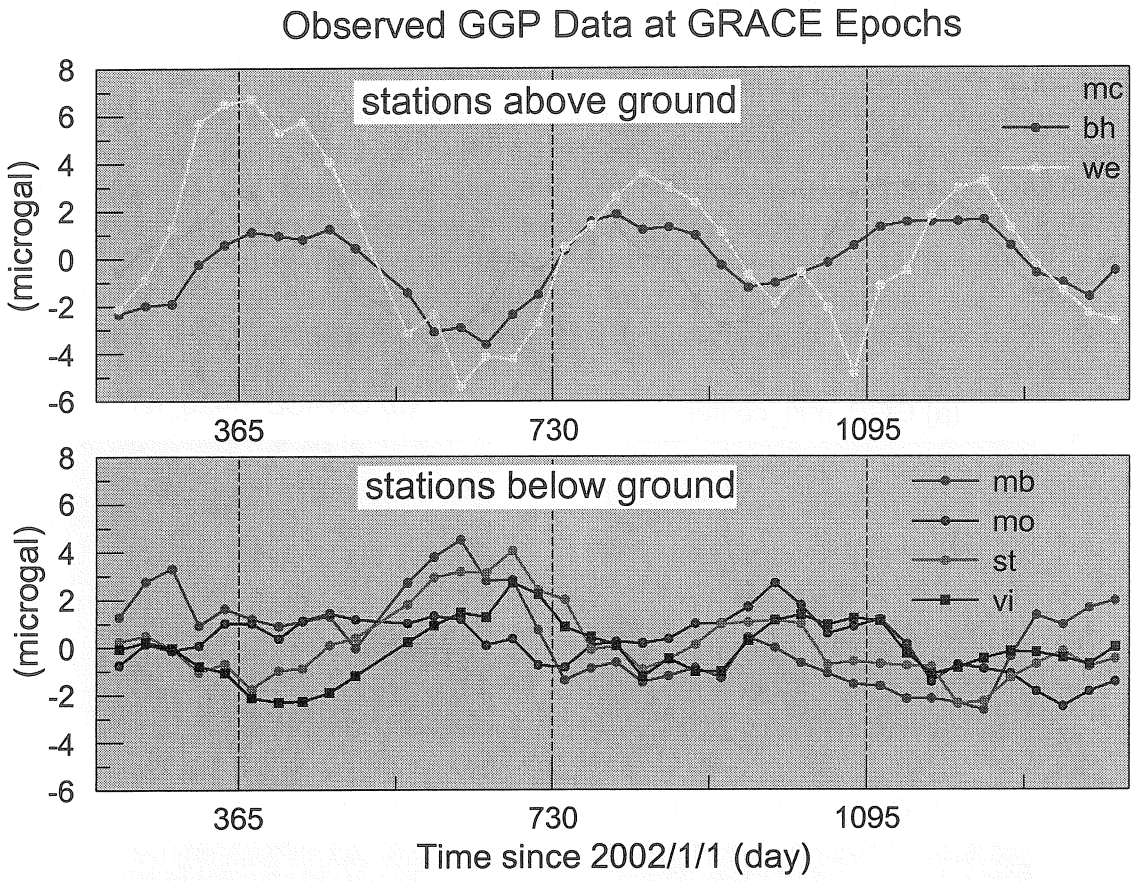

Figure 3. Residual SG data after processing described in text; stations are from Fig. 1.

The result is shown in Figure 3, in which we have grouped the stations according to whether the SGs are above or below ground level. It can be seen that a clear annual effect exists for all stations, although it is weak for station Moxa (MO) due to the complex hydrological situation (e.g. Kroner & Jahr, 2006). There are two small effects not accounted for in these residuals. The first is the 3-D atmospheric attraction, which reaches about 1 μGal amplitude (Neumeyer et al, 2004); we have most of the stations computed for this effect but not all of them for the whole time period, so elected to leave them out for the moment. The second effect is the vertical elevation effect that is sensed

by the SG but is not in the GRACE data. The effect is quite small, about 1 μGal, but ideally we should use GPS data from each station to estimate this contribution. Again this data was not readily available for all stations.

The spatial distribution of the GGP stations is so sparse that some means must be used to do appropriate space and time averaging for comparisons with the satellite data. We continue to use the minimum curvature algorithm to provide a surface at each 1 month epoch that has minimum distortion, and apart from inevitable edge effects, an appropriate average over the study area. The result for February 2003 is shown in Figure 4 (a). Note the phase difference between station WE that is above ground with VI that is below ground (the other stations are neutral for this month).

GRACE Data

We took the spherical harmonic coefficients provided by CSR Texas for the Level 2 solutions, both Release 1 and Release 2 fields (.e.g. Tapley et al., 2004). These were available from Apr/May 2002 until October 2005, and we elected to use Apr/May 02 as a reference level and took differences starting from August 2002. In all we had 38 data sets, specified at the 15th day of each month (missing June 2003). Instead of using the gravity anomaly supplied by GRACE, we computed the radial derivative of the potential field, called the gravity disturbance, on a 0.25° grid between latitudes 42-54° N and longitudes 2-18° E.

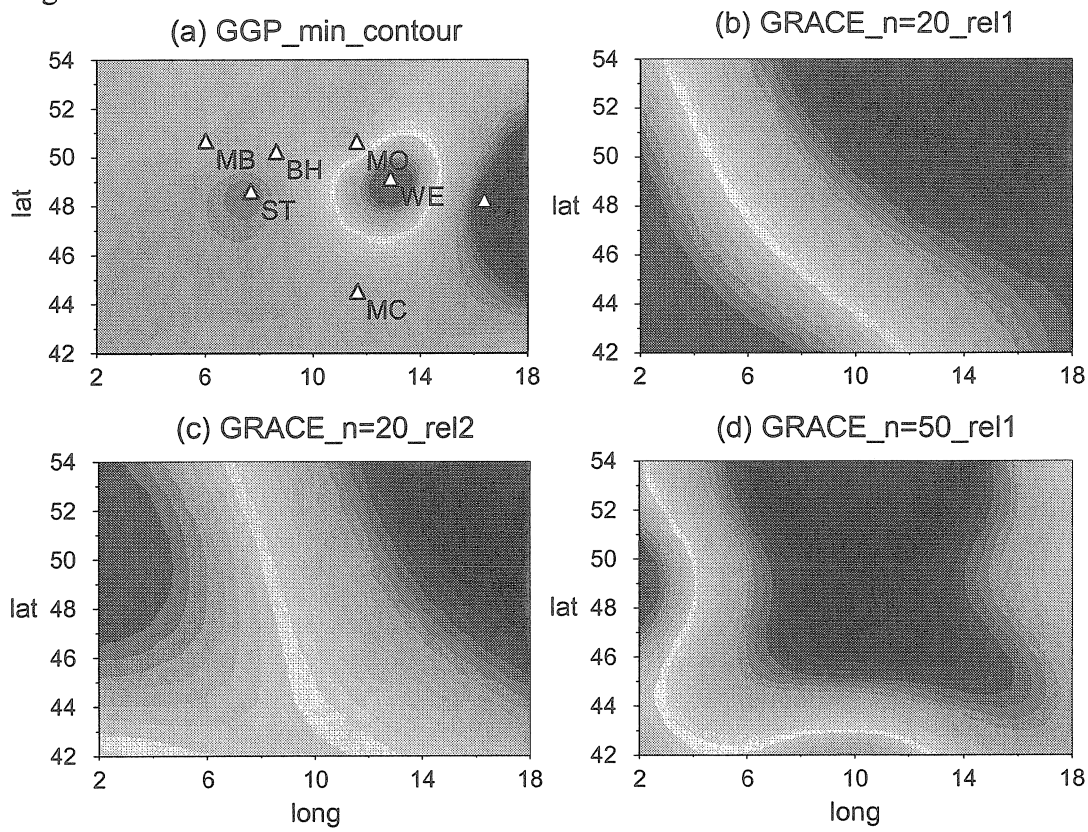

Figure 4. Gravity field over Europe for February 2003, each scaled independently (μGal) according to the ranges indicated: (a) GGP after smoothing [-4.6, 5.5], (b)-(d) GRACE Level 2 gravity disturbance (b) range [-5.4, 4.1], (c) range [-6.1, 4.8], and (d) range [-11.6, 9.4].

The Release 1 solution at a truncation of degree n=20 (about 1000 km), is shown in Figure 4 (b). Clearly the field is much more coherent that the GGP field and corresponds very little with the ground gravity. The Release 2 solutions incorporate some improvements in the processing (e.g. ocean tide models) that were added by the GRACE team retroactively, but only 22 months were available with this option. The first month available is February 2003, as in Figure 4 (c), which shows some differences from the Release 1 field but is of the same general character. Finally we experimented with a higher truncation of n=50 (about 400 km) for the Release 1 data, shown in Figure 4 (d). This field indicates more detail than n=20 and is consistent with the lower resolution data. Note, however, the scale of the n=50 solution is about twice that of the other GRACE fields and clearly much larger than the observed ground data.

EOF Decomposition

A month-by-month comparison of the GGP and GRACE fields would clearly be of limited use, especially because of the different locations of the SGs with respect to ground level. We therefore turned to the EOF decomposition of the fields that characterizes them in terms of eigenfunctions (the spatial part) and principal components (the temporal part).

We show the first (largest) principle component of the EOF decomposition in Figure 5. The upper panel compares GRACE to GGP; note the good agreement on the phase of the annual variation but the differing amplitudes. Figure 5 (b) compares the EOF decomposition of the original 38 months (Release 1) with a restricted set from Release 2 (22 months) and the same months for Release 1. The latter 2 solutions are quite similar and consistent with the full data set, indicating the EOF solution is quite robust. Note the large dip in the variation at about day 365 (middle of the 2003

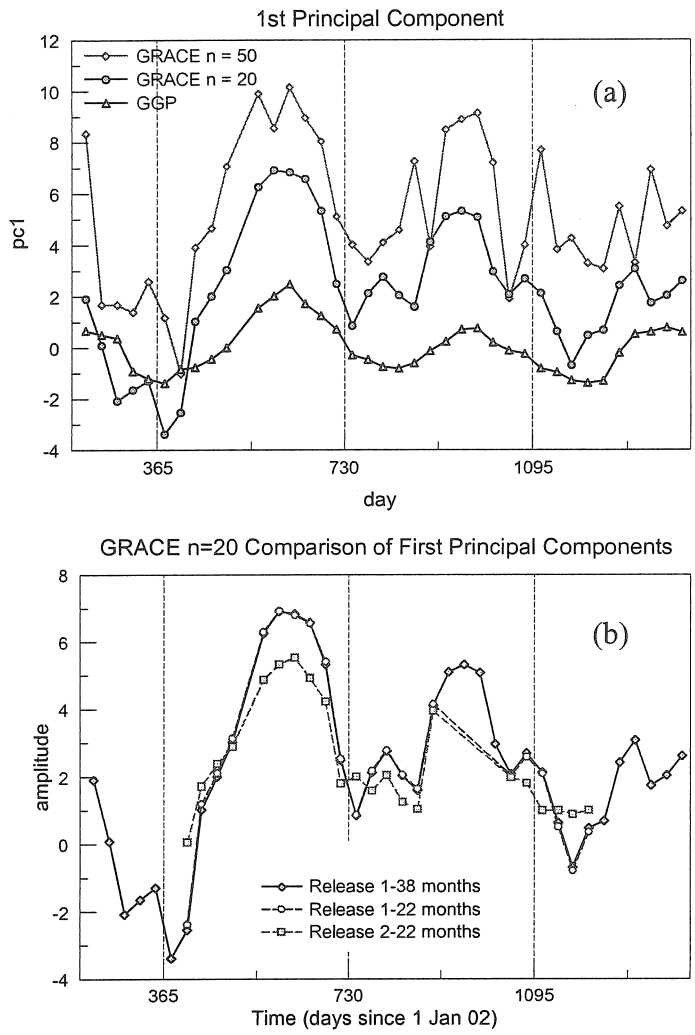

Figure 5. Principle components of the GGP and GRACE solutions showing that (a) the relative amplitudes show that GRACE tends to overestimate the ground- based values and (b) the use of only 22 months of GRACE solutions does not significantly change the EOF solution.

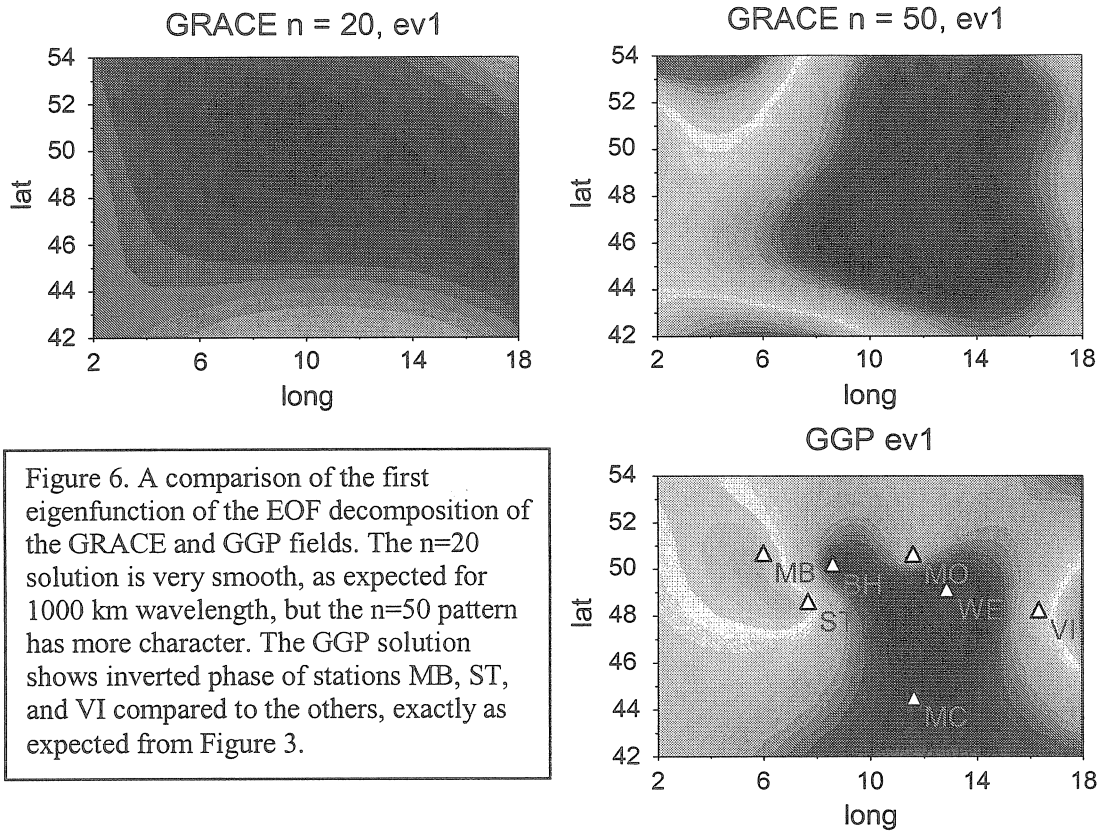

Figure 6. A comparison of the first eigenfunction of the EOF decomposition of the GRACE and GGP fields. The n=20 solution is very smooth, as expected for 1000 km wavelength, but the n=50 pattern has more character. The GGP solution shows inverted phase of stations MB, ST, and VI compared to the others, exactly as expected from Figure 3.

drought in Europe). Also we note the seasonal cycle seems to be getting weaker towards the end of the period in late 2005. This temporal behavior is better seen in the principal components than in simpler fitting of sinusoids as has been done elsewhere for the GRACE solutions.

The equivalent eigenfunctions are shown in Figure 6 for two of the GRACE solutions and for GGP. Despite the apparent similarity of the pattern for GRACE n=50 and GGP, this does not mean that the solutions support each other because the GGP pattern is clearly contaminated by the below-ground station effect. We also note that the eigenfunction of the Release 2 data is very similar to that for Release 1, n=20 (not shown)..

Each EOF decomposition can be assessed on the basis of the variance reduction when increasing numbers of eigenfunctions and principal components are included. This is shown in Figure 7 for the various solutions discussed above. Obviously the GGP solution is the most slowly convergent because of all the detail provided by the point-

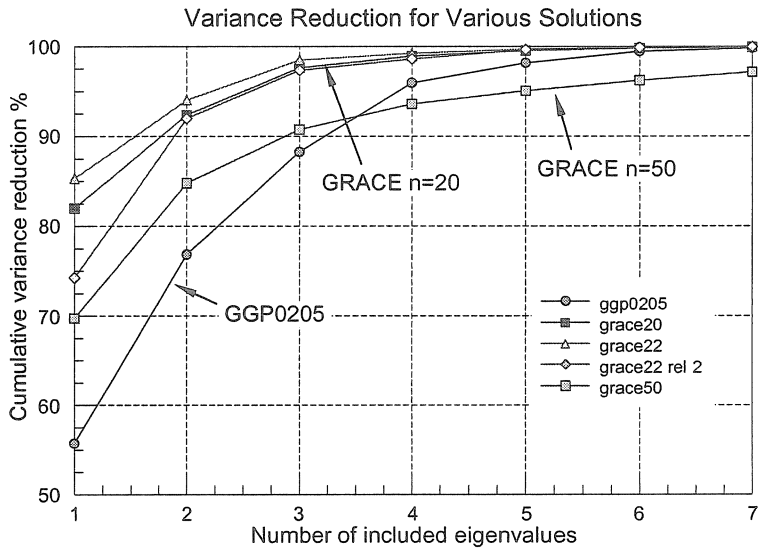

Figure 7. Variance reduction for the EOF solutions.

derived fields. It is also no surprise to see that the n=20 satellite solutions converge quickly due to the limited spatial resolution being comparable to our array size.

GLDAS Hydrology and Groundwater

Every study of the GRACE time varying solutions is compared to one or more versions of continental hydrology (e.g. LAD, Milly and Schmakin, 2002a, b; GLDAS, Rodell et al. 2004) and we do the same here. The GLDAS solutions are available at the NASA website and contain gridded solutions (0.25°) for soil moisture, snow cover, canopy water and other variables. They can be used directly for comparison with GRACE if the latter solutions are expressed in cm of water. The main difference for gravity is that the predicted water storage needs to be converted to a combination of loading (deformation) and Newtonian attraction where the location of the soil moisture with respect to the gravimeter must be correctly assessed. Our calculations show that the attraction can be further separated into a local effect, essentially a delta function right at the gravimeter, and a non-local effect (everywhere else). Of the 3 contributions to gravity, by far the largest is the local attraction (5-10 μGal for our 7 stations), and the deformation and non-local attraction are similar but smaller (1-2 μGal).

When combining these GLDAS effects we flip the sign of the local attraction for stations below the soil moisture horizon (MB, ST, and VI). The reason is that the soil moisture depth is usually only 1-2 m, and this is thin enough to place either completely above or below the SG. Station MO is partly above and partly below the soil horizon and the other stations (BH, MC, and WE) are above, or at, ground level.

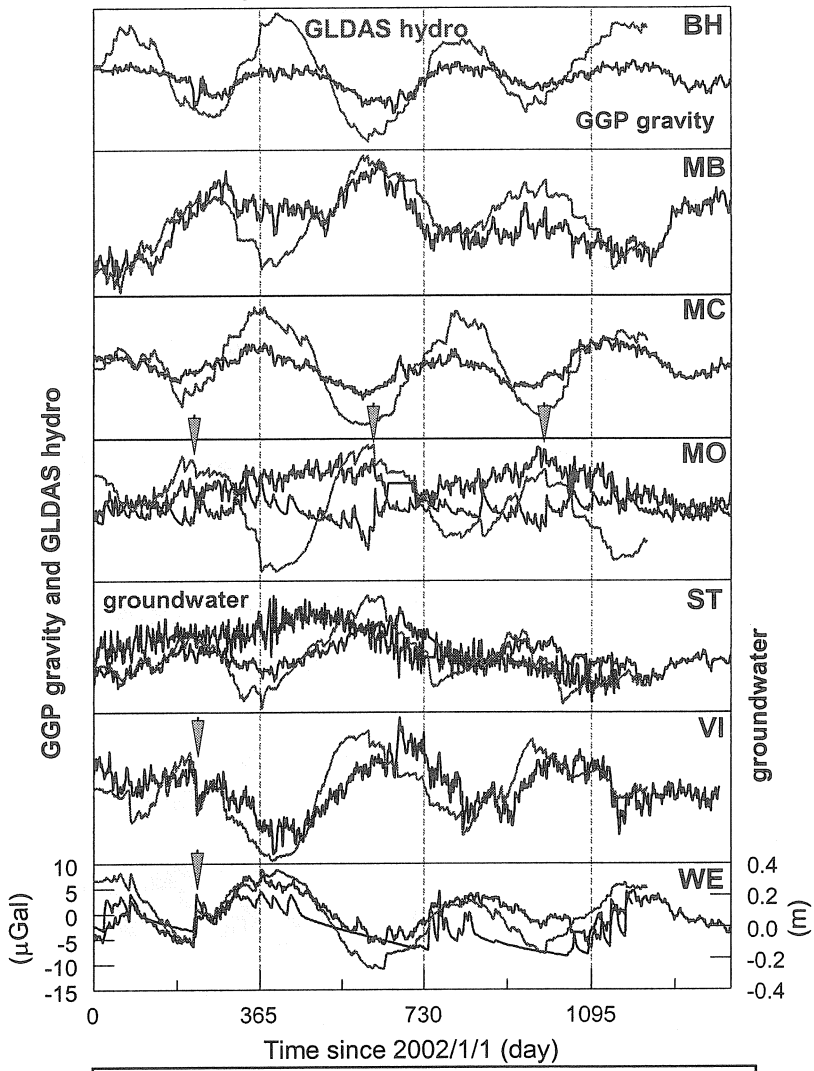

Figure 8. A comparison of GLDAS hydrology (red), SG gravity (black) and groundwater levels (blue) for each GGP station.

The resulting comparison is shown in Figure 8, together with the local groundwater data at 3 of the SG stations. Notice first that the GLDAS hydrology and SG gravity are very compatible in amplitude and phase for most stations. Second, the groundwater variations are not always a good indicator of the hydrology or gravity. The correlation coefficients for ST, MO and WE between groundwater and gravity are 0.05, 0.16, and 0.55 respectively; thus groundwater at ST has very little relation to either hydrology or gravity, whereas at WE the correlation is fairly high. This observation means that it is very difficult to 'correct' local hydrology at an SG site using groundwater data. Not only may the correlation be poor, but any admittance factor that is used will inevitably also respond to the soil moisture content that we would like to leave in the gravity residuals. Neumeyer et al. (2006) have shown some results from the point measurements and GRACE comparisons using this approach.

Finally we note that at the places marked by green arrows (Fig. 8), there is a significant offsets in all 3 signals, even at the same time at different stations. This indicates the widespread coherence of some rainfall and drainage patterns over several 100 km that is accurately captured by the SG measurements at widely separated point locations.

Hydrology Modeling

As in the past (Crossley et al. 1998) we prefer the empirical approach to modeling the hydrology at an SG station in terms of the 'leaky bucket' model with time constants. This was first used to good effect by Goodkind and Young (1991) and in later work by Harnisch and Harnisch (2006). The results shown above, however, demand an improvement over the simple approach of just rainfall and groundwater. Because the seasonal changes in gravity can be so well accounted for by placing the soil moisture level above the underground stations, this means that soil moisture must be retained in some environments for considerable time (before it leaks into the groundwater and runoff systems). We therefore need to add another stage to our previous model, to allow for the soil moisture horizon that is here represented as a thin horizontal layer, as in Figure 9

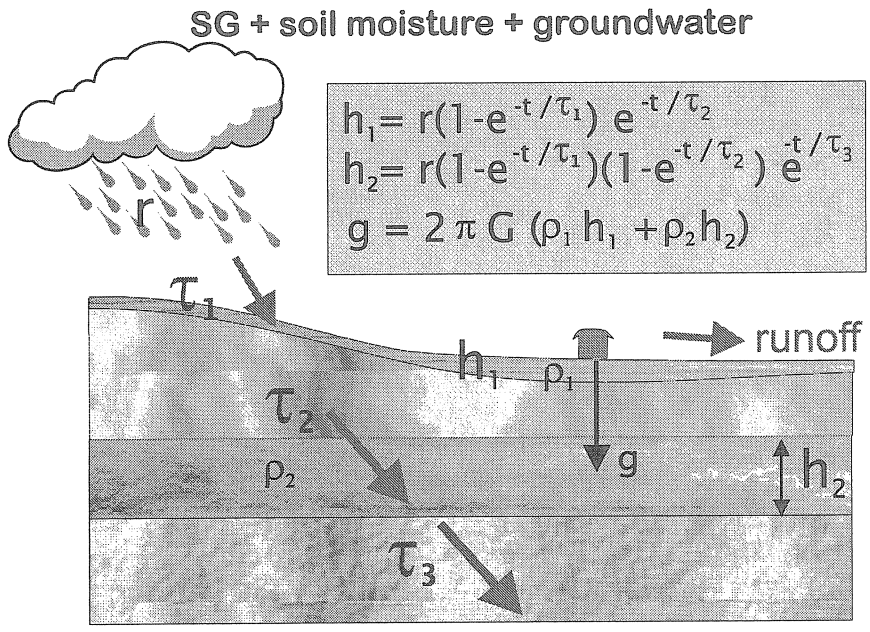

Figure 9. A 3-stage model for rainfall, soil moisture, groundwater, and gravity.

This hydrology problem can be solved empirically by modeling, using as

observations the time series of rainfall, soil moisture, groundwater, and ground gravity. It is in principle possible to establish values for the thickness and porosity of the two water layers and the 3 time constants τ_1, τ_2, τ_3 as indicated in Fig. 9. If the SG is below the soil moisture horizon, the sign of $\rho_1 h_1$ in the Bouguer slab attraction formula must be reversed. We intend to pursue this approach in future studies. The more physical approach to hydrology modeling is of course more satisfying (e.g. Llubes et al., 2004; Kroner and Jahr, 2006) but a complete description of the hydrology channels in complex areas such as hills and forests is a challenge yet to be solved.

Conclusions

(1) With more than 3 years of data from GGP and GRACE, we can now say with confidence that the seasonal variation of water storage at SG sites is consistent with satellite measurements and with hydrology models.
(2) The size of the annual variations is about ± 5 μGal at most stations, with highest gravity occurring during the winter months and the lowest gravity during summer when the soil moisture and canopy water evaporates.
(3) The higher degree truncation GRACE solution (n=50) gives surface gravity that has amplitudes twice that of the more reliable n=20 fields.
(4) The spatial inconsistency of the point wise SG data and the GRACE data does not seem to pose a major problem in the intercomparison. This has been demonstrated through the EOF decomposition of both fields.
(5) The principal components of the EOF analysis of the GRACE fields are a very useful measure of the time variation in the data, and show trends in amplitude and phase that are more satisfying than fitting a simple sinusoidal variation.
(6) The problem of some SG stations being underground poses special difficulties in with the soil moisture in hydrology, but these are not insurmountable and can be solved with effective empirical modeling. The simple reversal of sign of the local soil moisture attraction appears to be a crude, but effective, first strategy in such an approach.

Acknowledgments

We thank the GGP station operators for supplying the data for this paper, especially in some cases directly to us in advance, and also the B. Ducarme (ICET) and B. Ritschel (ISDC) in maintaining the GGP database. This material is based upon work supported by the National Science Foundation under Grant No. 0409381, and the CNRS (French Research Ministry).

References

Crossley D., J. Hinderer, Llubes, M., and Florsch, N, 2003. The potential of ground gravity measurements to validate GRACE data, *Advances in Geosciences*, **1**, 65-67.

Crossley D., J. Hinderer, and J.-P. Boy, 2004. Regional gravity variations in Europe from superconducting gravimeters, *J. Geodynamics*, **38**, 325-342.

Crossley, D., Xu, H., and Van Dam, T., 1998. Comprehensive analysis of 2 years of data from Table Mountain, Colorado, Proc. 13th Int. Symp. Earth Tides, pp. 659-668. eds. Ducarme, B., and Paquet, P., Brussels.

Goodkind, J.M. and Young, C., 1991, Gravity and hydrology at Kilauea Volcano, the Geysers and Miami, in *Proceedings of the Workshop: Non Tidal Gravity Changes Intercomparison between absolute and superconducting gravimeters*, 3, 163-167, ed Poitevin, C., Cahiers du Centre Européen de Géodynamique et de Séismologie, Luxembourg.

Harnisch, G., & Harnnisch, M., 2006. Hydrological influences in long gravimetric data series, *J. Geodynamics* 41 (1-3), 276-287.

Hinderer J., O. Anderson, F. Lemoine, D. Crossley, and J.-P. Boy, 2006. Seasonal changes in the European gravity field from GRACE: a comparison with superconducting gravimeters and hydrology model predictions, *J. Geodynamics*, 41, 59-68.

Kroner C. and T. Jahr, 2006. Hydrological experiments around the superconducting gravimeter at Moxa Observatory, *J. Geodynamics*, 41, 268-275.

Llubes, M., N. Florsch, J. Hinderer, L. Longueverne, and M. Amalvict, 2004. Local hydrology, Global Geodynamics Project and CHAMP/GRACE/GOCE perspectives: some case studies, *J. Geodesy*. 38, 355-374.

Merriam, J., 1992. Atmospheric pressure and gravity, *Geophys. J. Int.*, 109, 488-500.

Milly, P. C. D. and A. B. Shmakin, 2002a. Global modeling of land water and energy balances, Part I: the land dynamics (LaD) model, *J. Hydrometeorology,* 3, 283-299.

Milly, P. C. D. and A. B. Shmakin, 2002b. Global modeling of land water and energy balances, Part II: land characteristic contributions to spatial variability, *J. Hydrometeorology,* 3, 301-310.

Neumeyer, J., Hagedoorn, J., Leitloff, and Schmidt, R., 2004. Gravity reduction with three-dimensional atmospheric pressure data for precise ground gravity measurements, *J. Geodynamics*, 38, 437-450.

Neumeyer, J., Barthelmes, F., Dierks, O., Flechtner, F., Harnisch, M., Harnisch, G., Hinderer, J., Imanishi, Y., Kroner, C., Meurers, B., Petrovic, S., Reigber, C., Schmidt, R., Schwintzer, P., Sun, H.-P., & Virtanen, H., 2006. Combination of temporal gravity variations resulting from Superconducting Gravimeter (SG) recordings, GRACE satellite observations and global hydrology models, *J. Geodesy*, DOI: 10.1007/s00190-005-0014-8.

Rodell M., P.R. Houser, U. Jambor, J. Gottschack, K. Mitchell, C.-J. Meng, K. Arsenault, B. Cosgrove, J. Radkovich, M. Bosilovich, J.E. Entin, J.P. Walker, D. Lohmann, and D. Toll, 2004. The Global Land Data Assimilation System, *Bull. Am. Met. Soc.*, 85 (3), 381-394.

Tapley, B. S. Bettadpur, J. Reis, P. Thompson, & M. Watkins, 2004. GRACE measurements of mass variability in the Earth system, *Science*, 305, 503-505.

Wahr, J., S. Swenson, V. Zlotnicki, and I. Velicogna, 2004. Time-variable gravity from GRACE: first results, *Geophys. Res. Lett.*, 31 (11), L1150110

How to validate satellite-derived gravity observations with gravimeters at the ground?

Jacques Hinderer, Caroline de Linage & Jean-Paul Boy

EOST/IPG Strasbourg (UMR CNRS/ULP 7516)
5 rue Descartes
67084 Strasbourg Cedex France
jhinderer@eost.u-strasbg.fr

1. Introduction

There is a major international effort in the present decade to measure variations in the Earth's global gravity field using low orbit satellites. The first satellite CHAMP (Challenging Mini-satellite Payload) was launched in 2000 and was followed two years later by GRACE (Gravity Recovery and Climate Experiment). In the near future, there will be a third mission called GOCE (Gravity field and steady-state Ocean Circulation Explorer) that will orbit even closer to the ground and hence be even more sensitive to smaller scale gravity changes. The primary goal of these missions is to use the temporal changes of the Earth's gravity field to infer changes in regional and continental water storage, and ocean circulation (see Tapley et al. 2004; Wahr et al. 2004; Svenson et al. 2003).
In addition to satellite-derived gravity observations there is since 1997 a ground network of about 20 superconducting gravimeters (SG) within the frame of the GGP (Global Geodynamics Project). These instruments are able to study time variations in surface gravity over a very wide spectrum ranging from second to several year periods (see e.g. Hinderer & Crossley 2004).

	GRACE	Superconducting gravimeter
Gravity resolution (expected)	0.1 2 microgal	1-10 nanogal
Spatial resolution Half wavelength	500 250 km (nominal) ***1300 km (real)***	Point measurement
Spherical harmonic Expansion degree	40 80 (nominal) ***15 (real)***	
Temporal resolution	1 month	10 sec
Long term stability	No drift	Small drift < 3 microgal/year

Table 1. A comparison between satellite-derived and surface gravity performances.

Table 1 gives an overview of the similarities and differences between satellite and ground gravity measurements in terms of amplitude sensitivity (in μGal), space and time resolution and long term stability. Of course the highest resolution in time and amplitude is obtained with the SG at the Earth's surface but the SG measurements are point observations on the contrary to satellite-derived gravity which acts as a spatial integrator filter. Moreover these two types of data are not sensitive to the same gravity contributions as we will see in section 2.

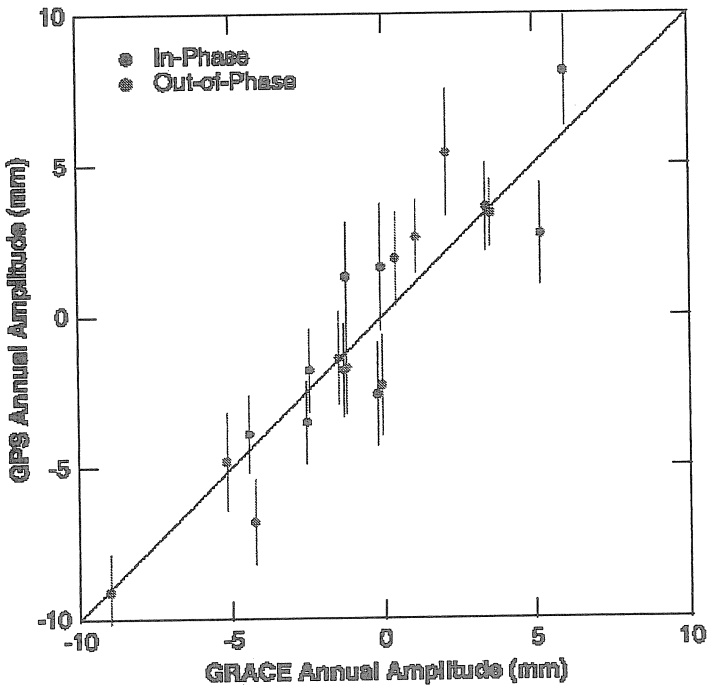

Figure 1. GPS versus GRACE derived observations of the annual hydrological signal in vertical displacement (mm) in the Amazon basin (from Davis et al. 2004).

Several methods have been proposed to calibrate/validate (CAL/VAL experiment) space-derived gravity observations:

- use of **models** for the atmosphere, oceans, hydrology, tides, or post-glacial rebound but this method does not appear very satisfactory from the conceptual point of view since satellite data are supposed to enhance these models;

- use of man-made '**controlled**' experiment like water impoundment of the Three-Gorges Reservoir in China (with detailed monitoring of water level + ground geodesy) (Boy & Chao 2002); it is however difficult because of the small spatial extension (40 km^3, 600 km x 1-2 km) and unknown underground contribution;

- use of in-situ Ocean Bottom Pressure (**OBP**) like the MOVE (Meridional Overturning Variability Experiment)) project in tropical northwest Atlantic (Kanzow et al. 2005)

or the Japanese project linked to the Kuroshio current in Western Pacific Ocean; this method is based on the capability of space-borne gravity measurements to detect the time variation of the oceanic mass redistribution and its currents; it is also difficult because of the small number of pressure sensors available;

- use of GPS observations of ground motion like in the study of hydrology-driven vertical deformation in the Amazon River Basin (Davis et al. 2004); this method is indirect (one compares displacement to gravity) but GPS has indeed the similar spatial sensitivity as GRACE data and the results are promising (see Fig. 1);

- use of **ground based gravity** data mainly with SG but also with repeated measurements using Absolute Gravimeter (AG) (Niebauer et al. 1995) in specific zones of interest (together with collocated GPS measurements); this will be the approach described in this paper.

2. Ground and satellite gravity transfer functions

There are three different contributions to ground gravity resulting from a surface loading process (Hinderer & Legros 1989):

1. the Newtonian attraction
2. the elastic term due to vertical motion in existing field (term depending on Love number h'_n of degree n)
3. the elastic term due to mass redistribution (term depending on Love number k'_n of degree n).

For instance the ratio of satellite-derived versus ground gravity transfer function for a hydrological surface load (due to soil moisture or snow coverage or underground aquifer) of degree n becomes:

$$\frac{\Delta g_{sat}}{\Delta g_{ground}} = \frac{(n+1)(1+k'_n)}{(n+1) - 2h'_n + (n+1)k'_n} \qquad (1)$$

Figure 2 shows the variation of this ratio as a function of the degree n of the spherical harmonic decomposition of the hydrological load. This ratio tends to unity for large n because the elastic deformational part in h'_n vanishes but is significantly different from unity for low degrees.

Notice that ground changes are always predicted to be larger than satellite changes for all degrees (ratio < 1). The reason is due to elasticity that systematically enhances the pure Newtonian attraction effect. When there is more water below the surface, gravity is increased and, at the same time, the crust is subsiding which again increases gravity.

3. A review of previous studies involving surface gravity

The 'ground truth' project based on GGP data was initiated some years ago to fulfil several goals among them the calibration, validation, or inter-comparison of ground gravity changes with satellite measurements (Crossley & Hinderer 2002). One goal was to provide an

independent method different from other approaches and to investigate a common reference signal which is the gravity variation driven by the seasonal changes in continental hydrology (see Wahr et al. 1998; Andersen et al. 2005a; Boy & Hinderer 2006).

A first study directly comparing CHAMP data to 6 SG ground observations was done by Neumeyer et al. (2004) and has led to satisfactory results for all the stations in the one year analysis period (from December 2000 to December 2001). The superposition of the monthly gravity mean values from the SG residuals (after correction for solid tides, ocean and atmospheric loadings, and polar motion) with the CHAMP reconstructed values at the SG sites is rather good. Neumeyer et al. (2006) recently extended this study to GRACE data pointing out again the partial agreement between surface and satellite-derived gravity at specific locations.
Before a detailed comparison can be made, however, one has to remember that ground gravity measurements include necessarily a contribution from the vertical motion of the instrument through the ambient gravity field as shown in part 2 (h'_n term).This signal does not affect the orbiting satellite and hence there is a difference in the gravity changes as seen at (moving) ground level and by the satellite (Hinderer et al. 2006).

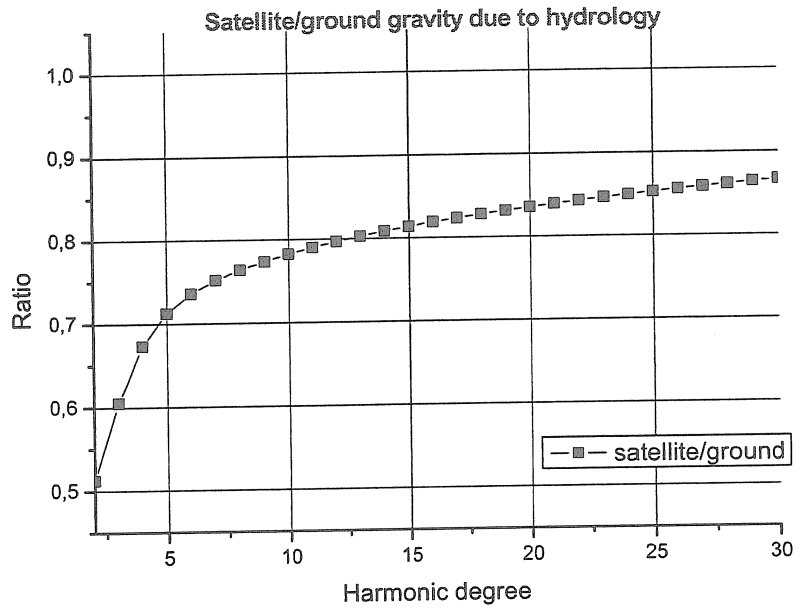

Figure 2. Ratio of the satellite versus ground gravity transfer function due to a hydrological load as a function of the degree n of the spherical harmonic decomposition.

We note in these studies that the comparison of single station results with the large-scale satellite solutions is problematic due to the completely different error budgets involved. GRACE data for example are good to 1 μGal only over length scales longer than 500- 1000 km, whereas SGs are good to the same accuracy (or better) at a single point. In order to average SG measurements and reduce local effects, there have been attempts to assemble a network solution from nearby SG stations rather than doing the above single station comparison; one way is for instance to do an Empirical Orthogonal Function (EOF) decomposition of the SG signals and to compare it to the same decomposition of the GRACE

field (Crossley et al. 2004). Within the existing rather sparse GGP network, Europe is obviously the best place to try such an approach.

The approach was first initiated using 1 year of SG data by Crossley and Hinderer (2002) and Crossley et al. (2003) and extended to longer data sets by Crossley et al. (2004, 2005). This approach was further extended to a 21 month time interval to inter-compare surface data (GGP European sub-network), satellite data from GRACE, and theoretical predictions for two global scale hydrology models (Andersen et al. 2005a; Hinderer et al. 2006).
The results show the existence of an annual signal that is coherent over Europe with an amplitude of a few μGal mostly due to the seasonal loading from continental hydrology (soil moisture + snow) according to recent models such as LaD (Milly & Shmakin 2002) or GLDAS (Rodell et al. 2004). There is even a possibility to detect in GRACE data inter-annual signals (Andersen & Hinderer 2005) and, in particular, there is a clear evidence that GRACE has been affected by the heat wave that occurred in summer 2003 in Europe (Andersen et al. 2005b). The Wettzell (Germany) and the Medicina (Italy) SG data seem to confirm this point as shown by Figure 3.

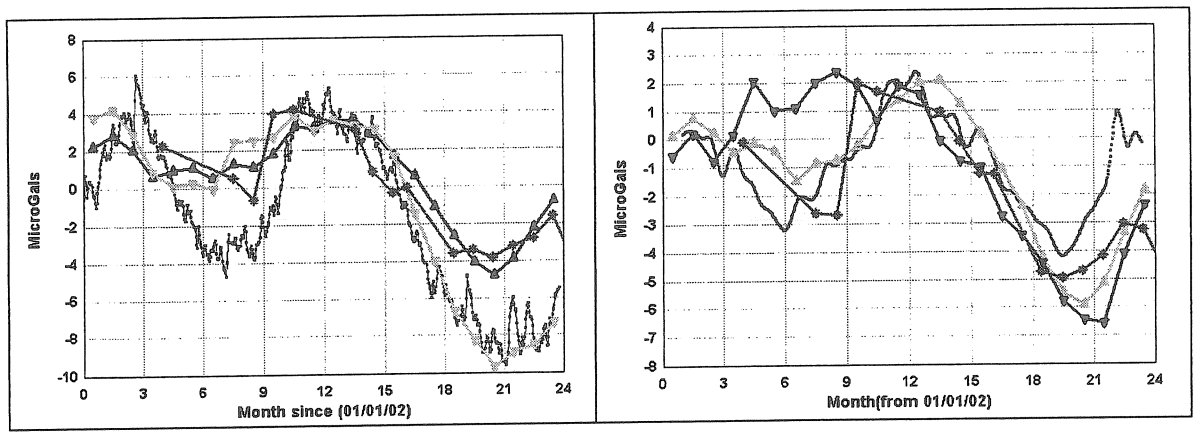

Figure 3. Direct observations of gravity field variations from two superconducting gravimeters located in Wettzell (Germany) and in Medicina (Italy). The SG gravity observations are shown in blue and the GRACE observations are shown in red. Predicted gravity changes from the GLDAS output are shown in green (triangles up) (raw, un-smoothed) and black (triangles down) (spatially smoothed to mimic GRACE observations) (from Andersen et al. 2005b).

4. A proposal for a pilot study: GHYRAF (Gravity, HYdRology in AFrica)

We have seen that continental hydrology changes are of limited amplitude in Europe where most of the ground based gravity validation experiments have been done. There are other regions where larger cyclic changes are expected and one is equatorial Africa. We propose hereafter a pilot study from the Sahara to the equatorial monsoon zone. The main target will be the comparison between models and multi-disciplinary observations (gravity, geodesy, hydrology, meteorology) of seasonal water storage changes in an arid region without any surface and underground water content variation and a very rainy region where we will be able to combine there a lack of hydrology in an arid region with a strong hydrology signal. The corollary is the ground validation of space-derived gravity (GRACE, GOCE).

Two types of ground-based measurement campaigns are involved (cf. figure 4):

- a repeated survey of 2 North-South absolute gravity profiles to assess the large soil moisture changes as predicted by recent hydrological models

- the installation of a high precision superconducting gravimeter (SG) at Nsimi (Cameroon) to act as a continuously monitored base station in a region of large water storage changes.

From the expression of the gravity transfer function (eqn. (1)) we know that it is important to determine the vertical motion at AG/SG points in order to correct for the free air gradient contribution which is not felt by the satellite.

Our project will include actual ground-based gravity measurements in a null zone (hydrologically) that will help constrain our observations for the other, high rainfall, zone in Central Africa. It will also enhance cooperation between various sub-disciplines (absolute and relative gravimetry, geodesy, hydrology, and satellite geodesy) and, finally, strengthen the activities of the AMMA (Multi Disciplinary Analysis of African Monsoon) international research program.

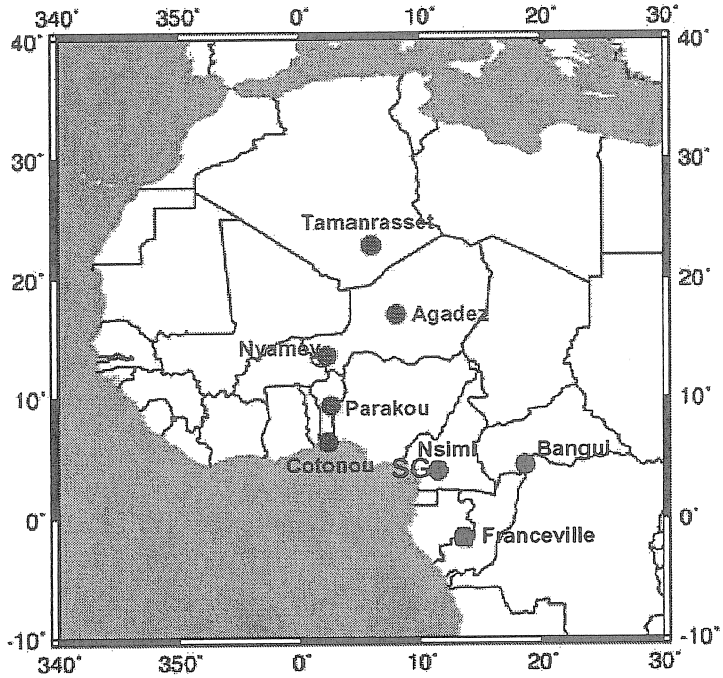

Figure 4. Location of the gravity measurement stations (Tamanrasset (Algeria), Agadez (Niger), Nyamey (Niger), Parakou (Benin), Cotonou (Benin), Franceville (Gabon), Nsimi (Cameroon), Bangui (Central African Republic)).

Our project will need a campaign of continuous precise GPS measurements along the profiles to assess the vertical deformation not seen by the GRACE satellites. Moreover in-situ measurements of hydrological parameters at each station are needed to assist us in modelling the local gravity effects at each station. Finally we also feel that new approaches to generating

highly tuned data from the GRACE satellites to maximize the time and spatial resolution of the satellite data (see Rowlands et al. 2005) are necessary in this area.

The extreme predictions are for Tamanrasset (TAM) station in the Sahara where the lack of water in the underground leads to almost no change in gravity (less than 0.4 μGal) and to small vertical motions (less than 2 mm) and for the Nsimi station in Cameroon (near Yaoundé) where gravity changes as large as 20 μGal and displacement of the order of 10 mm can be reached during the monsoon period (see Figure 5 below).

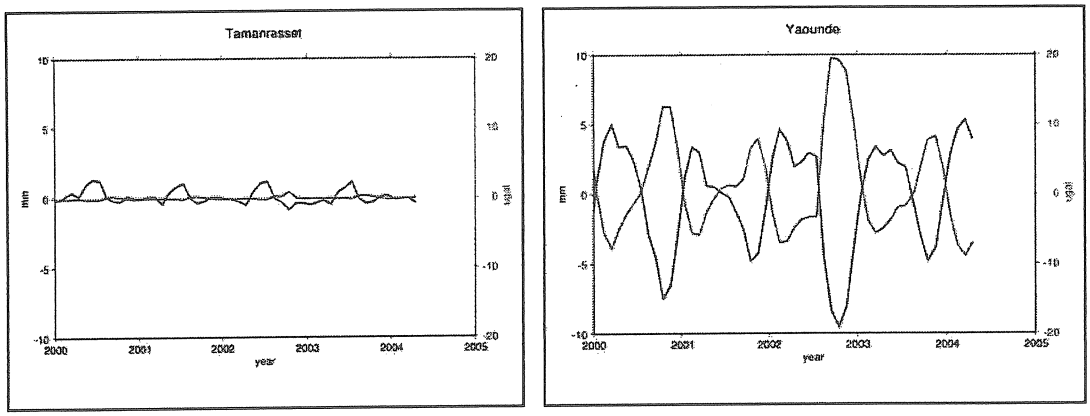

Figure 5. Hydrological predictions in gravity (in μGal) and in vertical displacement (in mm) in Tamanrasset (Algeria) and in Nsimi (Youndé) (Cameroon) stations.

5. Conclusion

In summary, we believe that in addition to other methods based on theoretical modeling, ocean bottom pressure or GPS vertical displacement, the validation of space-born gravity data with surface gravity observations is in progress. It appears clearly possible in Europe with the dense GGP sub-network available and using the annual signal of moderate amplitude due to continental hydrology (mainly soil moisture). However this method requires first to estimate the vertical motion from GPS in order to extract the gravity contribution arising from the motion in the existing gravity field (free air term). Second, since the gravity transfer function for surface measurements involves a Newtonian attraction term highly dependent on the location of the masses near the gravimeter, it is also required to model local hydrology in a very precise way. Another excellent opportunity to validate satellite gravity data is to perform new measurements in Africa with SG and AG focusing on two specific regions: the Sahara where a null test can be achieved and the monsoon region in the equatorial part where large signals are predicted from hydrology.

References

Andersen, O., and Hinderer, J., 2005. Global inter-annual gravity changes from GRACE: early results, Geophys. Res. Lett., 32, L01402, doi:10.1029/2004GL020948

Andersen, O., Hinderer, J., and Lemoine, F. G. , 2005a. Seasonal Gravity Field Variations from GRACE and Hydrological Models, in (eds) Jekeli, Bastos and Fernandes, Gravity, Geoid and Space Missions. IAG symposia vol. 129, 316-321, Springer Verlag.

Andersen O., Seneviratne, S. , Hinderer, J., and Viterbo, P., 2005b. GRACE-derived terrestrial water storage depletion associated with the 2003 European heat wave, Geophys. Res. Lett., 32, L18405, doi:10.1029/2005GL023574.

Boy, J.-P., and Hinderer, J., 2006. Study of the seasonal gravity signal in superconducting gravimeter data, Journal of Geodynamics, 41, 227-233.

Crossley, D., and Hinderer, J., 2002. GGP Ground Truth for Satellite Gravity Missions, BIM, 136, 10735-10742.

Crossley, D., Hinderer, J., Llubes, M., and Florsch, N., 2003. The potential of ground gravity measurements to validate GRACE data, Advances in Geosciences, 1, 1-7.

Crossley, D., Hinderer, J., and Boy, J.-P., 2004. Regional gravity variations in Europe from superconducting gravimeters, J. Geodynamics, 38, 325-342.

Crossley, D., Hinderer, J., and Boy, J.-P., 2005. Time variation of the European gravity field from superconducting gravimeters, Geophys. J. Int., 161, 257-264.

Davis, J., Elosegui, P., Mitrovica, J., and Tamisiea, M., 2004. Climate-driven deformation of the solid Earth from GRACE and GPS, Geophys. Res. Lett., 31, L24605, doi:10.1029/2004GL021435

Hinderer, J. and Legros, H., 1989. Elasto-gravitational deformation, relative changes in gravity and earth dynamics, Geophys. J., 97 , 481-495.

Hinderer, J., and Crossley, D., 2004. Scientific achievements from the first phase (1997-2003) of the Global Geodynamics Project using a worldwide network of superconducting gravimeters, J. Geodynamics, 38, 237-262.

Hinderer, J., Andersen, O., Lemoine, F., Crossley, D., and Boy, J.-P., 2006. Seasonal changes in the European gravity field from GRACE: A comparison with superconducting gravimeters and hydrology model predictions, Journal of Geodynamics, 41, 59-68.

Milly, C., and Shmakin, A., 2002. Global modeling of land water and energy balances. Part I: the land dynamics (LaD) model, J. of Hydrometeorology, 3, 283-299.

Neumeyer, J., Schwintzer, P., Barthelmes, F., Dierks, O., Imanishi, Y., Kroner, C., Meurers, B., Sun, H.-P., and Virtanen, H., 2004. Comparison of superconducting gravimeter and CHAMP satellite derived temporal gravity variations. In: Reigber, Ch., Lühr, H., Schwintzer, P., Wickert, J. (Eds.), Earth Observations with CHAMP Results from Three Years in Orbit, pp. 31–36.

Neumeyer, J., Barthelmes, F., Dierks, O., Flechtner, F., Harnisch, M., Harnisch, G., Hinderer, J., Imanishi, Y., Kroner, C., Meurers, B., Petrovic, S., Reigber, C., Schmidt, R.,

Schwintzer, P., Sun, H.-P., and Virtanen, H., 2006. Combination of temporal gravity variations resulting from Superconducting Gravimeter (SG) recordings, GRACE satellite observations and global hydrology models, J. of Geodesy, DOI: 10.1007/s00190-005-0014-8.

Niebauer, T., Sasagawa, G., Faller, J., Hilt, R., and Klopping, F., 1995. A new generation of absolute gravimeters, Metrologia, 32, 159-180.

Rodell, M., and Famiglietti, J., 1999. Detectability of variations in continental water storage from satellite observations of the time dependent gravity field, Water resources Res., 35, 9, 2705-2723.

Rodell, M., Houser, P.R., Jambor, U., Gottschalck, J., Mitchell, K., Meng, C.-J., Arsenault, K., Cosgrove, B., Radakovich, J., Bosilovich, M., Entin, J.K., Walker, J.P., Lohmann, D., and Toll, D., 2004. The global land data assimilation system, Bull. Am. Meteor. Soc. 85 (3), 381–394.

Rowlands, D., Luthcke, S., Klosko, S., Lemoine, F., Chinn, D., McCarthy, J. , Cox, C., and Andersen, O., 2005. Resolving mass flux at high spatial and temporal resolution using GRACE intersatellite measurements, Geophys. Res. Lett., VOL. 32, L04310, doi:10.1029/2004GL021908.

Swenson, S., Wahr, J., and Milly, P. C. D., 2003. Estimated accuracies of regional water storage variations inferred from the Gravity Recovery and Climate Experiment (GRACE), Water Resour. Res., 39(8), 1223, doi:10.1029/2002WR001808.

Tapley, B. D., Bettadpur, S., Watkins, M. , and Reigber, C. , 2004. The Gravity Recovery and Climate Experiment: Mission overview and early results, Geophys. Res. Lett., 31, L09607, doi:10.1029/2004GL019920.

Wahr, J., Molenaar, M. and Bryan, F., 1998. Time variability of the Earth's gravity field: Hydrological and oceanic effects and their possible detection using GRACE, J. Geophys. Res., 103, 30205– 30230.

Wahr, J., Svenson, S., Zlotnicki, V., and Velicogna, I., 2004. Time-variable gravity from GRACE: First results, Geophys. Res. Lett., Vol. 31, L11501, doi:10.1029/2004GL019779.